Sources, properties, and atmospheric effects of Amazonian biogenic aerosol

Dissertation

zur Erlangung des Grades

“Doktor rerum naturalium (Dr. rer. nat.)” der Fachbereiche

08 - Physik, Mathematik, Informatik
09 - Chemie, Pharmazie, Geographie und Geowissenschaften
10 - Biologie
Universitätsmedizin

verfasst und vorgelegt von

Leslie Ann Kremper

geb. in Lahnstein

Max Planck Graduate Center
mit der Johannes Gutenberg-Universität Mainz

angefertigt am Max-Planck-Institut für Chemie

Mainz, 13.12.2023

Tag der mündlichen Prüfung: 18.01.2024

I hereby declare that I wrote the dissertation submitted without any unauthorized external assistance and used only sources acknowledged in the work. All textual passages which are appropriated verbatim or paraphrased from published and unpublished texts as well as all information obtained from oral sources are duly indicated and listed in accordance with bibliographical rules. In carrying out this research, I complied with the rules of standard scientific practice as formulated in the statutes of Johannes Gutenberg-Universität Mainz to ensure standard scientific practice.

Mainz, 13.12.2023, Leslie Ann Kremper

“Wer die Schlauchverbindung nicht ehrt,
ist das Aerosol nicht wert!”

Me

Abstract

Atmospheric aerosol plays an important role in the Amazon rain forest as it influences ecological processes, clouds, precipitation, and climate. Over several decades, progress has been made in understanding the Amazonian aerosol life cycle, with its interplay of natural and anthropogenic emissions, transport, atmospheric processing, and effects. However, fundamental questions, such as on the roles and relevance of biogenic aerosol sources, have remained open. This dissertation provides experimental results and new insights into the sources, composition, and atmospheric cycling of natural and anthropogenic aerosol in the Amazon rain forest.

Aerosol samples were collected at the Amazon Tall Tower Observatory for single particle elemental analysis in combination with multi-year online atmospheric observations. It was found that the inorganic elemental signature of the wet season aerosol was defined by alternating episodes of pristine and long-range transport conditions. During long-range transport, African dust and smoke as well as sea spray predominated. Under pristine conditions, where rain forest emissions prevail, the inorganic element signature revealed a significant contribution of biogenic salts to the total aerosol population. Based on improved statistical validity, the data set reveals an intense biosphere-atmosphere exchange involving large parts of the aerosol size distribution. The results confirm the important role of biogenic salts in the Amazonian aerosol cycle and provide a basis for studying their influence on cloud microphysical processes.

In addition, multi-year measurements of aerosol particle number size distributions characterized the high seasonal, diel, and meteorology-driven variability of the aerosol population. This study focused on the effects of rain-related mixing on the occurrence and properties of particles smaller than 50 nm, originating from new particle formation in the upper troposphere and subsequent convective downdrafts. Not all events could be explained by this process, however, which emphasizes the potential involvement of biogenic sources for ultrafine particles in the forest. In a further study, the multi-year aerosol size distributions were linked to satellite-derived cloud microphysical parameters. The results showed a clear relation between aerosol abundance and size as well as cloud microphysics and, thereby, revealed that cloud droplet formation and growth processes in the Amazon are sensitive to changes in the aerosol population, even under polluted conditions in the dry season.

This dissertation emphasizes the diversity and source of Amazonian aerosol, their influence on aerosol-cloud-precipitation interactions, and subsequent effects on the rain forest ecosystem. It can advance our knowledge on pre-industrial aerosol processes and human impacts, and serve as baseline data for future studies.

Zusammenfassung

Atmosphärisches Aerosol spielt eine wichtige Rolle im Ökosystem des Amazonas-Regenwaldes. Es beeinflusst die Wolken- und Niederschlagsbildung sowie das Klima. Obwohl bereits Fortschritte im Verständnis des Aerosolkreislaufs, mit seinem Zusammenspiel von natürlichen und anthropogenen Emissionen, Transport, atmosphärischer Alterung und Auswirkungen im Amazonasgebite gemacht wurden, sind grundlegende Fragen, wie die nach der Rolle und der Relevanz biogener Aerosolquellen noch offen.

Diese Dissertation liefert experimentelle Ergebnisse und damit neue Erkenntnisse über die Quellen, die Zusammensetzung und atmosphärischen Auswirkungen von natürlichen und anthropogenen Aerosolen im Amazonas-Regenwald.

Zu diesem Zweck wurden am 'Amazon Tall Tower Observatory' Aerosolproben für die Analyse der elementaren Zusammensetzung einzelner Partikel, in Kombination mit Langzeit-Online-Messungen, genommen. Es wurde festgestellt, dass die anorganische Elementsignatur des Aerosols in der Regenzeit durch abwechselnde Perioden aus ungestörten Bedingungen und solchen mit starkem Einfluss von Ferntransport bestimmt wird.

Unter dem Einfluss von Ferntransport-Prozessen wurde die Aerosolzusammensetzung von Staub, Rauch und marinem Aerosol dominiert. Unter ungestörten Bedingungen, bei denen lokale Emissionen aus dem Regenwald vorherrschen, zeigte die anorganische Elementsignatur einen signifikanten Anteil biogener Salze. Basierend auf einer verbesserten statistischen Validierung zeigt der Datensatz einen intensiven Einfluss des Biosphäre-Atmosphäre-Austausches, der über weite Bereiche der Aerosolgrößenverteilung deutlich wird. Die Ergebnisse unterstreichen die wichtige Rolle biogener Salze im Aerosolkreislauf des Amazonas und bieten eine Grundlage zur weiteren Untersuchung ihres Einflusses auf die Wolkenmikrophysik.

Darüber hinaus haben mehrjährige Messungen von Aerosolpartikelgrößenverteilungen ausgeprägte tageszeitliche und jahreszeitliche, sowie meteorologisch bedingte Variabilität der Aerosolpopulation gezeigt. Die Studie konzentrierte sich auf die Auswirkungen der regenbedingten Durchmischung auf das Vorkommen und die Eigenschaften von Partikeln kleiner als 50 nm, die durch Partikelneubildung in der oberen Troposphäre und anschließende konvektive Abwinde eingetragen werden. Nicht alle Ereignisse konnten durch diesen Prozess erklärt werden, was auf die mögliche Beteiligung biogener Quellen von ultrafeinen Partikeln im Wald hinweist.

In einer weiteren Studie wurden Aerosolgrößenverteilungen mit satellitenbasierten mikrophysikalischen Wolkenparametern verknüpft. Die Ergebnisse zeigten einen klaren Zusammenhang zwischen der Häufigkeit und Größe der Aerosole und den mikro-

physikalischen Eigenschaften von Wolken. Sie zeigen damit, dass die Bildung und das Wachstum von Wolkentröpfchen im Amazonasgebiet empfindlich auf Änderungen der Aerosolpopulation reagieren, selbst unter verschmutzten Bedingungen in der Trockenzeit.

Zusammenfassend beschäftigt sich diese Dissertation mit der Vielfalt und den Quellen von Aerosolen im Amazonasgebiet, deren Einfluss auf die Aerosol-, Wolken- und Niederschlagsinteraktionen und den daraus resultierenden Auswirkungen auf das Ökosystem des Regenwaldes. Sie kann unser Wissen über vorindustrielle Aerosolprozesse und menschliche Einflüsse erweitern und als Basisdatensatz für zukünftige Studien dienen.

Contents

CHAPTER 1

Introduction

1.1 Atmospheric aerosol cycling and its relevance

An aerosol is defined as a suspension of solid, semisolid, or liquid particles in a gas (Prospero et al., 1983; Pandis et al., 1995). The aerosol in the Earth's atmosphere comprises a diverse mixture of particles from manifold sources. Aerosol particles are constantly and dynamically added to and removed from the atmosphere through its exchange with continental surfaces, vegetation, and the oceans (Pöschl and Shiraiwa, 2015). The dynamic life cycle of atmospheric aerosol particles is illustrated in Figure 1.1.

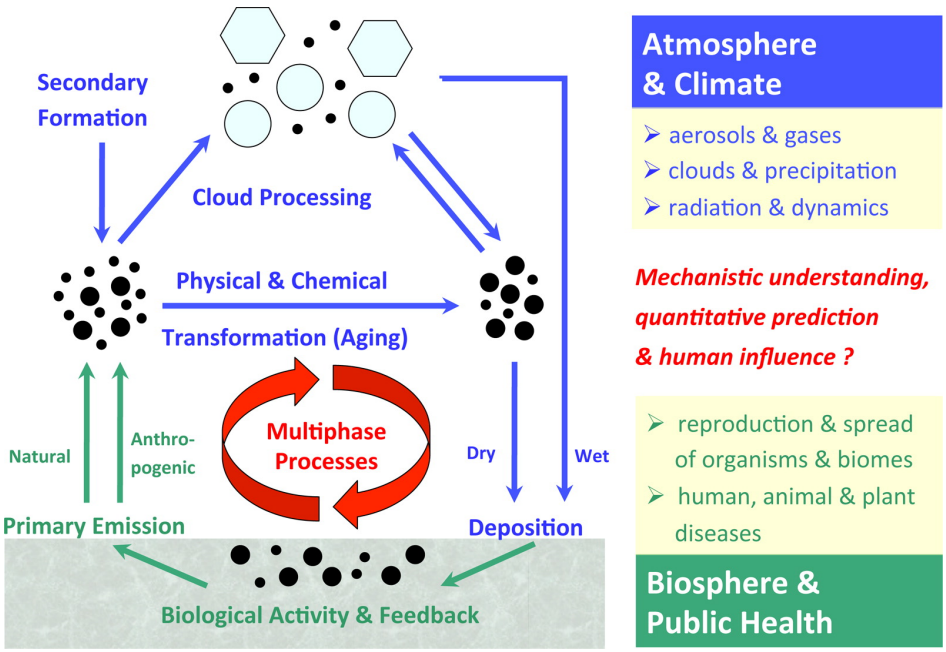

Figure 1.1: Scheme of the atmospheric life cycle of aerosol particles, emphasizing primary and secondary aerosol sources, atmospheric processing, and particle removal through wet and dry deposition. Further emphasized are the main fields of relevance for atmospheric cycling and climate as well as the biosphere and public health. Adopted from Pöschl and Shiraiwa (2015).

Aerosol particles can be broadly categorized into primary and secondary, according to their sources and formation processes. Primary particles are emitted directly from the Earth's surface into the atmosphere and include natural components, such as bacteria, fungal spores, pollen or viruses (Després et al., 2012; Fröhlich-Nowoisky et al., 2016), biogenic salts (Elbert et al., 2007; C. Pöhlker et al., 2012), sea spray (de Leeuw et al., 2011; Quinn et al., 2015) or mineral dust (Choobari et al., 2014; Adebiyi et al., 2023), as well as anthropogenic emissions like black carbon (BC) from combustion processes (Bond et al., 2013) or urban smog in mega cities (Raga et al., 2001). Secondary particles, such as secondary organic aerosol (SOA) or sulfate aerosol, are formed in the atmosphere through the oxidation of volatile organic compounds (VOCs) or sulfur dioxide, followed by the nucleation of the oxidation products in the formation of new particles or by their condensation on pre-existing particle surfaces (Kulmala, 2003; Hallquist et al., 2009; Lee et al., 2019). Atmospheric lifetimes of aerosol range from a few minutes to weeks (Raes et al., 2000;

Williams et al., 2002). During their atmospheric transport, particles can undergo physical and chemical transformations, such as coagulation, condensation and oxidation (Song and Carmichael, 1999; Kroll and Seinfeld, 2008; Zhang et al., 2008; George and Abbatt, 2010; Shiraiwa et al., 2011). These aging processes can change the particle properties significantly. They are removed from the atmosphere through precipitation (wet deposition), or diffusion and sedimentation (dry deposition).

Aerosol particles span a broad size range from a few nanometer to hundreds of micrometers. Their concentrations can vary widely, influenced by factors such as geographical location, weather conditions, and human activities (e.g. Pöschl, 2005; Fröhlich-Nowoisky et al., 2016; Paasonen et al., 2016; Brock et al., 2019). The particles exhibit distinct chemical compositions, which can include organic compounds, inorganic salts, and trace elements, each contributing to their individual characteristics (e.g. Pöschl et al., 2010; Laskin et al., 2012; M. L. Pöhlker et al., 2023). Based on their physicochemical properties, aerosol particles impact the Earth's climate system and water cycles. They influence cloud microphysics and precipitation formation by acting as cloud condensation nuclei (CCN), providing surfaces for water vapor to condense into cloud droplets (Bauer et al., 2003; Dusek et al., 2006; Sun and Ariya, 2006; Pope, 2010; Hassett et al., 2015), or act as ice nuclei (Hoose and Möhler, 2012; Huffman et al., 2013; Tang et al., 2022). The particles affect the Earth's radiation budget, either directly by scattering and absorbing solar radiation (Haywood and Boucher, 2000; Yu et al., 2006), or indirectly by modifying the radiative properties of clouds (Lohmann and Feichter, 2005; Möhler et al., 2007; Andreae and Rosenfeld, 2008). As a result, aerosol-cloud interactions contribute to large uncertainties in radiative forcing estimates (Carslaw et al., 2013; Mülmenstädt and Feingold, 2018). Further, aerosol particles can serve as transporters of biological organisms (Prospero et al., 1983; Elbert et al., 2007; Després et al., 2012) and vital nutrients over large geographical regions (Bristow et al., 2010; Jickells et al., 2016; Rizzolo et al., 2017), underlining their role in maintaining the planet's biodiversity and ecological balances.

1.2 The Amazon rain forest and its global significance

The Amazon Basin is the world's largest contiguous rain forest, representing one of the last intact ecosystems with the world's greatest biodiversity (Cardoso et al., 2017; Fearnside, 2021). Its service to the Earth's environmental stability is of huge importance (Bonan, 2008; Artaxo et al., 2022b; Borma et al., 2022). Among others, the Amazon rain forest plays an important role in the Earth's carbon cycle. With an estimated storage capacity of more than 100 billion tons of carbon (Malhi et al., 2006; Phillips et al., 2009), the rain forest contributes to the regulation of global carbon dioxide levels (Pan et al., 2011). In addition, the Amazon rain forest influences global water cycles and regulates temperatures. Through high levels of evaporation, the rain forest contributes water vapor, which enhances regional and global cloud formation (Artaxo et al., 2022a). This process, in turn, balances the radiation budget (Cecchini et al., 2017).

Nowadays, however, the Amazon ecosystem and its atmosphere are experiencing increasing perturbations due to human activities and climate change. These threats

are predicted to cause the rain forest to undergo a transition characterized by altered precipitation patterns, potential droughts, changes in vegetation, and increased risk of fire (Figure 1.2), leading to a potential reduction in carbon storage and shifts in the energy balance of the Amazon (e.g. Lenton et al., 2008; Pan et al., 2011; Davidson et al., 2012; Hilker et al., 2014; C. Pöhlker et al., 2019; Hubau et al., 2020; Gatti et al., 2021, and references therein).

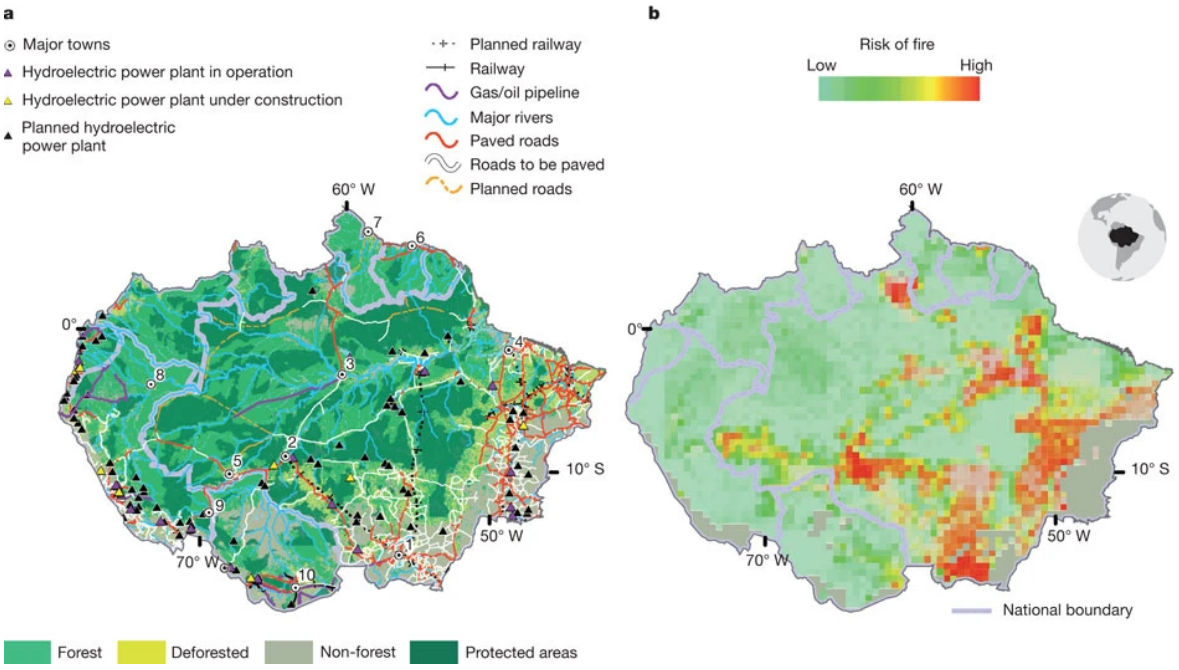

Figure 1.2: Map of land cover and land use of the Amazon basin today (a), emphasizing the trend from continuously wet conditions in the mostly undisturbed northwest, mainly representing forest and protected areas, in contrast to the pronounced dry conditions in the heavily disturbed southeast, with increasing deforestation and non-forest areas, along with future fire risk through 2050 (b), predicted by a model that takes into account human activities and weather conditions, where higher fire risk corresponds to more disturbed areas. Adopted from Silvestrini et al., 2011 & Davidson et al., 2012.

An intact hydrological cycle is essential to the integrity of the rain forest ecosystem and the global benefits it provides. So-called "flying rivers" transport water from the coast to the interior of the country and sustain the forest vegetation (Salati and Vose, 1984; Arraut and Satyamurty, 2009; Arraut et al., 2012; Staal et al., 2018). The airborne waterways are mainly driven by a repeated cycle of evaporation and transpiration, subsequent condensation into cloud droplets, transport and precipitation. Hence, beside environmental factors like solar radiation, temperature and wind, aerosol particles play a crucial role in the rain forest's hydrological cycle as they serve as CCN. In the scenario of increasing perturbation of the forest, the Amazonian aerosol population can be influenced from different perspectives. Alterations in the forest vegetation could lead to changes in natural emissions of aerosol (Hantson et al., 2017; Pugliese et al., 2023). Furthermore, the aerosol composition may be modified due to an increased contribution of combustion aerosol from human activities, causing changes in particle number size distributions as well as their optical and chemical properties (Saturno et al., 2018; Holanda et al., 2020, 2023a).

Given the critical role that aerosol play in the hydrological cycle, among others, these changes may have feedback within the unique ecosystem (Doughty et al., 2015; Barkhordarian et al., 2019; Boulton et al., 2022). Yet, the local and global consequences for the Amazon rain forest and beyond, including changes in aerosol-cloud interactions, cannot be fully estimated. However, to understand and assess the Amazon's future transition, it's important to understand its natural state. Therefore, it is important to take the opportunity to collect baseline data while the forest is still in its most natural and intact state. This data will serve as a reference for assessing ongoing perturbations and their effects, and will provide input for modeling approaches to predict future scenarios and understand underlying trends.

1.3 Seasonality of Amazonian aerosol between pristine and polluted states

The Amazon is one of the few remaining continental places with episodes that resemble almost pristine and pre-industrial atmospheric conditions (Andreae and Rosenfeld, 2008; Hamilton et al., 2014; M. L. Pöhlker et al., 2018). With its distinct seasonality, where the clean wet season with its almost pristine episodes is one extreme, and the dry season with its heavy biomass burning pollution is the other, it represents a suitable outdoor laboratory to contrast these two states (Koren et al., 2004; Andreae, 2007; Rizzo et al., 2013; Yáñez-Serrano et al., 2015; M. L. Pöhlker et al., 2018; Saturno et al., 2018). In recent decades, an increasing number of studies on atmospheric aerosol have shed light on particle sources and their seasonal changing composition (e.g. Talbot et al., 1988, 1990; Artaxo et al., 1993; Andreae et al., 2004; Martin et al., 2010; Andreae et al., 2018; Artaxo et al., 2022b, and references therein).

During the wet season, which spans from February to May, the atmospheric state in the Amazon is primarily influenced by the northern hemisphere (M. L. Pöhlker et al., 2018; C. Pöhlker et al., 2019). Throughout this period, the aerosol population is predominantly shaped by local biogenic emissions (Figure 1.3). This leads to almost pristine and preindustrial-like aerosol conditions that represent the forest background (e.g., Huffman et al., 2012; C. Pöhlker et al., 2012; China et al., 2016; Adachi et al., 2020; Löbs et al., 2020; Prass et al., 2021b; Barbosa et al., 2022). During clean episodes, aerosol number concentrations as low as 300- 500 cm^3 are frequently observed (Zhou et al., 2002; Varanda Rizzo et al., 2018).

Within the fine aerosol size range ($< 1\,\mu\mathrm{m}$), the typical particle number size distribution (PNSD) features a bimodal shape with distinct Aitken and accumulation modes, separated by a distinct 'Hoppel' minimum. The Aitken mode is centered between $\sim$ 50 and 80 nm and the accumulation mode at $\sim$ 100 and 200 nm (Zhou et al., 2002; Whitehead et al., 2016; M. L. Pöhlker et al., 2018). The accumulation mode covers the for cloud formation and cloud microphysics most relevant size range between $\sim$ 100 and 1000 nm (e.g., Roberts et al., 2003; Koren et al., 2004; Rissler et al., 2006; Martins et al., 2009; L. Liu et al., 2020), and is numerically the largest mode. Under pristine conditions, SOA is the major contributor to the fine mode population in the Amazon (Kesselmeier et al., 2009). It is formed by the oxidation products of

biogenic VOCs like monoterpenes or isporenes, which can either condense on existing particles (Figure 1.3) or contribute to the formation of new particles (Kulmala et al., 2012; Varanda Rizzo et al., 2018; Wimmer et al., 2018). However, compared to regions where new particles formation (NPF) and subsequent growth significantly influence aerosol concentrations, the Amazon does not exhibit the 'classical' NPF processes (Zhou et al., 2002; Varanda Rizzo et al., 2018). Unlike freshly nucleated particles where oxidized VOCs generate new molecular clusters, in the Amazon particle growth events are observed to initiate at larger sizes (Kulmala et al., 2012; Kerminen et al., 2018; Varanda Rizzo et al., 2018). This raises the ongoing discussion about the sources of these particles that maintain the Amazonian Aitken and accumulation mode in the absence of "classical" NPF (Andreae et al., 2018; Machado et al., 2021a; Khadir et al., 2023a). Previous studies suggest that NPF occurs in the upper troposphere, with downdraft transport introducing nano-sized particles into the tropical boundary layer (Wang et al., 2016; Andreae et al., 2018; T. Liu et al., 2023). Additional theories propose that biogenic salts from the forest biosphere may serve as seeds for SOA condensation (Pöschl et al., 2010; C. Pöhlker et al., 2012).

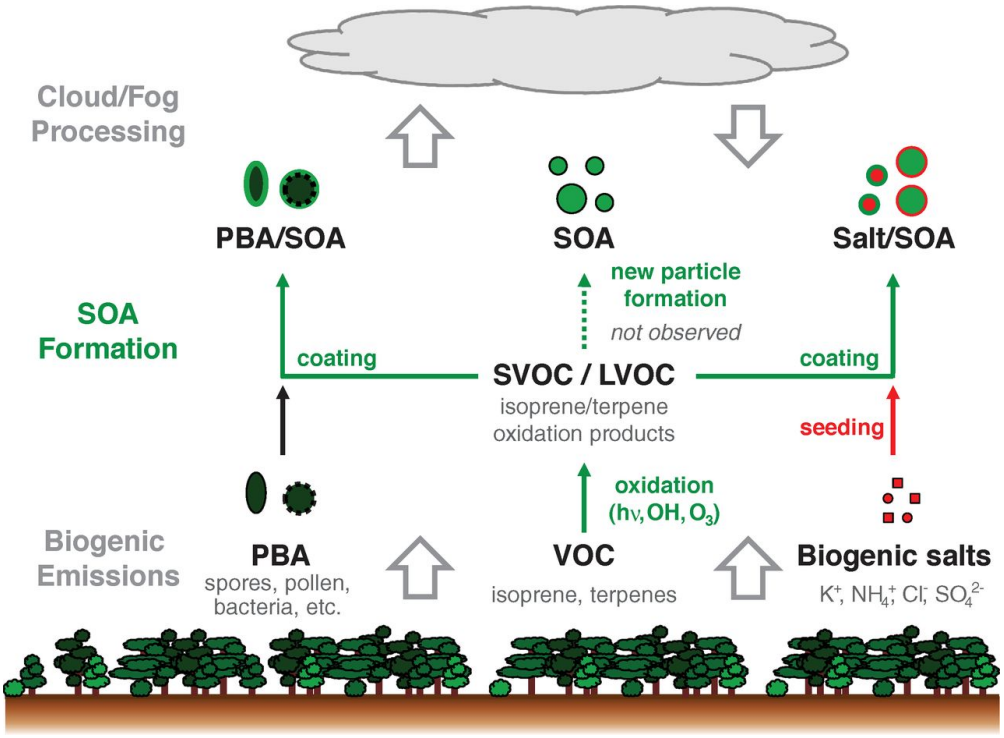

Figure 1.3: Aerosol sources and processing in the Amazon rain forest during pristine conditions including primary biological aerosol particles (PBAPs), secondary organic aerosol (SOA) formed by oxidation and condensation of biogenic volatile organic compounds (VOCs), and biogenic salts which can serve as seeds for SOA formation. Adopted from C. Pöhlker et al. (2012).

While the coarse mode ($> 1\,\mu m$) represents a smaller fraction in terms of number concentration, it dominates in terms of mass (Moran-Zuloaga et al., 2018). During pristine conditions, the coarse mode consist mainly of primary biological aerosol particles (PBAPs), including fungal spores, bacteria and fragments or excretions from plants and animals (Després et al., 2012; Fröhlich-Nowoisky et al., 2016). In addi-

tion to their important role in forest ecology, past and ongoing research suggests that PBAPs play an important role in atmospheric processes. They act as efficient CCN or ice nuclei and influence cloud and precipitation formation (Yin et al., 2000; Bauer et al., 2002; Elbert et al., 2007; Pope, 2010; Griffiths et al., 2012). However, specific information on their exact sources, properties and interactions remains limited (Elbert et al., 2007; Ramsay et al., 2020; Prass et al., 2021b; Barbosa et al., 2022).

Further, pristine conditions during the wet season are occasionally interrupted by the episodic occurrence of long range transport (LRT). During LRT episodes air masses coming over the Atlantic ocean, resulting in an influx of African mineral dust, biomass burning (BB) smoke and sea spray aerosol (Kaufman et al., 2005; Ansmann et al., 2009; Moran-Zuloaga et al., 2018). The intrusion of these particle types modifies the composition of the Amazonian background aerosol. The alteration is particularly characterized by an increase in coarse and accumulation mode concentrations, and is associated with increased BC mass concentrations (Wang et al., 2016; M. L. Pöhlker et al., 2018; Adachi et al., 2020; Holanda et al., 2023a).

In addition, during the dry season, which spans from August to November, the Amazon is under the predominant influence of the southern hemisphere (C. Pöhlker et al., 2019). Throughout this period, the region is strongly affected by anthropogenic activities, with local BB emissions strongly influence the aerosol state (e.g. Artaxo et al., 2013; Saturno et al., 2018; Holanda et al., 2020). Particle concentrations frequently exceed the natural background by up to two orders of magnitude, reaching number concentrations of 1000- 3000 cm^3 (Artaxo et al., 2013; Andreae et al., 2015; M. L. Pöhlker et al., 2018; Varanda Rizzo et al., 2018), and BC mass concentrations around $\sim 0.9\,\mu\mathrm{g\,m}^{-3}$ (Saturno et al., 2018). Due to the prevalence of BB aerosol, the shape of the natural PNSD is altered, resulting in a monomodal shape with a dominant accumulation mode, leading to modified aerosol-cloud interactions (Andreae et al., 2004; M. L. Pöhlker et al., 2018).

Substantial progress has been made in describing the Amazonian aerosol cycle with its various sources, associated processes and their effects. However, our understanding of the interactions between the biosphere and the atmosphere is far from complete. Therefore, intensive aerosol research is subject of the ongoing scientific activities in the Amazon rain forest.

1.4 Research objectives and thesis outline

Understanding the dynamics of biosphere-atmosphere interactions in the Amazon requires dedicated research. In 2010, the Amazon Tall Tower Observatory (ATTO) was established to study atmospheric processes in the unique rain forest system (Andreae et al., 2015). As a long-term research station located in a pristine rain forest region $150\,\mathrm{km}$ northeast of Manaus, the ATTO site allows monitoring the natural ecosystem in the context of ongoing climate change and increasing anthropogenic disturbance. With several measurement towers, including the $325\,\mathrm{m}$ tall tower, and a number of well-equipped laboratory containers, the site hosts a variety of specialized measurements for atmospheric aerosol (e.g. Saturno et al., 2017; Holanda et al., 2020; L. Liu et al., 2020; Schrod et al., 2020; Prass et al., 2021b; Leppla et al., 2023a), trace

gases (e.g. Yáñez-Serrano et al., 2015; Pfannerstill et al., 2018; Gomes Alves et al., 2023), meteorology (e.g. Oliveira et al., 2005; Chor et al., 2017; Dias-Júnior et al., 2022) and ecology (e.g. Löbs et al., 2020; Durgante et al., 2023).

The aerosol instrumentation at the ATTO site includes a wide range of measurement techniques. Continuous in-situ measurements allow real-time monitoring of aerosol properties in ambient air, commonly referred to as online techniques. These measurements typically detect and quantify aerosol characteristics like particle number concentrations, size distribution, optical properties, and chemical composition. Online measurements at ATTO provide long-term data with high time resolution and can capture short-lived events and detect rapid atmospheric changes. In contrast, discrete offline measurements refer to the collection of aerosol samples at specified intervals followed by laboratory analysis. The process requires the use of filter samplers or impactors to collect aerosol on substrates. Sampling strategy, including collection in defined size ranges or the use of specific substrates, can be adapted to specialized measurement techniques. Offline measurements like microscopy, spectroscopy or chemical analysis provide accurate in-depth data on particle characteristics like size, morphology, chemical composition and hygroscopicity, but are limited by their relatively low temporal resolution.

In this dissertation, continuous online as well as discrete offline measurements were used to obtain comprehensive information about the chemical composition and physical properties of Amazonian aerosol. The ATTO project provided the framework for my studies. Several field campaigns were an essential part of my project to collect aerosol samples for selected offline measurements. In addition, continuous support of online instrumentation was a central task.

My core project focuses on the analysis of the chemical composition of Amazonian aerosol particles using scanning electron microscopy combined with energy dispersive X-ray spectroscopy (SEM-EDX). SEM-EDX is a powerful tool for gaining detailed insight into individual particle properties by combining size, morphology and chemical information. The technique is particularly sensitive to probing the inorganic fraction, with efficient performance for particles larger than $250\,\mu\mathrm{m}$. In the following chapters 2.1 and 2.2, I will present two studies based on automated single particle SEM-EDX analysis. My investigations address the spatial and temporal variations in the Amazonian wet season aerosol, with a focal point on the inorganic composition of the accumulation and coarse mode size range. The studies employ a systematic aerosol collection strategy, designed to capture the diversity of environmental conditions in the Amazon. The collected samples have been analyzed in the context of various prevailing atmospheric conditions, monitored by complementary online measurements.

1. "*Contrasting the elemental composition of Amazonian aerosol under African dust influx vs. pristine conditions*" (chapter 2.1) focuses on the diversity of aerosol composition during the Amazonian wet season. Using complementary online data, aerosol samples were selected to represent the alternating episodes of pristine and long-range transport (LRT) conditions. This reveals the dominant sources contributing to the aerosol population during each episode. This approach facilitates the identification of elemental signatures and marker elements associated with LRT and pristine conditions.

2. "*Ubiquitous biogenic salts in the Amazonian aerosol observed by electron microspectroscopy*" (chapter 2.2) focuses on physicochemical properties of the natural Amazonian aerosol population under clean conditions. Based on complementary online measurements, the study distinguishes between clean and polluted states. It further examines day and night variations and explores biosphere-atmosphere exchange and mixing by considering below and above canopy conditions. This approach allows for the identification of specific elemental markers linked to distinct particle modes and discusses their potential sources, atmospheric abundance, and relevance.

In chapters 2.3 and 2.4, I present studies based on particle number size distributions (PNSD) obtained using a scanning mobility particle sizer (SMPS). The SMPS covers the Aitken mode and the lower accumulation mode size range from $10-400\,\mathrm{nm}$. PNSD measurements are essential for understanding the fundamental aerosol conditions. At ATTO, the continuous SMPS long-term measurements span over almost ten years and serve as important reference data for other aerosol instrumentation.

3. "*Occurrence and growth of sub-50 nm aerosol particles in the Amazonian boundary layer*" (Chapter 2.3) is an analysis of a long-term SMPS data set measured at the ATTO site. Combined with other meteorological data, the study observes the occurrence of sub-50 nm particles within the Amazonian aerosol population in respect to seasonal and diurnal cycles. This study facilitates the identification of potential sources of nanometer-sized particles that may serve as precursors to Aitken and accumulation mode particles.

4. "*High aerosol sensitivity of convective clouds over the Amazon*" (Chapter 2.4) is a study that combines in-situ ground-based measurements at the ATTO site, with satellite remote sensing data. The study focuses on aerosol-cloud interactions in tropical convective clouds. This study examines the variations in aerosol effects in relation to the variable PNSD during the heavily polluted dry season. The observations contribute to the understanding of the sensitivity of clouds to changes in aerosol concentrations.

CHAPTER 2

Results

2.1 Contrasting the elemental composition of Amazonian aerosol under African dust influx vs pristine conditions

This chapter contains the final draft of a manuscript that will be submitted to Atmospheric Chemistry and Physics.

Contribution to this publication by Leslie A. Kremper: I am the first author of this paper and played a major role in designing the study. I developed the codes for processing, analysis, and visualization of the data obtained by scanning electron microscopy with energy dispersive x-ray analysis, which are the core elements in this study. I took the lead preparing the figures and writing the manuscript.

Contrasting the elemental composition of Amazonian aerosol under African dust influx vs pristine conditions

Leslie A. Kremper[1], Daniel Moran-Zuloaga[1,2], Konrad Kandler[3], Jan-David Förster[1,2], Cléo Quaresma Dias-Júnior[4], Florian Ditas[1,2,a], Isabella Hrabe de Angelis[1], Jorge Saturno[1,2,b], David Walter[1,7], Paulo Artaxo[8], Meinrat O. Andreae[2,9], Ulrich Pöschl[1], and Christopher Pöhlker[1,2]

[1] Multiphase Chemistry Department, Max Planck Institute for Chemistry, 55128 Mainz, Germany
[2] Biogeochemistry Department, Max Planck Institute for Chemistry, 55128 Mainz, Germany
[3] Institut für Angewandte Geowissenschaften, Technische Universität Darmstadt, Darmstadt, Germany
[4] Department of Physics, Federal Institute of Pará (IFPA), Belém, PA, Brazil
[7] Climate Geochemistry Department, Max Planck Institute for Chemistry, 55128 Mainz, Germany
[8] Institute of Physics, University of São Paulo, São Paulo 05508-900, Brazil
[9] Scripps Institution of Oceanography, University of San Diego, La Jolla 92037, USA
[a] now at: Hessian Agency for Nature Conservation, Environment and Geology, 65203 Wiesbaden, Germany
[b] now at: Physikalisch-Technische Bundesanstalt, 38116 Braunschweig, Germany

Correspondence: Christopher Pöhlker (c.pohlker@mpic.de)

Abstract. Atmospheric aerosol in the Amazon rain forest influence biogeochemistry, clouds, and climate. Of particular importance is the clean wet season, which is determined by natural processes in the absence of human influence and is approaching pre-industrial conditions. However, the fundamental mechanisms of biosphere-atmosphere exchange remain enigmatic. In this study, we used scanning electron microscopy with energy dispersive x-ray spectroscopy (SEM-EDX) for a single particle analysis of the elemental composition of Amazonian wet season aerosol in the size range of 0.3 to 10 µm. Selected aerosol samples, representing defined atmospheric conditions according to a spectrum of online atmospheric parameters, allowed differentiation between atmospheric states with strong influence of long-range transported dust, smoke and sea spray versus pristine and rain forest-dominated conditions. All particles were dominated by organic matter, but also comprised a significant and diverse fraction of inorganic elements. Under the influence of long-range transport, the inorganic elemental signature was characterized by the dust and sea salt marker elements such as aluminum, iron, sodium and chlorine. Under the contrasting pristine conditions, it is characterized by biogenic tracer elements such as potassium. Overall, our results emphasize that the inorganic element signature of the Amazonian wet season aerosol is quite variable and can be characterized as alternating episodes of pristine vs long-range transport conditions, as well as a continuum of mixtures of both.

1 Introduction

The Amazon rain forest plays an important role in the biogeochemical cycles and climate system of the Earth (e.g., Davidson et al., 2012; Lenton et al., 2019; Yang et al., 2018; Staal et al., 2018). Major progress has been made in our understanding of the functioning of the forest ecosystem (e.g., ter Steege et al., 2013; Dias et al., 2002; Andreae et al., 2018; Yáñez-Serrano et al., 2018). Yet, a variety of fundamental processes – especially related to the biosphere-atmosphere exchange – are not well understood (Artaxo et al., 2022; Prospero et al., 2020). Atmospheric aerosol, comprising any kind of solid, semi-solid or liquid airborne particle from few nanometers to hundreds of micrometers, affect the rain forest ecology and biogeography (e.g., Swap et al., 1992; Rizzolo et al., 2017; Yu et al., 2015; Adachi et al., 2020) as well as cloud physics, the hydrological cycle and climate (e.g., Pöhlker et al., 2016; Pöschl et al., 2010; Liu et al., 2020; Lauer et al., 2022). Accordingly, aerosol have been a focal point of Amazonian research activities over decades (Martin et al., 2010; Andreae et al., 2015; Artaxo et al., 2022, and references therein). Of particular interest has been the Amazonian wet season approaching pristine and preindustrial-like aerosol conditions. Particularly over the continents, pristine atmospheric conditions have become rare worldwide (Andreae and Rosenfeld, 2008; Hamilton et al., 2014). While the clean wet season represents one extreme of the atmospheric seasonality in the Amazon, the dry season with its heavy biomass burning pollution is the other (e.g., Koren et al., 2004; Andreae et al., 2004; Rizzo et al., 2013; Saturno et al., 2018b). It is important to note, however, that the wet season is not characterized by a homogeneously clean atmosphere, but is strongly influenced by the episodic occurrence of long-range transported air masses bringing African dust, biomass burning smoke, and sea spray aerosol (Kaufman et al., 2005; Ansmann et al., 2009; Baars et al., 2011; Moran-Zuloaga et al., 2018; Holanda et al., 2020). Accordingly, the wet season conditions can be characterized as an alternating sequence of pristine periods, long-range transport periods, as well as a continuum of mixtures of both.

Pristine periods mostly occur in the late wet season, especially in the second half of April and first half of May (Pöhlker et al., 2018). Here, the aerosol population predominantly comprises biogenic emissions, including primary biological aerosol, such as bacteria and spores (e.g., Huffman et al., 2012; Löbs et al., 2020a; Prass et al., 2021), inorganic salts emitted from the biosphere (e.g., Nemeruyk, 1970; Artaxo and Hansson, 1995; Pöhlker et al., 2012; China et al., 2018), secondary organic aerosol (SOA) formed through the oxidation of volatile organic compounds (VOC) and their subsequent nucleation and particle growth (e.g., Chen et al., 2015; Andreae et al., 2018), as well as mixtures of all these particle classes. Pristine periods are characterized by the concentration of the pollution marker black carbon (BC) below detection limits (Pöhlker et al., 2018) and, therefore, reveal the rain forest background aerosol (e.g., Pöschl et al., 2010). Episodes of African LRT with its plume-wise advection of Saharan dust, African biomass burning smoke, and marine aerosol predominantly occur in the dry-to-wet season transition period (Dec and Jan) as well as the early wet season (Feb to Apr) (Ben-Ami et al., 2009, 2010; Moran-Zuloaga et al., 2018). The air mass influx through LRT alters the state of the Amazonian background aerosol profoundly (Adachi et al., 2020; Holanda et al., 2023). It affects the aerosol concentration and size distribution (i.e., enhanced accumulation mode and coarse mode concentrations), raises BC mass concentrations, and changes the aerosol chemical composition (Rizzo et al., 2018). This in turn has consequences for the aerosol hygroscopicity and CCN activity as well as optical properties (Saturno et al., 2018b; Holanda et al., 2020; Wang et al., 2016; Pöhlker et al., 2018; Saturno et al., 2018a).

Table 1. Literature synthesis compiling previous studies in the field of Amazonian aerosol research that present and discuss the occurrence and role of the listed elements ($Z \geq 12$) in the aerosol classes mineral dust, sea spray aerosol, biogenic emissions, and combustion. Table emphasizes that certain elements are relatively specific for a given source whereas others are ambiguous as occurring in multiple types of aerosol. The asterisk indicates that the main source of sulfur is secondary formation in the atmosphere in contrast to the other elements, which mostly originate from primary sources.

Element	Classes			
	Mineral dust	**Sea spray aerosol**	**Biogenic aerosol**	**Combustion aerosol**
Na		a, e, l, o, r, s	a, j, o	
Mg	e, k, m, o	a	o	
Al	a, e – g, i – m, o, s, t			
Si	a, e – g, i, j, l, m, o, s, t			
P	h, j, r		a, e, j, l, m, o, q, s, t	h, m
S*	a, g, o	a, o, t	a, c, e, l – o, s, t	a, d, e, m, u
Cl	g	a, e, l, o, r, s	a, f, m, s, t	u
K	f, i, l, o		a, e, j, l, m, o, q, s, t	a, b, m, p, u
Ca	a, e – g, i, k – m, s	o	o	b, p, s
Ti	e – g, k – m, s, t			
Fe	a, e – g, i – m, o, s, t			
Zn			e, l, m	m

[a] Adachi et al. (2020), [b] Andreae (1983), [c] Andreae and Andreae (1988), [d] Andreae et al. (1990), [e] Arana et al. (2014), [f] Artaxo et al. (1990), [g] Artaxo and Hansson (1995), [h] Barkley et al. (2019), [i] Bristow et al. (2010), [j] Chiapello et al. (1997), [k] China et al. (2018), [l] Formenti et al. (2001), [m] Guyon (2003), [n] Jardine et al. (2015), [o] Krejci et al. (2005), [p] Li et al. (2003), [q] Pöhlker et al. (2012), [r] Swap et al. (1992), [s] Worobiec et al. (2007), [t] Wu et al. (2019), [u] Yamasoe et al. (2000),

The elemental composition of the Amazonian aerosol provides insights into the interplay of sources and atmospheric processing and has been studied intensely since decades accordingly (e.g., Krejci et al., 2005; Wouters et al., 1993; Echalar et al., 1998; Artaxo et al., 1990). Particularly interesting are tracer elements that reflect the strength or relevance of one given source or atmospheric process and, therefore, help to disentangle the complex aerosol cycling. Most tracer elements – starting at sodium (Na, atomic number $Z = 12$) and heavier – are indicative of primary sources. Examples are (i) the desert or soil dust markers silicon (Si), aluminum (Al), iron (Fe), and titanium (Ti), (ii) the sea salt markers sodium (Na) and chlorine (Cl) as well as (iii) the biogenic tracers potassium (K), phosphorous (P), and zink (Zn). Sulfur (S) mostly occurs as sulfate (SO_4^{2-}) in the aerosol phase and originates from gaseous S species through secondary aerosol formation. Biogenic S-bearing gases, such as hydrogen sulfide (H_2S), dimethylsulfide (DMS), and carbonyl sulfide (COS), as well as anthropogenic emissions can act as precursors (Andreae et al., 1990; Andreae and Andreae, 1988). However, the assignment of marker elements is often ambiguous because the elements can originate from multiple sources. Examples are, for instance, K and Na which can be

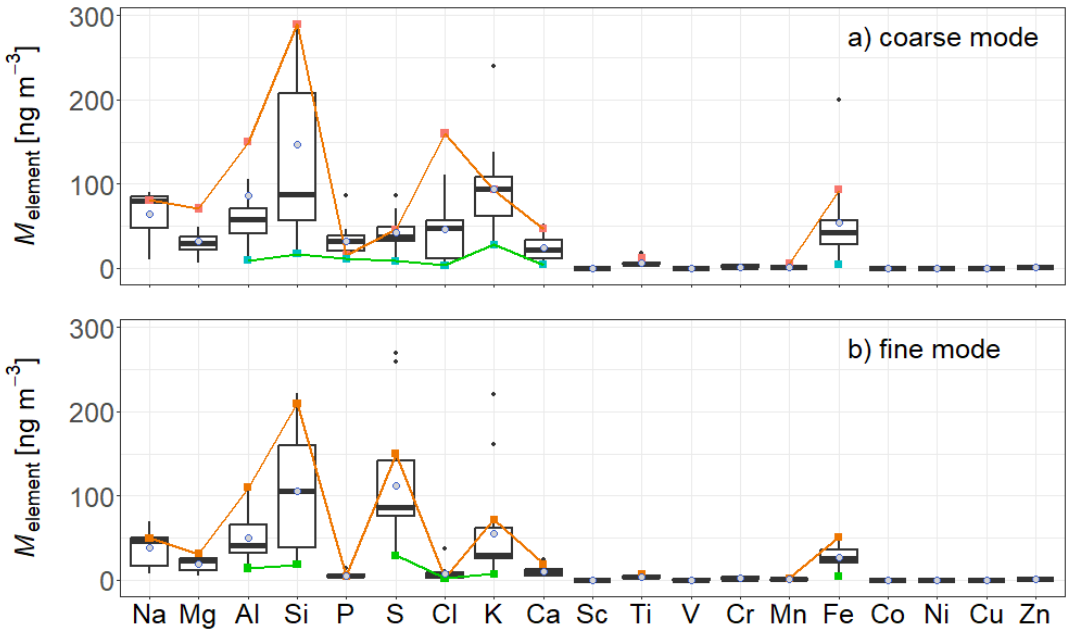

Figure 1. Overview of elemental mass concentrations $M_{element}$ in the Amazonian aerosol coarse (>2.5 µm, **a**), and fine (<2.5 µm, **b**) particle size ranges, compiled from previous studies. The figure provides a summary of the overall variability of $M_{element}$ under Amazonian wet season conditions. The data points represent the average values reported in previous studies (i.e., Arana et al., 2014; Moran-Zuloaga et al., 2018; Maenhaut et al., 2002; Artaxo et al., 2013; Guyon, 2003; Artaxo et al., 1990). In the box-whisker plots, medians are shown as horizontal lines and mean values as circular markers. Boxes represent the first and third quartiles, and whiskers extend to the largest or smallest within the 1.5 times interquartile range (IQR). Outlying values are displayed individually. Results from Moran-Zuloaga et al. (2018) are emphasized, as this study differentiates pristine conditions (in green) and major LRT influx (in orange), which provides reference values for the defined conditions.

emitted by the biosphere (e.g., Artaxo and Hansson, 1995; China et al., 2018), combustion processes (e.g., Andreae, 1983; Chen et al., 2013) as well as associated with sea spray (e.g., Bertram et al., 2018) and/or mineral dust (e.g., Kandler et al., 2007). Table 1 summarizes selected studies on the presence of the most abundant trace elements in the Amazonian aerosol ($Z = 12$) to illustrate which ones are somewhat specific for a given source and which ones are rather ambiguous. Along these lines, Figure 1 summarizes typical concentration levels from previous studies for selected elements ($Z = 12$) under Amazonian wet season conditions. Emphasized in colors are the results from Moran-Zuloaga et al. (2018), which discriminate pristine vs LRT-influenced conditions, whereas in many other studies, wet season averages are provided, which typically represent mixtures of the rain forest background and LRT aerosol. Figure 1 shows, for instance, the clear enhancement of Si, Al, and Fe

under LRT conditions and their near-absence in the pristine atmosphere. It further shows that the biogenic tracer K is present throughout the seasons.

This study goes a step further, building on previous findings. Specifically, scanning electron microscopy with energy-dispersive x-ray spectroscopy (SEM-EDX) for an elemental analysis of Amazonian aerosol samples on single particle basis was applied. The samples were collected at the Amazon Tall Tower Observatory (ATTO), closely linked to a broad range of online aerosol characterization. This allows us to analyze the abundance of relevant elements and their covariance as a function of particle size. Further and importantly, the aerosol samples were selected to represent the typical gradient of aerosol states in the Amazonian wet season, ranging from pristine conditions over mixed states to major LRT influx. This approach distinguishes the biogenic vs LRT-dominated aerosol states that many previous studies have – intentionally or unintentionally – analyzed intermingled. The chemical characterization of these distinct states provides insights into the occurrence and distribution of marker elements in the aerosol population to better determine the role and relevance of the major sources.

2 Experimental section

2.1 The Amazon Tall Tower Observatory

The Amazon Tall Tower Observatory (ATTO) has been established in 2011/12 as a long-term research station for atmospheric aerosol (e.g., Schrod et al., 2020; Liu et al., 2020; Prass et al., 2021; Franco et al., 2022; Holanda et al., 2020), trace gases (e.g., Yanez-Serrano et al., 2015; Pfannerstill et al., 2018; Alves et al., 2023), meteorology (e.g., Oliveira et al., 2020; Chor et al., 2017; Dias-Júnior et al., 2022), and ecology (e.g., Löbs et al., 2020b; Durgante et al., 2023) in the central Amazon rain forest. It is located $\sim$150 km northeast of Manaus, Brazil, at S 02° 08.602', W 59° 00.033' (130 m above sea level) in a largely untouched rain forest region. Details on atmospheric, geographic, and ecological conditions at the ATTO site and on its footprint region can be found elsewhere (Pöhlker et al., 2019; Andreae et al., 2015). In this study, aerosol sampling and in situ measurements – both sampling from a 60 m inlet at the 80 m tall triangular mast – were combined. The inlet is located about 30 m above the average canopy height. The instrumentation is located in an air-conditioned laboratory container at the foot of the tower. Sample air is transported through a 25 mm stainless steel tube (finetron tubes, Dockweiler AG, Neustadt-Glewe, Germany) and dried by silica gel adsorption dryers upstream the instrumentation to a relative humidity (RH) below 40 %. Further information on the aerosol setup at ATTO can be found elsewhere (e.g., Andreae et al., 2015; Pöhlker et al., 2016; Saturno et al., 2018b). Aerosol samples and online data for this work have been obtained in the wet season 2014 (Feb – May) – a period that has been well characterized by previous studies (Pöhlker et al., 2016; Moran-Zuloaga et al., 2018; Saturno et al., 2018b). Further, the sampling period overlapped with the first intensive operating period (IOP, 1 February 2014 to 31 March 2014) of the international field campaign Observation and modeling of the Green Ocean Amazon (GoAmazon2014/5), conducted in and around the city of Manaus from 1 January 2014 through 31 December 2015 (Martin et al., 2016).

2.2 Online observations at ATTO

Aerosol, trace gas, and meteorological measurements have been conducted at ATTO since 2012 (e.g., Andreae et al., 2015; Saturno et al., 2018b). Below is a summary of the ATTO data sets as well as complementary remote sensing and trajectory model data used in this study.

- An Optical Particle Sizer (OPS, model 3330, TSI Inc. Shoreview, MN, USA) measured the particle number size distributions (PNSDs) from 0.3 to 10 µm. The size range of $1-10\,\mu\mathrm{m}$ covers most of the aerosol coarse mode with $N_{1\text{-}10}$ as the coarse mode particle number concentration and $M_{1\text{-}10}$ as the coarse mode mass concentration. The size range of $0.3-1\,\mu\mathrm{m}$ covers the large particle fraction of the accumulation mode with $N_{0.3\text{-}1}$ as a proxy for the accumulation mode particle number concentration and $M_{0.3\text{-}1}$ as a proxy for the accumulation mode mass concentration. For number to mass concentration conversion, a density of $\rho = 1\,\mathrm{g\,cm^{-3}}$ was assumed (details in supplement of Moran-Zuloaga et al., 2018).

- A Multi-Angle Absorption Photometer (MAAP, model 5012, Thermo Electron Group) was used to measure an aerosol absorption coefficient at $\lambda = 637\,\mathrm{nm}$. The MAAP reports the equivalent black carbon mass concentration (M_{BCe}) assuming the widely used standard mass absorption cross section (MAC) of $6.6\,\mathrm{m^2\,g^{-1}}$. Note that typical MAC values in the Amazon are higher (i.e., $11-12\,\mathrm{m^2\,g^{-1}}$) (Saturno et al., 2018b), which means that M_{BCe} tends to be overestimated here. Generally, M_{BCe} serves as a pollution marker and biomass burning tracer.

- Scattering coefficients were measured using an Aurora 3000 nephelometer (Ecotech Pty Ltd., Knoxfield, Australia), which measures scattering coefficients at 450, 525, and $635\,\mathrm{nm}$ wavelength. CO_2 calibrations were periodically performed. For further details, refer to Saturno et al. (2018b).

- The micrometerological data was obtained at the $60\,\mathrm{m}$ height of the $80\,\mathrm{m}$ INSTANT tower and comprises (i) measurements of precipitation (rain gauge, TB4, Hydrological Services Pty. Ltd., Australia) and (ii) solar radiation (pyranometer, CMP21, Kipp & Zonen, Netherlands).

- Backward trajectory (BT) and remote sensing data were used to characterize the arriving air masses and overall atmospheric conditions. BTs are based on the Hybrid Single-Particle Lagrangian Integrated Trajectorymodel (HYSPLIT, NOAA-ARL) with meteorological input data from the Global Data Assimilation System (GDAS1,1° resolution) (Draxler and Hess, 1998; Stein et al., 2015). The BT analysis was adapted from Pöhlker et al. (2019), where details can be found. The cumulative precipitation along the BT tracks, P_{BT}, has been calculated based on the HYSPLIT model output (see also Moran-Zuloaga et al., 2018). The P_{BT} values represent a measure for potential aerosol scavenging by rain. The analysis of remote sensing data, such as from the moderate resolution imaging spectroradiometers (MODIS) on the satellites Terra and Aqua, were adapted from Moran-Zuloaga et al. (2018), where details can be found.

Data processing was conducted with the software packages IGOR Pro (version 6.3.7.2, Wavemetrics, Inc.;Portland, OR, USA) and RStudio (Posit team, 2023).

2.3 Aerosol sampling

Aerosol samples for single particle analysis were collected with a custom-build single-stage impactor with a nozzle diameter of $1.1\,\mathrm{mm}$. Particles were deposited onto silicon nitride (Si_3N_4) substrates (size $5\,\mathrm{mm}$ x $5\,\mathrm{mm}$, Silson Ltd., Northhampton, UK). The impactor was operated with flow rates between $3-7\,\mathrm{L\,min^{-1}}$, resulting in theoretical $50\,\%$ particle cutoff sizes (D_{50}) between $0.5-0.75\,\mu\mathrm{m}$. In the size range around D_{50}, the particle collection efficiency decreases steeply, however, also a certain fraction of particles in $< D_{50}$ is typically still collected and therefore available for analysis. Accordingly, the present study focuses on coarse mode aerosol particles (defined here as $>1\,\mu\mathrm{m}$) and further covers the large particle fraction (i.e., larger $0.3\,\mu\mathrm{m}$) of the accumulation mode (defined here as $0.1-1\mu\mathrm{m}$). The duration of each sampling run was rather short ($1-2$ minutes), which ensures appropriately thin particle coverage on the substrate for single particle analysis. Because of the short sampling times, the individual samples represent 'snapshots' of the given aerosol population at the time of sampling. All samples were stored in airtight containers at -20°C immediately after sampling.

During the 2014 wet season IOP, a large sample set was collected. Samples with an appropriate particle coverage and representing relevant aerosol conditions were analyzed with different techniques. The six best samples in terms of sample quality and particle coverage as well as relevance of probed conditions were selected for in-depth SEM-EDX analysis (see Table 2). Samples were classified into categories of ambient aerosol conditions: (i) samples 12 and 23 representing strong long-range transport from Africa; (ii) samples 54 and 55 representing pristine rain forest conditions; and (iii) samples 19 and 58 representing comparatively weak long-range transport from Africa. For parts of the subsequent analysis, samples 12 and 23, on one hand, and samples 54 and 55 were pooled as sampling conditions were quite similar.

Table 2. Selected and analyzed aerosol samples collected at ATTO in the wet season 2014 along with sampling times and conditions.

Sample name	Date	Start time (UTC)	Duration [min]	Cut-off size [μm]	Air volume [L]
$2014-12$	2014-02-15	18:56	2	0.75	6
$2014-19$	2014-02-17	12:24	1	0.50	6
$2014-23$	2014-02-17	18:23	2	0.50	14
$2014-54$	2014-03-16	20:05	2	0.60	9
$2014-55$	2014-03-17	19:15	2	0.60	9
$2014-58$	2014-03-29	17:39	2	0.75	6

2.4 Scanning electron microscopy with energy dispersive x-ray analysis

The sampled SiN substrates were analyzed automatically with a scanning electron microscope (SEM, FEI ESEM Quanta 200 FEG) combined with energy-dispersive x-ray analysis (EDX, EDAX Phoenix, EDAX, Tilburg, The Netherlands) with the software EDAX/AMETEK GENESIS 5.231. The samples were analyzed in vacuum ($\sim 10^{-2}\,\mathrm{Pa}$) with an acceleration voltage of

150 $12.5\,\mathrm{kV}$ with a beam diameter of $3\,\mathrm{nm}$ and a working distance of $\sim 10\,\mathrm{mm}$, without pre-treatment. The scanning resolution during automated analysis corresponded to $18\,\mathrm{nm}$ per pixel. Prior to automated analysis, target areas on the samples had been selected manually based on the particle distribution and were screened for surface defects, atypical particles or deposition patterns indicating possible contamination. Target areas were characterized by a preferably high number of clearly separated particles and are therefore located within the periphery of the impaction spot. During scanning, particles were separated auto-
155 matically from the background via thresholding based on the backscatter electron signal. Depending on the sample properties, the thresholds were defined for each sample individually. Particle sizes here represent the average diameters of the particles' projected areas. All measured particles were grouped into four size bins as specified in Table 3.

Table 3. Size bins used in SEM-EDX analysis of this study. Size resolution has been purposefully kept low to increase particle statistics in individual bins.

Size bin	lower limit [μm]	upper limit [μm]
1	0.30	0.5
2	0.50	1.0
3	1.00	2.5
4	2.50	10

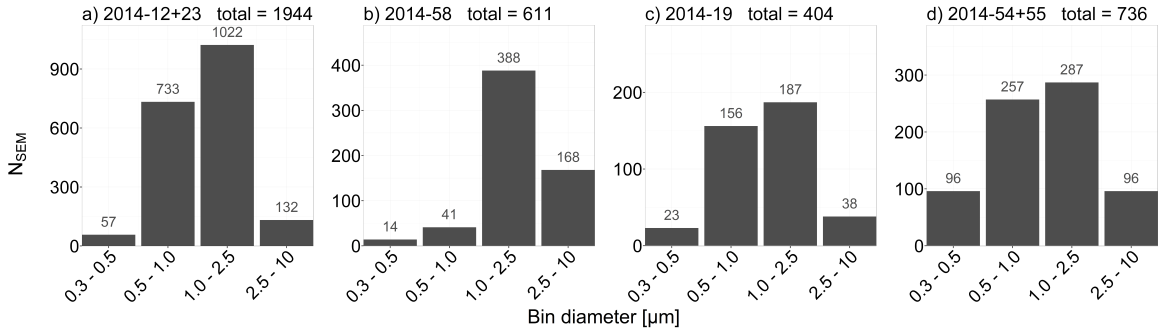

Figure 2. Particle number size distributions (PNSD) of analyzed particles as bar plots, representing the following ambient aerosol conditions: **(a)** strong long-range transport (LRT) influence from Africa, **(b & c)** weak to medium LRT influence from Africa, and **(d)** pristine rain forest conditions. The SEM-derived physical particle diameters represent the projected particle area on the substrates, which was grouped here into four size bins defined in Table 3. Above each size bin, the total particle number of analyzed particles (N_{SEM}) is reported. Particle number concentrations (N_{SEM}) are not normalized by bin width here.

Element detection and quantification in single particles was conducted by EDX microanalysis. The system records characteristic x-ray emissions for all elements with an atomic number $Z > 5$. Due to comparatively small particle sizes, the quantification

160 method by Cliff and Lorimer (1975) was applied. Elemental quantities are given in atomic concentrations (at.%, defined as the percentage of the number of atoms of a particular element relative to the total number of atoms in a compound). The concentration of silicon (Si) and nitrogen (N) could not be quantified as the signals from the aerosol particles are masked by the strong background from the SiN substrates. Si and N are therefore excluded from further analysis. In addition, oxygen (O) is excluded as well, due to the poor reliability of EDX for O quantification. The following elements could be detected within 165 more than 1 % of particles per sample and were therefore considered for analysis: Carbon (C), sodium (Na), magnesium (Mg), aluminum (Al), phosphorus (P), sulphur (S), chlorine (Cl), potassium (K), calcium (Ca), iron (Fe), titanium (Ti) and copper (Cu). For further details on automated SEM-EDX analysis refer to Kandler et al. (2018). The SEM-EDX data analysis and processing were done with RStudio (Posit team, 2023).

2.5 Element index definition and particle classification

170 The relative abundance of carbon within a single particle is represented by the carbon index defined as

$$\text{C-index} = \frac{at.\%C}{\sum at.\%E_{all}} \tag{1}$$

where $at.\%C$ is the atomic concentration of carbon and $at.\%E_{all}$ is the atomic concentration of a given element within all elements measured (E_{all} = C, Na, Mg, Al, P, S, Cl, K, Ca, Ti, Fe, Cu). To observe the inorganic element composition within a single particle exclusively, the inorganic elemental index is defined as

175 $$E_i\text{-index}_{inorg} = \frac{at.\%E_\mathrm{i}}{\sum at.\%E_\mathrm{i}} \tag{2}$$

where $at.\%E_i$ is the atomic concentration of the element of interest (E_i = Na, Mg, Al, P, S, Cl, K, Ca, Ti, Fe, Cu). Note that for the E_i-Index$_{inorg}$ calculation $at.\%C$ is not included. Based on E_i-Index$_{inorg}$ three additional parameter were introduced, defined as

$$\text{NaCl-index} = \text{Na-index}_{inorg} + \text{Cl-index}_{inorg} \tag{3}$$

180

$$\text{ClNa-ratio} = \frac{\text{Cl-index}_{inorg}}{\text{Na-index}_{inorg}} \tag{4}$$

$$\text{AlFeTi-index} = \text{Al-index}_{inorg} + \text{Fe-index}_{inorg} + \text{Ti-index}_{inorg} \tag{5}$$

In total, four main parameters (C-index, NaCl-index, ClNa-ratio, AlFeTi-index) were used to classify each single particle into seven main groups: Sea-spray aerosol (SSA), carbonaceous sea-spray aerosol (C-SSA), mineral dust (MD), carbonaceous mineral dust (C-MD), particles with mixed properties (mix), carbonaceous particles with mixed properties (C-mix) and carbon dominated particles (C-rich). The classification process is illustrated in a decision tree in Figure 3 with the defining parameters for each class summarized in Table 4.

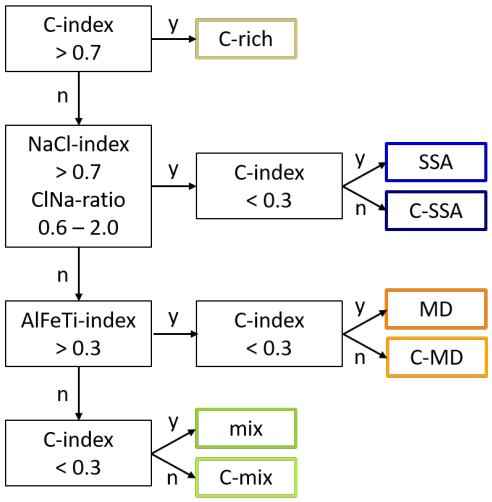

Figure 3. Decision tree for particle classification based on elemental parameters in Table 4. Particles were classified into seven groups: sea-spray aerosol (SSA), carbonaceous sea-spray aerosol (C-SSA), mineral dust (MD), carbonaceous mineral dust (C-MD), particles with mixed properties (mix), carbonaceous particles with mixed properties (C-mix) and carbon dominated particles (C-rich). Positive decisions are marked with 'y' if the corresponding conditions of elemental composition are met. Negative decisions are marked with 'n' accordingly.

Table 4. Parameters and thresholds for particle classification based on defined element indices derived from atomic concentrations. Compare illustration in Figure 3.

Class	Description	C-index	NaCl-index	ClNa-ratio	AlFeTi-index
SSA	Sea-spray aerosol	0 - 0.3	0.7 - 1	0.6 - 2.0	0 - 0.3
C-SSA	Carbon with sea-spray	0.3 - 0.7	0.7 - 1	0.6 - 2.0	0 - 0.3
MD	Mineral dust	0 - 0.3	0 - 0.7	0 - ínf	0.3 - 1
C-MD	Carbon with mineral dust	0.3 - 0.7	0 - 0.7	0 - ínf	0.3 - 1
mix	Mixed properties	0 - 0.3	0.3 - 0.7	0 - ínf	0 - 0.3
C-mix	Carbon with mixed properties	0.3 - 0.7	0 - 0.3	0 - ínf	0 - 0.3
C-rich	Rich in Carbon	0.7 - 1	0 - 1	0 - ínf	0 -1

3 Results and Discussion

3.1 Typical wet season conditions and sampling

The aerosol states probed here represent typical wet season conditions in the Amazon. This is illustrated in Figure 4, which shows selected aerosol and trace gas time series from February to May 2014 at ATTO. Figure 4 has been adapted from Bridges et al. (1966), where detailed information on the wet season aerosol characterization can be found. The following aspects are worth mentioning: The Amazonian wet season – and therefore also the sampling period – are characterized by frequent rainfall. The rain showers largely affect the aerosol population through wet deposition, as shown through the co-variability of aerosol abundance and rain in Figure 4a and c. Generally, the wet season 2014 was slightly dryer than the long-term average conditions, as indicated by a moderately negative anomaly in the rainfall around ATTO for that time (refer to Pöhlker et al., 2019). Still, the conditions in Figure 4 can be regarded as typical for central Amazonian wet season conditions. Backward trajectories (BTs) typically arrive from northeastern and east-northeastern directions. The corresponding northeastern footprint region of ATTO is defined by widely untouched rain forest regions (Pöhlker et al., 2019). Moran-Zuloaga et al. (2018) further showed that the northeasternmost BTs are particularly prone to transport African LRT aerosol (i.e., African dust, smoke and sea spray) into the central Amazon. Figure 4 emphasizes the alternating pattern of relatively clean conditions (white background shading) vs LRT conditions (gray background shading).

Episodes that can be considered pristine according to Pöhlker et al. (2018) (cyan background shading), are relatively rare. Holanda et al. (2023) reported that only about 7 % of the time per year at ATTO can be considered as pristine periods. These episodes are mostly concentrated in the wet season months April and May (for details, see Pöhlker et al., 2018). Under wet season conditions in the absence of LRT influence, mean coarse mode concentrations $M_{1\text{-}10}$ are around 3 to $4\,\mu g\,m^{-3}$ and the corresponding mean BC mass concentrations (M_{BCe}) around $0.02\,\mu g\,m^{-3}$ (Moran-Zuloaga et al., 2018). LRT aerosol influx is associated with a clearly increased coarse mode due to transported African dust and Atlantic sea salt (Scheuvens and Kandler, 2014; Moran-Zuloaga et al., 2018; Wang et al., 2023) as well as a correlated increase in the accumulation mode due to co-transported African smoke (Holanda et al., 2023). The LRT smoke fraction also results in increased mean M_{BCe}) around $0.2\,\mu g\,m^{-3}$. The mean $M_{1\text{-}10}$ under LRT influence is around 10 to $15\,\mu g\,m^{-3}$ Moran-Zuloaga et al. (2018).
From a larger pool of samples collected, the six selected and comprehensively analyzed samples can be subdivided into three groups of atmospheric conditions:

1. The samples 2014-12 and 2014-23 were collected during comparatively strong LRT-influenced conditions. During sampling, the coarse mode and BC mass concentrations were significantly enhanced (Figure 5). Sample 12 was characterized by a mean $M_{1\text{-}10}$ of about $10\,\mu g\,m^{-3}$ and a mean M_{BCe} of about $0.9\,\mu g\,m^{-3}$. Sample 23 was characterized by a mean $M_{1\text{-}10}$ of about $30\,\mu g\,m^{-3}$ and a mean M_{BCe} of about $0.8\,\mu g\,m^{-3}$. The samples comprise a mixture of African dust and smoke, aged sea spray, and the prevailing rain forest background aerosol. The results from samples 12 and 23 were pooled for the subsequent analysis and jointly represent the LRT influence on the elemental composition of the central Amazonian aerosol.

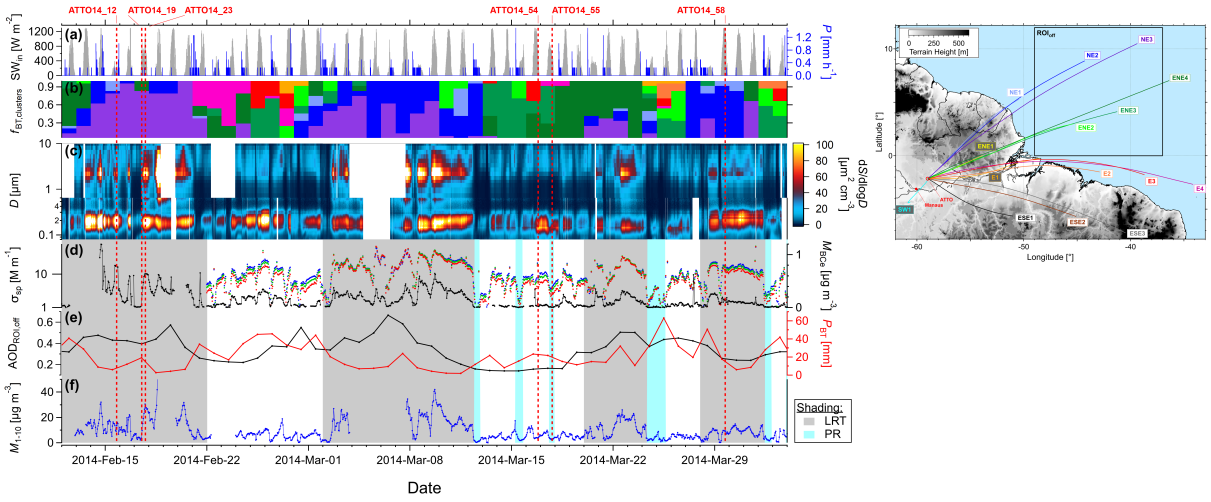

Figure 4. Overview of meteorological and aerosol conditions in the wet season 2014 when aerosol samples were collected. Sampling periods are shown as vertical, dashed red lines. Figure has been adapted from Moran-Zuloaga et al. (2018), where further information on atmospheric conditions and experimental details can be found. **(a)** Meteorological parameters at ATTO: Incoming shortwave radiation, SW_{in}, as marker for day vs night, and precipitation rate, P. **(b)** Frequency of occurrence, f_{BT}, of 15 backward trajectory clusters, showing variability in air mass advection. Colors and BT clusters are specified in the map insert. For details, refer to Pöhlker et al. (2019). **(c)** Image plot of aerosol particle surface size distributions spanning from 80 nm to 10 µm. **(d, left axis)** Time series of the aerosol scattering coefficients, ρ_{sp}, at three different wavelengths. **(d, right axis)** Pollution marker equivalent black carbon mass concentration, M_{BCe}, calculated assuming a mass absorption cross section MAC of $6.6\,m^2\,g^{-1}$. For details on ρ_{sp} and M_{BCe}, refer to Saturno et al. (2018b). **(e, left axis)** Satellite-retrieved aerosol optical depth at 550 nm, area-averaged over offshore and upwind region of interest (ROI_{off}) as shown in the map insert. $AOD_{ROI,off}$ is a marker for the arrival of Saharan dust at the northeast Brazilian coast and the time series represent the average of the MODIS data sets from the satellites Aqua and Terra. **(e, right axis)** HYSPLIT-retrieved accumulated precipitation, P_{BT}, along the trajectory tracks as a measure for precipitation and aerosol scavenging during air mass transport. For details, see AnderssonEngels et al. (1997). **(f)** Aerosol mass concentrations in the coarse mode 1-10 μm ($M_{1\text{-}10}$). Grey vertical bands mark episodes when Saharan long-range transport aerosol was measured at ATTO according to Moran-Zuloaga et al. (2018). Light blue vertical bands mark pristine episodes with M_{BCe} below detection limits according to Pöhlker et al. (2018).

2. The samples 2014-54 and 2014-55 were collected under the cleanest conditions of the sampling period with M_{BCe} below $0.01\,\mu g\,m^{-3}$ and $M_{1\text{-}10}$ around 3 to $4\,\mu g\,m^{-3}$, which corresponds to typical wet season background conditions (Moran-Zuloaga et al., 2018). Accordingly, both samples were primarily influenced by local biogenic sources in the absence of LRT influence. The results from samples 54 and 55 were pooled for the subsequent analysis and jointly represent the elemental composition during pristine conditions of the central Amazonian aerosol.

3. For the samples 2014-19 and 2014-58, conditions were weakly to moderately influenced by LRT and therefore represent an intermediate state between the pristine and strongly LRT-influences states. Sample 19 was collected during a major LRT episode, after a strong rainfall (see peaks in P and P_{BT} in Figure 4) and just before $M_{1\text{-}10}$ and M_{BCe} increased again in the course of further LRT aerosol entrainment (see Figure 4). It therefore represents the remaining fraction of a previous LRT plume after strong scavenging together with the biogenic background aerosol, which can be considered as a typical case in the Amazon. Sample 58 was collected during a moderately pronounced event of LRT aerosol influx. M_{BCe} reached around 0.2 μg m^{-3} and $M_{1\text{-}10}$ around 9.2 μg m^{-3} (Figure 5a and b).

Using M_{BCe} and $M_{1\text{-}10}$, the samples were ordered along the gradient from strong LRT influence to pristine conditions as shown in Figure 5a and b.

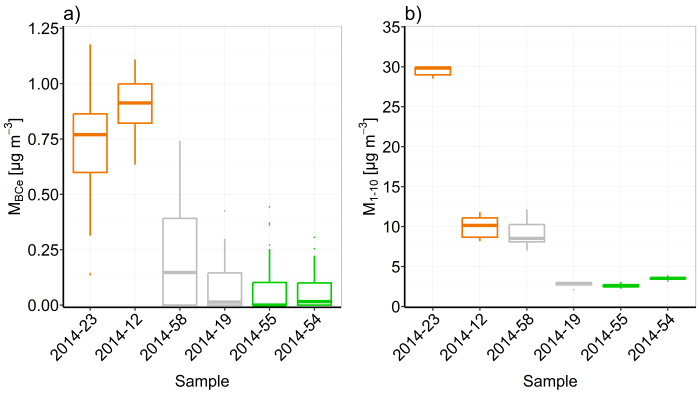

Figure 5. Atmospheric conditions during sampling, characterized here by the equivalent black carbon (BCe) mass concentration (M_{BCe}) in **(a)**, serving as a pollution marker, as well as the coarse mode mass concentration ($M_{1\text{-}10}$) in **(b)**, tracing the aerosol mass increase during LRT influx. Box-whisker plots characterize conditions for each sample along the gradient from strong LRT influence to pristine conditions. M_{BCe} and $M_{1\text{-}10}$ statistics are calculated for the sampling time intervals, starting 25 min before and ending 5 min after sampling. Medians are shown as horizontal lines. Boxes represent the first and third quartiles. Whiskers extend to the largest and smallest values within the 1.5 times interquartile range (IQR). Outlying points are displayed individually.

3.2 Elemental composition and particle classification

With SEM-EDX analysis, data on the size and elemental composition of ~3700 individual particles from the six selected samples was obtained. The analysis covered the particle size range between ~0.3 µm and ~10 µm. Figure 2 shows that the best particle statistics was achieved between ~0.5 µm and ~2.5 µm. Towards larger diameters (i.e., >4 µm) the number of analyzed particles decreased due to the decreasing abundance of atmospheric particles and it also decreased towards smaller diameters due to a decreasing efficiency of the impactor sampling. The size-resolved elemental composition obtained from this analyzed particle ensemble is discussed below. Figure 6 shows the size dependence of the carbon-index distribution calculated

with Equation 1 and reflecting the ratio of C relative to all inorganic elements (E_i) together with C. The higher the C-index, the higher the C fraction. In the samples with weak to moderate LRT influence (i.e., 2014-58 and 2014-19) as well as in the clean samples (i.e., 2014-54 and 2014-55), a majority of more than 60 % of the particles showed C-index values above 0.6. In the LRT samples (i.e., 2014-12 and 2014-23), in contrast, the majority of particles showed a C-index below 0.6. This underlines the clean and expected decrease in C-dominated particles upon LRT influx of mineral dust and sea spray aerosol.

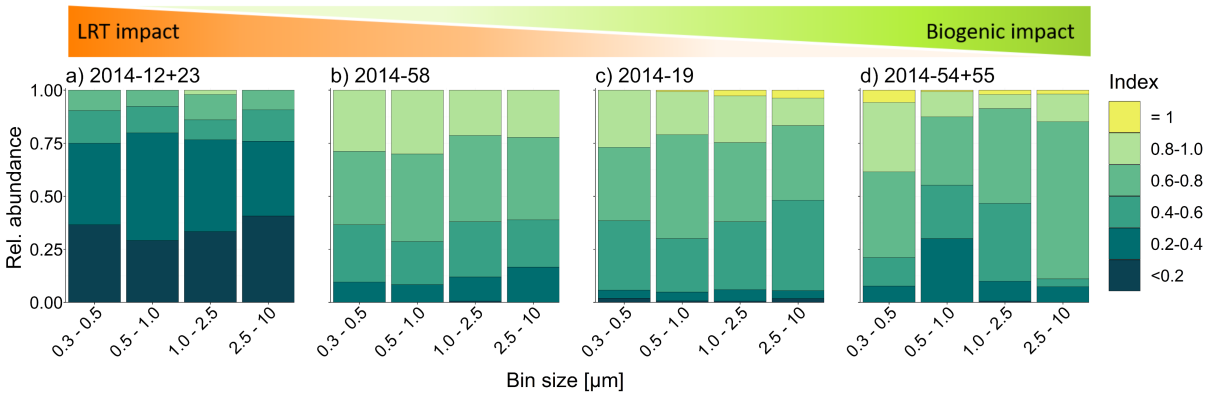

Figure 6. Size dependence of carbon-index distribution for contrasting aerosol conditions, ranging from **(a)** strong LRT influence, **(b & c)** over medium to weak LRT influences, to **(d)** pristine conditions. C-index reflects the content of carbon in the particles, relative to all detected inorganic elements, except oxygen which has been excluded here (Equation 1). A high C-index indicates high C fractions, with C-index = 1 corresponding to pure carbon (oxygen not considered).

It further emphasizes the observation that only a few particles – between 2 and 4 % even in the clean samples – have a C-index approaching 1, which indicates in agreement with previous studies (Artaxo et al., 1990; Echalar et al., 1998) that the Amazonian aerosol is characterized by persistent and significant fractions of inorganic elements, originating from both, LRT influx as well as biogenic sources. Along these lines, Figures 7 and 8 show the size dependence of element-index distribution for the elements Na, Mg, Al, S and Cl as well as K, Ca, Fe and Cu. The element-indices were obtained through Equation 2 and show diverse patterns of element abundance in different size ranges.

Based on the elemental composition, a particle classification procedure related to specific atmospheric conditions was developed, as outlined in Section 2.5 (refer to Figure 3 and Table 4). Four particle classes related to LRT influence were determined, including sea-spray aerosol (SSA), carbonaceous sea-spray aerosol (C-SSA), mineral dust (MD) and carbonaceous mineral dust (C-MD). Three classes for particles of initially undefined origin were determined, including carbon-rich (C-rich), mixed properties (mix) and carbonaceous with mixed properties (C-mix). Figure 10 shows the size dependence of the abundance of all classes.

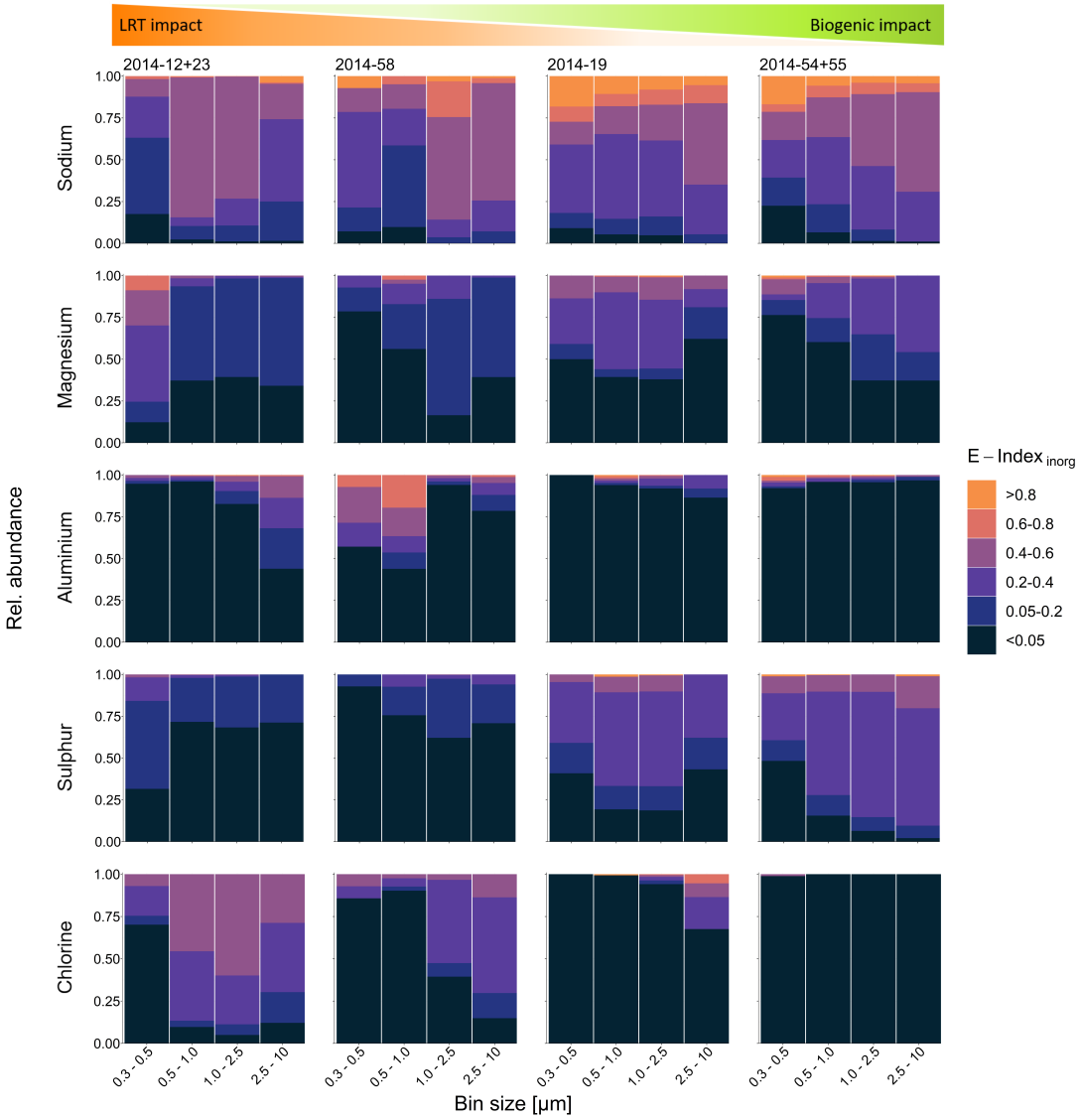

Figure 7. Size dependence of element-index distributions for sodium, magnesium, aluminium, sulphur and chlorine under contrasting aerosol conditions, ranging from strong LRT influence, over medium to weak LRT influences, to pristine conditions. The element-index reflects the content of the respective element with carbon and oxygen being excluded (Equation 2). A high element-index indicates a high fraction of the particular element, relative to all elements except C and O.

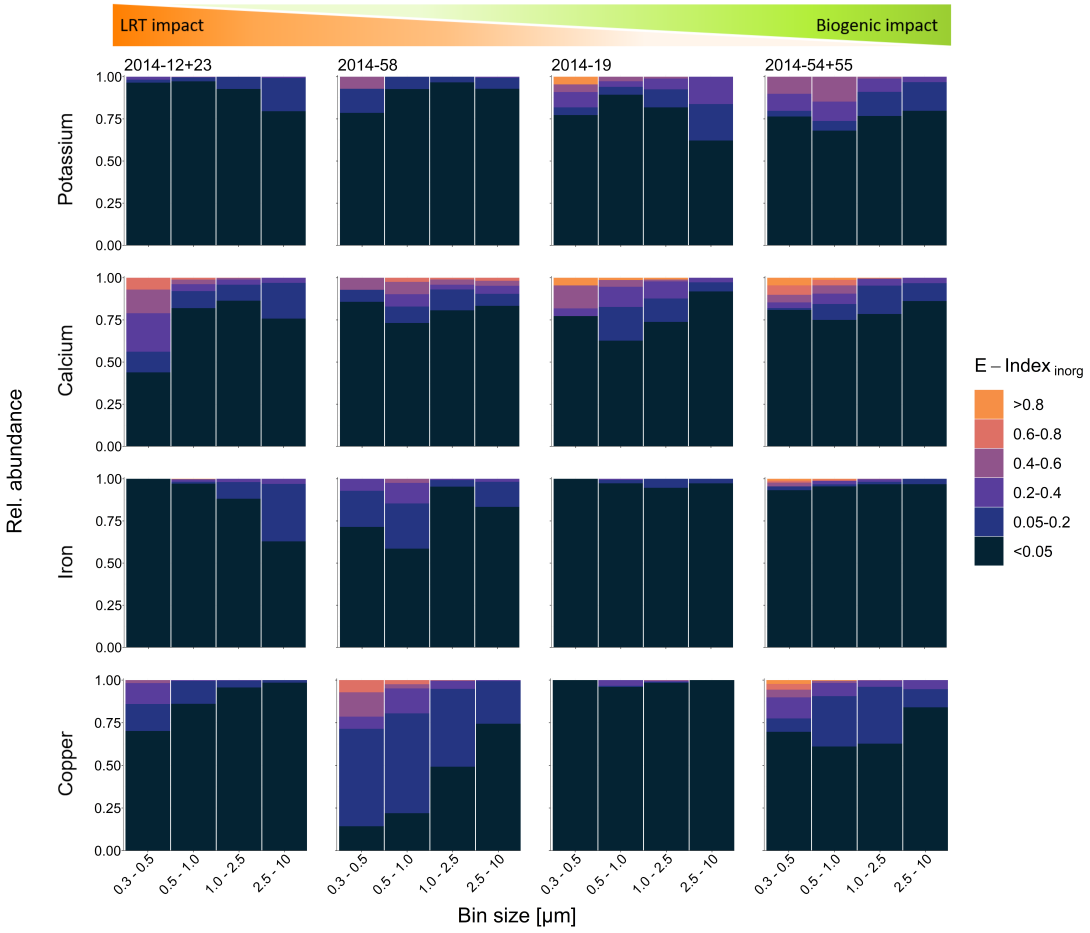

Figure 8. Size dependence of element-index distributions for potassium, calcium, iron and copper under contrasting aerosol conditions, ranging from strong LRT influence, over medium to weak LRT influences, to pristine conditions. The element-index reflects the content of the respective element with carbon and oxygen being excluded (Equation 2). A high element-index indicates a high fraction of the particular element, relative to all elements except C and O.

260 The common occurrence of Na and Cl in SSA and C-SSA was considered as primary indication for SSA and C-SSA (see classification procedure Figure 3 and Table 4), as Na^+ and Cl^- are the main ionic species in sea water and are well-known as main components of SSA produced by various mechanisms at the sea surface (e.g., bubble bursting, Lewis and Schwartz (2004); Salter et al. (2016)). The difference between C-SSA and SSA is the particles' carbon content, with C-SSA having a carbon content >30 % per particle. Besides that, both classes have similar inorganic composition characteristics (Figure S1). In

LRT-related samples, the presence of Cl is closely connected to the presence of Na. This is evident through a strong positive correlation between Cl and Na (Figure 9 a, b, e & f), but also visible in similar distributions of the Na and Cl indices in Figure 7. Since seawater contains other dissolved salts such as SO_4^{2-}, Mg^{2+}, Ca^{2+} and K^+, and atmospheric aging can occur, it is known that the chemical composition of SSA can differ significantly from the typical Cl/Na ratios of bulk seawater (e.g., an enrichment of Mg, S or Ca) (Su et al., 2022). Compared to Na and Cl, we only detected small amounts of other inorganic elements within particles classified as SSA or C-SSA (Figure S1). In addition, our correlation analysis did not yield further comparative strong trends linked to Na and Cl in SSA. However, within an SSA internal correlation analysis, the strongest correlations exist between S, Ca, and Mg themselves (also slightly visible in the overall correlation analysis in Figure 9 a, b, e & f), indicating minerals like glauberite ($Na_2Ca(SO_4)_2$) or bloedite ($Na_2Mg(SO)_2$), which are found to be associated with sea spray aerosol (Andreae et al., 1986).

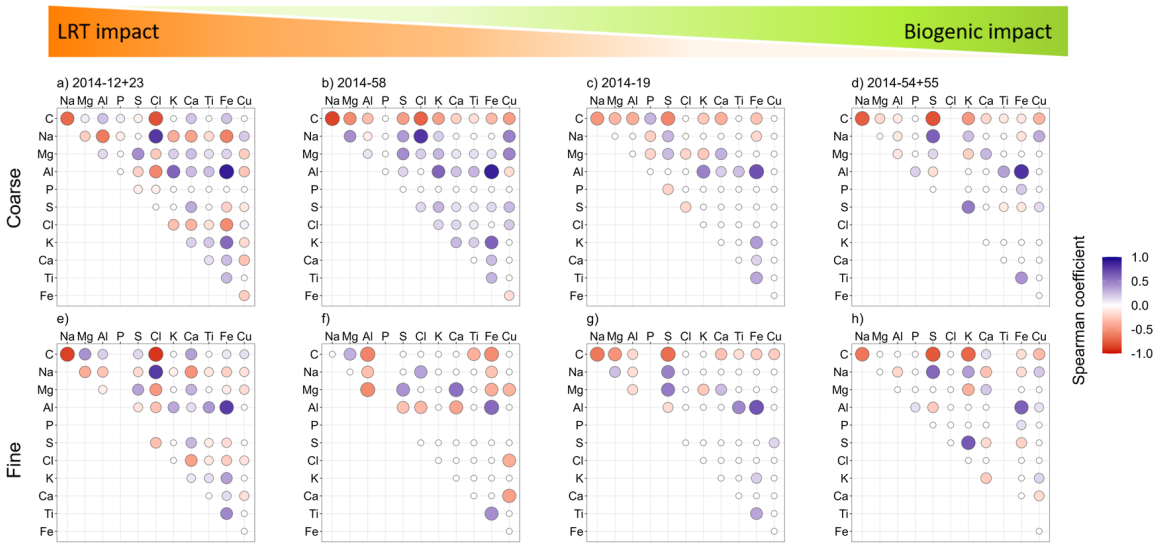

Figure 9. Spearman correlation analysis on elemental co-occurrence on a single particle scale within the aerosol coarse and fine mode ranges under contrasting aerosol conditions, ranging from (a & e) strong LRT influence, over (b & f) and (c & g) medium to weak LRT influences, to (d & h) pristine conditions. The strength and direction of the Spearman correlation coefficient (R) are visually represented by the color and the size of the circles, indicated in the colour scale. Circles in bluish color and large size indicate a strong correlation, while reddish color with a small circle suggests a weak correlation. Only correlations with R significantly different from zero (p-value <0.05) are shown, with non-significant correlations presented as white circles. Empty slots represent the absence of a particular element.

For MD and C-MD, the occurrence of Al, Fe and Ti is considered as primary indication (see classification procedure Figure 3 and Table 4), as Al, Fe and Ti are common elements in soil constituents like silicate minerals, including feldspar or clay

minerals, which can be associated with African mineral dust (Kandler et al., 2007; Formenti et al., 2001; Linke et al., 2006; Chiapello et al., 1997). The difference between C-MD and MD is the particles' carbon content, with C-MD having a carbon content >30 % per particle, while the inorganic composition is similar (Figure S1). Actually, Si would give a good indication for MD as well, as Si-oxides are expected to be major constituents in MD particles. However, Si was excluded from our analysis, due to the strong Si background from the SiN substrates. By focusing on Al, Fe and Ti as MD indicators, it is clear that the elements are highly related, as significant strong positive correlations between Al, Fe and Ti within all samples were found (Figure 9). In the LRT-influenced samples, particularly in the coarse mode, there is a noticeable correlation between Al and Fe with K, which is also a commonly found component in MD particles. Further elements like Ca or Mg are also known to be some major mineral dust constituents (Kandler et al., 2007; Adachi et al., 2020). However, for Ca and Mg, we found only weak correlations with Al, Fe and Ti. In addition, the analysis showed that MD-classified particles are mostly mixed with small amounts of sea spray-like components (NaCl). Hence, at this point the source of K, Ca, and Mg cannot be clearly determined. Most likely, the particle composition is affected by both sea spray and mineral dust, as SSA and MD particles can mix during their transport over the Atlantic ocean. In addition, MD internal correlation analysis indicates that the presence of S is linked to Na and Cl, which suggests a contribution from SSA. In all cases, a contribution of anthropogenic sources in Africa as well as biogenic sources from the Amazon rain forest has to be taken into account.

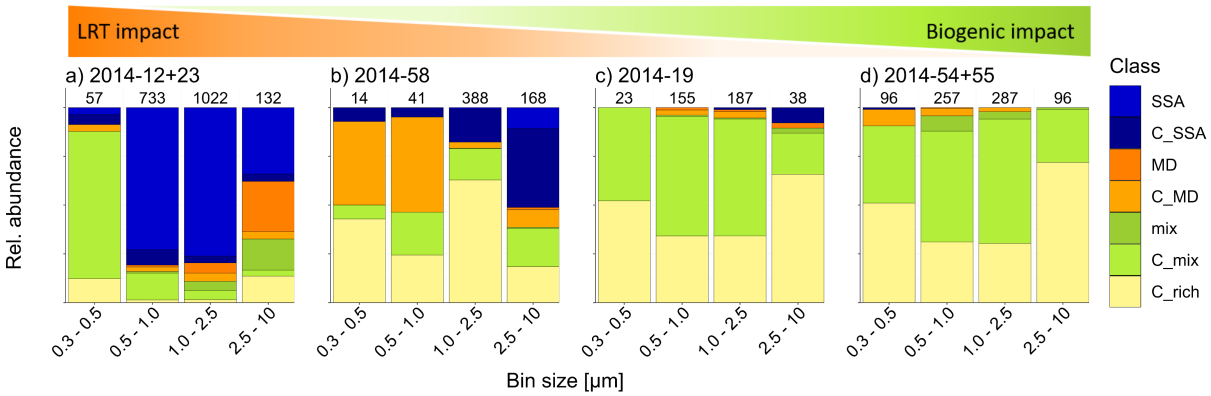

Figure 10. Size dependence of the abundance of particle classes under contrasting aerosol conditions, ranging from **(a)** strong LRT influence, over **(b,c)** medium to weak LRT influences, **(d)** to pristine conditions. The particles have been classified into seven different classes, as follows: Sea-spray aerosol (SSA), carbonaceous sea-spray aerosol (C-SSA), mineral dust (MD), carbonaceous mineral dust (C-MD), particles with mixed properties (mix), carbonaceous particles with mixed properties (C-mix) and carbon dominated particles (C-rich). For details, refer to Figure 3.

C-rich particles are categorized based on their high carbon content (>70 % per particle, Figure 3). The particles with mixed properties (mix and C-mix) do not match the criteria for any other particle class. C-mix particles are differentiated from mixed

particles only based on their higher carbon content (C > 30% per particle, Figure 3 and Table 4), whereas mix particles are primarily composed of pure inorganic salts with only a small fraction of carbon (C < 30% per particle). A comparison of the inorganic composition of the three classes from clean with LRT samples shows a noticeable difference (Figure S1). The inorganic composition of LRT-affected samples suggests a combination of SSA and MD-like particles originating from a variety of typical LRT sources (refer to Section 3.1). C-rich and C-mix particles found on the clean samples are dominated by Na, S and Mg. Here the presence of Na is not linked to Cl. It should be noted that this analysis refers explicitly to the inorganic composition, which makes up only a small fraction in the case of the C-rich and C-mix particles. In the case of the almost pure salty mix particles, the amount of K is significantly increased. Due to the sampling location and condition a biological origin from the forest explicitly can be assumed.

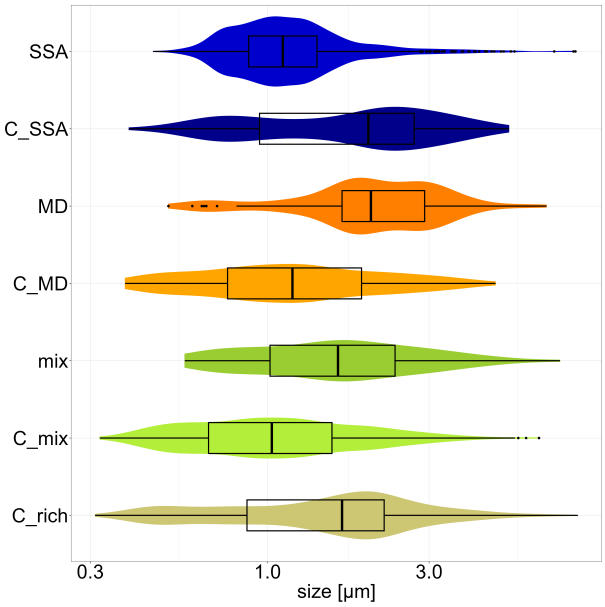

Figure 11. Particle class characterization by size using a combination of box-whisker and violin plots to visualize the size distribution of each particle class. Medians are shown as horizontal lines. The boxes represent the first and third quartiles, the whiskers extend to the largest and smallest values within the 1.5 times interquartile range (IQR). The violin plots represent the shape of the element-specific particle size distributions. Color coding is identical to Figures 3 and 10.

The distributions of the different particle classes in Figure 10 clearly display the gradient of decreasing LRT impact. The LRT samples are dominated by SSA (70%), particularly within the size range >0.5 µm (Figure 11), and compared to other samples a high fraction of MD is found in the coarse mode (5 %). Sample 2014-58 is also dominated by LRT aerosol particles, but with a low presence of SSA and MD (3.5 %, 0.3 %), but a higher presence of C-SSA and C-MD (22.5 %, 0.7 %). C-SSA

is more dominant in the coarse mode, while C-MD is also found in the fine mode range (Figure 11). The observed particle class distribution pattern for sample 2014-19, as well as of the clean samples, is significantly different from the LRT-influenced samples (Figure 10). Here almost no particles were classified as SSA, C-SSA, MD and C-MD. Only a small fraction of C-SSA, MD and C-MD can be found on sample 2014-19 in a size range >0.5 µm.

The presence of C-rich particles clearly varies between the samples. The class contributes only 2.5 % to the LRT, 47 % to sample 2014-58, and about 38 % to sample 2014-19 and the clean ones (Figure 10). The C-mix particles contribute only 10 % to the LRT samples, mostly in the fine mode, and 17 % to sample 2014-58. In sample 19 and the clean samples, the C-mix class represents over half of the total particles, 56 % and 53 % respectively. In this case, the class covers the entire size range, but is most prevalent in the range from 0.5 µm to 2.5 µm (Figure 11).

The mixture class constitutes only a minor portion of the total composition across all samples (3.8 % LRT samples, 0.3 % sample 2014-58, 0.7 % sample 2014-19. 4.3 % clean samples). An accumulation of mix particles is only observed within the coarse mode in the LRT samples, as well as within the 0.5 µm to 2.5 µm range in the clean samples.

4 Conclusion

The broad setup of ATTO online instrumentation for aerosol measurements, combined with remote sensing techniques and modelling, provides a comprehensive description of prevailing aerosol conditions at the ATTO site. This data allows to differentiate the Amazonian wet season conditions into categories, such as LRT, transmission and clean episodes, and allows for the identification of potential aerosol sources or exclusion of others. During LRT episodes, an increase in the presence of African mineral dust, as well as biomass burning smoke from Africa and sea spray aerosol from the Atlantic Ocean is observed. LRT episodes are characterized by high values of AOD_{ROI} and low values of P_{BT} as well as increased levels of M_{BCe} and $M_{1\text{-}10}$. In contrast, the main aerosol source during clean episodes is expected to be local biogenic emissions, with little to no contribution from other sources. Clean episodes exhibit lower AOD_{ROI} values and higher P_{BT}, with relatively low levels of M_{BCe} and $M_{1\text{-}10}$. Initially, the collected aerosol samples were categorized into particular environmental conditions based on the corresponding online data and the characteristics of LRT or clean episodes described previously. Samples were sorted along a gradient of decreasing LRT impact.

Complementary, the chemical composition of the particles measured by SEM-EDX confirms the expected aerosol sources as indicated by the online data. The analysis confirmed SSA and MD as LRT indicators. In accordance with our classification procedure, in particular the presence of Na and Cl with a ratio close to that of sea water is indicative for SSA, while the presence of Al, Fe and Ti suggests the presence of MD. The LRT-affected samples are dominated by particles classified as SSA, C-SSA, MD or C-MD. As expected, the impact decreases along the LRT gradient, and the clean samples show no or very few SSA or MD-related particles. Carbon-rich particles, carbonaceous salts, and almost pure salts dominate the clean samples. The exact

source of these particles cannot be determined here, but local biological sources are likely responsible. It is noticeable that almost no pure carbon particles are present. This suggests that biogenic salts could widely act as seeds for carbonaceous SOA condensation. First findings in this study indicate that K and Na may serve as indicators for natural biogenic inorganic and/or organic salts.

In conclusion, this study shows that the combination of complementary online and offline data is a powerful strategy to characterize prevailing aerosol populations in terms of their origin. In this study the alternating episodes of pristine and long-range transport conditions were characterized by their prevailing aerosol sources. With a focus on the inorganic fraction, this approach facilitates the identification of elemental signatures and marker elements associated with LRT or pristine conditions. Thereby, the almost ubiquitous presence of inorganic salts within the clean samples emphasizes a significant contribution of biogenic emissions. However, many questions remain unanswered, especially regarding their release mechanisms and atmospheric relevance. Therefore, the natural forest emissions will be addressed in follow-up studies.

Data availability. The datasets presented here are available under https://doi.org/10.XXX/3.XX (). The ATTO data used in this study are available via the ATTO data portal through https://www.attoproject.org/. For data requests beyond the available data, please refer to the corresponding author.

Author contributions. According to Contributor Roles Taxonomy (CRediT, https://casrai.org/credit/):

Conceptualization: LAK, CP

Data curation: LAK, DW

Formal analysis: LAK, DMZ

Investigation: LAK, DMZ, JDF, CQDJ, FD, IHdA, JS

Software: LAK, KK

Supervision: UP, CP

Validation: PA, MOA

Visualization: LAK, CP

Writing – original draft: LAK, CP

Writing – review & editing: All authors

Competing interests. The authors declare that they have no conflict of interest.

Acknowledgements. This research has been funded by the Bundesministerium für Bildung und Forschung (BMBF contracts 01LB1001A, 01LK1602B, and 01LK2101B), the Brazilian Ministério da Ciência, Tecnologia e Inovação (MCTI/FINEP contract 01.11.01248.00), the Max Planck Society, the Conselho Nacional de Desenvolvimento Científico e Tecnológico (CNPq, Brazil) (process 200723/2015-4), and the Max Planck Graduate Center with the Johannes Gutenberg University Mainz (MPGC). For the operation of the ATTO site, we acknowledge the support by the Instituto Nacional de Pesquisas da Amazônia (INPA), the Amazon State University (UEA), the Large-Scale Biosphere-Atmosphere Experiment (LBA), FAPEAM, and the Reserva de Desenvolvimento Sustentável do Uatumã (SDS/CEUC/RDS-Uatumã). Particularly, we would like to thank the ATTO team members including Susan Trumbore, Alberto Quesada, Bruno Takeshi, Reiner Ditz, Stefan Wolff, Björn Nillius, Fernando Morais, Thomas Klimach, Roberta Pereira de Souza, Jürgen Kesselmeier, Andrew Crozier, Sam Jones, Delano Campos, Juarez Viegas, Sipko Bulthuis, Francisco Alcinei Gomes da Silva, Isabella Diogenes, Hermes Braga Xavier, Nagib Alberto de Castro Souza, Antonio Huxley Melo Nascimento, Valmir Ferreira de Lima, Feliciano de Souza Coelho, André Luiz Matos, Wallace Rabelo Costa, Amauri Rodriguês Perreira, Adir Vasconcelos Brandão, Davirley Gomes Silva, Thomas Disper, Torsten Helmer, Steffen Schmidt, Uwe Schulz, Uwe Schultz, Karl Kübler, Olaf Kolle, Martin Hertel, Kerstin Hippler, Steffen Schmidt and all further colleagues involved in the technical, logistical, and scientific support.

References

Adachi, K., Oshima, N., Gong, Z., de Sá, S., Bateman, A. P., Martin, S. T., de Brito, J. F., Artaxo, P., Cirino, G. G., Sedlacek III, A. J., and Buseck, P. R.: Mixing states of Amazon basin aerosol particles transported over long distances using transmission electron microscopy, Atmospheric Chemistry and Physics., 20, 11 923–11 939, https://doi.org/10.5194/acp-20-11923-2020, https://acp.copernicus.org/articles/20/11923/2020/, 2020.

Alves, E. G., Santana, R. A., Dias-Junior, C. Q., Botia, S., Taylor, T., Yanez-Serrano, A. M., Kesselmeier, J., Bourtsoukidis, E., Williams, J., de Assis, P. I. L. S., Martins, G., de Souza, R., Duvoisin Jr, S., Guenther, A., Gu, D., Tsokankunku, A., Soergel, M., Nelson, B., Pinto, D., Komiya, S., Rosa, D. M., Weber, B., Barbosa, C., Robin, M., Feeley, K. J., Duque, A., Lemos, V. L., Contreras, M. P., Idarraga, A., Lopez, N., Husby, C., Jestrow, B., and Toro, I. M. C.: Intra- and interannual changes in isoprene emission from central Amazonia, Atmospheric Chemistry and Physics, 23, 8149–8168, https://doi.org/10.5194/acp-23-8149-2023, 2023.

AnderssonEngels, S., afKlinteberg, C., Svanberg, K., and Svanberg, S.: In vivo fluorescence imaging for tissue diagnostics, Physics in Medicine and Biology, 42, 815–824, <GotoISI>://A1997WZ95300006, 1997.

Andreae, M. and Rosenfeld, D.: Aerosol–cloud–precipitation interactions. Part 1. The nature and sources of cloud-active aerosols, Earth-Science Reviews, 89, 13–41, https://doi.org/https://doi.org/10.1016/j.earscirev.2008.03.001, https://www.sciencedirect.com/science/article/pii/S0012825208000317, 2008.

Andreae, M. O.: Soot Carbon and Excess Fine Potassium: Long-Range Transport of Combustion-Derived Aerosols, Science, 220, 1148–1151, https://doi.org/10.1126/science.220.4602.1148, https://www.science.org/doi/10.1126/science.220.4602.1148, 1983.

Andreae, M. O. and Andreae, T. W.: The cycle of biogenic sulfur-compounds over the Amazon Basin .1. Dry season, Journal of Geophysical Research-Atmospheres, 93, 1487–1497, https://doi.org/10.1029/JD093iD02p01487, <GotoISI>://WOS:A1988M303000014, 1988.

Andreae, M. O., Charlson, R. J., Bruynseels, F., Storms, H., Van Grieken, R., and Maenhaut, W.: Internal Mixture of Sea Salt, Silicates, and Excess Sulfate in Marine Aerosols, Science, 232, 1620–1623, https://doi.org/10.1126/science.232.4758.1620, https://www.sciencemag.org/lookup/doi/10.1126/science.232.4758.1620, 1986.

Andreae, M. O., Berresheim, H., Bingemer, H., Jacob, D. J., Lewis, B. L., Li, S. M., and Talbot, R. W.: The atmospheric sulfur cycle over the Amazon Basin: 2. Wet season, Journal of Geophysical Research-Atmosphere, 95, 16 813–16 824, https://doi.org/10.1029/JD095iD10p16813, 1990.

Andreae, M. O., Rosenfeld, D., Artaxo, P., Costa, A. A., Frank, G. P., Longo, K. M., and Silva-Dias, M. A. F.: Smoking rain clouds over the Amazon, Science, 303, 1337–1342, https://doi.org/10.1126/science.1092779, <GotoISI>://WOS:000189238600042, 2004.

Andreae, M. O., Acevedo, O. C., Araùjo, A., Artaxo, P., Barbosa, C. G. G., Barbosa, H. M. J., Brito, J., Carbone, S., Chi, X., Cintra, B. B. L., da Silva, N. F., Dias, N. L., Dias-Júnior, C. Q., Ditas, F., Ditz, R., Godoi, A. F. L., Godoi, R. H. M., Heimann, M., Hoffmann, T., Kesselmeier, J., Könemann, T., Krüger, M. L., Lavric, J. V., Manzi, A. O., Lopes, A. P., Martins, D. L., Mikhailov, E. F., Moran-Zuloaga, D., Nelson, B. W., Nölscher, A. C., Santos Nogueira, D., Piedade, M. T. F., Pöhlker, C., Pöschl, U., Quesada, C. A., Rizzo, L. V., Ro, C.-U., Ruckteschler, N., Sá, L. D. A., de Oliveira Sá, M., Sales, C. B., dos Santos, R. M. N., Saturno, J., Schöngart, J., Sörgel, M., de Souza, C. M., de Souza, R. A. F., Su, H., Targhetta, N., Tóta, J., Trebs, I., Trumbore, S., van Eijck, A., Walter, D., Wang, Z., Weber, B., Williams, J., Winderlich, J., Wittmann, F., Wolff, S., and Yáñez-Serrano, A. M.: The Amazon Tall Tower Observatory (ATTO): overview of pilot measurements on ecosystem ecology, meteorology, trace gases, and aerosols, Atmospheric Chemistry and Physics, 15, 10 723–10 776, https://doi.org/10.5194/acp-15-10723-2015, https://acp.copernicus.org/articles/15/10723/2015/, 2015.

Andreae, M. O., Afchine, A., Albrecht, R., Holanda, B. A., Artaxo, P., Barbosa, H. M. J., Borrmann, S., Cecchini, M. A., Costa, A., Dollner, M., Fütterer, D., Järvinen, E., Jurkat, T., Klimach, T., Konemann, T., Knote, C., Krämer, M., Krisna, T., Machado, L. A. T., Mertes, S., Minikin, A., Pöhlker, C., Pöhlker, M. L., Pöschl, U., Rosenfeld, D., Sauer, D., Schlager, H., Schnaiter, M., Schneider, J., Schulz, C., Spanu, A., Sperling, V. B., Voigt, C., Walser, A., Wang, J., Weinzierl, B., Wendisch, M., and Ziereis, H.: Aerosol characteristics and particle production in the upper troposphere over the Amazon Basin, Atmospheric Chemistry and Physics,, 18, 921–961, https://doi.org/10.5194/acp-18-921-2018, https://www.atmos-chem-phys.net/18/921/2018/, 2018.

Ansmann, A., Baars, H., Tesche, M., Muller, D., Althausen, D., Engelmann, R., Pauliquevis, T., and Artaxo, P.: Dust and smoke transport from Africa to South America: Lidar profiling over Cape Verde and the Amazon rainforest, Geophysical Research Letters, 36, https://doi.org/10.1029/2009gl037923, <GotoISI>://WOS:000266741500001, 2009.

Arana, A., Loureiro, A. L., Barbosa, H. M. J., Van Grieken, R., and Artaxo, P.: Optimized energy dispersive X-ray fluorescence analysis of atmospheric aerosols collected at pristine and perturbed Amazon Basin sites: Optimized EDXRF analysis of atmospheric aerosols in the Amazon Basin, 43, 228–237, https://doi.org/10.1002/xrs.2544, https://onlinelibrary.wiley.com/doi/10.1002/xrs.2544, 2014.

Artaxo, P. and Hansson, H. C.: Size Distribution of Biogenic Aerosol Particles from the Amazon Basin, Atmospheric Environment, 29, 393–402, <GotoISI>://A1995QK40600010, 1995.

Artaxo, P., Maenhaut, W., Storms, H., and Vangrieken, R.: Aerosol characteristics and sources for the Amazon Basin during wet season, Journal of Geophysical Research-Atmospheres, 95, 16 971–16 985, https://doi.org/10.1029/JD095iD10p16971, <GotoISI>://WOS:A1990EB20200051, 1990.

Artaxo, P., V. Rizzo, L., F. Brito, J., J. Barbosa, H. M., Arana, A., T. Sena, E., G. Cirino, G., Bastos, W., T. Martin, S., and O. Andreae, M.: Atmospheric Aerosols in Amazonia and Land Use Change: From Natural Biogenic to Biomass Burning Conditions, Faraday Discussions, 165, 203–235, https://doi.org/10.1039/C3FD00052D, 2013.

Artaxo, P., Hansson, H.-C., Andreae, M. O., Bäck, J., Alves, E. G., Barbosa, H. M. J., Bender, F., Bourtsoukidis, E., Carbone, S., Chi, J., Decesari, S., Després, V. R., Ditas, F., Ezhova, E., Fuzzi, S., Hasselquist, N. J., Heintzenberg, J., Holanda, B. A., Guenther, A., Hakola, H., Heikkinen, L., Kerminen, V.-M., Kontkanen, J., Krejci, R., Kulmala, M., Lavric, J. V., de Leeuw, G., Lehtipalo, K., Machado, L. A. T., McFiggans, G., Franco, M. A. M., Meller, B. B., Morais, F. G., Mohr, C., Morgan, W., Nilsson, M. B., Peichl, M., Petäjä, T., Praß, M., Pöhlker, C., Pöhlker, M. L., Pöschl, U., Randow, C. V., Riipinen, I., Rinne, J., Rizzo, L. V., Rosenfeld, D., Dias, M. A. F. S., Sogacheva, L., Stier, P., Swietlicki, E., Sörgel, M., Tunved, P., Virkkula, A., Wang, J., Weber, B., Yáñez-Serrano, A. M., Zieger, P., Mikhailov, E., Smith, J. N., and Kesselmeier, J.: Tropical and Boreal Forest – Atmosphere Interactions: A Review, 74, 24–163, https://doi.org/10.16993/tellusb.34, 2022.

Baars, H., Ansmann, A., Althausen, D., Engelmann, R., Artaxo, P., Pauliquevis, T., and Souza, R.: Further evidence for significant smoke transport from Africa to Amazonia, Geophysical Research Letters, 38, L20 802, https://doi.org/L20802 10.1029/2011gl049200, <GotoISI>://WOS:000296157100002, 2011.

Barkley, A. E., Prospero, J. M., Mahowald, N., Hamilton, D. S., Popendorf, K. J., Oehlert, A. M., Pourmand, A., Gatineau, A., Panechou-Pulcherie, K., Blackwelder, P., and Gaston, C. J.: African biomass burning is a substantial source of phosphorus deposition to the Amazon, Tropical Atlantic Ocean, and Southern Ocean, Proceedings of the National Academy of Sciences, 116, 16 216–16 221, https://doi.org/10.1073/pnas.1906091116, https://www.pnas.org/doi/full/10.1073/pnas.1906091116, publisher: Proceedings of the National Academy of Sciences, 2019.

Ben-Ami, Y., Koren, I., and Altaratz, O.: Patterns of North African dust transport over the Atlantic: winter vs. summer, based on CALIPSO first year data, Atmospheric Chemistry and Physics, 9, 7867–7875, https://doi.org/10.5194/acp-9-7867-2009, https://www.atmos-chem-phys.net/9/7867/2009/, 2009.

Ben-Ami, Y., Koren, I., Rudich, Y., Artaxo, P., Martin, S. T., and Andreae, M. O.: Transport of North African dust from the Bodélé depression to the Amazon Basin: a case study, Atmospheric Chemistry and Physics, 10, 7533–7544, https://doi.org/10.5194/acp-10-7533-2010, <GotoISI>://WOS:000281432800001, 2010.

Bertram, T. H., Cochran, R. E., Grassian, V. H., and Stone, E. A.: Sea spray aerosol chemical composition: elemental and molecular mimics for laboratory studies of heterogeneous and multiphase reactions, Chemical Society Reviews, 47, 2374–2400, https://doi.org/10.1039/c7cs00008a, 2018.

Bridges, J. W., Davies, D. S., and Williams, R. T.: Fluorescence studies on some hydropyridines including compounds of vitamin B6 group, Biochemical Journal, 98, 451–468, <GotoISI>://A19667287000014, 1966.

Bristow, C. S., Hudson-Edwards, K. A., and Chappell, A.: Fertilizing the Amazon and equatorial Atlantic with West African dust, Geophysical Research Letters, 37, https://doi.org/10.1029/2010GL043486, https://onlinelibrary.wiley.com/doi/abs/10.1029/2010GL043486, _eprint: https://onlinelibrary.wiley.com/doi/pdf/10.1029/2010GL043486, 2010.

Chen, H., Grassian, V. H., Saraf, L. V., and Laskin, A.: Chemical imaging analysis of environmental particles using the focused ion beam/scanning electron microscopy technique: microanalysis insights into atmospheric chemistry of fly ash, Analyst, 138, 451–460, https://doi.org/10.1039/c2an36318f, 2013.

Chen, Q., Farmer, D. K., Rizzo, L. V., Pauliquevis, T., Kuwata, M., Karl, T. G., Guenther, A., Allan, J. D., Coe, H., Andreae, M. O., Poschl, U., Jimenez, J. L., Artaxo, P., and Martin, S. T.: Submicron particle mass concentrations and sources in the Amazonian wet season (AMAZE-08), Atmospheric Chemistry and Physics, 15, 3687–3701, https://doi.org/10.5194/acp-15-3687-2015, <GotoISI>://WOS:000352957400004, 2015.

Chiapello, I., Bergametti, G., Chatenet, B., Bousquet, P., Dulac, F., and Soares, E. S.: Origins of African dust transported over the northeastern tropical Atlantic, Journal of Geophysical Research: Atmospheres, 102, 13 701–13 709, https://doi.org/10.1029/97JD00259, http://doi.wiley.com/10.1029/97JD00259, 1997.

China, S., Burrows, S. M., Wang, B., Harder, T. H., Weis, J., Tanarhte, M., Rizzo, L. V., Brito, J., Cirino, G. G., Ma, P.-L., Cliff, J., Artaxo, P., Gilles, M. K., and Laskin, A.: Fungal spores as a source of sodium salt particles in the Amazon basin, Nature Communications, 9, 4793, https://doi.org/10.1038/s41467-018-07066-4, https://doi.org/10.1038/s41467-018-07066-4, 2018.

Chor, T. L., Dias, N. L., Araujo, A., Wolff, S., Zahn, E., Manzi, A., Trebs, I., Sa, M. O., Teixeira, P. R., and Sorgel, M.: Flux-variance and flux-gradient relationships in the roughness sublayer over the Amazon forest, Agricultural and Forest Meteorology, 239, 213–222, https://doi.org/10.1016/j.agrformet.2017.03.009, <GotoISI>://WOS:000401884800020, 2017.

Cliff, G. and Lorimer, G. W.: The quantitative analysis of thin specimens, Journal of Microscopy, https://doi.org/10.1111/j.1365-2818.1975.tb03895.x, https://onlinelibrary.wiley.com/doi/abs/10.1111/j.1365-2818.1975.tb03895.x, 1975.

Davidson, E. A., de Araujo, A. C., Artaxo, P., Balch, J. K., Brown, I. F., Bustamante, M. M. C., Coe, M. T., DeFries, R. S., Keller, M., Longo, M., Munger, J. W., Schroeder, W., Soares-Filho, B. S., Souza, Carlos M., J., and Wofsy, S. C.: The Amazon basin in transition, Nature, 481, 321–328, https://doi.org/10.1038/nature10717, <GotoISI>://WOS:000299210600034, 2012.

Dias, M., Rutledge, S., Kabat, P., Dias, P. L. S., Nobre, C., Fisch, G., Dolman, A. J., Zipser, E., Garstang, M., Manzi, A. O., Fuentes, J. D., Rocha, H. R., Marengo, J., Plana-Fattori, A., Sa, L. D. A., Alvala, R. C. S., Andreae, M. O., Artaxo, P., Gielow, R., and Gatti, L.: Cloud

and rain processes in a biosphere-atmosphere interaction context in the Amazon Region, Journal of Geophysical Research-Atmospheres, 107, https://doi.org/10.1029/2001jd000335, <GotoISI>://WOS:000180466200028, 2002.

Dias-Júnior, C. Q., Carneiro, R. G., Fisch, G., D'Oliveira, F. A. F., Sörgel, M., Botía, S., Machado, L. A. T., Wolff, S., Santos, R. M. N. d., and Pöhlker, C.: Intercomparison of Planetary Boundary Layer Heights Using Remote Sensing Retrievals and ERA5 Reanalysis over Central Amazonia, Remote Sensing, 14, https://doi.org/10.3390/rs14184561, https://www.mdpi.com/2072-4292/14/18/4561, 2022.

Draxler, R. R. and Hess, G. D.: An overview of the HYSPLIT 4 modelling system for trajectories, dispersion and deposition, Australian Meteorological Magazine, 47, 295–308, <GotoISI>://WOS:000078594400003, 1998.

Durgante, F. M., Higuchi, N., Ohashi, S., Householder, J. E., Lima, A. J. N., Ishizuka, M., Wittmann, F., dos Santos, J., Carneiro, V. M. C., Xu, X., do Nascimento, C. C., Schongart, J., Piedade, M. T. F., Schmitt, A. R. K., Alves, Y. L. A., Lehman, J., Gimenez, B. O., Baggio, P. M., de Ourique, L. K., and Trumbore, S.: Soil fertility and drought interact to determine large variations in wood production for a hyperdominant Amazonian tree species, Frontiers in Forest and Global Change, 5, https://doi.org/10.3389/ffgc.2022.1065645, 2023.

Echalar, F., Artaxo, P., Martins, J. V., Yamasoe, M., Gerab, F., Maenhaut, W., and Holben, B.: Long-term monitoring of atmospheric aerosols in the Amazon Basin: Source identification and apportionment, Journal of Geophysical Research-Atmospheres, 103, 31 849–31 864, https://doi.org/10.1029/98jd01749, <GotoISI>://WOS:000077967000025, 1998.

Formenti, P., Andreae, M. O., Lange, L., Roberts, G., Cafmeyer, J., Rajta, I., Maenhaut, W., Holben, B. N., Artaxo, P., and Lelieveld, J.: Saharan dust in Brazil and Suriname during the Large-Scale Biosphere-Atmosphere Experiment in Amazonia (LBA) - Cooperative LBA Regional Experiment (CLAIRE) in March 1998, Journal of Geophysical Research: Atmospheres, 106, 14 919–14 934, https://doi.org/10.1029/2000JD900827, http://doi.wiley.com/10.1029/2000JD900827, 2001.

Franco, M. A., Ditas, F., Kremper, L. A., Machado, L. A. T., Andreae, M. O., Araújo, A., Barbosa, H. M. J., de Brito, J. F., Carbone, S., Holanda, B. A., Morais, F. G., Nascimento, J. P., Pöhlker, M. L., Rizzo, L. V., Sá, M., Saturno, J., Walter, D., Wolff, S., Pöschl, U., Artaxo, P., and Pöhlker, C.: Occurrence and Growth of Sub-50 Nm Aerosol Particles in the Amazonian Boundary Layer, Tech. Rep. 5, https://doi.org/10.5194/acp-22-3469-2022, 2022.

Guyon, P.: In-canopy gradients, composition, sources, and optical properties of aerosol over the Amazon forest, 108, 4591, https://doi.org/10.1029/2003JD003465, http://doi.wiley.com/10.1029/2003JD003465, 2003.

Hamilton, D. S., Lee, L. A., Pringle, K. J., Reddington, C. L., Spracklen, D. V., and Carslaw, K. S.: Occurrence of pristine aerosol environments on a polluted planet, Proceedings of the National Academy of Sciences of the United States of America, 111, 18 466–18 471, https://doi.org/10.1073/pnas.1415440111, <GotoISI>://WOS:000347444400030, 2014.

Holanda, B. A., Pöhlker, M. L., Walter, D., Saturno, J., Sörgel, M., Ditas, J., Ditas, F., Schulz, C., Franco, M. A., Wang, Q., Donth, T., Artaxo, P., Barbosa, H. M. J., Borrmann, S., Braga, R., Brito, J., Cheng, Y., Dollner, M., Kaiser, J. W., Klimach, T., Knote, C., Krüger, O. O., Fütterer, D., Lavrič, J. V., Ma, N., Machado, L. A. T., Ming, J., Morais, F. G., Paulsen, H., Sauer, D., Schlager, H., Schneider, J., Su, H., Weinzierl, B., Walser, A., Wendisch, M., Ziereis, H., Zöger, M., Pöschl, U., Andreae, M. O., and Pöhlker, C.: Influx of African biomass burning aerosol during the Amazonian dry season through layered transatlantic transport of black carbon-rich smoke, Atmospheric Chemistry and Physics, 20, 4757–4785, https://doi.org/10.5194/acp-20-4757-2020, https://www.atmos-chem-phys.net/20/4757/2020/, 2020.

Holanda, B. A., Franco, M. A., Walter, D., Artaxo, P., Carbone, S., Cheng, Y., Chowdhury, S., Ditas, F., Gysel-Beer, M., Klimach, T., Kremper, L. A., Krueger, O. O., Lavric, V, J., Lelieveld, J., Ma, C., Machado, L. A. T., Modini, R. L., Morais, F. G., Pozzer, A., Saturno, J., Su, H., Wendisch, M., Wolff, S., Poehlker, M. L., Andreae, M. O., Poeschl, U., and Poehlker, C.: African biomass burning affects aerosol cycling over the Amazon, COMMUNICATIONS EARTH & ENVIRONMENT, 4, https://doi.org/10.1038/s43247-023-00795-5, 2023.

Huffman, J. A., Sinha, B., Garland, R. M., Snee-Pollmann, A., Gunthe, S. S., Artaxo, P., Martin, S. T., Andreae, M. O., and Pöschl, U.: Size distributions and temporal variations of biological aerosol particles in the Amazon rainforest characterized by microscopy and real-time UV-APS fluorescence techniques during AMAZE-08, Atmos. Chem. Phys., 12, 11 997–12 019, https://doi.org/10.5194/acp-12-11997-2012, https://acp.copernicus.org/articles/12/11997/2012/, 2012.

Jardine, K., Yañez-Serrano, A. M., Williams, J., Kunert, N., Jardine, A., Taylor, T., Abrell, L., Artaxo, P., Guenther, A., Hewitt, C. N., House, E., Florentino, A. P., Manzi, A., Higuchi, N., Kesselmeier, J., Behrendt, T., Veres, P. R., Derstroff, B., Fuentes, J. D., Martin, S. T., and Andreae, M. O.: Dimethyl sulfide in the Amazon rain forest: DMS in the Amazon, Global Biogeochemical Cycles, 29, 19–32, https://doi.org/10.1002/2014GB004969, http://doi.wiley.com/10.1002/2014GB004969, 2015.

Kandler, K., Benker, N., Bundke, U., Cuevas, E., Ebert, M., Knippertz, P., Rodriguez, S., Schuetz, L., and Weinbruch, S.: Chemical composition and complex refractive index of Saharan Mineral Dust at Izana, Tenerife (Spain) derived by electron microscopy, Atmospheric Environment, 41, 8058–8074, https://doi.org/10.1016/j.atmosenv.2007.06.047, 2007.

Kandler, K., Schneiders, K., Ebert, M., Hartmann, M., Weinbruch, S., Prass, M., and Pöhlker, C.: Composition and mixing state of atmospheric aerosols determined by electron microscopy: method development and application to aged Saharan dust deposition in the Caribbean boundary layer, Atmospheric Chemistry and Physics, 2018, 1–59, https://doi.org/10.5194/acp-2018-417, https://www.atmos-chem-phys-discuss.net/acp-2018-417/, 2018.

Kaufman, Y. J., Koren, I., Remer, L. A., Rosenfeld, D., and Rudich, Y.: The effect of smoke, dust, and pollution aerosol on shallow cloud development over the Atlantic Ocean, Proceedings of the National Academy of Sciences of the United States of America, 102, 11 207–11 212, https://doi.org/10.1073/pnas.0505191102, <GotoISI>://WOS:000231253400017, 2005.

Koren, I., Kaufman, Y. J., Remer, L. A., and Martins, J. V.: Measurement of the effect of Amazon smoke on inhibition of cloud formation, Science, 303, 1342–1345, https://doi.org/10.1126/science.1089424, <GotoISI>://WOS:000189238600043, 2004.

Krejci, R., Ström, J., de Reus, M., and Sahle, W.: Single particle analysis of the accumulation mode aerosol over the northeast Amazonian tropical rain forest, Surinam, South America, Atmospheric Chemistry and Physics, 5, 3331–3344, https://doi.org/10.5194/acp-5-3331-2005, 2005.

Lauer, O., Kremper, L. A., Rosenfeld, D., Franco, Marco A.and Andreae, M. O., Artaxo, P., Campos Braga, R., Dias-Júnior, C. Q., de Araújo, A. C., Ditas, F., Efraim, A., Ervens, B., Holanda, B. A., Jungandreas, L., Krüger, O. O., Machado, L. A. T., Hernández Pardo, L., Pöschl, U., Pulik, G., Quaas, J., Zheng, Y., Zhu, Y., Pöhlker, C., and Pöhlker, M. L.: High aerosol sensitivity of Amazonian clouds throughout the seasons, in prep., 2022.

Lenton, T. M., Rockstrom, J., Gaffney, O., Rahmstorf, S., Richardson, K., Steffen, W., and Schellnhuber, H. J.: Climate tipping points - too risky to bet against, Nature, 575, 592–595, https://doi.org/10.1038/d41586-019-03595-0, <GotoISI>://WOS:000500036800038, 2019.

Lewis, E. R. and Schwartz, S. E.: Fundamentals, chap. 2, pp. 9–99, American Geophysical Union (AGU), https://doi.org/https://doi.org/10.1002/9781118666050.ch2, https://agupubs.onlinelibrary.wiley.com/doi/abs/10.1002/9781118666050.ch2, 2004.

Li, J., Pósfai, M., Hobbs, P. V., and Buseck, P. R.: Individual aerosol particles from biomass burning in southern Africa: 2, Compositions and aging of inorganic particles: COMPOSITIONS AND AGING OF INORGANIC PARTICLES, Journal of Geophysical Research: Atmospheres, 108, n/a–n/a, https://doi.org/10.1029/2002JD002310, http://doi.wiley.com/10.1029/2002JD002310, 2003.

Linke, C., Mohler, O., Veres, A., Mohacsi, A., Bozoki, Z., Szabo, G., and Schnaiter, M.: Optical properties and mineralogical composition of different Saharan mineral dust samples: a laboratory study, Atmospheric Chemistry and Physics, p. 9, 2006.

Liu, L., Cheng, Y., Wang, S., Wei, C., Pöhlker, M. L., Pöhlker, C., Artaxo, P., Shrivastava, M., Andreae, M. O., Pöschl, U., and Su, H.: Impact of biomass burning aerosols on radiation, clouds, and precipitation over the Amazon: relative importance of aerosol–cloud and aerosol–radiation interactions, Atmospheric Chemistry and Physics, 20, 13 283–13 301, https://doi.org/10.5194/acp-20-13283-2020, https://acp.copernicus.org/articles/20/13283/2020/, publisher: Copernicus GmbH, 2020.

Löbs, N., Barbosa, C. G. G., Brill, S., Walter, D., Ditas, F., de Oliveira Sá, M., de Araújo, A. C., de Oliveira, L. R., Godoi, R. H. M., Wolff, S., Piepenbring, M., Kesselmeier, J., Artaxo, P., Andreae, M. O., Pöschl, U., Pöhlker, C., and Weber, B.: Aerosol measurement methods to quantify spore emissions from fungi and cryptogamic covers in the Amazon, Atmospheric Measurement Techniques, 13, 153–164, https://doi.org/10.5194/amt-13-153-2020, https://www.atmos-meas-tech.net/13/153/2020/, 2020a.

Löbs, N., Walter, D., Barbosa, C. G. G., Brill, S., Alves, R. P., Cerqueira, G. R., de Oliveira Sá, M., de Araújo, A. C., de Oliveira, L. R., Ditas, F., Moran-Zuloaga, D., Pires Florentino, A. P., Wolff, S., Godoi, R. H. M., Kesselmeier, J., Mota de Oliveira, S., Andreae, M. O., Pöhlker, C., and Weber, B.: Microclimatic conditions and water content fluctuations experienced by epiphytic bryophytes in an Amazonian rain forest, Biogeosciences, 17, 5399–5416, https://doi.org/10.5194/bg-17-5399-2020, https://bg.copernicus.org/articles/17/5399/2020/bg-17-5399-2020.html, 2020b.

Maenhaut, W., Fernandez-Jimenez, M. T., Rajta, I., and Artaxo, P.: Two-year study of atmospheric aerosols in Alta Floresta, Brazil: Multielemental composition and source apportionment, Nuclear Instruments Methods in Physics Research Section B-Beam Interactions with Materials and Atoms, 189, 243–248, https://doi.org/10.1016/s0168-583x(01)01050-3, <GotoISI>://WOS:000175595500044, 2002.

Martin, S., Artaxo, P., Machado, L., Manzi, A., Souza, R., Schumacher, C., Wang, J., Biscaro, T., Brito, J., Calheiros, A., Jardine, K., Medeiros, A., Portela, B., Sá, S. d., Adachi, K., Aiken, A., Albrecht, R., Alexander, L., Andreae, M., Barbosa, H., Buseck, P., Chand, D., Comstock, J., Day, D., Dubey, M., Fan, J., Fast, J., Fisch, G., Fortner, E., Giangrande, S., Gilles, M., Goldstein, A., Guenther, A., Hubbe, J., Jensen, M., Jimenez, J., Keutsch, F., Kim, S., Kuang, C., Laskin, A., McKinney, K., Mei, F., Miller, M., Nascimento, R., Pauliquevis, T., Pekour, M., Peres, J., Petäjä, T., Pöhlker, C., Pöschl, U., Rizzo, L., Schmid, B., Shilling, J., Dias, M. S., Smith, J., Tomlinson, J., Tóta, J., and Wendisch, M.: The Green Ocean Amazon Experiment (GoAmazon2014/5) Observes Pollution Affecting Gases, Aerosols, Clouds, and Rainfall over the Rain Forest, Bulletin of the American Meteorological Society, 0, null, https://doi.org/10.1175/bams-d-15-00221.1, http://journals.ametsoc.org/doi/abs/10.1175/BAMS-D-15-00221.1, 2016.

Martin, S. T., Andreae, M. O., Artaxo, P., Baumgardner, D., Chen, Q., Goldstein, A. H., Guenther, A., Heald, C. L., Mayol-Bracero, O. L., McMurry, P. H., Pauliquevis, T., Poschl, U., Prather, K. A., Roberts, G. C., Saleska, S. R., Dias, M. A. S., Spracklen, D. V., Swietlicki, E., and Trebs, I.: Sources and properties of Amazonian aerosol particles, Reviews of Geophysics, 48, RG2002, https://doi.org/10.1029/2008rg000280, <GotoISI>://000276831600001, 2010.

Moran-Zuloaga, D., Ditas, F., Walter, D., Saturno, J., Brito, J., Carbone, S., Chi, X., Hrabě de Angelis, I., Baars, H., Godoi, R. H. M., Heese, B., Holanda, B. A., Lavrič, J. V., Martin, S. T., Ming, J., Pöhlker, M. L., Ruckteschler, N., Su, H., Wang, Y., Wang, Q., Wang, Z., Weber, B., Wolff, S., Artaxo, P., Pöschl, U., Andreae, M. O., and Pöhlker, C.: Long-term study on coarse mode aerosols in the Amazon rain forest with the frequent intrusion of Saharan dust plumes, Atmospheric Chemistry and Physics, 18, 10 055–10 088, https://doi.org/10.5194/acp-18-10055-2018, https://acp.copernicus.org/articles/18/10055/2018/, 2018.

Nemeruyk, G. E.: Migration of salts into the atmosphere during transpiration, Sov. Plant Physiol., 17, 1970.

Oliveira, M. I., Acevedo, O. C., Sörgel, M., Nascimento, E. L., Manzi, A. O., Oliveira, P. E. S., Brondani, D. V., Tsokankunku, A., and Andreae, M. O.: Planetary boundary layer evolution over the Amazon rainforest in episodes of deep moist convection at the Amazon Tall Tower Observatory, Atmospheric Chemistry and Physics, 20, 15–27, https://doi.org/10.5194/acp-20-15-2020, https://www.atmos-chem-phys.net/20/15/2020/, 2020.

Pfannerstill, E. Y., Nölscher, A. C., Yáñez-Serrano, A. M., Bourtsoukidis, E., Keßel, S., Janssen, R. H. H., Tsokankunku, A., Wolff, S., Sörgel, M., Sá, M. O., Araújo, A., Walter, D., Lavrič, J., Dias-Júnior, C. Q., Kesselmeier, J., and Williams, J.: Total OH Reactivity Changes Over the Amazon Rainforest During an El Niño Event, Frontiers in Forests and Global Change, 1, 12, https://www.frontiersin.org/article/10.3389/ffgc.2018.00012, 2018.

Pöhlker, C., Wiedemann, K. T., Sinha, B., Shiraiwa, M., Gunthe, S. S., Smith, M., Su, H., Artaxo, P., Chen, Q., Cheng, Y., Elbert, W., Gilles, M. K., Kilcoyne, A. L. D., Moffet, R. C., Weigand, M., Martin, S. T., Pöschl, U., and Andreae, M. O.: Biogenic Potassium Salt Particles as Seeds for Secondary Organic Aerosol in the Amazon, Science, 337, 1075–1078, https://doi.org/10.1126/science.1223264, 2012.

Posit team: RStudio: Integrated Development Environment for R, Posit Software, PBC, Boston, MA, http://www.posit.co/, 2023.

Prass, M., Andreae, M. O., de Araùjo, A. C., Artaxo, P., Ditas, F., Elbert, W., Franco, M. A., Hrabe de Angelis, I., Kesselmeier, J., Klimach, T., Kremper, L. A., Thines, E., Walter, D., Weber, J., Weber, B., Fuchs, B. M., Pöschl, U., and Pöhlker, C.: Bioaerosols in the Amazon rain forest: Temporal variations and vertical profiles of Eukarya, Bacteria and Archaea, Biogeosciences Discussions, https://doi.org/10.5194/bg-2020-469, https://bg.copernicus.org/preprints/bg-2020-469, 2021.

Prospero, J. M., Barkley, A. E., Gaston, C. J., Gatineau, A., Campos y Sansano, A., and Panechou, K.: Characterizing and Quantifying African Dust Transport and Deposition to South America: Implications for the Phosphorus Budget in the Amazon Basin, Global Biogeochemical Cycles, 34, e2020GB006 536, https://doi.org/10.1029/2020GB006536, https://onlinelibrary.wiley.com/doi/abs/10.1029/2020GB006536, _eprint: https://onlinelibrary.wiley.com/doi/pdf/10.1029/2020GB006536, 2020.

Pöhlker, C., Walter, D., Paulsen, H., Könemann, T., Rodríguez-Caballero, E., Moran-Zuloaga, D., Brito, J., Carbone, S., Degrendele, C., Després, V. R., Ditas, F., Holanda, B. A., Kaiser, J. W., Lammel, G., Lavrič, J. V., Ming, J., Pickersgill, D., Pöhlker, M. L., Praß, M., Löbs, N., Saturno, J., Sörgel, M., Wang, Q., Weber, B., Wolff, S., Artaxo, P., Pöschl, U., and Andreae, M. O.: Land cover and its transformation in the backward trajectory footprint region of the Amazon Tall Tower Observatory, Atmospheric Chemistry and Physics, 19, 8425–8470, https://doi.org/10.5194/acp-19-8425-2019, https://www.atmos-chem-phys.net/19/8425/2019/, 2019.

Pöhlker, M. L., Pöhlker, C., Klimach, T., Hrabe de Angelis, I., Barbosa, H. M. J., Brito, J., Carbone, S., Cheng, Y., Chi, X., Ditas, F., Ditz, R., Gunthe, S. S., Kesselmeier, J., Könemann, T., Lavrič, J. V., Martin, S. T., Moran-Zuloaga, D., Rose, D., Saturno, J., Su, H., Thalman, R., Walter, D., Wang, J., Wolff, S., Artaxo, P., Andreae, M. O., and Pöschl, U.: Long-term observations of cloud condensation nuclei in the Amazon rain forest – Part 1: Aerosol size distribution, hygroscopicity, and new model parameterizations for CCN prediction, Atmos. Chem. Phys., 16, 15 709–15 740, https://doi.org/10.5194/acp-2016-519, http://www.atmos-chem-phys-discuss.net/acp-2016-519/, 2016.

Pöhlker, M. L., Ditas, F., Saturno, J., Klimach, T., Hrabě de Angelis, I., Araùjo, A. C., Brito, J., Carbone, S., Cheng, Y., Chi, X., Ditz, R., Gunthe, S. S., Holanda, B. A., Kandler, K., Kesselmeier, J., Könemann, T., Krüger, O. O., Lavrič, J. V., Martin, S. T., Mikhailov, E., Moran-Zuloaga, D., Rizzo, L. V., Rose, D., Su, H., Thalman, R., Walter, D., Wang, J., Wolff, S., Barbosa, H. M. J., Artaxo, P., Andreae, M. O., Pöschl, U., and Pöhlker, C.: Long-term observations of cloud condensation nuclei over the Amazon rain forest – Part 2: Variability and characteristics of biomass burning, long-range transport, and pristine rain forest aerosols, Atmospheric Chemistry and Physics., 18, 10 289–10 331, https://doi.org/10.5194/acp-18-10289-2018, https://www.atmos-chem-phys.net/18/10289/2018/, 2018.

Pöschl, U., Martin, S. T., Sinha, B., Chen, Q., Gunthe, S. S., Huffman, J. A., Borrmann, S., Farmer, D. K., Garland, R. M., Helas, G., Jimenez, J. L., King, S. M., Manzi, A., Mikhailov, E., Pauliquevis, T., Petters, M. D., Prenni, A. J., Roldin, P., Rose, D., Schneider, J., Su, H., Zorn, S. R., Artaxo, P., and Andreae, M. O.: Rainforest Aerosols as Biogenic Nuclei of Clouds and Precipitation in the Amazon, Science, 329, 1513–1516, https://doi.org/10.1126/science.1191056, https://www.science.org/doi/full/10.1126/science.1191056, publisher: American Association for the Advancement of Science, 2010.

Rizzo, L. V., Artaxo, P., Mueller, T., Wiedensohler, A., Paixao, M., Cirino, G. G., Arana, A., Swietlicki, E., Roldin, P., Fors, E. O., Wiedemann, K. T., Leal, L. S. M., and Kulmala, M.: Long term measurements of aerosol optical properties at a primary forest site in Amazonia, Atmospheric Chemistry and Physics, 13, 2391–2413, https://doi.org/10.5194/acp-13-2391-2013, <GotoISI>://WOS:000316960500006, 2013.

Rizzo, L. V., Roldin, P., Brito, J., Backman, J., Swietlicki, E., Krejci, R., Tunved, P., Petaja, T., Kulmala, M., and Artaxo, P.: Multi-year statistical and modeling analysis of submicrometer aerosol number size distributions at a rain forest site in Amazonia, Atmospheric Chemistry and Physics, 18, 10 255–10 274, https://doi.org/10.5194/acp-18-10255-2018, <GotoISI>://WOS:000439171300001, 2018.

Rizzolo, J. A., Barbosa, C. G. G., Borillo, G. C., Godoi, A. F. L., Souza, R. A. F., Andreoli, R. V., Manzi, A. O., Sá, M. O., Alves, E. G., Pöhlker, C., Angelis, I. H., Ditas, F., Saturno, J., Moran-Zuloaga, D., Rizzo, L. V., Rosário, N. E., Pauliquevis, T., Santos, R. M. N., Yamamoto, C. I., Andreae, M. O., Artaxo, P., Taylor, P. E., and Godoi, R. H. M.: Soluble iron nutrients in Saharan dust over the central Amazon rainforest, Atmospheric Chemistry and Physics, 17, 2673–2687, https://doi.org/10.5194/acp-17-2673-2017, https://acp.copernicus.org/articles/17/2673/2017/, 2017.

Salter, M. E., Hamacher-Barth, E., Leck, C., Werner, J., Johnson, C. M., Riipinen, I., Nilsson, E. D., and Zieger, P.: Calcium enrichment in sea spray aerosol particles, Geophysical research letters, 43, 8277–8285, 2016.

Saturno, J., Ditas, F., Penning de Vries, M., Holanda, B. A., Pöhlker, M. L., Carbone, S., Walter, D., Bobrowski, N., Brito, J., Chi, X., Gutmann, A., Hrabe de Angelis, I., Machado, L. A. T., Moran-Zuloaga, D., Rüdiger, J., Schneider, J., Schulz, C., Wang, Q., Wendisch, M., Artaxo, P., Wagner, T., Pöschl, U., Andreae, M. O., and Pöhlker, C.: African volcanic emissions influencing atmospheric aerosols over the Amazon rain forest, Atmospheric Chemistry and Physics, 18, 10 391–10 405, https://doi.org/10.5194/acp-18-10391-2018, https://www.atmos-chem-phys.net/18/10391/2018/, 2018a.

Saturno, J., Holanda, B. A., Pöhlker, C., Ditas, F., Wang, Q., Moran-Zuloaga, D., Brito, J., Carbone, S., Cheng, Y., Chi, X., Ditas, J., Hoffmann, T., Hrabe de Angelis, I., Könemann, T., Lavrič, J. V., Ma, N., Ming, J., Paulsen, H., Pöhlker, M. L., Rizzo, L. V., Schlag, P., Su, H., Walter, D., Wolff, S., Zhang, Y., Artaxo, P., Pöschl, U., and Andreae, M. O.: Black and brown carbon over central Amazonia: long-term aerosol measurements at the ATTO site, Atmospheric Chemistry and Physics, 18, 12 817–12 843, https://doi.org/10.5194/acp-18-12817-2018, https://www.atmos-chem-phys.net/18/12817/2018/, 2018b.

Scheuvens, D. and Kandler, K.: On Composition, Morphology, and Size Distribution of Airborne Mineral Dust, book section 2, pp. 15–49, Springer Netherlands, https://doi.org/10.1007/978-94-017-8978-3_2, http://dx.doi.org/10.1007/978-94-017-8978-3_2, 2014.

Schrod, J., Thomson, E. S., Weber, D., Kossmann, J., Pöhlker, C., Saturno, J., Ditas, F., Artaxo, P., Clouard, V., Saurel, J.-M., Ebert, M., Curtius, J., and Bingemer, H. G.: Long-term deposition and condensation ice-nucleating particle measurements from four stations across the globe, Atmospheric Chemistry and Physics, 20, 15 983–16 006, https://doi.org/10.5194/acp-20-15983-2020, https://acp.copernicus.org/articles/20/15983/2020/, 2020.

Staal, A., Tuinenburg, O. A., Bosmans, J. H. C., Holmgren, M., van Nes, E. H., Scheffer, M., Zemp, D. C., and Dekker, S. C.: Forest-rainfall cascades buffer against drought across the Amazon, Nature Climate Change, 8, 539+, https://doi.org/10.1038/s41558-018-0177-y, 2018.

Stein, A. F., Draxler, R. R., Rolph, G. D., Stunder, B. J. B., Cohen, M. D., and Ngan, F.: NOAA'S HYSPLIT ATMOSPHERIC TRANSPORT AND DISPERSION MODELING SYSTEM, Bulletin of the American Meteorological Society, 96, 2059–2077, https://doi.org/10.1175/bams-d-14-00110.1, <GotoISI>://WOS:000368500900001, 2015.

Su, B., Wang, T., Zhang, G., Liang, Y., Lv, C., Hu, Y., Li, L., Zhou, Z., Wang, X., and Bi, X.: A Review of Atmospheric Aging of Sea Spray Aerosols: Potential Factors Affecting Chloride Depletion, Atmospheric Environment, 290, 119 365, https://doi.org/10.1016/j.atmosenv.2022.119365, 2022.

Swap, R., Garstang, M., Greco, S., Talbot, R., and Kållberg, P.: Saharan dust in the Amazon Basin, Tellus B, 44, 133–149, https://doi.org/10.1034/j.1600-0889.1992.t01-1-00005.x, https://onlinelibrary.wiley.com/doi/abs/10.1034/j.1600-0889.1992.t01-1-00005.x, _eprint: https://onlinelibrary.wiley.com/doi/pdf/10.1034/j.1600-0889.1992.t01-1-00005.x, 1992.

ter Steege, H., Pitman, N. C. A., Sabatier, D., Baraloto, C., Salomao, R. P., Guevara, J. E., Phillips, O. L., Castilho, C. V., Magnusson, W. E., Molino, J.-F., Monteagudo, A., Nunez Vargas, P., Carlos Montero, J., Feldpausch, T. R., Coronado, E. N. H., Killeen, T. J., Mostacedo, B., Vasquez, R., Assis, R. L., Terborgh, J., Wittmann, F., Andrade, A., Laurance, W. F., Laurance, S. G. W., Marimon, B. S., Marimon, Jr., B.-H., Guimaraes Vieira, I. C., Amaral, I. L., Brienen, R., Castellanos, H., Cardenas Lopez, D., Duivenvoorden, J. F., Mogollon, H. F., de Almeida Matos, F. D., Davila, N., Garcia-Villacorta, R., Stevenson Diaz, P. R., Costa, F., Emilio, T., Levis, C., Schietti, J., Souza, P., Alonso, A., Dallmeier, F., Duque Montoya, A. J., Fernandez Piedade, M. T., Araujo-Murakami, A., Arroyo, L., Gribel, R., Fine, P. V. A., Peres, C. A., Toledo, M., Gerardo, A. A. C., Baker, T. R., Ceron, C., Engel, J., Henkel, T. W., Maas, P., Petronelli, P., Stropp, J., Eugene Zartman, C., Daly, D., Neill, D., Silveira, M., Rios Paredes, M., Chave, J., de Andrade Lima, D., Jorgensen, P. M., Fuentes, A., Schoengart, J., Cornejo Valverde, F., Di Fiore, A., Jimenez, E. M., Penuela Mora, M. C., Fernando Phillips, J., Rivas, G., van Andel, T. R., von Hildebrand, P., Hoffman, B., Zent, E. L., Malhi, Y., Prieto, A., Rudas, A., Ruschell, A. R., Silva, N., Vos, V., Zent, S., Oliveira, A. A., Cano Schutz, A., Gonzales, T., Nascimento, M. T., Ramirez-Angulo, H., Sierra, R., Tirado, M., Umana Medina, M. N., van der Heijden, G., Vela, C. I. A., Vilanova Torre, E., Vriesendorp, C., Wang, O., Young, K. R., Baider, C., Balslev, H., Ferreira, C., Mesones, I., Torres-Lezama, A., Urrego Giraldo, L. E., Zagt, R., Alexiades, M. N., Hernandez, L., Huamantupa-Chuquimaco, I., Milliken, W., Palacios Cuenca, W., Pauletto, D., Valderrama Sandoval, E., Valenzuela Gamarra, L., Dexter, K. G., Feeley, K., Lopez-Gonzalez, G., and Silman, M. R.: Hyperdominance in the Amazonian Tree Flora, Science, 342, 325+, https://doi.org/10.1126/science.1243092, 2013.

Wang, Q., Saturno, J., Chi, X., Walter, D., Lavric, J. V., Moran-Zuloaga, D., Ditas, F., Pöhlker, C., Brito, J., Carbone, S., Artaxo, P., and Andreae, M. O.: Modeling investigation of light-absorbing aerosols in the Amazon Basin during the wet season, Atmospheric Chemistry and Physics, 16, 14 775–14 794, https://doi.org/10.5194/acp-16-14775-2016, http://www.atmos-chem-phys.net/16/14775/2016/, 2016.

Wang, X., Wang, Q., Prass, M., Pöhlker, C., Moran-Zuloaga, D., Artaxo, P., Gu, J., Yang, N., Yang, X., Tao, J., Hong, J., Ma, N., Cheng, Y., Su, H., and Andreae, M. O.: The export of African mineral dust across the Atlantic and its impact over the Amazon Basin, Atmospheric Chemistry and Physics, 23, 9993–10 014, https://doi.org/10.5194/acp-23-9993-2023, https://acp.copernicus.org/articles/23/9993/2023/, 2023.

Worobiec, A., Szalóki, I., Osán, J., Maenhaut, W., Anna Stefaniak, E., and Van Grieken, R.: Characterisation of Amazon Basin Aerosols at the Individual Particle Level by X-ray Microanalytical Techniques, Atmospheric Environment, 41, 9217–9230, https://doi.org/10.1016/j.atmosenv.2007.07.056, 2007.

Wouters, L., Hagedoren, S., Dierck, I., Artaxo, P., and Vangrieken, R.: Laser Microprobe Mass Analysis of Amazon Basin Aerosols, Atmospheric Environment Part A - General Topics, 27, 661–668, https://doi.org/10.1016/0960-1686(93)90184-z, <GotoISI>://WOS:A1993KY38100003, 1993.

Wu, L., Li, X., Kim, H., Geng, H., Godoi, R. H. M., Barbosa, C. G. G., Godoi, A. F. L., Yamamoto, C. I., de Souza, R. A. F., Pöhlker, C., Andreae, M. O., and Ro, C.-U.: Single-particle characterization of aerosols collected at a remote site in the Amazonian rainforest and an urban site in Manaus, Brazil, 19, 1221–1240, https://doi.org/10.5194/acp-19-1221-2019, https://acp.copernicus.org/articles/19/1221/2019/, 2019.

Yamasoe, M. A., Artaxo, P., Miguel, A. H., and Allen, A. G.: Chemical composition of aerosol particles from direct emissions of vegetation fires in the Amazon Basin: water-soluble species and trace elements, Atmospheric Environment, 34, 1641–1653, 2000.

Yanez-Serrano, A. M., Noelscher, A. C., Williams, J., Wolff, S., Alves, E., Martins, G. A., Bourtsoukidis, E., Brito, J., Jardine, K., Artaxo, P., and Kesselmeier, J.: Diel and seasonal changes of biogenic volatile organic compounds within and above an Amazonian rainforest, Atmospheric Chemistry and Physics, 15, 3359–3378, https://doi.org/10.5194/acp-15-3359-2015, <GotoISI>://WOS:000352157600024, 2015.

Yang, Y., Saatchi, S. S., Xu, L., Yu, Y., Choi, S., Phillips, N., Kennedy, R., Keller, M., Knyazikhin, Y., and Myneni, R. B.: Post-drought decline of the Amazon carbon sink, Nature Communications, 9, https://doi.org/10.1038/s41467-018-05668-6, 2018.

Yu, H. B., Chin, M., Yuan, T. L., Bian, H. S., Remer, L. A., Prospero, J. M., Omar, A., Winker, D., Yang, Y. K., Zhang, Y., Zhang, Z. B., and Zhao, C.: The fertilizing role of African dust in the Amazon rainforest: A first multiyear assessment based on data from Cloud-Aerosol Lidar and Infrared Pathfinder Satellite Observations, Geophysical Research Letters, 42, 1984–1991, https://doi.org/10.1002/2015gl063040, <GotoISI>://WOS:000353170000047, 2015.

Yáñez-Serrano, A. M., Nölscher, A. C., Bourtsoukidis, E., Gomes Alves, E., Ganzeveld, L., Bonn, B., Wolff, S., Sa, M., Yamasoe, M., Williams, J., Andreae, M. O., and Kesselmeier, J.: Monoterpene chemical speciation in a tropical rainforest:variation with season, height, and time of dayat the Amazon Tall Tower Observatory (ATTO), Atmospheric Chemistry and Physics., 18, 3403–3418, https://doi.org/10.5194/acp-18-3403-2018, https://www.atmos-chem-phys.net/18/3403/2018/, 2018.

Supplement of

Contrasting the elemental composition of Amazonian aerosol under African dust influx vs pristine conditions

Leslie Ann Kremper et al.

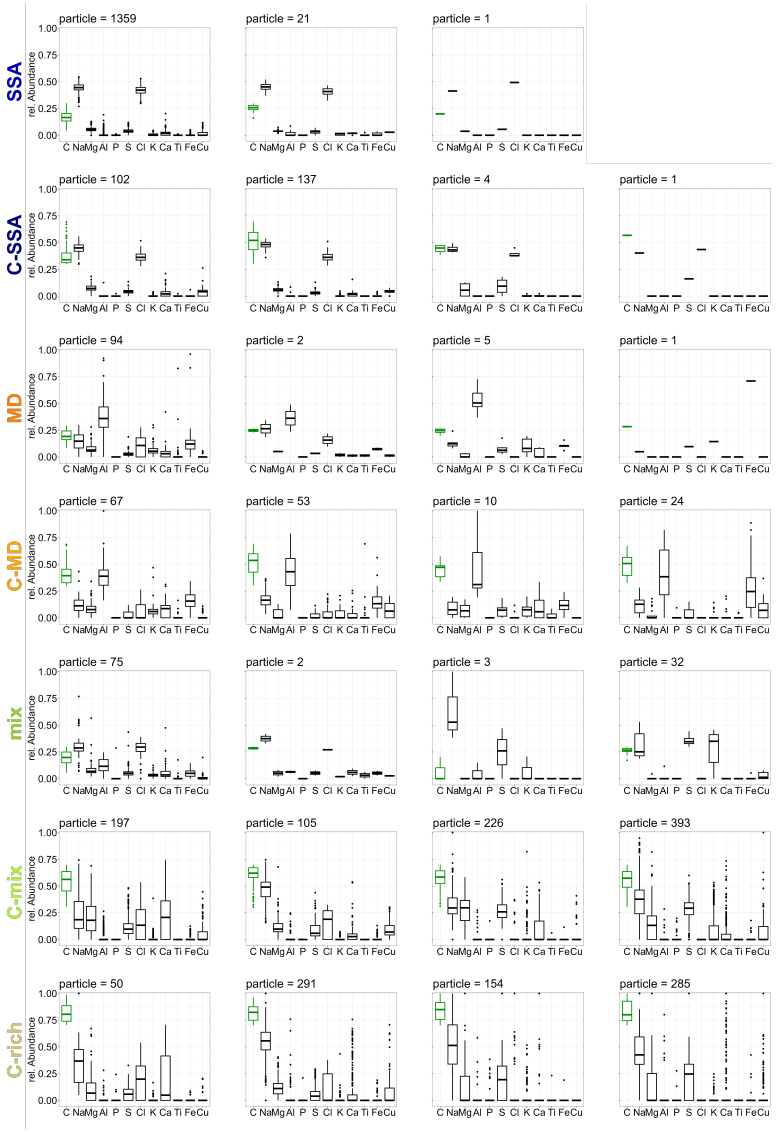

Figure S1. Particle class characterization by elemental composition derived from SEM-EDX single particle analyses using box-whisker plots. The median value is indicated by a horizontal line and the boxes represent the first and third quartiles, the whiskers extend to the largest and smallest values within the 1.5 times inter quartile range (IQR). Additionally, any outlying point are displayed individually. The amount of Carbon is represented by the C-index (Equation 1) as green boxes, while remaining elements are represented by the Element index considering the inorganic fraction exclusively (Equation 2) as black boxes.

2.2 Ubiquitous biogenic salts in the Amazonian aerosol observed by electron microspectroscopy

This chapter contains a first complete manuscript draft. After some remaining optimizations, it will be submitted to a journal to be defined.

Contribution to this publication by Leslie A. Kremper: I am the first author of this paper and played a major role in planning the study. I designed the sampling strategy and performed the collection of the samples that are the basis of this study. I participated in several measurement campaigns at ATTO, where I refined and implemented the sampling approach. I also performed the laboratory analysis by scanning electron microscopy with energy dispersive x-ray analysis and developed a strategy for post-processing and quality assurance of the data. I developed the codes for analysis and visualization. In addition, I contributed to the in-situ measurements during the field campaigns, which are crucial for interpreting the results. I prepared the figures and took the lead in writing the manuscript.

Ubiquitous biogenic salts in the Amazonian aerosol observed by electron microspectroscopy

Leslie A. Kremper[1], Sebastian Brill[1], Jan-David Förster[1,2], Paulo Artaxo[3], Ulrich Pöschl[1], Konrad Kandler[4], and Christopher Pöhlker[1]

[1] Multiphase Chemistry Department, Max Planck Institute for Chemistry, 55128 Mainz, Germany
[2] Atmospheric Microphysics Department, Leibniz Institute for Tropospheric Research, 04318 Leipzig, Germany
[3] Institute of Physics, University of São Paulo, São Paulo 05508-900, Brazil
[4] Institut für Angewandte Geowissenschaften, Technische Universität Darmstadt, Darmstadt, Germany

Correspondence: Christopher Pöhlker (c.pohlker@mpic.de), Leslie A. Kremper (l.kremper@mpic.de)

Abstract. Understanding the Amazonian aerosol cycle is crucial for unraveling the interactions between the biosphere, anthropogenic impacts, and climate processes. Previous research indicates a complex aerosol composition in the Amazon, influenced by seasonal variations and different sources, where the polluted dry season contrasts with the clean wet season dominated by natural emissions. However, knowledge of the precise particle sources, especially those that contribute to the fine particle fraction during clean conditions, is limited. This study shows the contribution of inorganic salts within the Amazonian accumulation and coarse mode population. Scanning electron microscopy combined with energy dispersive x-ray spectroscopy is used for single particle analysis, revealing temporal and spatial variations within the inorganic particle composition. An almost ubiquitous presence of inorganic components within the carbon-dominated particles was observed. Furthermore, the particles could be classified into distinct groups based on their inorganic composition. These results indicate a significant contribution of inorganic salts to the Amazonian aerosol accumulation and coarse mode population. Based on the observed spatial and temporal patterns, it is most likely that biogenic processes from the rain forest are related. Therefore, this study suggests that biogenic salts are a relevant component within the Amazonian aerosol cycle and play a significant role as seeds for secondary aerosol formation. Thus, the current results support previous assumptions that under clean conditions, locally emitted biogenic salts help to maintain the accumulation mode that is most relevant for aerosol-cloud interactions. Although more research is needed, this study is a further step in linking biogenic inorganic emissions to cloud microphysics in the Amazon.

1 Introduction

Studying the atmospheric aerosol in the Amazon rain forest is essential to understand the interactions between the natural biosphere, anthropogenic impacts and climatic processes in an globally important ecosystem. Over the last few decades, progress has been made in exploring the aerosol cycle in the Amazon (Talbot et al., 1988, 1990; Martin et al., 2010; Andreae et al., 2004, 2018; Artaxo et al., 1993, 2022, and references therein). The composition of the Amazonian aerosol population is highly variable and strongly influenced by seasonal variations in prevailing aerosol sources (e.g Rizzo et al., 2013; Pöhlker et al., 2016; Saturno et al., 2018; Moran-Zuloaga et al., 2018). During the dry season, anthropogenic activities, especially local slash-and-burn fires, strongly influence the aerosol state (e.g Artaxo et al., 2013; Pöhlker et al., 2018; Saturno et al., 2018). This leads to a dominance of biomass burning (BB) emissions, resulting in a significantly increased concentration of particles, particularly in the accumulation mode, which is the size range most relevant for cloud formation and cloud microphysical properties (~ 100 – 1000 nm) (e.g Roberts et al., 2003; Koren et al., 2004; Rissler et al., 2006; Martins et al., 2009; Liu et al., 2020). In contrast, the wet season is characterized by predominantly clean atmospheric conditions. Apart from occasional interruptions due to the influx of BB smoke from Africa (Pöhlker et al., 2018; Holanda et al., 2023), the aerosol composition is largely defined by natural sources. This includes mineral dust and sea spray aerosol introduced by long-range transport (LRT) across the Atlantic (Prospero et al., 1981; Swap et al., 1992; Formenti et al., 2001; Ansmann et al., 2009; Moran-Zuloaga et al., 2018; Wang et al., 2023). During periods when LRT is negligible, the aerosol composition is predominantly influenced by local sources and the aerosol population consists mainly of primary biological aerosol particles (PBAPs), biogenic salts and secondary organic aerosol (SOA) (e.g., Pöschl et al., 2010; Elbert et al., 2007; Graham et al., 2003; Artaxo et al., 1990).

PBAPs are particles originating from living organisms, which are emitted directly into the atmosphere, including fungal spores, bacteria and fragments or excretions from plants and animals (Després et al., 2012; Fröhlich-Nowoisky et al., 2016). In the Amazon, PBAPs contribute significantly to the coarse mode particle population (> 1 µm), but are also present within the fine mode (< 1 µm). Previous and ongoing research suggests a significant role for PBAPs in atmospheric processes, but specific information on their exact sources, properties and interactions remains limited (Elbert et al., 2007; Ramsay et al., 2020; Prass et al., 2021; Barbosa et al., 2022). During clean conditions, biogenic SOA represent numerically the largest fraction, contributing significantly to the fine mode range (Chen et al., 2009), and play a critical role in cloud formation processes (Andreae et al., 2018; Williamson et al., 2019). SOA are formed by the oxidation of biogenic volatile organic compounds (BVOC), forming low or semi-volatile oxidation products that can either condense on existing particles or contribute to new particle formation (NPF, Pöschl, 2005; Pöhlker et al., 2012; Huffman et al., 2012; Chen et al., 2015; Liu et al., 2016). Compared to other regions where NPF with subsequent particle growth contribute significantly to the aerosol concentration (Kerminen et al., 2018, and references therein), this 'classical' NPF is not observed in the Amazon (Kulmala et al., 2012; Wimmer et al., 2018; Varanda Rizzo et al., 2018). Unlike characteristic sizes of freshly nucleated particles, in the Amazon particles initiating growth events are observed to occur at larger sizes between ~ 20 – 40 nm (Kulmala et al., 2012; Kerminen et al., 2018; Varanda Rizzo et al., 2018; Franco et al., 2022). This raises a basic question: In the absence of the typical NPF, what are the sources of these

particles that maintain the Amazonian accumulation particle population under clean conditions? Previous studies proposed a mechanism in which NPF takes place in the upper troposphere (Andreae et al., 2018; Liu et al., 2023). Subsequently, the downdraft transport of the newly formed particles serves as a source of particles in the sub-50 nm size range within the tropical boundary layer (Wang et al., 2016). However, this process alone cannot explain their entire occurrence (Varanda Rizzo et al., 2018; Franco et al., 2022). Further research has proposed additional sources and mechanisms (Machado et al., 2021; Khadir et al., 2023), including the release of biogenic salts from the forest biosphere, which could serve as seeds for SOA condensation (Pöschl et al., 2010; Pöhlker et al., 2012). Hence, biogenic salts may play a crucial role in the formation of CCN-relevant aerosol particles. The precise sources and release mechanisms, however, remain unclear.

Following previous studies characterizing the elemental composition of the Amazonian aerosol population (Artaxo et al., 1990, 1994, 2000; Pöhlker et al., 2012; Adachi et al., 2020; Wu et al., 2019, e.g.), this study aims to deepen the knowledge of the natural particle composition and to identify potential sources. It provides insights into the Amazonian aerosol composition by systematically investigating selected aerosol conditions. The study distinguishes between clean and (moderately) polluted states, examines day and night variations, and explores biosphere-atmosphere exchange and mixing by considering below and above-canopy conditions. The approach of scanning electron microscopy with energy dispersive X-ray analysis of single particles provides size-resolved chemical information, allowing the identification of distinct particle modes along with their corresponding physicochemical properties. By focusing on the inorganic composition of individual particles, this research provides new insights into the atmospheric abundance and relevance of (biogenic) salts, particularly in their potential role as seeds for SOA formation. Understanding these processes could be a crucial step in linking biogenic emissions to cloud microphysics in the Amazon rain forest.

2 Experimental section

2.1 The Amazon Tall Tower Observatory

Aerosol sampling and measurements were conducted at the Amazon Tall Tower Observatory (ATTO), which is a long-term research station located in a largely untouched rain forest area, $\sim$150 km northeast of Manaus, Brazil (2.146° S, 59.006° W, 130 m above sea level). Details on atmospheric, geographic, and ecological conditions at the ATTO site and on its footprint region can be found elsewhere (Andreae et al., 2015; Pöhlker et al., 2019; Oliveira et al., 2020; Durgante et al., 2023). For this study, sampling and measurements were conducted at the 325 m tall tower and the 80 m triangular mast (see details in Andreae et al., 2015). Instruments were housed in air-conditioned laboratory containers at the base of the towers. Sample air was collected trough stainless steel tubes (25.4 mm outer diameter and (22.1 mm inner diameter, finetron tubes, Dockweiler AG, Neustadt-Glewe, Germany) with total suspended particle (TSP) inlet heads at varying heights (specified in Section 2.2 and 2.3). The sample air for the online aerosol instruments was dried by a custom-build and automated condensation dryer to a relative humidity (RH) <40 %. The sample air for aerosol sample collection was purposefully not dried to reduce the effect

of particle bouncing in the impactors (e.g., Stein et al., 1994; Virtanen et al., 2010). The aerosol samplers were either operated inside the laboratory containers or mounted directly on the towers without additional inlet lines.

2.2 Continuous measurements of aerosol and related properties

The ATTO site is equipped with a broad range of instrumentation for continuous observation of aerosol properties (for details, see e.g., Pöhlker et al., 2018; Saturno et al., 2018; Holanda et al., 2023). In this study, data from an Optical Particle Sizer (OPS, model 3330, TSI Inc. Shoreview, MN, USA), sampling from the 60 m inlet at the triangular mast, measured the particle number size distributions (PNSDs) from 0.3 – 10 µm. This data covers the coarse mode aerosol population (1 – 10 µm) and the large size fraction of the accumulation mode (0.3 – 1 µm) (see also Moran-Zuloaga et al., 2018). In addition, a Multi-Angle Absorption Photometer (MAAP, model 5012, Thermo Electron Group) was used to measure the aerosol absorption coefficient at $\lambda = 637\,\mathrm{nm}$. The MAAP reports the equivalent black carbon mass concentration (M_{BCe}) assuming the widely used standard mass absorption cross section (MAC) of $6.6\,\mathrm{m^2\,g^{-1}}$ (Bond and Bergstrom, 2006). Note that typical MAC values in the Amazon are higher (i.e., $11 - 12\,\mathrm{m^2\,g^{-1}}$) (Saturno et al., 2018; Holanda et al., 2023), which means that M_{BCe} tends to be overestimated here. M_{BCe} is used as a pollution marker and biomass burning tracer here. The cumulative precipitation, P_{BT}, for individual HYSPLIT 3-day backward trajectories (BTs, starting height at ATTO at 200 m above ground level) was obtained by integrating the precipitation data along the BT tracks (Draxler and Hess, 1998). Details are described in Pöhlker et al. (2019) and Moran-Zuloaga et al. (2018). P_{BT} represents the amount of rain that the air parcels experienced during their last 3 days of atmospheric transport towards ATTO and, therefore, reflects the extent of rain-related aerosol scavenging. The analysis and processing of the aforementioned data sets were done with RStudio (Posit team, 2023).

2.3 Aerosol sampling

2.3.1 Setup and equipment for aerosol collection

Aerosol samples for single particle analysis were collected with three distinct custom-built single-stage impactors. The impactors' nominal cut-off diameters (i.e., D_{50}, calculated 50 % collection efficiency) are calculated assuming a unit particle density of $1.5\,\mathrm{g\,cm^{-3}}$ (see details in Supplement of Moran-Zuloaga et al., 2018). Note that a certain fraction of particles in $< D_{50}$ is is commonly collected as well due to diffusive and interceptive processes, but with a lower efficiency. Nevertheless, owing to the usually higher numbers of the smaller particles, sufficient numbers of smaller particles are therefore available for analysis.

- **I-1**: Impactor 1 is a multi-impactor with up to 42 substrates. With a nozzle diameter of 1.1 mm and a flow rate of $1\,\mathrm{L\,min^{-1}}$, it has a D_{50} of ~ 0.9 µm. The impactor is operated with automatic control software.
- **I-2**: Impactor 2 is a multi-impactor with up to 12 substrates. With a nozzle diameter of 0.5 mm and a flow rate of $0.85\,\mathrm{L\,min^{-1}}$, it has a D_{50} of ~ 0.36 µm. The impactor is operated with automatic control software.

– **I-3**: Impactor 3 has a nozzle diameter of $0.8\,\mathrm{mm}$ and flow rates in the range of $0.3-0.65\,\mathrm{L\,min^{-1}}$, which results in a D_{50} in the range of $0.9-1.4\,\mu\mathrm{m}$. The impactor is not software-controlled and requires manual operation.

Further sampling details are specified in Table 2. I-1 and I-3 are stationary instruments, operated within a container, and connected to inlet lines of either $5\,\mathrm{m}$ at the $80\,\mathrm{m}$-tall mast or $60\,\mathrm{m}$ at the $325\,\mathrm{m}$-tall tower. I-2 is a transportable unit and was either placed in a container connected to the $5\,\mathrm{m}$ inlet or installed directly on the tall tower without an additional inlet. Particles were deposited onto silicon nitride (SiN) substrates of 5 x 5 mm dimension and a 100 or 150 nm thin membrane (Silson Ltd., Northhampton, UK & Norcada Inc., Edmonton, Canada). To ensure appropriate particle coverage on the substrate for single particle analysis, sampling duration was adjusted based on ambient conditions (Table 2). After collection, the samples underwent a preliminary quality check under a light microscope and were subsequently stored in airtight containers at $-20°\mathrm{C}$.

2.3.2 Sampling strategy and sample categories

Aerosol sampling took place during three intensive sampling campaigns in November 2021 (dry season), April 2022 (wet season), and December 2022 (transmission period from dry to wet season, overlapping with the CAFE-Brazil aircraft campaign). Day- and nighttime samples were collected to capture aerosol variations throughout the diel cycle. At ATTO, sunrise is at ~ 06:00 local time (LT) and sunset at ~ 18:00 LT. The onset of significant convective mixing is about 1 h after sunrise (Carneiro and Fisch, 2020; Henkes et al., 2021; Dias-Júnior et al., 2022). Therefore, we defined daytime here as 07:00 to 19:00 LT and nighttime as 19:00 to 07:00 LT. To capture aerosol variations across the forest canopy space, samples were collected at $60\,\mathrm{m}$), which is about $30\,\mathrm{m}$) above average canopy height and at $5\,\mathrm{m}$), well below the canopy. As this study focuses on the day-to-night contrast and the aerosol transport across the canopy space, the samples were categorized into four groups: **(i)** day-time samples at $60\,\mathrm{m}$, **(ii)** day-time samples at $5\,\mathrm{m}$, **(iii)** night-time samples at $60\,\mathrm{m}$, and **(vi)** night-time samples at $5\,\mathrm{m}$. Figure 2 illustrates this classification and the subsequent figures are designed in a panel-like layout, accordingly. Table 2 specifies details and the classification for all samples.

The primary objective of this study is the physicochemical analysis of the natural aerosol population under Amazonian wet season conditions. Accordingly, samples were classified into clean vs (moderately) polluted based on $\mathrm{M_{BCe}}$ levels at ATTO. Clean samples are defined as $\mathrm{M_{BCe}} < 0.15\,\mu\mathrm{g\,m^{-3}}$) and polluted samples as $\mathrm{M_{BCe}} > 0.15\,\mu\mathrm{g\,m^{-3}}$. The $\mathrm{M_{BCe}}$ threshold was selected according to previous studies: Pöhlker et al. (2018) defined $\mathrm{M_{BCe}} = 0.01\,\mu\mathrm{g\,m^{-3}}$ as pristine rain forest conditions with regard to the aerosol load. Holanda et al. (2023) showed that pristine conditions according to this definition account for only 7 % of the year at ATTO and are comparatively rare, accordingly. The threshold selected here (i.e., $\mathrm{M_{BCe}} < 0.15\,\mu\mathrm{g\,m^{-3}}$)) is a compromise between conditions that widely free from pollution, on one hand, and a reasonably high sample and particle statistics for the background conditions on the other hand (Figure 1 a). A sensitivity study showed that the results of the chemical analysis do not significantly change if different $\mathrm{M_{BCe}}$ thresholds are chosen. The following specific thresholds were tested: ($< 0.05\,\mu\mathrm{g\,m^{-3}}$, $< 0.10\,\mu\mathrm{g\,m^{-3}}$, $< 0.15\,\mu\mathrm{g\,m^{-3}}$, $< 0.20\,\mu\mathrm{g\,m^{-3}}$, $< 0.25\,\mu\mathrm{g\,m^{-3}}$, and $< 0.30\,\mu\mathrm{g\,m^{-3}}$, Figure 1 b – l).

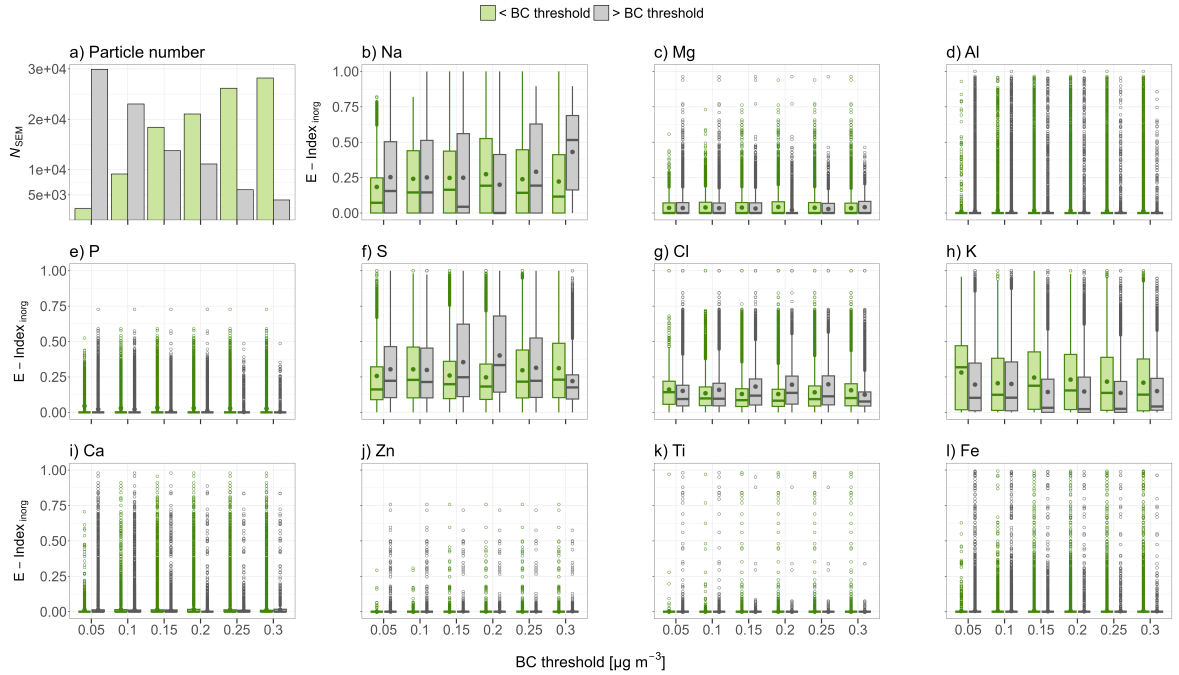

Figure 1. Sensitivity study to test the effects of the choice of black carbon mass concentration (M_{BCe}) threshold on the measured aerosol chemical composition. As a function of M_{BCe}, the variation in the number of analyzed particles (panel a) and the element index distributions for the following inorganic elements Na, Mg, P, S, Cl, K, Ca, Ti, Fe and Zn (E-index$_{inorg}$, panels b to l) are shown. Each individual sample is categorized by the mean M_{BCe} value calculated from a 30 min time interval before and 30 min after sampling. The bar plots in (a) show the number of particles detected on samples for given M_{BCe} category (below M_{BCe}: green, above M_{BCe}: grey). The box plots in (b to l) illustrate the E-index$_{inorg}$ (Equation 4) distribution. The median (horizontal line) and mean (dot) values are calculated from the E-index$_{inorg}$ of individual particles associated with each M_{BCe} threshold. The boxes represent the first and third quartiles, whiskers extend to the largest and smallest values within the 1.5 times interquartile range (IQR), and outliers are shown individually.

2.4 Scanning electron microscopy with energy dispersive x-ray analysis

The sampled Si_3N_4 (shortly SiN) substrates were analyzed with computer-controlled scanning electron microscopy using a FEI Quanta 400 FEG instrument (FEI, Eindhoven, the Netherlands) equipped, with energy-dispersive x-ray analysis (X-Max150, Oxford, Oxfordshire, United Kingdom), with the Oxford software AZtec (version 4.4). To ensure a consistently
145 low background signal by minimizing initial beam interactions with the sample substrate or instrumental surfaces, the SiN substrates were placed in a custom-built copper sample holder. Furthermore, scanned areas were selected exclusively on the SiN membranes and not on the silicon frame. The samples were analyzed in vacuum (~ 10^{-5} Pa) with an acceleration voltage

of 12.5 kV and a working distance of ∼10 mm. Samples were analyzed without pre-treatment or sputtering. In a first image acquisition pass, a backscatter electron image was acquired from which the particles were segmented from the background by image analysis based on a suitably adjusted threshold brightness. In a second step, the identified features (i.e. the particle cross sections) were scanned by the electron beam and the resulting x-ray spectrum was recorded. The x-ray signal collection time was adjusted to a minimum of 100 000 to yield a spectrum with suitable counting statistics for all elements of interest.

2.4.1 Element quantification in single particles

Element quantification for each spectrum was caried out using the automatic 'standard-less' (i.e. system-calibrated) x-ray quantification algorithms (ZAF correction systems) built-in into the manufacturer's software. Quantification was done for all elements with an atomic number number $Z < 4$. To ensure accurate quantification, sensitivity tests for the quantification threshold were done, yielding an optimum of 2.5 for the sigma level. This value allowed for identifying trace compounds while at the same time not over-interpreting statistical noise. The following elements were considered for interpretation: carbon (C), oxygen (O), sodium (Na), magnesium (Mg), aluminum (Al), phosphorous (P), sulfur (S), chlorine (Cl), potassium (K), calcium (Ca), titanium (Ti), iron (Fe), and zinc (Zn) (= E_x). Note that silicon (Si), nitrogen (N), and copper (Cu) concentrations could not be quantified due to the SiN substrate contributions and were therefore excluded from further analysis.

The software provided weight percentages ($wt\%$) for each detected element. For interpretation of the quantified data, atomic concentration ($at\%$) were used. To calculate $at\%$, the standard mole number (n) equation is used:

$$n_{E_x} = \frac{wt\%_{E_x}}{M_{E_x}} \tag{1}$$

where M represents the atomic mass and $wt\%_{E_x}$ is the mass of E_x in 100 g of the total mixture. The atomic concentrations are calculated for the elements E_x using the following equation:

$$at\%_{E_x} = \frac{n_{E_x}}{\sum n_{E_x}} \tag{2}$$

All ratio values given in this study refer to $at\%$. To measure the ratio of most abundant inorganic elements (i.e., E_i = Na, Mg, Al, P, S, Cl, K, Ca, Ti, Fe, Zn) to carbon within a particle, a salt-index is defined as

$$\text{salt-index} = \frac{\sum at\%_{E_i}}{at\%_C + \sum at\%_{E_i}} \tag{3}$$

In order to consider the inorganic elemental composition exclusively, another inorganic elemental index, representing the proportion of E_i within the inorganic fraction in a particle, is defined as

$$E_i\text{-index}_{inorg} = \frac{at\%_{E_i}}{\sum at\%_{E_i}} \tag{4}$$

The SEM-EDX data analysis and processing were done with RStudio (Posit team, 2023).

2.4.2 Particle sizing and sample quality assurance

The SEM image analysis determines the physical particle size as the equivalent circle diameter, D_{ec} (in the AZtec software defined as ECD). The D_{ec} is defined as

$$D_{ec} = \sqrt{\frac{4A}{\pi}} \tag{5}$$

and represents the diameter of a circular particle with the same projected area, A, as the area covered by the actual particle on the substrate.

To ensure the reliability of the EDX data, only particles $> 0.25\,\mu m$ were included for analysis. The microscope has a slight inherent inaccuracy in the positioning of the moving stage during scanning, resulting in small shifts and overlaps of the individual scanned fields. This effect required manual inspection and filtering of the image data. Specifically, cropped particles at the margins of individual fields as well as duplicated particles, appearing on two fields due to a shifted stage, were removed. Impaction-induced fragmentation, appearing as dispersed smaller particles near and/or around the primary particle, were also excluded. Detection artifacts, including features misinterpreted as single particles due to blurred or irregular boundaries of larger particles, as well as misinterpreted signals from background noise, were removed manually or mostly by the size limit selection ($> 0.25\,\mu m$).

All particles analyzed with SEM-EDX were grouped into 17 size bins as specified in Table 1. The bin limits were chosen according to the bin definitions of the OPS instrument (see Sect. 2.2) to ensure direct comparability of the results. The SEM-derived PNSDs are shown in Figure 2 for the clean and in Figure 3 for the (moderately) polluted sampling conditions. Each PNSD takes all particles of all samples of a given category (Sect. 2.3.2) into account. The resulting particle number concentrations within each bin (N_{SEM}) of the histograms in Figures 2 & 3 a, c, e, & g were not normalized by bin widths.

The SEM-derived PNSDs based on the physical particle diameters (D_{ec}) were compared with the corresponding OPS-derived PNSDs based on the optical particle diameters (D_o). For the comparison with the OPS-derived $dN_{OPS}/d\log D_o$ distribution, each SEM-derived PNSD was converted to $dN_{SEM}/d\log D_{ec}$ using the formula:

$$\frac{dN_{SEM}}{d\log D_{ec}} = \frac{\frac{N_{SEM}}{V} \times f_{spot}}{\log(\frac{D_u}{D_l})} \tag{6}$$

where V represents the total sample air volume in liters (Table 2), f_{spot} is a correction factor accounting for the smaller size of the analyzed area in relation to the entire sampling spot, and D_l and D_u represent the lower and upper bin limits in Table 1.

To test whether and across which size range the SEM-derived PNSDs agree with the OPS-derived PNSDs, both were compared for clean conditions in Figure 2 b, d, f & h and for polluted conditions in Figure 3 b, d, f & h. The comparison was conducted separately for the four sample categories defined in Sect. 2.3.2 because of the different impactors in use with their different

Table 1. Lower (D_l) and upper (D_u) size bins used for size classification of all particles analyzed with SEM-EDX. Bin definitions here were adopted from bin definitions of OPS instrument (see Sect. 2.2).

Size bin	D_l [µm]	D_u [µm]
1	0.25	0.30
2	0.30	0.37
3	0.37	0.46
4	0.46	0.58
5	0.58	0.72
6	0.72	0.90
7	0.90	1.12
8	1.23	1.40
9	1.40	1.73
10	1.73	2.16
11	2.16	2.69
12	2.69	3.34
13	3.34	4.16
14	4.16	5.18
15	5.18	6.45
16	6.45	8.03
17	8.03	10.0

sampling efficiencies and cut-off diameters (see Sect. 2.3). Figures 2 & 3 show that $\mathrm{d}N_{\mathrm{OPS}}/\mathrm{dlog}D_{\mathrm{o}}$ and $\mathrm{d}N_{\mathrm{SEM}}/\mathrm{dlog}D_{\mathrm{ec}}$ generally compare well for diameters larger $\sim$1 µm. For diameters smaller $\sim$1 µm, $\mathrm{d}N_{\mathrm{OPS}}/\mathrm{dlog}D_{\mathrm{o}}$ and $\mathrm{d}N_{\mathrm{SEM}}/\mathrm{dlog}D_{\mathrm{ec}}$ deviate depending on the impactor primarily used per sample category. Specifically, for both sample categories collected at 60 m height, the deviation is comparatively large because of the rather large cut-off diameter of impactor I-3 (i.e., D_{50} in the range of 0.9 – 1.4 µm) that was primarily used here. For both sample categories collected at 5 m height, the comparison $<$1 µm is much better because of the comparatively low cut-off diameter of impactor I-2 (i.e., D_{50} of ~ 0.36 µm) that was primarily used at this height. The PNSD comparison in Figure 2 and Figure 3 underlines that the particle ensemble analyzed by SEM-EDX is representative for the ambient aerosol population as detected by the OPS and that no major particles fractions are systematically lost, for instance, due to particle bouncing in the impactors.

The comparability in the accumulation mode size range (i.e., 0.25 to 1 µm), depends on the characteristics of the impactor used. For impactor I-2 with its relatively low cut-off diameter, we tested specifically the comparability of SEM-derived and OPS-derived PNSDs in Figure 4. A good agreement between $\mathrm{d}N_{\mathrm{SEM}}/\mathrm{dlog}D_{\mathrm{ec}}$ and $\mathrm{d}N_{\mathrm{OPS}}/\mathrm{dlog}D_{\mathrm{o}}$ was observed down to about 0.5 µm, which indicates that particularly for the I-2-samples a good representation of large particle tail of the accumulation mode was achieved. Through the systematic comparison of the PNSDs along with the assessment of the impactor collection

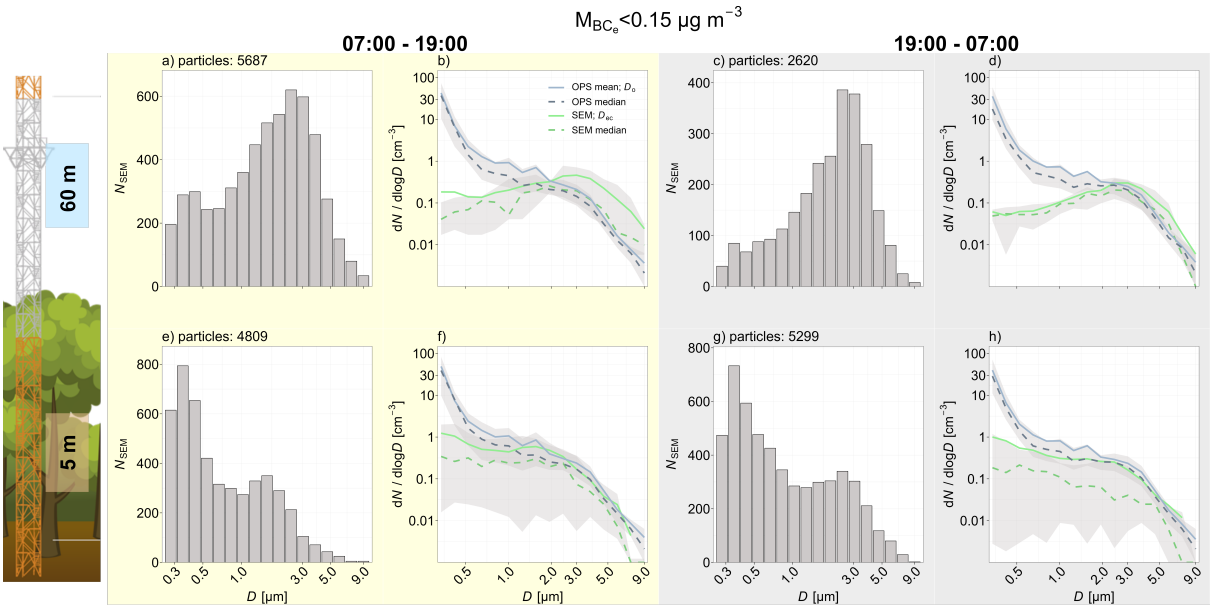

Figure 2. PNSDs from SEM measurements in comparison to OPS-derived PNSDs for the same sampling periods, associated to clean conditions ($M_{BCe} < 0.15\,\mu g\,m^{-3}$). Samples are distinguished between day at 60 m (a & b), night at 5 m (c & d), day at 5 m (e & f), and night at 60 m (g & h). Day is defined from 07:00 to 19:00 LT and night 19:00 to 07:00 LT. Data at 60 m refer to measurements above the canopy and data at 5 m were taken below the canopy. SEM-derived PNSDs are shown as bar plots (a, c, e & g) representing the cumulative PNSDs (N_{SEM}) including all samples in one category, and as corresponding $dN_{SEM}/d\log D_{ec}$ (b, d, f & g) representation (green), in comparison to OPS-derived $dN_{OPS}/d\log D_o$ (blue). Solid lines represent mean values, and dashed lines represent median values. Quantiles (25% to 75%) are represented by gray shading. The $dN_{SEM}/d\log D_{ec}$ values are calculated based on Equation 6. The $dN_{OPS}/d\log D_o$ values include data from the 30 min time intervals before and 30 min after the start of each sample collection.

efficiencies, we consider it unlikely that our results are systematically biased by impactor sampling artifacts within the covered particle size range.

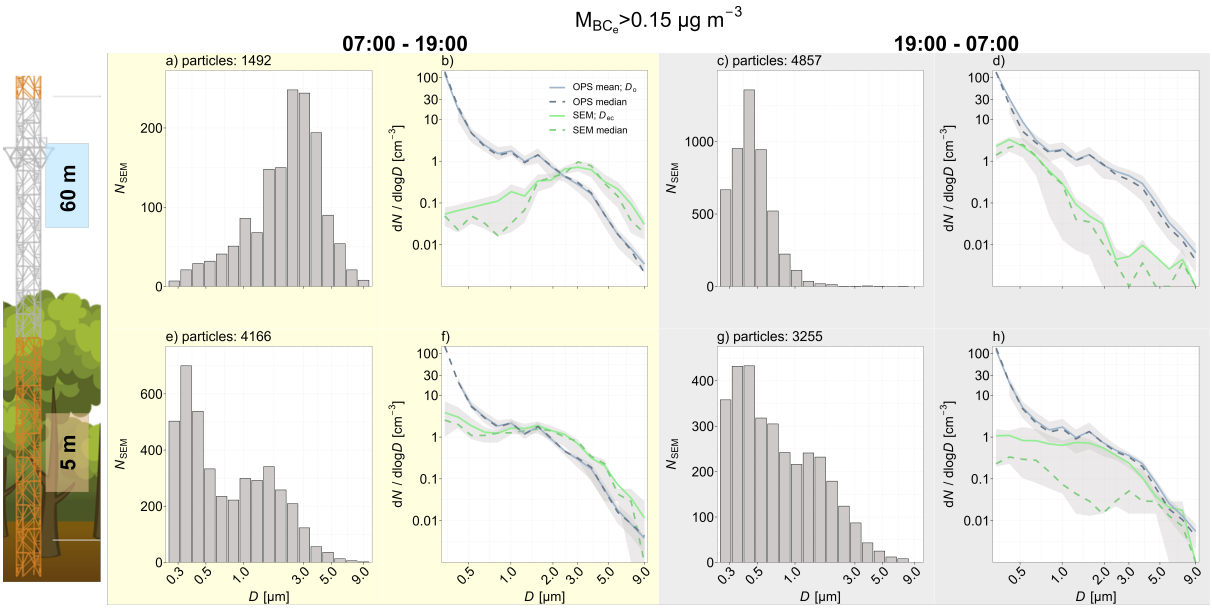

Figure 3. PNSDs from SEM measurements in comparison to OPS-derived PNSDs for the same sampling periods, associated to moderately polluted conditions ($M_{BCe} > 0.15\,\mu g\,m^{-3}$). Samples are distinguished between day at 60 m, (a & b), night at 60 m (c & d), day at 5 m (e & f), and night at 5 m (g & h). Day is defined from 07:00 to 19:00 LT and night 19:00 to 07:00 LT. Data at 60 m refer to measurements above the canopy and data at 5 m were taken below the canopy. SEM-derived PNSDs are shown as bar plots (a, c, e & g) representing the cumulative PNSDs (N_{SEM}) including all samples in one category, and as corresponding $dN_{SEM}/d\log D_{ec}$ (b, d, f & g) representation (green), in comparison to OPS-derived $dN_{OPS}/d\log D_o$ (blue). Solid lines represent mean values, and dashed lines represent median values. Quantiles (25% to 75%) are represented by gray shading. The $dN_{SEM}/d\log D_{ec}$ values are calculated based on Equation 6. The $dN_{OPS}/d\log D_o$ values include data from the 30 min time intervals before and 30 min after the start of each sample collection.

Table 2: Overview of all samples analyzed in this study. Table specifies: sample name; date and start time of collection in format [yyyy-mm-dd hh:mm in LT]; sampling height above ground H_s; sampling with or without sampling lines at tower (yes or no), * indicate dried sample air (RH ~ 40 %); type of impactor used (I-1, I-2, or I-3 – see Sect. 2.3); duration of sampling t_s; air volume sampled V_s; cut-off diameter considering type of impactor and flow rate D_50; and category of sample according to Sect. 2.3.2.

Name	Date	Start time	H_s [m]	Inlet	Imp	t_s [min]	V_s [L]	D_{50} [μm]	Category
60_211104_2	2021-11-04	07:11	60	y*	I-1	420	7	0.93	n60p
60_211104_3	2021-11-04	10:21	60	y*	I-1	420	7	0.93	n60p
05_211108_14	2021-11-08	23:22	5	y	I-1	600	10	0.84	n5p
05_211109_1	2021-11-09	02:17	5	y	I-1	600	10	0.84	n5p

Table 2 – continued from previous page

Name	Date	Start time	H_s [m]	Inlet	Imp	H_s [min]	V_s [L]	D_{50} [μm]	Category
05_211110_6	2021-11-10	08:52	5	y	I-1	600	10	0.84	n5p
05_211111_3	2021-11-11	08:13	5	y	I-1	600	10	0.84	n5p
60_211111_4	2021-11-11	08:25	60	y*	I-1	600	10	0.84	n60p
60_211111_5	2021-11-11	08:40	60	y*	I-1	600	10	0.84	n60p
05_220420_1	2022-04-20	03:00	5	y	I-1	1500	25	0.93	n5c
05_220420_2	2022-04-20	07:00	5	y	I-1	1500	25	0.93	n5c
05_220420_3	2022-04-20	09:00	5	y	I-1	1500	25	0.93	n5c
05_220420_4	2022-04-20	10:30	5	y	I-1	1500	25	0.93	n5c
05_220420_5	2022-04-20	12:00	5	y	I-1	1500	25	0.93	d5c
60_220420_1	2022-04-20	14:30	60	n	I-2	900	7.5	0.49	d60c
60_220420_2	2022-04-20	16:00	60	n	I-2	900	12.75	0.36	d60c
60_220420_4	2022-04-20	22:00	60	n	I-2	900	12.75	0.36	d60c
60_220421_1	2022-04-21	02:00	60	n	I-2	900	12.75	0.36	n60c
60_220421_2	2022-04-21	07:00	60	n	I-2	900	12.75	0.36	n60c
60_220421_3	2022-04-21	10:30	60	n	I-2	900	12.75	0.36	n60c
60_220423_1	2022-04-23	00:30	60	n	I-2	900	12.75	0.36	n60c
60_220423_4	2022-04-23	10:00	60	n	I-2	900	12.75	0.36	n60c
05_220423_1	2022-04-23	15:35	5	y	I-1	1800	30	0.93	d5c
60_220423_7	2022-04-23	18:00	60	n	I-2	900	12.75	0.36	d60c
05_220423_2	2022-04-23	18:00	5	y	I-1	1800	30	0.93	d5c
05_220423_3	2022-04-23	22:00	5	y	I-1	1800	30	0.93	d5c
60_220423_8	2022-04-23	22:00	60	n	I-2	1200	17	0.36	d60c
60_220424_1	2022-04-24	02:00	60	n	I-2	1200	17	0.36	n60c
60_220424_3	2022-04-24	09:30	60	n	I-2	900	12.75	0.36	n60c
05_220424_4	2022-04-24	19:00	5	y	I-1	1800	30	0.93	d5c
05_220424_7	2022-04-24	23:55	5	y	I-1	1800	30	0.93	n5c
05_220424_1	2022-04-24	23:55	5	n	I-2	1200	17	0.36	n5c
05_220425_1	2022-04-25	01:00	5	n	I-2	1200	17	0.36	n5c
05_220425_3	2022-04-25	09:30	5	y	I-1	1800	30	0.93	n5c
60_220425_3	2022-04-25	17:38	60	y	I-3	1080	11.7	0.93	d60c
05_220425_7	2022-04-25	17:49	5	y	I-1	1800	30	0.93	d5c
60_220425_4	2022-04-25	20:10	60	y	I-3	930	10.075	0.93	d60c
05_220426_1	2022-04-26	00:01	5	n	I-2	1200	17	0.36	n5p
05_220426_3	2022-04-26	06:00	5	n	I-2	1200	17	0.36	n5c
05_220426_4	2022-04-26	08:00	5	n	I-2	1200	17	0.36	n5c
60_220426_1	2022-04-26	12:27	60	y	I-3	1080	11.7	0.93	d60p

Table 2 – continued from previous page

Name	Date	Start time	H_s [m]	Inlet	Imp	H_s [min]	V_s [L]	D_{50} [μm]	Category
60_220426_2	2022-04-26	14:17	60	y	I-3	720	7.8	0.93	d60c
60_221207_7	2022-12-07	22:12	60	y	I-3	1080	5.4	1.41	d60c
05_221209_2	2022-12-09	04:01	5	y	I-2	180	2.55	0.36	n5c
05_221209_3	2022-12-09	08:00	5	y	I-2	180	2.55	0.36	n5c
05_221209_4	2022-12-09	12:00	5	y	I-2	180	2.55	0.36	d5c
60_221209_1	2022-12-09	12:27	60	y	I-3	720	3.6	1.41	d60c
05_221209_6	2022-12-09	15:00	5	y	I-2	180	2.55	0.36	d5c
05_221209_7	2022-12-09	16:00	5	y	I-2	180	2.55	0.36	d5c
05_221209_8	2022-12-09	17:00	5	y	I-2	180	2.55	0.36	d5c
05_221209_13	2022-12-09	23:00	5	y	I-2	180	2.55	0.36	d5p
05_221210_1	2022-12-10	02:00	5	y	I-2	180	2.55	0.36	n5p
05_221210_2	2022-12-10	05:00	5	y	I-2	180	2.55	0.36	n5p
05_221210_3	2022-12-10	08:00	5	y	I-2	180	2.55	0.36	n5p
05_221210_5	2022-12-10	16:00	5	y	I-2	180	2.55	0.36	n5p
05_221210_6	2022-12-10	23:00	5	y	I-2	180	2.55	0.36	d5p
05_221213_1	2022-12-13	02:00	5	y	I-2	180	2.55	0.36	n5p
60_221213_2	2022-12-13	14:00	60	y	I-3	900	4.5	1.41	d60p
05_221213_4	2022-12-13	14:00	5	y	I-2	180	2.55	0.36	d5p
60_221217_2	2022-12-17	15:00	60	y	I-3	900	9.75	0.93	d60c
05_221217_4	2022-12-17	15:30	5	y	I-2	210	2.975	0.36	d5c
05_221217_5	2022-12-17	18:00	5	y	I-2	210	2.975	0.36	d5c
60_221217_1	2022-12-17	18:00	60	y	I-3	900	9.75	0.93	d60c
05_221218_1	2022-12-18	03:00	5	y	I-2	210	2.975	0.36	n5c
05_221218_2	2022-12-18	05:00	5	y	I-2	210	2.975	0.36	n5c
60_221218_1	2022-12-18	05:00	60	y	I-3	900	9.75	0.93	n60c
05_221218_3	2022-12-18	09:00	5	y	I-2	210	2.975	0.36	n5c
05_221218_4	2022-12-18	12:00	5	y	I-2	210	2.975	0.36	d5c
05_221218_5	2022-12-18	17:00	5	y	I-2	210	2.975	0.36	d5c
05_221219_3	2022-12-19	09:00	5	y	I-2	180	2.55	0.36	n5c
05_221219_4	2022-12-19	12:30	5	y	I-2	240	3.4	0.36	d5c
60_221219_3	2022-12-19	12:30	60	y	I-3	900	9.75	0.93	d60c
05_221219_5	2022-12-19	18:00	5	y	I-2	240	3.4	0.36	d5p
60_221219_4	2022-12-19	18:00	60	y	I-3	900	9.75	0.93	d60p

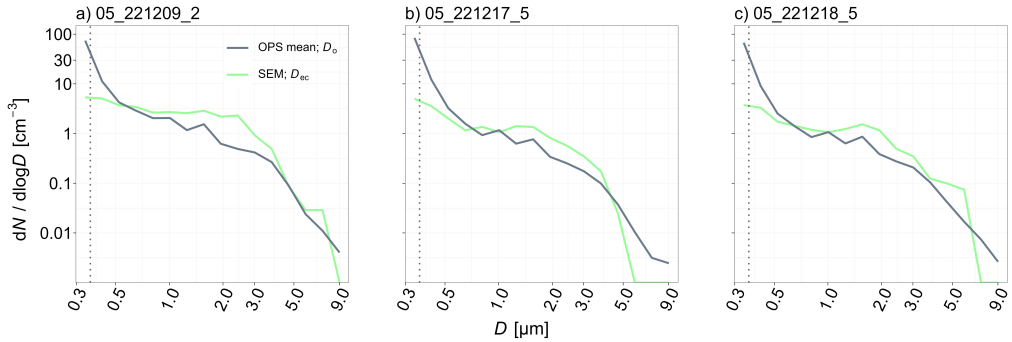

Figure 4. PNSDs from SEM measurements of three selected samples (05_221209_2, 05_221217_05 & 05_221218_5), compared with OPS-derived PNSDs for the respective sampling periods. SEM-derived $\mathrm{d}N_{\mathrm{SEM}}/\mathrm{dlog}D_{\mathrm{ec}}$ (green) is shown along with OPS-derived mean $\mathrm{d}N_{\mathrm{OPS}}/\mathrm{dlog}D_{\mathrm{o}}$ (blue). All three samples are collected with impactor 2, which exhibits a D_{50} of ~ 0.36 µm (dashed vertical line).

3 Results and discussion

3.1 Elemental composition in clean and polluted samples

Based on the single particle SEM-EDX measurements the overall elemental particle composition has been examined and is shown in Figure 5. This analysis distinguish between the clean ($M_{BCe} < 0.15\,\mu g\,m^{-3}$, Figure 5 a, b & c) and moderately polluted ($M_{BCe} > 0.15\,\mu g\,m^{-3}$, Figure 5 d, e & f) sample set. As already indicated in Figure 1 in Section 2.3.2, the overall elemental composition shows almost identical patterns with slight variations between clean and more polluted samples. Ratios remain consistent, with minor variations observed mainly in absolute numbers. Therefore, the observations described here apply to both conditions.

Carbon is the most dominant element and accounts for > 60 % of the total composition, while oxygen makes up ~ 30 %, and the inorganic fraction (Na, Mg, Al, P, S, Cl, K, Ca, Ti, Fe, Zn) contributes 5 % (Figure 5 a & d). Figure 5 b & e shows the salt-index distribution, which reflects the variation in the inorganic fraction across aerosol particles (Equation 3). The inorganic elemental composition (C and O excluded) is shown in Figure 5 c & f. The prevailing elements within the inorganic fraction include sodium, sulfur, chlorine and potassium. Magnesium and phosphor make up only a small amount, followed by a small fraction of aluminium, calcium and some traces of titanium, iron and zinc. The salt-index is expressed by the ratio of carbon to the remaining inorganic elements (Equation 3), where higher salt-index values indicate a higher proportion of salts. A salt-index of zero (C 100 %) indicate particles composed entirely of carbon, or at least where no other inorganic element is detected. Note that oxygen is not included in this analysis. The majority of particles are dominated by carbon, but more than 99 % have a salt-index > 0 and are mixed with a various fraction of diverse inorganic elements (Figure 5 b & e).

Potential sources of inorganic constituents within the Amazonian aerosol population are diverse and depend on seasonal fluctuations and the episodic occurrence of LRT (Saturno et al., 2018; Pöhlker et al., 2018; Moran-Zuloaga et al., 2018; Holanda et al., 2020). The main sources include combustion and industrial processes, mineral dust (MD), sea spray (SSA) and biological material. Combustion processes, especially slash-and-burn fires in the Amazon region, but also from Africa, can contribute large amounts of BB aerosol, typically associated with

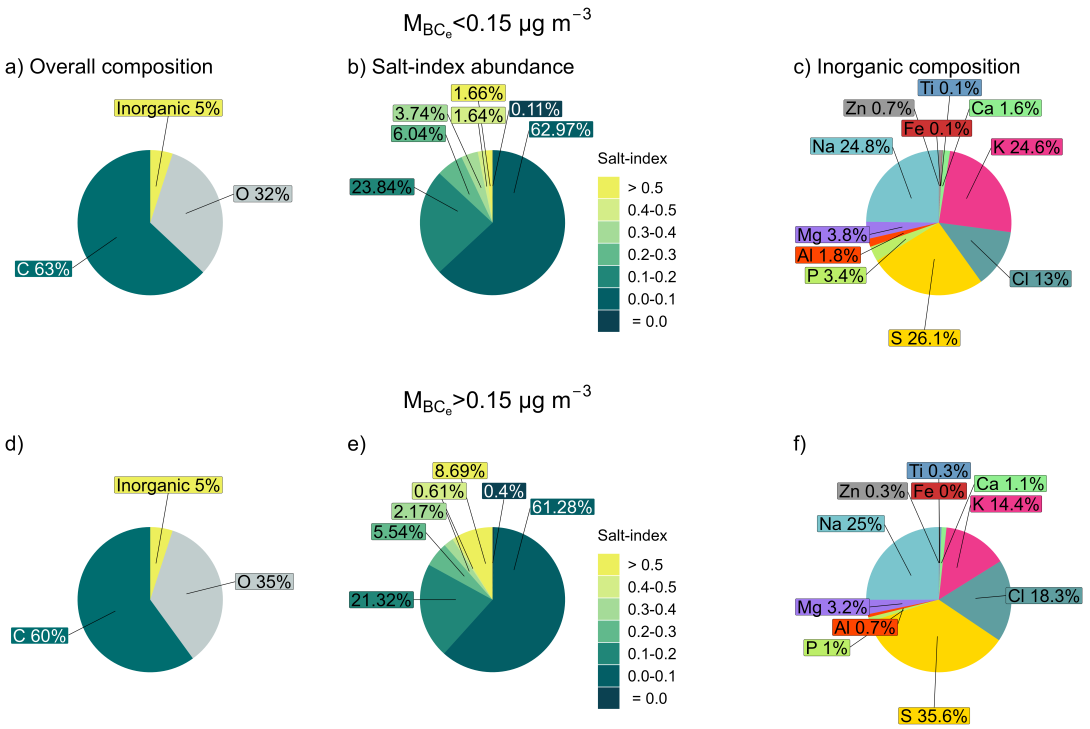

Figure 5. Analysis of the aerosol particle composition comparing clean samples ($M_{BCe} < 0.15\,\mu g\,m^{-3}$, a – c) and moderately polluted ($M_{BCe} > 0.15\,\mu g\,m^{-3}$), d – f). The pie charts show the overall carbon, oxygen and inorganic contribution in a & d, the salt-index distribution, representing the salt (inorganic) fraction within individual particles (Equation 3), with higher salt-index values indicating a higher proportion of salt in b & e, and the inorganic elemental composition (E_i, Equation 4) in c & f.

elements such as phosphorus, potassium, or sulfur (e.g. Andreae, 1983; Li et al., 2003; Barkley et al., 2019; Adachi et al., 2020). To check the potential effects of pollution, the relation between M_{BCe} as an BB marker, on individual elemental concentrations was analyzed (Figure 6). The Spearman correlation analysis shows a significant (p-value < 0.05), but slight negative correlation with M_{BCe} only for phosphorus (R = -0.32, Figure 6 e) and potassium (R = -0.35, Figure 6 h). Zinc shows a slight significant positive correlation with M_{BCe} (R = 0.30, Figure 6 j). These findings suggest that within the analyzed levels of atmospheric pollution (e.i. M_{BCe} approaching zero up to ~ $0.35\,\mu g\,m^{-3}$) the aerosol elemental composition seems to be not affected by BB aerosol. Contrary to expectations of a substantial increase in characteristic BB tracers such as potassium and phosphorus, their levels tend to decrease, confirming the mostly undisturbed aerosol conditions.

In addition, a potential relationship between accumulated precipitation (P_{BT}) and the abundance of individual elements was tested (Figure 7). P_{BT} is a measure of the amount of precipitation and subsequent aerosol scavenging during the atmospheric transport of air masses. Higher P_{BT} values indicate a higher contribution from local emission sources and a decrease or absence of LRT aerosol (Moran-Zuloaga et al.,

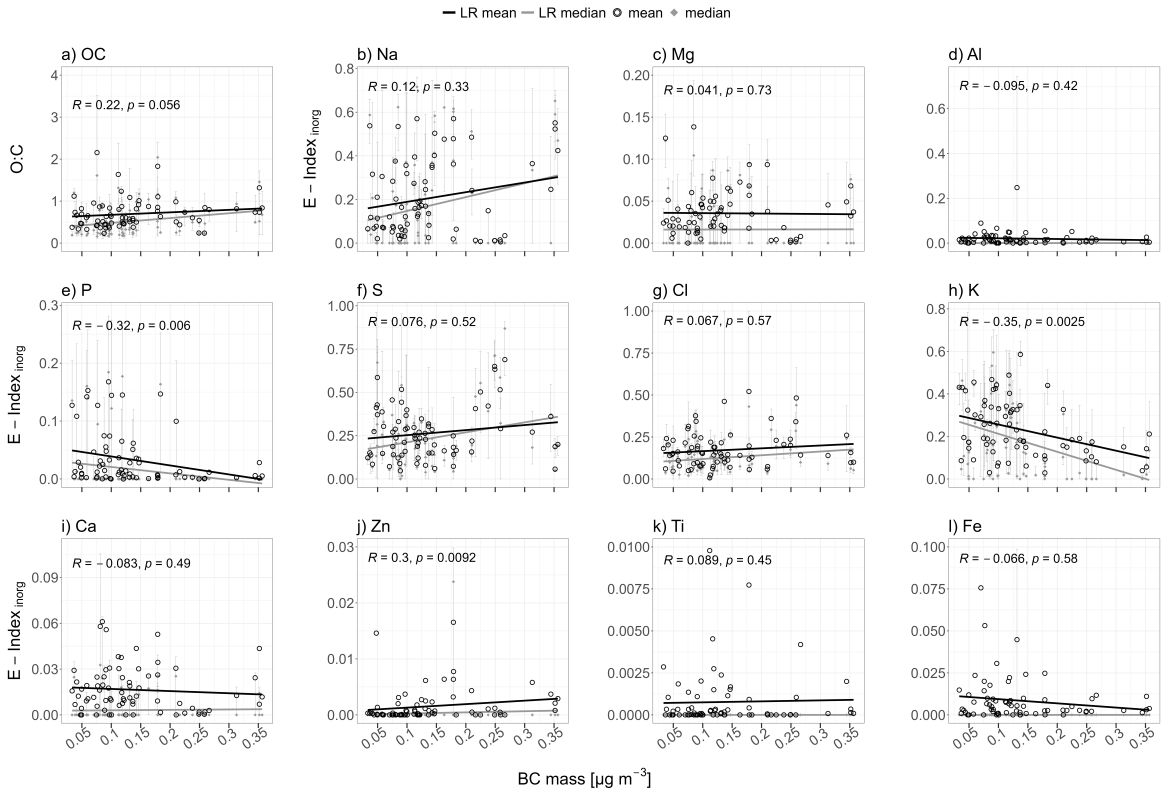

Figure 6. Relationship between ambient black carbon mass (M_{BCe}) and aerosol particle composition metrics: Oxygen to carbon ratio (O:C, a) and inorganic element index for Na, Mg, P, S, Cl, K, Ca, Ti, Fe and Zn (E-index$_{inorg}$, b – l). Mean (black circles) and median (grey squares) values, along with error bars representing the first and third quartiles, are calculated from the E-index$_{inorg}$ of individual particles associated with each sample. The linear regression lines (LR) are fitted to the mean (black line) and median (grey line) values. The Spearman correlation coefficient (R) together with the corresponding p-value show the strength and significance of the relationship between M_{BCe} and samples' mean E-index$_{inorg}$. M_{BCe} represent the mean value calculated from a 30 min time interval before and 30 min after sampling. Each element has its individual y-scale.

2018; Pöhlker et al., 2019). MD is typically related to LRT and originates mostly from the Sahara Desert in Africa (Swap et al., 1992; Rizzolo et al., 2017; Barkley et al., 2019). It is linked to an increase in BC and typically traced by elements such as silicon, aluminum, and iron (Moran-Zuloaga et al., 2018). Additionally, SSA is typically associated with the plume-wise injection of BB and MD (Moran-Zuloaga et al., 2018), but can also occur separately (). Particular SSA tracers are sodium and chlorine but also magnesium, potassium and calcium (Lewis and Schwartz, 2004; Quinn et al., 2015; Salter et al., 2016). Similar to the M_{BCe} sensitivity study, most of the trends for the relationship between P_{BT} and individual elements are mostly not statistically significant, indicating independence from LRT. Therefore,

255 a significant contribution of MD can be neglected. This is confirmed by the low concentrations of MD tracer elements such as aluminum and iron. However, the Spearman correlation analysis shows a significant negative correlation with P_{BT} for sodium (R = -0.50, Figure 7 b) and magnesium (R = -0.43, Figure 7 c), indicating a potential effect of LRT on sodium and magnesium concentrations, indicating a potential impact of SSA.

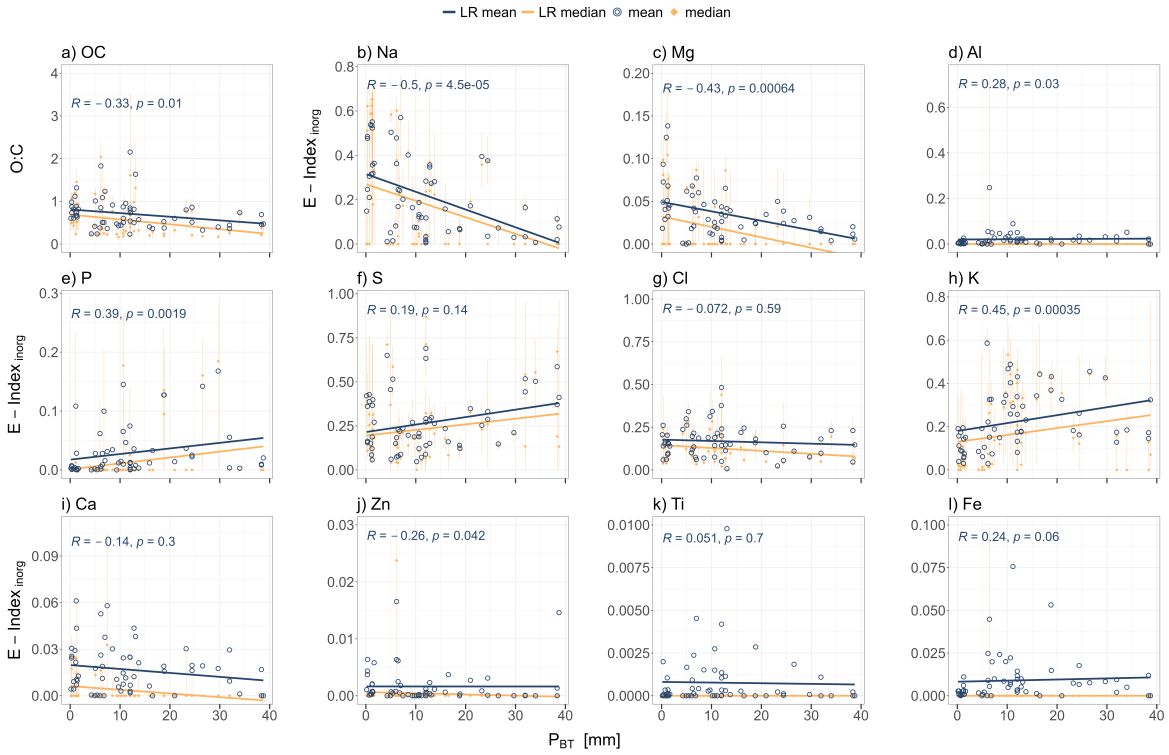

Figure 7. Relationship between HYSPLIT-retrieved accumulated precipitation (P_{BT}) and aerosol particle composition metrics: Oxygen to carbon ratio (O:C, a) and inorganic element index for Na, Mg, P, S, Cl, K, Ca, Ti, Fe and Zn (E-index$_{inorg}$, b – l). Mean (blue circles) and median (orange squares) values, along with error bars representing the first and third quartiles, are calculated from the E-index$_{inorg}$ of individual particles associated with each sample. The linear regression lines (LR) are fitted to the mean (blue line) and median (orange line) values. The Spearman correlation coefficient (R) together with the corresponding p-value show the strength and significance of the relationship between P_{BT} and samples' mean E-index$_{inorg}$. P_{BT} represent the mean value calculated from a 3 hour time interval before sampling. Each element has its individual y-scale.

Inorganic elements like sodium, sulfate, chlorine and potassium are known to be present in living organisms. They are involved in various
260 metabolic processes, osmoregulation, enzyme activity, and other regulatory processes in biological organisms ranging from microbes to

higher plants (e.g. Kelly et al., 1997; Maathuis, 2009; Benito et al., 2014, and references therein). Potassium is one of the most common elements in most living cells (Benito et al., 2002; Johnson et al., 2022). Phosphorus, in particular, is also characteristic of material of biological origin due to its essential role as a component of DNA and cell membranes (Raghothama, 2005). Consequently, PBAPs typically carry a mixture of these inorganic elements, with potassium and phosphorus being particularly characteristic tracer elements (e.g. Artaxo et al., 1990; Pöhlker et al., 2012; Arana et al., 2014; Wu et al., 2019). While this is particularly true for PBAPs in the coarse mode size range ($>1\,\mu m$, such as fungal spores or plant and animal debris, the identity of biogenic particles in the fine mode size range ($<1\,\mu m$ is largely unexplored. A particular difficulty is the low concentration of phosphorus, which may be below the detection limit in small particles and therefore unavailable as a biogenic tracer. Within the current sample set significant positive correlations are shown for phosphorus ($R = 0.39$, Figure 7 e) and potassium ($R = 0.45$, Figure 7 h). These results suggest that these elements are related to local biogenic sources, rather than BB aerosol or MD from LRT.

Previous studies have suggested that inorganic ions could be emitted into the atmosphere through the transpiration of plants (Nemeryuk, 1970; Kazarov and Plieva, 1989; Beauford et al., 1977; Jayaratne et al., 2011). In addition, fungal spores, including active release mechanisms as well as bursting, are suggested as a significant source of potassium (Elbert et al., 2007) or sodium (China et al., 2016, 2018). However, knowledge of mechanisms that could lead to the transfer of inorganic species to the atmosphere is sparse. Therefore, the analysis in the next section focuses on the natural aerosol in order to observe the biogenic emissions in more detail. Despite initial results showing slight effects of pollution and MD on all samples, the study narrows its focus to only clean samples for a analysis of Amazonian natural aerosols, excluding moderately polluted samples. Therefore, this strategy can confidently exclude the contribution of BB aerosol to the observed elemental composition, providing a reference for mostly natural conditions.

3.2 Variability in elemental concentrations

The clean aerosol samples were categorized into four different environmental conditions: **(i)** day-time samples at $60\,m$, **(ii)** day-time samples at $5\,m$, **(iii)** night-time samples at $60\,m$, and **(vi)** night-time samples at $5\,m$ (Section 2.3.2). Additionally, the particles have been divided into 17 size bins (Table 1). Following this approach, the abundance size distributions for the total salt-index and individual elements sodium, magnesium, potassium, calcium (cation forming) and phosphorus, sulfur and chlorine (anion forming) are shown in Figure 8. Analogous to this structure, the O:C ratio as a function of particle size together with the salt and individual element indices are shown in Figure 9. This approach allows for size-resolved analysis of the particle data set.

Salt-index: The salt index distributions in Figure 8 & 9 show that the the majority of particles are dominated by carbon. However, more than 99 % have a salt-index >0, indicating that the particles to contain a varying fraction of diverse inorganic elements. This estimate only applies to the particles that are successfully detected. It does not take into account potential losses of purely organic matter, which may occur due to vacuum degradation, detection limitations and damage caused by the electron beam. Although carbon dominated particles (salt-index <0.5) are the predominant particle type, the size resolved presentation suggest an ubiquitous presence of inorganic salts over the entire size range. This finding makes it worth noting that inorganic salts are consistently present in detected aerosol particles. Figure 9 shows the general trend that more salty particles exhibit higher oxygenation level (higher O:C ratio value) for all conditions. In order to explore the variability of inorganic elements the following section focuses on the analysis of the inorganic composition. To explore the variability of inorganic

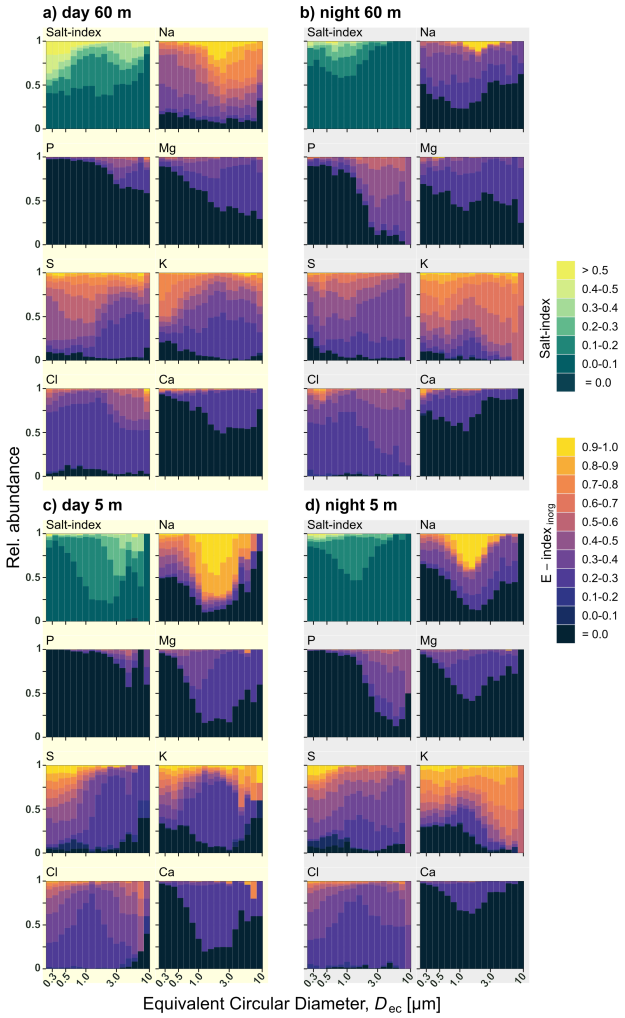

Figure 8. Index abundance size distributions for sodium (Na), potassium (P), magnesium (Mg), sulfur (S), potassium (P), chlorine (Cl) and calcium (Ca). The distributions show the temporal and spatial variations of aerosol elemental composition for day at 60 m (a), night at 60 m (b), day at 5 m (c), and night at 5 m (d) conditions. The salt-index indicates the fraction of inorganic element, described as salt to carbon ratio (Equation 3) with higher values indicating a greater proportion of salt. The E_i-index$_{inorg}$ quantifies each E_i fraction within the inorganic composition (Equation 4), with higher index values indicating a higher fraction of the respective element. Particles are categorized by their D_{ec} into size bins, according to the bin limits defined in Table 1. The height of each bar corresponds to the relative abundance of particles that fall in a particular index range (indicated by the color code) within a given size bin.

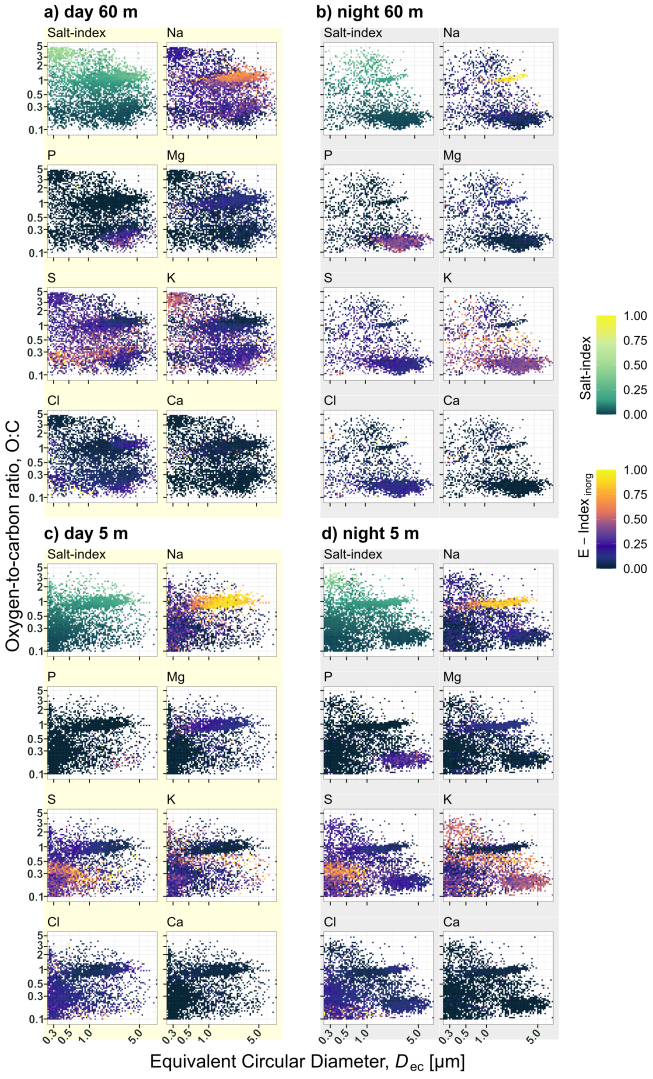

Figure 9. Oxygen to carbon ratio (O:C) as a function of particles size (D_{ec}) together with the E_i-index$_{inorg}$ for sodium (Na), potassium (P), magnesium (Mg), sulfur (S), potassium (P), chlorine (Cl) and calcium (Ca) represented by the color code. The distributions show the temporal and spatial variations of aerosol elemental composition for day at 60 m (a), night at 60 m (b), day at 5 m (c), and night at 5 m (d) conditions. The salt-index indicates the fraction of inorganic element, described as salt to carbon ratio (Equation 3) with higher values indicating a greater proportion of salt. The E_i-index$_{inorg}$ quantifies each E_i fraction within the inorganic composition (Equation 4), with higher index values indicating a higher fraction of the respective element.

elements, the following section focuses on the analysis of inorganic composition. Information on inorganic elemental concentrations refers only to the inorganic fraction of individual particles based on the calculated E_i-index$_{inorg}$ (equation 4, excluding carbon and oxygen).

Sodium: The Na-index size distributions show that sodium is not ubiquitous in the collected particles (Figure 8). At night, ~40 % of the particle lack sodium (Figure 8b & d). During day, sodium is more abundant with >50 % of the particles having an index >0.4 (Figure 8 a) & i)).

Magnesium and calcium: The Mg- and Ca-index size distributions show that the presence of magnesium and calcium appears to be related to sodium. Although the concentrations of magnesium and calcium are much lower than those of sodium, their distributions are mostly similar and there is a positive correlation among all three elements over the entire size range under all conditions (Figure10). Additionally, in the coarse mode range chlorine shows a significant positive correlation with all these elements (Figure10 b, d, f & g).

Sulfur: The analysis of the S-index size distributions show that sulfur is with >95 % of particles containing sulfur, present in almost all collected particles under all conditions (Figure 8). However, even if present in small amounts the majority of the particles have a relatively low sulfur content, with an index between 0 and 0.4. Especially at 5 m within the fine mode range, sulfur shows a significant positive correlation with chlorine Figure10 e & g) where also their distributions are similar (Figure 8 c & d).

Potassium: The K-index size distributions reveal that at 60 m with >90% the majority of particles contain potassium (Figure 8 a & b). At 5 m ~20 % lack potassium (Figure 8 c & d), but particles with increased concentrations are more prevalent. Potassium shows a slight increase in the fine mode range, but especially in the coarse mode (Figure 8).

Phosphorous: The P-index size distribution show that phosphorus is mostly detected within the coarse mode, in particular within the >3 µm range. Here the presence of phosphorous is connected to potassium (Figure 8 & 9).

Chlorine: The Cl-index size distributions across all conditions show that >94% of the collected particles contain chlorine (Figure 8). However, with >95 % of the particles have an index <0.4, and >75 % have an index <0.2, the majority has a relative low chlorine content.

3.3 Particle classes

The aerosol particle classification process categorized each particle according to its inorganic composition. This classification was primarily determined by the concentration of the major elements sodium, sulfur, and potassium within each particle. A particle is assigned to a particular class when the inorganic fraction of that particle is made up of at least 60% of a specific element. This can be numerically represented by an element index that is >0.6. Chlorine is not attributed to a specific particle, due to its overall low concentration in individual particles. Resulting classes are sodium-dominated (Na-rich), sulfur-dominated (S-rich), and potassium-dominated (K-rich) particles. Given its important role in biogenic matter, the concentration of phosphorus in the particles was also considered. However, the threshold set for phosphorus was comparatively lower, with a particle requiring only a 10% concentration of phosphorus to be classified as phosphorous-rich (P-rich). This is represented by a phosphorus index greater than 0.1 (P-index >0.1). The classes are examined for morphological features. The measurements are not specifically designed to produce high quality images, but rather for efficient elemental quantification. The resulting images, however, allow the observation of specific particle class characteristics. In addition, particles that could not be assigned to a class using this procedure were assigned to the total inorganic element concentration, resulting in low-salt, high-salt, and carbon-dominated (C-rich) particles.

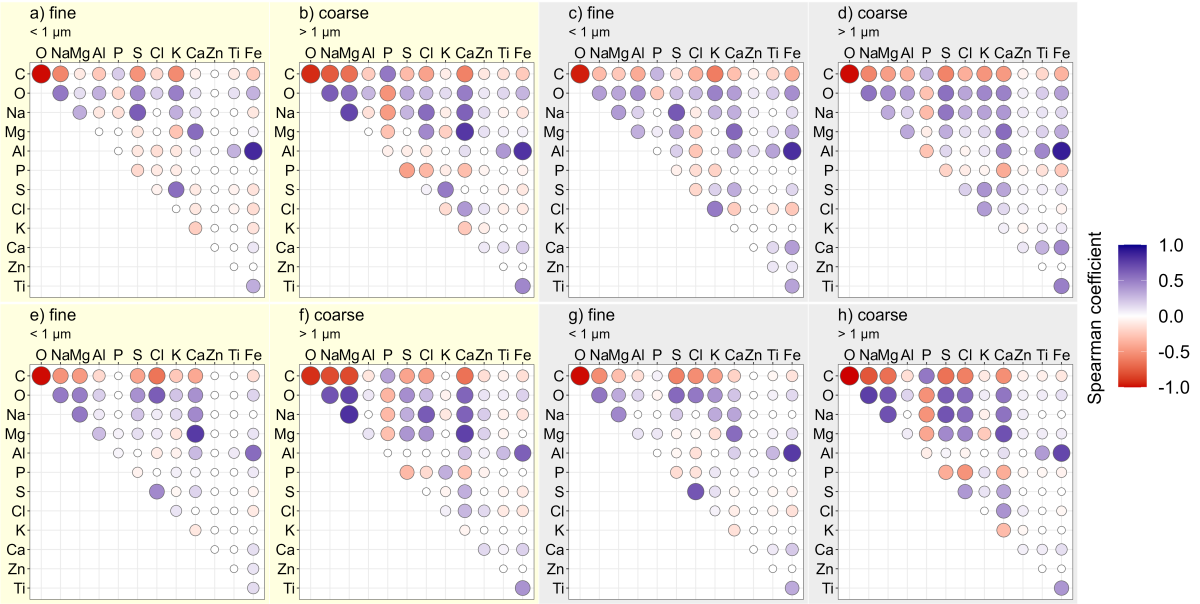

Figure 10. Spearman correlation analysis to investigate the elemental co-occurrence at the single particle scale within the aerosol fine mode (0.25 – 1 µm) and coarse mode (1 – 10 µm) ranges under different aerosol conditions: day at 60 m (a & b), night at 60 m (c & d), day at 5 m (e & f), and night at 5 m (g & h). The strength and direction of the Spearman correlation coefficient (R) are visually represented by the colour and size of the circles, indicated in the colour code. Circles with a bluish color and large size indicate a strong correlation, while a reddish colour with a small circle indicates a weak correlation. Only correlations with R significantly different from zero (p-value <0.05) are shown, while non-significant correlations are shown as white circles.

3.3.1 Na-rich particles

Na-rich particles are characterized by a Na-index > 0.6. Within the remaining inorganic fraction magnesium, sulfur, and chlorine make up the largest fraction. Na-rich particles contribute to the saltier particles, with > 50 % having a salt-index ranging between 0.15 and 0.2. These particles show distinct O:C ratio values centered around 1, but range from ~ 0.8 to 1.2 (Figure 9). As a result, the salt-index distributions are predominantly influenced by the sodium concentrations. The Na-rich class forms a well-defined mode in a size range between 0.5 and 5 µm, peaking at ~ 2 µm. Na-rich particles exhibit a largely uniform round shape, with an internal heterogeneous appearance (Figure 11). The morphology implies the formation of an amorphous organic shell that encloses inorganic components, visible as bright enclosures.

The Na-rich class is most abundant during the day at 5 m, accounting for ~ 25 % of the particles (Figure 15 c). This fraction decreases at 5 m during the night (12 % Figure 15 d), similar at 60 m (17 %, Figure 15 a), and becoming even less at 60 m during the night (5 %, Figure 15 b). Compared to other particle classes such as K-rich, high- and low-salt particles, Na-rich particles show a clearly emerging mode with distinct characterization properties in terms of size, morphology and chemistry. They are one of the most common particles in all conditions, making them a subject of particular interest. For this reason, their possible sources and interactions will be the subject of further discussion.

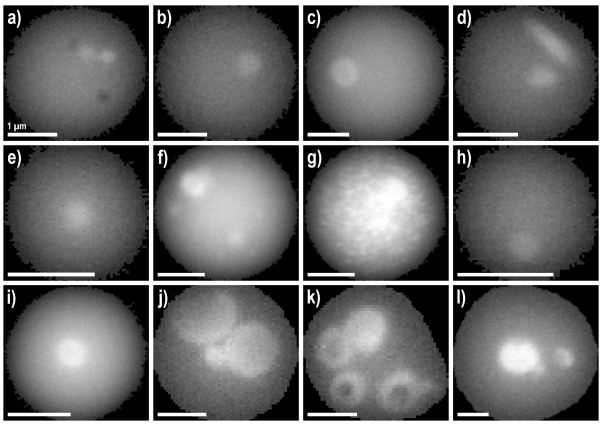

Figure 11. Representative selection of sodium dominated particles showing characteristic morphologies within the identified Na-rich particle class (Na-index > 0.6). The images provide a visual overview of the predominantly uniform structures observed within the Na-rich category. The particles have a round shape with an internal heterogeneous appearance suggesting the formation of an amorphous organic shell enclosing inorganic components visible as bright cores or partially crystalline structures. The backscattered electron images were acquired during a first image acquisition pass for automated SEM-EDX single particle analysis. Each scale bar corresponds to 1 µm.

In the current sample set, the primary origin of the Na-rich particle class cannot be conclusively determined. Both, local and transport related origins are considered. Based on an increase in the abundance of Na-rich particles within the 5 m samples, compared to the 60 m samples, a primary local source of Na-rich particles can be assumed. Assuming that the highest concentration of particles is near the source, it can be concluded that a local source below the canopy is likely. If spores were the source of the Na-rich particles as suggested by (China et al., 2016, 2018), a parallel increase in Na-rich and spore occurrence would be expected. However, there is no evidence of a direct relationship between the occurrence of Na-rich particles and the presence of spores and other PBAPs (represented by P-rich particles). SSA might be another, transport related source for sodium. Although a primary local origin of sodium within the forest is not excluded, LRT is another likely source of the Na-rich particles that must be considered. Although the Na-rich particles have a significantly lower chlorine concentration than typical SSA, the presence of magnesium in particular is indicative of an SSA origin. Therefore, the Na-rich particles are likely to represent atmospherically aged, chlorine-depleted SSA (Laskin et al., 2012; Chen et al., 2021). This assumption is supported by the comparison of the morphology of the Na-rich particles in this study with that observed for originally sodium chloride particles mixed with organic acids that underwent chloride depletion by (Laskin et al., 2012), which looks similar 11. Nevertheless, the presence of Na-rich particle might be affected by SSA and non-SSA related processed.

3.3.2 S-rich particles

S-rich particles are characterized by a S-index > 0.6. Most of these S-rich particles represent only a small inorganic fraction, falling within a salt-index range of < 0.05, and exhibit O:C ratio values between 0.2 and 0.5 (Figure 9. The particles tend to be more S-rich the higher their oxygen content. Beside sulfur, chlorine represents the largest fraction and is often the only inorganic element other than S that can be detected. As S-rich classified particles are common within the fine size range (< 1 µm), especially those with an index > 0.8, where also

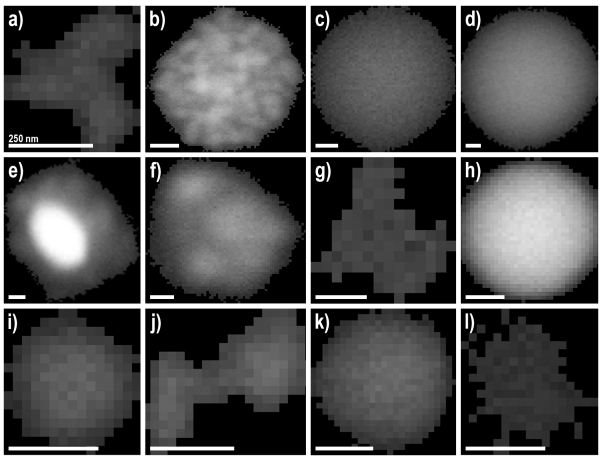

Figure 12. Exemplary selection of sulfur dominated particles showing individual morphologies within the identified S-rich particle class (S-index > 0.6). The backscattered electron images were acquired during a first image acquisition pass for automated SEM-EDX single particle analysis. Each scale bar corresponds to 250 nm.

the correlation analysis shows a relation with small amounts of chlorine (Figure 10 e & f). In the coarse mode range, S-rich particles are rarely found. The S-rich show individual morphologies. Within an exemplary selection of S-rich particles in the size range between 0.35 and 2.0 µm (Figure 12, some show an irregular shape while others are more spherical (Figure 12). For the smaller particles, further morphological features cannot be observed due to the limited resolution of the images. However, examples of larger particles with mostly spherical shapes show partially homogeneous, but also internally heterogeneous textures with bright enclosures. S-rich particles are particularly abundant at 5 m during day and night (14 % & 16 % Figure 15 c & d). During the day at 60 m the S-rich fraction is significant lower (5 %), almost absent during the night (1 %), and spans almost equally over the entire size range (Figure 15 a & b).

3.3.3 K-rich particles

K-rich particles are characterized by a K-index > 0.6. In addition to potassium, sulfur makes up the largest fraction of these particles, followed by chlorine and sodium. The particles occur in diverse oxygenation levels, with a salt-index primarily ranging between 0.03 and 0.1. In contrast to the Na- and S-rich particles this class do not conform to a specific size range. Like S-rich particles, the K-rich class show individual morphologies (Figure 13). An exemplary selection of particles between 1.3 and 5 µm is shown in Figure 13. Some particles are irregular in shape, others are more spherical. Most images suggest a heterogeneous mixture. Some show core-shell-like features with bright enclosures of partially crystalline structure. In addition to the selected examples in Fugure 13, a huge fraction of particles with typical morphology of PBAPs, especially spores, similar to those shown in Figure 14 are identified within the K-rich class. Due to a selection bias, fine mode K-rich particles are not well represented in this image selection. This under-representation is due to their inherently low contrast, which results in reduced visibility. The K-rich particles are most abundant during the night at 5 m (17 % Figure 15 d). During night at at 60 m and day at 5 m the K-rich fraction is lower (< 10 %, Figure 15 b & c), and almost absent during day at 60 m (1 %, Figure 15 a).

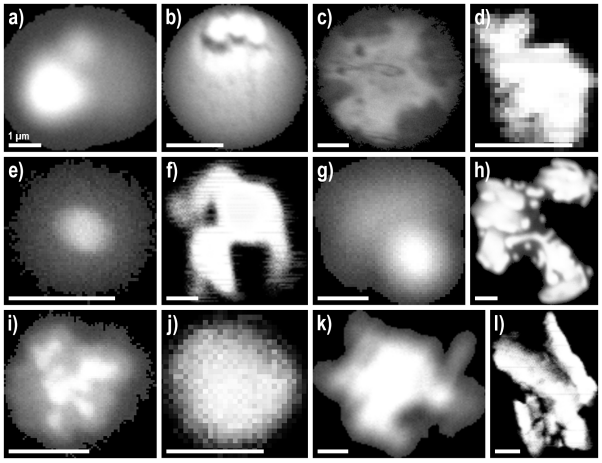

Figure 13. Exemplary selection of potassium dominated particles showing individual morphologies within the identified K-rich particle class (K-index > 0.6). The images provide a visual overview of the diverse structures of K-rich particles in a size range between 1.3 and 5 µm. The backscattered electron images were acquired during a first image acquisition pass for automated SEM-EDX single particle analysis. Each scale bar corresponds to 1 µm.

3.3.4 P-rich particles

P-rich particles are characterized by a P-index > 0.1. This threshold means that the particles classified as P-rich can still be potassium dominated. This class has a minimal salt fraction where most particles showing a salt-index < 0.02. Within their inorganic fraction, P-rich particles are dominated by potassium, followed by smaller amounts of sulfur and chlorine and sodium. P-rich particles exhibit distinct O:C ratio values < 0.3. Within all conditions they predominantly occur within the coarse mode range (Figure 15). There is a noticeable difference in the abundance of the P-rich particles between day and night, with a significantly higher presence during nighttime. During night at 60 m P-rich particles contribute more than 50 % (Figure 15 b).

3.3.5 High- and low-salt particles

High-salt particles are characterized by a salt-index > 0.2. Low-salt particles are characterized by a salt-index 0.1 – 0.2. The inorganic fraction of both high-salt and low-salt particles is primarily characterized by the presence of sodium, sulfur, and potassium, albeit in varying proportions. In high-salt particles, potassium is the dominant constituent, whereas in low-salt particles, sodium is more present. Sulfate, however, maintains a consistent presence in both types of particles. Furthermore, the high-salt particles have C:O ratio values > 1, while the low-salt particles exhibit O:C ratio values ranging between 0.5 and 2. In terms of spatial and temporal distribution, both high- and low-salt particles display similar patterns. They are most abundant at 60 m, primarily during daytime where they contribute about 30 %. Here the salt particles are more dominant within the fine mode (Figure 15 a). Conversely, at 5 m, both high- and low-salt particles constitute a smaller fraction of the overall particles (~ 10 %, Figure 15 c & d).

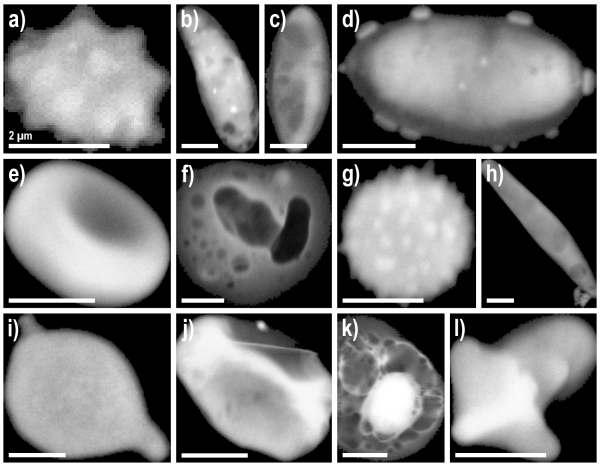

Figure 14. Representative selection of particles showing characteristic morphologies within the identified P-rich particle class (P-index >0.1). The images provide a visual overview of the diverse structures observed within the P-rich category which represent the PBAP fraction. Particles show fungal spores (a - e & g – j). The backscattered electron images were acquired during a first image acquisition pass for automated SEM-EDX single particle analysis. Each scale bar corresponds to $2\,\mu m$.

3.3.6 C-rich particles

C-rich particles are characterized by a salt-index <0.1). The inorganic fraction of C-rich particles, although minor, is composed of varying proportions of sodium, sulfur, chlorine, and potassium. The C:O ratio values in these particles are <1. This class represent on of the most abundant particle types within all conditions, contributing between ~ 27 % at 60 m(Figure 15 a & b) and ~ 34 % at 5 m (Figure 15 c & d).

3.4 Particle composition in clean vs polluted conditions

The samples classified as moderately polluted were categorized in the same environmental conditions as the clean samples (Section 2.3.2). As already noted in Section 2.4.2, both sample categories collected at 60 m height show significant deviations between the SEM-derived and the OPS-derived PNSDs. This makes the polluted 60 m conditions unrepresentative and are therefore neglected when comparing to the clean sample. The night at 60 m condition is not only characterized by the difference in PNSD, but especially by the different S-rich abundance pattern (Figure 16 b). Here, the dominance of S-rich particles can be related primarily to two different samples, making this pooled condition not comparable in another way.

Comparing the 5 m samples from clean and polluted conditions, an increase in the proportion of the more salt-rich fraction (higher concentration of inorganic elements) in polluted samples is observed (Figure 16 c & d). This includes the high- and low-salt as well as the Na-rich classes, accounting for more than 50 % in both polluted5 m conditions. Among these, especially the Na-rich particles show a significant increase by 17 % during the day and by 12 % during the night. In parallel, the fraction of the K-rich and P-rich particles is decreased in the polluted samples. Since the results in the clean samples suggest that these two classes are a marker for PBAPs and other biological

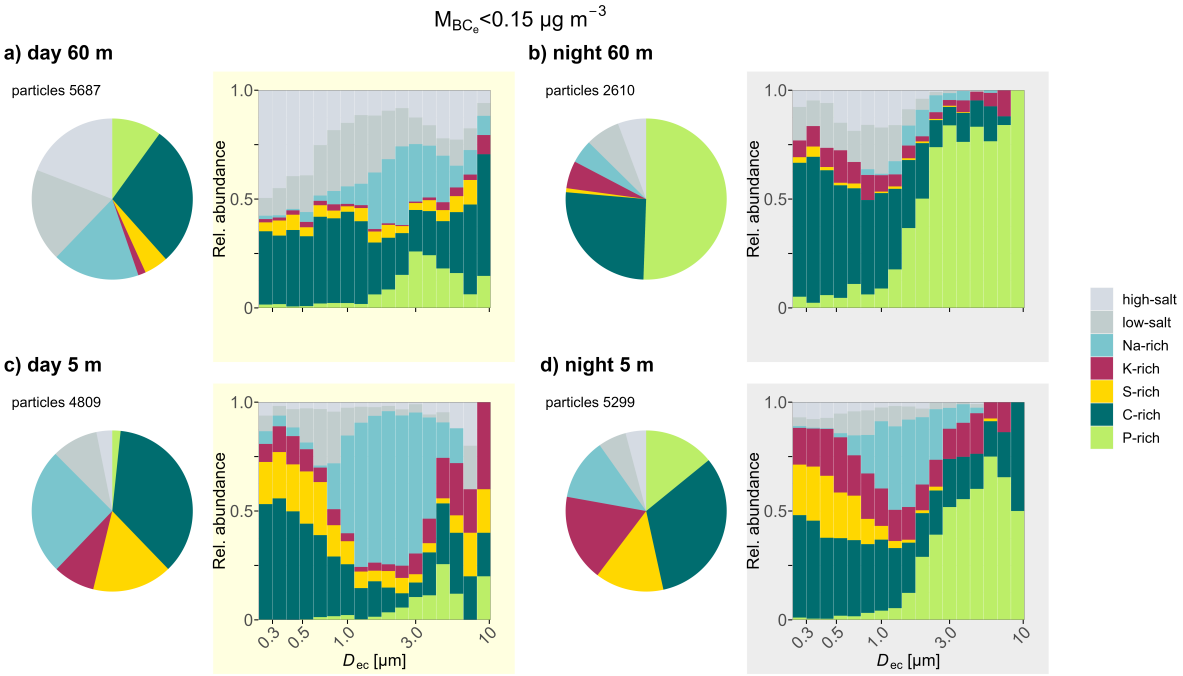

Figure 15. Variability in particle class abundance for day at 60 m (a), night at 60 m (b), day at 5 m (c), and night at 5 m (d) under clean conditions. The pie charts show the total fraction of each class per condition within. Additionally, abundance size distributions show variations in class abundance across different size ranges. Particles are categorized by their D_{ec} into size bins, according to the bin limits defined in Table 1. The height of each bar corresponds to the relative abundance of each class (high-salt, low-salt, Na-rich, K-rich, S-rich, C-rich and P-rich) as indicated in in the color code.

compounds, this trend shows a reduced influence of these biogenic sources. Moreover, the overall pattern of dominant classes with respect to the size range remains similar. This is an indication of the overall presence of the background aerosol in the forest. In addition, these results suggest that there is no significant addition of polluting aerosol that dominates the composition of the aerosol.

4 Summary and outlook

A particular strength of this study is the method of SEM-EDX measurements of individual aerosol particles. This allowed the determination of the composition of individual particles as a measure of the internal mixing of components, particularly within their inorganic fraction. In addition, this approach allowed the acquisition of size-resolved chemical information, by analyzing the abundance of elemental concentrations as a function of particle size. The systematical sampling approach allowed to observe the variability of aerosol elemental composition in terms of the dial cycle and below and above canopy conditions. Further, the use of complementary online measurements has proven to be essential in providing both atmospheric aerosol and meteorological parameters. As a result, defined relationships between environmental fac-

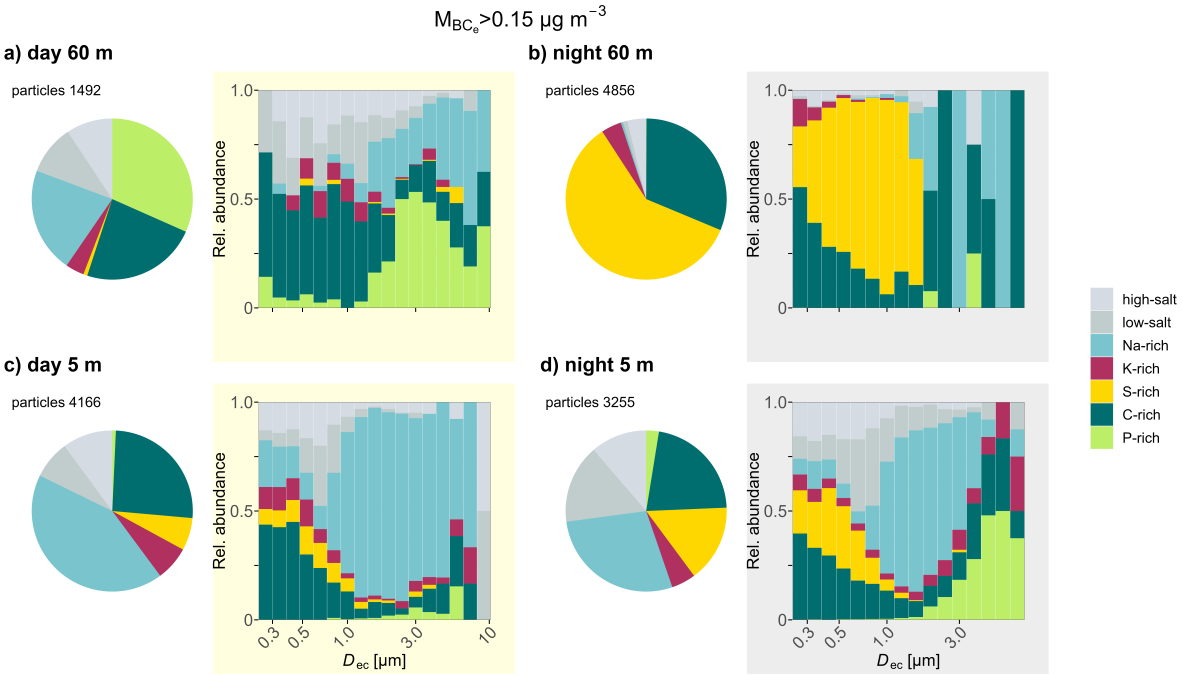

Figure 16. Variability in particle class abundance for day at 60 m (a), night at 60 m (b), day at 5 m (c), and night at 5 m (d) under moderately polluted conditions. The pie charts show the total fraction of each class per condition. Additionally, abundance size distributions show variations in class abundance across different size ranges. Particles are categorized by their D_{ec} into size bins, according to the bin limits defined in Table 1. The height of each bar corresponds to the relative abundance of each class (high-salt, low-salt, Na-rich, K-rich, S-rich, C-rich and P-rich) as indicated in in the color code.

tors and the observed particle composition could be established. In addition, OPS measurements facilitated the validation of the SEM-EDX technique by comparing SEM-derived PNSDs with OPS-derived PNSDs. The results of this comparison are in good agreement, indicating that the samples collected accurately represent the ambient conditions. This suggests that there is no systematic loss of particles, further confirming the reliability of our methods. However, potential losses of pure organic particles due to vacuum degradation and instrumentation limitations must be considered and require further investigation. Although the time resolution of the discrete sampling approach is much lower than that of most continuous online measurements, it is significantly higher than that of previous studies also based on aerosol sampling and subsequent chemical analysis. While other studies have used sampling times ranging from several hours up to days (Artaxo et al., 1990), the current study uses relatively short sampling times ranging from a few minutes up to 30 minutes. This allows in-depth chemical analysis of individual particles derived from different aerosol conditions defined by atmospheric parameters, whereas many other studies provide mixtures of rain forest background, LRT and/or pollution aerosol(Adachi et al., 2020; Artaxo et al., 1994). In addition, the large number of samples collected, combined with the large capacity of automated SEM-EDX measurements, allowed a huge number of individual aerosol particles to be analyzed within each defined condition. As a result, statistical validation was greatly improved compared

to previous studies that had poor statistical capabilities (Pöhlker et al., 2012; Kremper et al., in preparation). As a result, this study provides a robust and representative data set for aerosol conditions in the Amazon.

In agreement with previous studies, the current work reveals a significant presence of inorganic components in the carbon-dominated particles, with a diverse composition of elements such as sodium, sulfur, chlorine, and potassium, primarily associated with a rain forest biosphere origin. The particles were classified into different types based on the abundance of these elements, revealing characteristic properties in size and composition. In addition, phosphorus, a common biogenic marker element, was identified as an effective tracer for PBAPs. This diversity in particle composition, including both internal and external mixing, implies the contribution of different sources in the biosphere-atmosphere exchange over a broad aerosol size distribution.

This data set offers additional opportunities for in-depth data analysis. In particular, there is potential to improve particle classification to identify more detailed clusters. This can be achieved both manually, where preliminray results are promising, and through the application of data mining and machine learning techniques for efficient data clustering based on common characteristics. In addition, the knowledge gained, combined with advances in aerosol sampler techniques, provide the basis for more accurate aerosol sampling. For example, targeted sampling from specific sources within the forest biosphere, using samplers designed for certain particle sizes, could generate distinct fingerprint data that can be compared to the atmospheric mixtures sampled in this study. Moreover, the integration of other microspectroscopic techniques, such as scanning transmission x-ray microscopy with near edge x-ray absorption fine structure (STXM-NEXAFS), known for its efficiency in characterizing organic composition, would enhance the single particle data.

While the exact sources remain unidentified, the study demonstrates the potential of combining systematic aerosol sampling with continuous online observations for approximate source localization, especially under clean conditions. Building on previous research, it highlights the important role of biogenic salts from multiple sources in the Amazonian aerosol cycle. Beyond their primary emission role, these results suggest that diverse biogenic processes contribute to the aerosol population. This highlights the need for additional research on this possibly underestimated aspect of the Amazonian aerosol cycle.

Data availability. The datasets presented here are available under https://doi.org/10.XXX/3.XX (). The ATTO data used in this study are available via the ATTO data portal through https://www.attoproject.org/. For data requests beyond the available data, please refer to the corresponding author.

Author contributions. According to Contributor Roles Taxonomy (CRediT, https://casrai.org/credit/):

Conceptualization: LAK, CP

Data curation: LAK, KK

Formal analysis: LAK

Investigation: LAK, SB, JDF

Software: LAK, KK

Supervision: CP

Validation: PA, KK

Visualization: LAK

Writing – original draft: LAK, CP

Writing – review & editing: All authors

Competing interests. The authors declare that they have no conflict of interest.

Acknowledgements. This research has been funded by the Bundesministerium für Bildung und Forschung (BMBF contracts 01LB1001A, 01LK1602B, and 01LK2101B), the Brazilian Ministério da Ciência, Tecnologia e Inovação (MCTI/FINEP contract 01.11.01248.00), the Max Planck Society, the Conselho Nacional de Desenvolvimento Científico e Tecnológico (CNPq, Brazil) (process 200723/2015-4), and the Max Planck Graduate Center with the Johannes Gutenberg University Mainz (MPGC). For the operation of the ATTO site, we acknowledge the support by the Instituto Nacional de Pesquisas da Amazônia (INPA), the Amazon State University (UEA), the Large-Scale Biosphere-Atmosphere Experiment (LBA), FAPEAM, and the Reserva de Desenvolvimento Sustentável do Uatumã (SDS/CEUC/RDS-Uatumã). Particularly, we would like to thank the ATTO team members including Susan Trumbore, Alberto Quesada, Bruno Takeshi, Reiner Ditz, Stefan Wolff, Björn Nillius, Fernando Morais, Thomas Klimach, Roberta Pereira de Souza, Jürgen Kesselmeier, Andrew Crozier, Sam Jones, Delano Campos, Juarez Viegas, Sipko Bulthuis, Francisco Alcinei Gomes da Silva, Isabella Diogenes, Hermes Braga Xavier, Nagib Alberto de Castro Souza, Antonio Huxley Melo Nascimento, Valmir Ferreira de Lima, Feliciano de Souza Coelho, André Luiz Matos, Wallace Rabelo Costa, Amauri Rodriguês Perreira, Adir Vasconcelos Brandão, Davirley Gomes Silva, Thomas Disper, Torsten Helmer, Steffen Schmidt, Uwe Schulz, Uwe Schultz, Karl Kübler, Olaf Kolle, Martin Hertel, Kerstin Hippler, Steffen Schmidt and all further colleagues involved in the technical, logistical, and scientific support.

References

Adachi, K., Oshima, N., Gong, Z., de Sá, S., Bateman, A. P., Martin, S. T., de Brito, J. F., Artaxo, P., Cirino, G. G., Sedlacek III, A. J., and Buseck, P. R.: Mixing States of Amazon Basin Aerosol Particles Transported over Long Distances Using Transmission Electron Microscopy, Atmospheric Chemistry and Physics, 20, 11 923–11 939, https://doi.org/10.5194/acp-20-11923-2020, 2020.

Andreae, M. O.: Soot Carbon and Excess Fine Potassium: Long-Range Transport of Combustion-Derived Aerosols, Science, 220, 1148–1151, https://doi.org/10.1126/science.220.4602.1148, 1983.

Andreae, M. O., Rosenfeld, D., Artaxo, P., Costa, A. A., Frank, G. P., Longo, K. M., and Silva-Dias, M. A. F.: Smoking Rain Clouds over the Amazon, Science, 303, 1337–1342, https://doi.org/10.1126/science.1092779, 2004.

Andreae, M. O., Acevedo, O. C., Araùjo, A., Artaxo, P., Barbosa, C. G. G., Barbosa, H. M. J., Brito, J., Carbone, S., Chi, X., Cintra, B. B. L., da Silva, N. F., Dias, N. L., Dias-Júnior, C. Q., Ditas, F., Ditz, R., Godoi, A. F. L., Godoi, R. H. M., Heimann, M., Hoffmann, T., Kesselmeier, J., Könemann, T., Krüger, M. L., Lavric, J. V., Manzi, A. O., Lopes, A. P., Martins, D. L., Mikhailov, E. F., Moran-Zuloaga, D., Nelson, B. W., Nölscher, A. C., Santos Nogueira, D., Piedade, M. T. F., Pöhlker, C., Pöschl, U., Quesada, C. A., Rizzo, L. V., Ro, C.-U., Ruckteschler, N., Sá, L. D. A., de Oliveira Sá, M., Sales, C. B., dos Santos, R. M. N., Saturno, J., Schöngart, J., Sörgel, M., de Souza, C. M., de Souza, R. a. F., Su, H., Targhetta, N., Tóta, J., Trebs, I., Trumbore, S., van Eijck, A., Walter, D., Wang, Z., Weber, B., Williams, J., Winderlich, J., Wittmann, F., Wolff, S., and Yáñez-Serrano, A. M.: The Amazon Tall Tower Observatory (ATTO): Overview of Pilot Measurements on Ecosystem Ecology, Meteorology, Trace Gases, and Aerosols, Atmospheric Chemistry and Physics, 15, 10 723–10 776, https://doi.org/10.5194/acp-15-10723-2015, 2015.

Andreae, M. O., Afchine, A., Albrecht, R., Holanda, B. A., Artaxo, P., Barbosa, H. M. J., Borrmann, S., Cecchini, M. A., Costa, A., Dollner, M., Fütterer, D., Järvinen, E., Jurkat, T., Klimach, T., Konemann, T., Knote, C., Krämer, M., Krisna, T., Machado, L. A. T., Mertes, S., Minikin, A., Pöhlker, C., Pöhlker, M. L., Pöschl, U., Rosenfeld, D., Sauer, D., Schlager, H., Schnaiter, M., Schneider, J., Schulz, C., Spanu, A., Sperling, V. B., Voigt, C., Walser, A., Wang, J., Weinzierl, B., Wendisch, M., and Ziereis, H.: Aerosol Characteristics and Particle Production in the Upper Troposphere over the Amazon Basin, Atmospheric Chemistry and Physics, 18, 921–961, https://doi.org/10.5194/acp-18-921-2018, 2018.

Ansmann, A., Baars, H., Tesche, M., Müller, D., Althausen, D., Engelmann, R., Pauliquevis, T., and Artaxo, P.: Dust and Smoke Transport from Africa to South America: Lidar Profiling over Cape Verde and the Amazon Rainforest, Geophysical Research Letters, 36, https://doi.org/10.1029/2009GL037923, 2009.

Arana, A., Loureiro, A. L., Barbosa, H. M. J., Van Grieken, R., and Artaxo, P.: Optimized Energy Dispersive X-ray Fluorescence Analysis of Atmospheric Aerosols Collected at Pristine and Perturbed Amazon Basin Sites, X-Ray Spectrometry, 43, 228–237, https://doi.org/10.1002/xrs.2544, 2014.

Artaxo, P., Maenhaut, W., Storms, H., and Van Grieken, R.: Aerosol Characteristics and Sources for the Amazon Basin during the Wet Season, Journal of Geophysical Research: Atmospheres, 95, 16 971–16 985, https://doi.org/10.1029/JD095iD10p16971, 1990.

Artaxo, P., Gerab, F., and Rabello, M. L. C.: Elemental Composition of Aerosol Particles from Two Atmospheric Monitoring Stations in the Amazon Basin, Nuclear Instruments and Methods in Physics Research Section B: Beam Interactions with Materials and Atoms, 75, 277–281, https://doi.org/10.1016/0168-583X(93)95658-R, 1993.

Artaxo, P., Gerab, F., Yamasoe, M. A., and Martins, J. V.: Fine Mode Aerosol Composition at Three Long-Term Atmospheric Monitoring Sites in the Amazon Basin, Journal of Geophysical Research: Atmospheres, 99, 22 857–22 868, https://doi.org/10.1029/94JD01023, 1994.

Artaxo, P., Calixto de Campos, R., Fernandes, E. T., V. Martins, J., Xiao, Z., Lindqvist, O., Fernández-Jiménez, M. T., and Maenhaut, W.: Large Scale Mercury and Trace Element Measurements in the Amazon Basin, Atmospheric Environment, 34, 4085–4096, https://doi.org/10.1016/S1352-2310(00)00106-0, 2000.

Artaxo, P., V. Rizzo, L., F. Brito, J., J. Barbosa, H. M., Arana, A., T. Sena, E., G. Cirino, G., Bastos, W., T. Martin, S., and O. Andreae, M.: Atmospheric Aerosols in Amazonia and Land Use Change: From Natural Biogenic to Biomass Burning Conditions, Faraday Discussions, 165, 203–235, https://doi.org/10.1039/C3FD00052D, 2013.

Artaxo, P., Hansson, H.-C., Andreae, M. O., Bäck, J., Alves, E. G., Barbosa, H. M. J., Bender, F., Bourtsoukidis, E., Carbone, S., Chi, J., Decesari, S., Després, V. R., Ditas, F., Ezhova, E., Fuzzi, S., Hasselquist, N. J., Heintzenberg, J., Holanda, B. A., Guenther, A., Hakola, H., Heikkinen, L., Kerminen, V.-M., Kontkanen, J., Krejci, R., Kulmala, M., Lavric, J. V., de Leeuw, G., Lehtipalo, K., Machado, L. A. T., McFiggans, G., Franco, M. A. M., Meller, B. B., Morais, F. G., Mohr, C., Morgan, W., Nilsson, M. B., Peichl, M., Petäjä, T., Praß, M., Pöhlker, C., Pöhlker, M. L., Pöschl, U., Randow, C. V., Riipinen, I., Rinne, J., Rizzo, L. V., Rosenfeld, D., Dias, M. A. F. S., Sogacheva, L., Stier, P., Swietlicki, E., Sörgel, M., Tunved, P., Virkkula, A., Wang, J., Weber, B., Yáñez-Serrano, A. M., Zieger, P., Mikhailov, E., Smith, J. N., and Kesselmeier, J.: Tropical and Boreal Forest – Atmosphere Interactions: A Review, 74, 24–163, https://doi.org/10.16993/tellusb.34, 2022.

Barbosa, C. G. G., Taylor, P. E., Sá, M. O., Teixeira, P. R., Souza, R. A. F., Albrecht, R. I., Barbosa, H. M. J., Sebben, B., Manzi, A. O., Araújo, A. C., Prass, M., Pöhlker, C., Weber, B., Andreae, M. O., and Godoi, R. H. M.: Identification and Quantification of Giant Bioaerosol Particles over the Amazon Rainforest, npj Climate and Atmospheric Science, 5, 1–10, https://doi.org/10.1038/s41612-022-00294-y, 2022.

Barkley, A. E., Prospero, J. M., Mahowald, N., Hamilton, D. S., Popendorf, K. J., Oehlert, A. M., Pourmand, A., Gatineau, A., Panechou-Pulcherie, K., Blackwelder, P., and Gaston, C. J.: African Biomass Burning Is a Substantial Source of Phosphorus Deposition to the Amazon, Tropical Atlantic Ocean, and Southern Ocean, Proceedings of the National Academy of Sciences, 116, 16 216–16 221, https://doi.org/10.1073/pnas.1906091116, 2019.

Beauford, W., Barber, J., and Barringer, A. R.: Release of Particles Containing Metals from Vegetation into the Atmosphere, Science, 195, 571–573, https://doi.org/10.1126/science.195.4278.571, 1977.

Benito, B., Garciadeblás, B., and Rodríguez-Navarro, A.: Potassium- or Sodium-Efflux ATPase, a Key Enzyme in the Evolution of fungiThe GenBank Accession Numbers for the Sequences Reported in This Paper Are: Pleurotus Ostreatus ENA1, AJ420741; Phycomyces Blakesleeanus ENA1, AJ420742; Ph. Blakesleeanus PCA1, AJ420743; Blakeslea Trispora ENA1, AJ420744; B. Trispora BCA1, AJ420745; B. Trispora BCA2, AJ420746., Microbiology, 148, 933–941, https://doi.org/10.1099/00221287-148-4-933, 2002.

Benito, B., Haro, R., Amtmann, A., Cuin, T. A., and Dreyer, I.: The Twins K+ and Na+ in Plants, Journal of Plant Physiology, 171, 723–731, https://doi.org/10.1016/j.jplph.2013.10.014, 2014.

Bond, T. C. and Bergstrom, R. W.: Light Absorption by Carbonaceous Particles: An Investigative Review, Aerosol Science and Technology, 40, 27–67, https://doi.org/10.1080/02786820500421521, 2006.

Carneiro, R. G. and Fisch, G.: Observational Analysis of the Daily Cycle of the Planetary Boundary Layer in the Central Amazon during a Non-El Niño Year and El Niño Year (GoAmazon Project 2014/5), Atmospheric Chemistry and Physics, 20, 5547–5558, https://doi.org/10.5194/acp-20-5547-2020, 2020.

Chen, Q., Farmer, D. K., Schneider, J., Zorn, S. R., Heald, C. L., Karl, T. G., Guenther, A., Allan, J. D., Robinson, N., Coe, H., Kimmel, J. R., Pauliquevis, T., Borrmann, S., Pöschl, U., Andreae, M. O., Artaxo, P., Jimenez, J. L., and Martin, S. T.: Mass Spectral Characterization of Submicron Biogenic Organic Particles in the Amazon Basin, Geophysical Research Letters, 36, https://doi.org/10.1029/2009GL039880, 2009.

Chen, Q., Farmer, D. K., Rizzo, L. V., Pauliquevis, T., Kuwata, M., Karl, T. G., Guenther, A., Allan, J. D., Coe, H., Andreae, M. O., Pöschl, U., Jimenez, J. L., Artaxo, P., and Martin, S. T.: Submicron Particle Mass Concentrations and Sources in the Amazonian Wet Season (AMAZE-08), Atmospheric Chemistry and Physics, 15, 3687–3701, https://doi.org/10.5194/acp-15-3687-2015, 2015.

Chen, Z., Liu, P., Liu, Y., and Zhang, Y.-H.: Strong Acids or Bases Displaced by Weak Acids or Bases in Aerosols: Reactions Driven by the Continuous Partitioning of Volatile Products into the Gas Phase, Accounts of Chemical Research, 54, 3667–3678, https://doi.org/10.1021/acs.accounts.1c00318, 2021.

China, S., Wang, B., Weis, J., Rizzo, L., Brito, J., Cirino, G. G., Kovarik, L., Artaxo, P., Gilles, M. K., and Laskin, A.: Rupturing of Biological Spores As a Source of Secondary Particles in Amazonia, Environmental Science & Technology, 50, 12 179–12 186, https://doi.org/10.1021/acs.est.6b02896, 2016.

China, S., Burrows, S. M., Wang, B., Harder, T. H., Weis, J., Tanarhte, M., Rizzo, L. V., Brito, J., Cirino, G. G., Ma, P.-L., Cliff, J., Artaxo, P., Gilles, M. K., and Laskin, A.: Fungal Spores as a Source of Sodium Salt Particles in the Amazon Basin, Nature Communications, 9, 4793, https://doi.org/10.1038/s41467-018-07066-4, 2018.

Després, V. R., Huffman, J. A., Burrows, S. M., Hoose, C., Safatov, A. S., Buryak, G., Fröhlich-Nowoisky, J., Elbert, W., Andreae, M. O., Pöschl, U., and Jaenicke, R.: Primary Biological Aerosol Particles in the Atmosphere: A Review, Tellus B: Chemical and Physical Meteorology, 64, 15 598, https://doi.org/10.3402/tellusb.v64i0.15598, 2012.

Dias-Júnior, C. Q., Carneiro, R. G., Fisch, G., D'Oliveira, F. A. F., Sörgel, M., Botía, S., Machado, L. A. T., Wolff, S., dos Santos, R. M. N., and Pöhlker, C.: Intercomparison of Planetary Boundary Layer Heights Using Remote Sensing Retrievals and ERA5 Reanalysis over Central Amazonia, Remote Sensing, 14, 4561, https://doi.org/10.3390/rs14184561, 2022.

Draxler, R. R. and Hess, G. D.: An overview of the HYSPLIT 4 modelling system for trajectories, dispersion and deposition, Australian Meteorological Magazine, 47, 295–308, <GotoISI>://WOS:000078594400003, 1998.

Durgante, F. M., Higuchi, N., Ohashi, S., Householder, J. E., Lima, A. J. N., Ishizuka, M., Wittmann, F., dos Santos, J., Carneiro, V. M. C., Xu, X., do Nascimento, C. C., Schöngart, J., Piedade, M. T. F., Schmitt, A. R. K., Alves, Y. L. A., Lehman, J., Gimenez, B. O., Baggio, P. M., de Ourique, L. K., and Trumbore, S.: Soil Fertility and Drought Interact to Determine Large Variations in Wood Production for a Hyperdominant Amazonian Tree Species, Frontiers in Forests and Global Change, 5, 2023.

Elbert, W., Taylor, P. E., Andreae, M. O., and Pöschl, U.: Contribution of Fungi to Primary Biogenic Aerosols in the Atmosphere: Wet and Dry Discharged Spores, Carbohydrates, and Inorganic Ions, Atmospheric Chemistry and Physics, 7, 4569–4588, https://doi.org/10.5194/acp-7-4569-2007, 2007.

Formenti, P., Andreae, M. O., Lange, L., Roberts, G., Cafmeyer, J., Rajta, I., Maenhaut, W., Holben, B. N., Artaxo, P., and Lelieveld, J.: Saharan Dust in Brazil and Suriname during the Large-Scale Biosphere-Atmosphere Experiment in Amazonia (LBA) - Cooperative LBA Regional Experiment (CLAIRE) in March 1998, Journal of Geophysical Research: Atmospheres, 106, 14 919–14 934, https://doi.org/10.1029/2000JD900827, 2001.

Franco, M. A., Ditas, F., Kremper, L. A., Machado, L. A. T., Andreae, M. O., Araújo, A., Barbosa, H. M. J., de Brito, J. F., Carbone, S., Holanda, B. A., Morais, F. G., Nascimento, J. P., Pöhlker, M. L., Rizzo, L. V., Sá, M., Saturno, J., Walter, D., Wolff, S., Pöschl, U., Artaxo, P., and Pöhlker, C.: Occurrence and Growth of Sub-50 Nm Aerosol Particles in the Amazonian Boundary Layer, Atmospheric Chemistry and Physics, 22, 3469–3492, https://doi.org/10.5194/acp-22-3469-2022, 2022.

Fröhlich-Nowoisky, J., Kampf, C. J., Weber, B., Huffman, J. A., Pöhlker, C., Andreae, M. O., Lang-Yona, N., Burrows, S. M., Gunthe, S. S., Elbert, W., Su, H., Hoor, P., Thines, E., Hoffmann, T., Després, V. R., and Pöschl, U.: Bioaerosols in the Earth System: Climate, Health, and Ecosystem Interactions, Atmospheric Research, 182, 346–376, https://doi.org/10.1016/j.atmosres.2016.07.018, 2016.

Graham, B., Guyon, P., Maenhaut, W., Taylor, P. E., Ebert, M., Matthias-Maser, S., Mayol-Bracero, O. L., Godoi, R. H. M., Artaxo, P., Meixner, F. X., Moura, M. A. L., Rocha, C., Van Grieken, R., Glovsky, M. M., Flagan, R. C., and Andreae, M. O.: Composition and diurnal variability of the natural Amazonian aerosol, Journal of Geophysical Research-Atmospheres, 108, 4765, https://doi.org/4765 10.1029/2003jd004049, 2003.

Henkes, A., Fisch, G., Machado, L. A. T., and Chaboureau, J.-P.: Morning Boundary Layer Conditions for Shallow to Deep Convective Cloud Evolution during the Dry Season in the Central Amazon, Atmospheric Chemistry and Physics, 21, 13 207–13 225, https://doi.org/10.5194/acp-21-13207-2021, 2021.

Holanda, B. A., Pöhlker, M. L., Walter, D., Saturno, J., Sörgel, M., Ditas, J., Ditas, F., Schulz, C., Franco, M. A., Wang, Q., Donth, T., Artaxo, P., Barbosa, H. M. J., Borrmann, S., Braga, R., Brito, J., Cheng, Y., Dollner, M., Kaiser, J. W., Klimach, T., Knote, C., Krüger, O. O., Fütterer, D., Lavrič, J. V., Ma, N., Machado, L. A. T., Ming, J., Morais, F. G., Paulsen, H., Sauer, D., Schlager, H., Schneider, J., Su, H., Weinzierl, B., Walser, A., Wendisch, M., Ziereis, H., Zöger, M., Pöschl, U., Andreae, M. O., and Pöhlker, C.: Influx of African Biomass Burning Aerosol during the Amazonian Dry Season through Layered Transatlantic Transport of Black Carbon-Rich Smoke, Atmospheric Chemistry and Physics, 20, 4757–4785, https://doi.org/10.5194/acp-20-4757-2020, 2020.

Holanda, B. A., Franco, M. A., Walter, D., Artaxo, P., Carbone, S., Cheng, Y., Chowdhury, S., Ditas, F., Gysel-Beer, M., Klimach, T., Kremper, L. A., Krueger, O. O., Lavric, V, J., Lelieveld, J., Ma, C., Machado, L. A. T., Modini, R. L., Morais, F. G., Pozzer, A., Saturno, J., Su, H., Wendisch, M., Wolff, S., Poehlker, M. L., Andreae, M. O., Poeschl, U., and Poehlker, C.: African biomass burning affects aerosol cycling over the Amazon, COMMUNICATIONS EARTH & ENVIRONMENT, 4, https://doi.org/10.1038/s43247-023-00795-5, 2023.

Huffman, J. A., Sinha, B., Garland, R. M., Snee-Pollmann, A., Gunthe, S. S., Artaxo, P., Martin, S. T., Andreae, M. O., and Pöschl, U.: Size Distributions and Temporal Variations of Biological Aerosol Particles in the Amazon Rainforest Characterized by Microscopy and Real-Time UV-APS Fluorescence Techniques during AMAZE-08, Atmospheric Chemistry and Physics, 12, 11 997–12 019, https://doi.org/10.5194/acp-12-11997-2012, 2012.

Jayaratne, E., Ling, X., and Morawska, L.: Role of Vegetation in Enhancing Radon Concentration and Ion Production in the Atmosphere., Environmental Science & Technology, 45, 6350–6355, https://doi.org/10.1021/es201152g, 2011.

Johnson, R., Vishwakarma, K., Hossen, M. S., Kumar, V., Shackira, A. M., Puthur, J. T., Abdi, G., Sarraf, M., and Hasanuzzaman, M.: Potassium in Plants: Growth Regulation, Signaling, and Environmental Stress Tolerance, PLANT PHYSIOLOGY AND BIOCHEMISTRY, 172, 56–69, https://doi.org/10.1016/j.plaphy.2022.01.001, 2022.

Kazarov, A. A. and Plieva, L. S.: Evolution of Ions into the Atmosphere during Transpiration by Plants of Several Zones of the Northern Caucasus, Soviet Plant Physiology, 36, 761–766, <GotoISI>://WOS:A1989DA39300001, 1989.

Kelly, D. P., Shergill, J. K., Lu, W.-P., and Wood, A. P.: Oxidative Metabolism of Inorganic Sulfur Compounds by Bacteria, Antonie van Leeuwenhoek, 71, 95–107, https://doi.org/10.1023/A:1000135707181, 1997.

Kerminen, V.-M., Chen, X., Vakkari, V., Petäjä, T., Kulmala, M., and Bianchi, F.: Atmospheric New Particle Formation and Growth: Review of Field Observations, Environmental Research Letters, 13, 103 003, https://doi.org/10.1088/1748-9326/aadf3c, 2018.

Khadir, T., Riipinen, I., Talvinen, S., Heslin-Rees, D., Pöhlker, C., Rizzo, L., Machado, L. A. T., Franco, M. A., Kremper, L. A., Artaxo, P., Petäjä, T., Kulmala, M., Tunved, P., Ekman, A. M. L., Krejci, R., and Virtanen, A.: Sink, Source or Something In-Between? Net Effects of Precipitation on Aerosol Particle Populations, Geophysical Research Letters, 50, e2023GL104 325, https://doi.org/10.1029/2023GL104325, 2023.

Koren, I., Kaufman, Y. J., Remer, L. A., and Martins, J. V.: Measurement of the Effect of Amazon Smoke on Inhibition of Cloud Formation, Science, 303, 1342–1345, https://doi.org/10.1126/science.1089424, 2004.

Kremper, L. A., Moran-Zuloaga, D., Kandler, K., Förster, J.-D., Quaresma Dias-Júnior, C., Ditas, F., Hrabe de Angelis, I., Saturno, J., Walter, D., Artaxo, P., Andreae, M. O., Pöschl, U., and Pöhlker, C.: Contrasting the elemental composition of Amazonian aerosols under African dust influx vs pristine conditions, in preparation.

Kulmala, M., Petäjä, T., Nieminen, T., Sipilä, M., Manninen, H. E., Lehtipalo, K., Dal Maso, M., Aalto, P. P., Junninen, H., Paasonen, P., Riipinen, I., Lehtinen, K. E. J., Laaksonen, A., and Kerminen, V.-M.: Measurement of the Nucleation of Atmospheric Aerosol Particles, Nature Protocols, 7, 1651–1667, https://doi.org/10.1038/nprot.2012.091, 2012.

Laskin, A., Moffet, R. C., Gilles, M. K., Fast, J. D., Zaveri, R. A., Wang, B., Nigge, P., and Shutthanandan, J.: Tropospheric Chemistry of Internally Mixed Sea Salt and Organic Particles: Surprising Reactivity of NaCl with Weak Organic Acids, Journal of Geophysical Research: Atmospheres, 117, 2012JD017 743, https://doi.org/10.1029/2012JD017743, 2012.

Lewis, E. R. and Schwartz, S. E.: Sea Salt Aerosol Production: Mechanisms, Methods, Measurements, and Models, American Geophysical Union, 2004.

Li, J., Pósfai, M., Hobbs, P. V., and Buseck, P. R.: Individual Aerosol Particles from Biomass Burning in Southern Africa: 2, Compositions and Aging of Inorganic Particles, Journal of Geophysical Research: Atmospheres, 108, https://doi.org/10.1029/2002JD002310, 2003.

Liu, L., Cheng, Y., Wang, S., Wei, C., Pöhlker, M. L., Pöhlker, C., Artaxo, P., Shrivastava, M., Andreae, M. O., Pöschl, U., and Su, H.: Impact of Biomass Burning Aerosols on Radiation, Clouds, and Precipitation over the Amazon: Relative Importance of Aerosol–Cloud and Aerosol–Radiation Interactions, Atmospheric Chemistry and Physics, 20, 13 283–13 301, https://doi.org/10.5194/acp-20-13283-2020, 2020.

Liu, T., Zhang, J., Cao, J., Zheng, H., Zhan, C., Liu, H., Zhang, L., Xiao, K., Liu, S., Xiang, D., and Zhang, D.: Identification of Coexistence of Biological and Non-Biological Aerosol Particles with DAPI (4′,6-Diamidino-2-Phenylindole) Stain, Particuology, 72, 49–57, https://doi.org/10.1016/j.partic.2022.02.009, 2023.

Liu, Y., Brito, J., Dorris, M. R., Rivera-Rios, J. C., Seco, R., Bates, K. H., Artaxo, P., Duvoisin, S., Keutsch, F. N., Kim, S., Goldstein, A. H., Guenther, A. B., Manzi, A. O., Souza, R. A. F., Springston, S. R., Watson, T. B., McKinney, K. A., and Martin, S. T.: Isoprene Photochemistry over the Amazon Rainforest, Proceedings of the National Academy of Sciences, 113, 6125–6130, https://doi.org/10.1073/pnas.1524136113, 2016.

Maathuis, F. J.: Physiological Functions of Mineral Macronutrients, Current Opinion in Plant Biology, 12, 250–258, https://doi.org/10.1016/j.pbi.2009.04.003, 2009.

Machado, L. A. T., Franco, M. A., Kremper, L. A., Ditas, F., Andreae, M. O., Artaxo, P., Cecchini, M. A., Holanda, B. A., Pöhlker, M. L., Saraiva, I., Wolff, S., Pöschl, U., and Pöhlker, C.: How Weather Events Modify Aerosol Particle Size Distributions in the Amazon Boundary Layer, Atmospheric Chemistry and Physics, 21, 18 065–18 086, https://doi.org/10.5194/acp-21-18065-2021, 2021.

Martin, S. T., Andreae, M. O., Artaxo, P., Baumgardner, D., Chen, Q., Goldstein, A. H., Guenther, A., Heald, C. L., Mayol-Bracero, O. L., McMurry, P. H., Pauliquevis, T., Pöschl, U., Prather, K. A., Roberts, G. C., Saleska, S. R., Silva Dias, M. A., Spracklen, D. V., Swietlicki, E., and Trebs, I.: Sources and Properties of Amazonian Aerosol Particles, Reviews of Geophysics, 48, https://doi.org/10.1029/2008RG000280, 2010.

Martins, J. A., Silva Dias, M. a. F., and Gonçalves, F. L. T.: Impact of Biomass Burning Aerosols on Precipitation in the Amazon: A Modeling Case Study, Journal of Geophysical Research: Atmospheres, 114, https://doi.org/10.1029/2007JD009587, 2009.

Moran-Zuloaga, D., Ditas, F., Walter, D., Saturno, J., Brito, J., Carbone, S., Chi, X., Hrabě de Angelis, I., Baars, H., Godoi, R. H. M., Heese, B., Holanda, B. A., Lavrič, J. V., Martin, S. T., Ming, J., Pöhlker, M. L., Ruckteschler, N., Su, H., Wang, Y., Wang, Q., Wang, Z., Weber, B., Wolff, S., Artaxo, P., Pöschl, U., Andreae, M. O., and Pöhlker, C.: Long-Term Study on Coarse Mode Aerosols in the Amazon Rain Forest with the Frequent Intrusion of Saharan Dust Plumes, Atmospheric Chemistry and Physics, 18, 10 055–10 088, https://doi.org/10.5194/acp-18-10055-2018, 2018.

Nemeryuk, G. E.: Migration of salts into the atmosphere during transpiration, Soviet Plant Physiology, 17, 560–566, <GotoISI>://BIOSIS:PREV197107027808, 1970.

Oliveira, M. I., Acevedo, O. C., Sörgel, M., Nascimento, E. L., Manzi, A. O., Oliveira, P. E. S., Brondani, D. V., Tsokankunku, A., and Andreae, M. O.: Planetary Boundary Layer Evolution over the Amazon Rainforest in Episodes of Deep Moist Convection at the Amazon Tall Tower Observatory, Atmospheric Chemistry and Physics, 20, 15–27, https://doi.org/10.5194/acp-20-15-2020, 2020.

Pöhlker, C., Wiedemann, K. T., Sinha, B., Shiraiwa, M., Gunthe, S. S., Smith, M., Su, H., Artaxo, P., Chen, Q., Cheng, Y., Elbert, W., Gilles, M. K., Kilcoyne, A. L. D., Moffet, R. C., Weigand, M., Martin, S. T., Pöschl, U., and Andreae, M. O.: Biogenic Potassium Salt Particles as Seeds for Secondary Organic Aerosol in the Amazon, Science, 337, 1075–1078, https://doi.org/10.1126/science.1223264, 2012.

Pöhlker, C., Walter, D., Paulsen, H., Könemann, T., Rodríguez-Caballero, E., Moran-Zuloaga, D., Brito, J., Carbone, S., Degrendele, C., Després, V. R., Ditas, F., Holanda, B. A., Kaiser, J. W., Lammel, G., Lavrič, J. V., Ming, J., Pickersgill, D., Pöhlker, M. L., Praß, M., Löbs, N., Saturno, J., Sörgel, M., Wang, Q., Weber, B., Wolff, S., Artaxo, P., Pöschl, U., and Andreae, M. O.: Land Cover and Its Transformation in the Backward Trajectory Footprint Region of the Amazon Tall Tower Observatory, Atmospheric Chemistry and Physics, 19, 8425–8470, https://doi.org/10.5194/acp-19-8425-2019, 2019.

Pöhlker, M. L., Pöhlker, C., Ditas, F., Klimach, T., Hrabe de Angelis, I., Araújo, A., Brito, J., Carbone, S., Cheng, Y., Chi, X., Ditz, R., Gunthe, S. S., Kesselmeier, J., Könemann, T., Lavrič, J. V., Martin, S. T., Mikhailov, E., Moran-Zuloaga, D., Rose, D., Saturno, J., Su, H., Thalman, R., Walter, D., Wang, J., Wolff, S., Barbosa, H. M. J., Artaxo, P., Andreae, M. O., and Pöschl, U.: Long-Term Observations of Cloud Condensation Nuclei in the Amazon Rain Forest – Part 1: Aerosol Size Distribution, Hygroscopicity, and New Model Parametrizations for CCN Prediction, Atmospheric Chemistry and Physics, 16, 15 709–15 740, https://doi.org/10.5194/acp-16-15709-2016, 2016.

Pöhlker, M. L., Ditas, F., Saturno, J., Klimach, T., Hrabě de Angelis, I., Araùjo, A. C., Brito, J., Carbone, S., Cheng, Y., Chi, X., Ditz, R., Gunthe, S. S., Holanda, B. A., Kandler, K., Kesselmeier, J., Könemann, T., Krüger, O. O., Lavrič, J. V., Martin, S. T., Mikhailov, E., Moran-Zuloaga, D., Rizzo, L. V., Rose, D., Su, H., Thalman, R., Walter, D., Wang, J., Wolff, S., Barbosa, H. M. J., Artaxo, P., Andreae, M. O., Pöschl, U., and Pöhlker, C.: Long-Term Observations of Cloud Condensation Nuclei over the Amazon Rain Forest – Part 2: Variability and Characteristics of Biomass Burning, Long-Range Transport, and Pristine Rain Forest Aerosols, Atmospheric Chemistry and Physics, 18, 10 289–10 331, https://doi.org/10.5194/acp-18-10289-2018, 2018.

Pöschl, U.: Atmospheric Aerosols: Composition, Transformation, Climate and Health Effects, Angewandte Chemie International Edition, 44, 7520–7540, https://doi.org/10.1002/anie.200501122, 2005.

Pöschl, U., Martin, S. T., Sinha, B., Chen, Q., Gunthe, S. S., Huffman, J. A., Borrmann, S., Farmer, D. K., Garland, R. M., Helas, G., Jimenez, J. L., King, S. M., Manzi, A., Mikhailov, E., Pauliquevis, T., Petters, M. D., Prenni, A. J., Roldin, P., Rose, D., Schneider, J., Su, H., Zorn, S. R., Artaxo, P., and Andreae, M. O.: Rainforest Aerosols as Biogenic Nuclei of Clouds and Precipitation in the Amazon, Science, 329, 1513–1516, https://doi.org/10.1126/science.1191056, 2010.

Posit team: RStudio: Integrated Development Environment for R, Posit Software, PBC, Boston, MA, http://www.posit.co/, 2023.

Prass, M., Andreae, M. O., de Araùjo, A. C., Artaxo, P., Ditas, F., Elbert, W., Förster, J.-D., Franco, M. A., Hrabe de Angelis, I., Kesselmeier, J., Klimach, T., Kremper, L. A., Thines, E., Walter, D., Weber, J., Weber, B., Fuchs, B. M., Pöschl, U., and Pöhlker, C.: Bioaerosols in

the Amazon Rain Forest: Temporal Variations and Vertical Profiles of Eukarya, Bacteria, and Archaea, Biogeosciences, 18, 4873–4887, https://doi.org/10.5194/bg-18-4873-2021, 2021.

Prospero, J. M., Glaccum, R. A., and Nees, R. T.: Atmospheric Transport of Soil Dust from Africa to South America, Nature, 289, 570–572, https://doi.org/10.1038/289570a0, 1981.

Quinn, P. K., Collins, D. B., Grassian, V. H., Prather, K. A., and Bates, T. S.: Chemistry and Related Properties of Freshly Emitted Sea Spray Aerosol, Chemical Reviews, 115, 4383–4399, https://doi.org/10.1021/cr500713g, 2015.

Raghothama, K. G.: Phosphorus and Plant Nutrition: An Overview, in: Phosphorus: Agriculture and the Environment, chap. 11, pp. 353–378, John Wiley & Sons, Ltd, https://doi.org/10.2134/agronmonogr46.c11, 2005.

Ramsay, R., Di Marco, C. F., Sörgel, M., Heal, M. R., Carbone, S., Artaxo, P., de Araùjo, A. C., Sá, M., Pöhlker, C., Lavric, J., Andreae, M. O., and Nemitz, E.: Concentrations and Biosphere–Atmosphere Fluxes of Inorganic Trace Gases and Associated Ionic Aerosol Counterparts over the Amazon Rainforest, Atmospheric Chemistry and Physics, 20, 15 551–15 584, https://doi.org/10.5194/acp-20-15551-2020, 2020.

Rissler, J., Vestin, A., Swietlicki, E., Fisch, G., Zhou, J., Artaxo, P., and Andreae, M. O.: Size Distribution and Hygroscopic Properties of Aerosol Particles from Dry-Season Biomass Burning in Amazonia, Atmospheric Chemistry and Physics, 6, 471–491, https://doi.org/10.5194/acp-6-471-2006, 2006.

Rizzo, L. V., Artaxo, P., Müller, T., Wiedensohler, A., Paixão, M., Cirino, G. G., Arana, A., Swietlicki, E., Roldin, P., Fors, E. O., Wiedemann, K. T., Leal, L. S. M., and Kulmala, M.: Long Term Measurements of Aerosol Optical Properties at a Primary Forest Site in Amazonia, Atmospheric Chemistry and Physics, 13, 2391–2413, https://doi.org/10.5194/acp-13-2391-2013, 2013.

Rizzolo, J. A., Barbosa, C. G. G., Borillo, G. C., Godoi, A. F. L., Souza, R. A. F., Andreoli, R. V., Manzi, A. O., Sá, M. O., Alves, E. G., Pöhlker, C., Angelis, I. H., Ditas, F., Saturno, J., Moran-Zuloaga, D., Rizzo, L. V., Rosário, N. E., Pauliquevis, T., Santos, R. M. N., Yamamoto, C. I., Andreae, M. O., Artaxo, P., Taylor, P. E., and Godoi, R. H. M.: Soluble Iron Nutrients in Saharan Dust over the Central Amazon Rainforest, Atmospheric Chemistry and Physics, 17, 2673–2687, https://doi.org/10.5194/acp-17-2673-2017, 2017.

Roberts, G. C., Nenes, A., Seinfeld, J. H., and Andreae, M. O.: Impact of Biomass Burning on Cloud Properties in the Amazon Basin, Journal of Geophysical Research: Atmospheres, 108, https://doi.org/10.1029/2001JD000985, 2003.

Salter, M. E., Hamacher-Barth, E., Leck, C., Werner, J., Johnson, C. M., Riipinen, I., Nilsson, E. D., and Zieger, P.: Calcium Enrichment in Sea Spray Aerosol Particles, Geophysical Research Letters, 43, 8277–8285, https://doi.org/10.1002/2016GL070275, 2016.

Saturno, J., Holanda, B. A., Pöhlker, C., Ditas, F., Wang, Q., Moran-Zuloaga, D., Brito, J., Carbone, S., Cheng, Y., Chi, X., Ditas, J., Hoffmann, T., Hrabe de Angelis, I., Könemann, T., Lavrič, J. V., Ma, N., Ming, J., Paulsen, H., Pöhlker, M. L., Rizzo, L. V., Schlag, P., Su, H., Walter, D., Wolff, S., Zhang, Y., Artaxo, P., Pöschl, U., and Andreae, M. O.: Black and Brown Carbon over Central Amazonia: Long-Term Aerosol Measurements at the ATTO Site, Atmospheric Chemistry and Physics, 18, 12 817–12 843, https://doi.org/10.5194/acp-18-12817-2018, 2018.

Stein, S. W., Turpin, B. J., Cai, X., Huang, P.-F., and Mcmurry, P. H.: Measurements of Relative Humidity-Dependent Bounce and Density for Atmospheric Particles Using the DMA-impactor Technique, Atmospheric Environment, 28, 1739–1746, https://doi.org/10.1016/1352-2310(94)90136-8, 1994.

Swap, R., Garstang, M., Greco, S., Talbot, R., and Kållberg, P.: Saharan Dust in the Amazon Basin, 44, 133, https://doi.org/10.3402/tellusb.v44i2.15434, 1992.

Talbot, R. W., Andreae, M. O., Andreae, T. W., and Harriss, R. C.: Regional Aerosol Chemistry of the Amazon Basin during the Dry Season, Journal of Geophysical Research: Atmospheres, 93, 1499–1508, https://doi.org/10.1029/JD093iD02p01499, 1988.

Talbot, R. W., Andreae, M. O., Berresheim, H., Artaxo, P., Garstang, M., Harriss, R. C., Beecher, K. M., and Li, S. M.: Aerosol Chemistry during the Wet Season in Central Amazonia: The Influence of Long-Range Transport, Journal of Geophysical Research: Atmospheres, 95, 16 955–16 969, https://doi.org/10.1029/JD095iD10p16955, 1990.

Varanda Rizzo, L., Roldin, P., Brito, J., Backman, J., Swietlicki, E., Krejci, R., Tunved, P., Petäjä, T., Kulmala, M., and Artaxo, P.: Multi-Year Statistical and Modeling Analysis of Submicrometer Aerosol Number Size Distributions at a Rain Forest Site in Amazonia, Atmospheric Chemistry and Physics, 18, 10 255–10 274, https://doi.org/10.5194/acp-18-10255-2018, 2018.

Virtanen, A., Joutsensaari, J., Koop, T., Kannosto, J., Yli-Pirilä, P., Leskinen, J., Mäkelä, J. M., Holopainen, J. K., Pöschl, U., Kulmala, M., Worsnop, D. R., and Laaksonen, A.: An Amorphous Solid State of Biogenic Secondary Organic Aerosol Particles, Nature, 467, 824–827, https://doi.org/10.1038/nature09455, 2010.

Wang, J., Krejci, R., Giangrande, S., Kuang, C., Barbosa, H. M. J., Brito, J., Carbone, S., Chi, X., Comstock, J., Ditas, F., Lavric, J., Manninen, H. E., Mei, F., Moran-Zuloaga, D., Pöhlker, C., Pöhlker, M. L., Saturno, J., Schmid, B., Souza, R. A. F., Springston, S. R., Tomlinson, J. M., Toto, T., Walter, D., Wimmer, D., Smith, J. N., Kulmala, M., Machado, L. A. T., Artaxo, P., Andreae, M. O., Petäjä, T., and Martin, S. T.: Amazon Boundary Layer Aerosol Concentration Sustained by Vertical Transport during Rainfall, Nature, 539, 416–419, https://doi.org/10.1038/nature19819, 2016.

Wang, X., Wang, Q., Prass, M., Pöhlker, C., Moran-Zuloaga, D., Artaxo, P., Gu, J., Yang, N., Yang, X., Tao, J., Hong, J., Ma, N., Cheng, Y., Su, H., and Andreae, M. O.: The Export of African Mineral Dust across the Atlantic and Its Impact over the Amazon Basin, Atmospheric Chemistry and Physics, 23, 9993–10 014, https://doi.org/10.5194/acp-23-9993-2023, 2023.

Williamson, C. J., Kupc, A., Axisa, D., Bilsback, K. R., Bui, T., Campuzano-Jost, P., Dollner, M., Froyd, K. D., Hodshire, A. L., Jimenez, J. L., Kodros, J. K., Luo, G., Murphy, D. M., Nault, B. A., Ray, E. A., Weinzierl, B., Wilson, J. C., Yu, F., Yu, P., Pierce, J. R., and Brock, C. A.: A Large Source of Cloud Condensation Nuclei from New Particle Formation in the Tropics, Nature, 574, 399–403, https://doi.org/10.1038/s41586-019-1638-9, 2019.

Wimmer, D., Buenrostro Mazon, S., Manninen, H. E., Kangasluoma, J., Franchin, A., Nieminen, T., Backman, J., Wang, J., Kuang, C., Krejci, R., Brito, J., Goncalves Morais, F., Martin, S. T., Artaxo, P., Kulmala, M., Kerminen, V.-M., and Petäjä, T.: Ground-Based Observation of Clusters and Nucleation-Mode Particles in the Amazon, Atmospheric Chemistry and Physics, 18, 13 245–13 264, https://doi.org/10.5194/acp-18-13245-2018, 2018.

Wu, L., Li, X., Kim, H., Geng, H., Godoi, R. H. M., Barbosa, C. G. G., Godoi, A. F. L., Yamamoto, C. I., de Souza, R. A. F., Pöhlker, C., Andreae, M. O., and Ro, C.-U.: Single-Particle Characterization of Aerosols Collected at a Remote Site in the Amazonian Rainforest and an Urban Site in Manaus, Brazil, Atmospheric Chemistry and Physics, 19, 1221–1240, https://doi.org/10.5194/acp-19-1221-2019, 2019.

2.3 Occurrence and growth of sub-50 nm aerosol particles in the Amazonian boundary layer

This chapter has been published as:

Franco, M. A.; Ditas, F.; Kremper, L. A.; Machado, L. A. T.; Andreae, M. O.; Araújo, A.; Barbosa, H. M. J.; de Brito, J. F.; Carbone, S.; Holanda, B. A.; Morais, F. G.; Nascimento, J. P.; Pöhlker, M. L.; Rizzo, L. V.; Sá, M.; Saturno, J.; Walter, D.; Wolff, S.; Pöschl, U.; Artaxo, P., and Pöhlker, C.: "Occurrence and growth of sub-50 nm aerosol particles in the Amazonian boundary layer". *Atmospheric Chemistry and Physics*, 22, 5. (Mar. 2022), pp. 3469–3492. DOI: 10.5194/acp-22-3469-2022

Supplementary Material: The Supplementary Material for this article can be found online at: https://doi.org/10.5194/acp-18-10289-2018-supplement

Contribution to this publication by Leslie A. Kremper: I am the third author of this paper, following the shared first authors Marco A. Franco and Florian Ditas. In collaboration with F. Ditas and then taking over in 2019, I have been responsible as an instrument operator for the ATTO measurements of aerosol particle number size distributions obtained by a scanning mobility particle sizer (SMPS) as well as of total aerosol particle concentrations obtained by a condensation particle counter (CPC). I largely contributed to the data acquisition, field instrument maintenance, and data quality assurance. The unique SMPS and CPC long-term time series are the experimental core of the manuscript in this chapter. Beyond the actual data acquisition and processing, I contributed to the writing and data interpretation (e.g., analysis of long time series, seasonality, statistics) of this manuscript.

Atmos. Chem. Phys., 22, 3469–3492, 2022
https://doi.org/10.5194/acp-22-3469-2022

Atmospheric Chemistry and Physics
Open Access
EGU

Occurrence and growth of sub-50 nm aerosol particles in the Amazonian boundary layer

Marco A. Franco[1,2], Florian Ditas[2,a], Leslie A. Kremper[2], Luiz A. T. Machado[1,2], Meinrat O. Andreae[2,3,4], Alessandro Araújo[5], Henrique M. J. Barbosa[1], Joel F. de Brito[6], Samara Carbone[7], Bruna A. Holanda[2], Fernando G. Morais[1], Janaína P. Nascimento[8,b], Mira L. Pöhlker[2,11], Luciana V. Rizzo[9], Marta Sá[8], Jorge Saturno[2,c], David Walter[2,10,d], Stefan Wolff[2], Ulrich Pöschl[2], Paulo Artaxo[1], and Christopher Pöhlker[2]

[1]Institute of Physics, University of São Paulo, São Paulo 05508-900, Brazil
[2]Multiphase Chemistry Department, Max Planck Institute for Chemistry, 55128 Mainz, Germany
[3]Scripps Institution of Oceanography, University of California San Diego, La Jolla, CA 92037, USA
[4]Department of Geology and Geophysics, King Saud University, Riyadh, Saudi Arabia
[5]Empresa Brasileira de Pesquisa Agropecuária (Embrapa) Amazonia Oriental, CEP 66095-100, Belém, Brazil
[6]IMT Lille Douai, Institut Mines-Télécom, Université de Lille, Centre for Energy and Environment, 59000 Lille, France
[7]Agrarian Sciences Institute, Federal University of Uberlândia, Uberlândia-MG, 38408-100, Brazil
[8]National Institute for Amazonian Research, Manaus, AM, 69.060-000, Brazil
[9]Federal University of Sao Paulo, Department of Environmental Sciences, Diadema, Brazil
[10]Department of Biogeochemical Systems, Max Planck Institute for Biogeochemistry, 07701 Jena, Germany
[11]Experimental Aerosol and Cloud Microphysics Department, Leibniz Institute for Tropospheric Research, Leipzig, Germany
[a]now at: Hessian Agency for Nature Conservation, Environment and Geology, 65203 Wiesbaden, Germany
[b]now at: NOAA Global Systems Laboratory, Boulder, CO 80305, USA
[c]now at: Department 3.4 Analytical Chemistry of the Gas Phase, Physikalisch-Technische Bundesanstalt, 38116 Braunschweig, Germany
[d]now at: Climate Geochemistry Department, Max Planck Institute for Chemistry, 55128 Mainz, Germany

Correspondence: Marco A. Franco (marco.franco@usp.br) and Christopher Pöhlker (c.pohlker@mpic.de)

Received: 6 September 2021 – Discussion started: 9 September 2021
Revised: 17 January 2022 – Accepted: 20 January 2022 – Published: 16 March 2022

Abstract. New particle formation (NPF), referring to the nucleation of molecular clusters and their subsequent growth into the cloud condensation nuclei (CCN) size range, is a globally significant and climate-relevant source of atmospheric aerosols. Classical NPF exhibiting continuous growth from a few nanometers to the Aitken mode around 60–70 nm is widely observed in the planetary boundary layer (PBL) around the world but not in central Amazonia. Here, classical NPF events are rarely observed within the PBL, but instead, NPF begins in the upper troposphere (UT), followed by downdraft injection of sub-50 nm ($CN_{<50}$) particles into the PBL and their subsequent growth. Central aspects of our understanding of these processes in the Amazon have remained enigmatic, however. Based on more than 6 years of aerosol and meteorological data from the Amazon Tall Tower Observatory (ATTO; February 2014 to September 2020), we analyzed the diurnal and seasonal patterns as well as meteorological conditions during 254 of such Amazonian growth events on 217 event days, which show a sudden occurrence of particles between 10 and 50 nm in the PBL, followed by their growth to CCN sizes. The occurrence of events was significantly higher during the wet season, with 88 % of all events from January to June, than during the dry season, with 12 % from July to December, probably due to differences in the condensation sink (CS), atmospheric aerosol load, and meteorological conditions. Across all events, a median

Published by Copernicus Publications on behalf of the European Geosciences Union.

growth rate (GR) of 5.2 nm h^{-1} and a median CS of 1.1×10^{-3} s^{-1} were observed. The growth events were more frequent during the daytime (74 %) and showed higher GR (5.9 nm h^{-1}) compared to nighttime events (4.0 nm h^{-1}), emphasizing the role of photochemistry and PBL evolution in particle growth. About 70 % of the events showed a negative anomaly of the equivalent potential temperature ($\Delta\theta'_e$) – as a marker for downdrafts – and a low satellite brightness temperature (Tir) – as a marker for deep convective clouds – in good agreement with particle injection from the UT in the course of strong convective activity. About 30 % of the events, however, occurred in the absence of deep convection, partly under clear-sky conditions, and with a positive $\Delta\theta'_e$ anomaly. Therefore, these events do not appear to be related to downdraft transport and suggest the existence of other currently unknown sources of sub-50 nm particles.

1 Introduction

New particle formation (NPF) refers to the nucleation of nanometer-sized molecular clusters from gaseous precursors and their subsequent condensational growth (e.g., Kulmala et al., 2004; Dal Maso, 2005; Kirkby et al., 2011; Kulmala et al., 2012; Kerminen et al., 2018). Under favorable atmospheric conditions, the newly formed particles grow through condensation of semi-volatile and low-volatility gases as well as coagulation into the cloud- and, thus, climate-relevant size range with diameters, D, larger than $\sim$ 80 nm (see definitions in Kulmala et al., 2012; Kerminen et al., 2018). NPF has been observed worldwide in the course of ground-based observations in different environments, such as rural and remote continental areas, urban environments, the Arctic and Antarctica, marine areas, and mountain sites (Kerminen et al., 2018, and references therein). A brief overview of the current knowledge on the occurrence of NPF worldwide and the chemical mechanisms involved can be found in Andreae et al. (2021). Its wide and frequent occurrence makes NPF a major and possible even dominant source of aerosol particle number concentrations and cloud condensation nuclei (CCN) on global scales (e.g., Merikanto et al., 2009; Spracklen et al., 2008; Nieminen et al., 2018; Yli-Juuti et al., 2020).

In the long list of locations where "classical NPF" has been detected in the planetary boundary layer (PBL) (Kerminen et al., 2018), the Amazon rain forest is a remarkable exception (e.g., Andreae, 2013; Varanda Rizzo et al., 2018; Wimmer et al., 2018). Here, events have been observed that indeed resemble the classical "banana plots" of NPF but differ clearly in the initial diameter of the growth curve. While the smallest diameters in, for instance, boreal forest are typically in the range of a few nanometers, the "Amazonian bananas" rather start between about 20 and 40 nm (Kulmala et al., 2012; Kerminen et al., 2018). Varanda Rizzo et al. (2018) discussed the occurrence of such sub-50 nm particle growth events in the Amazon and found them only in 3 % of the 749 d examined, associated mainly with convective downdrafts. Accordingly, the Amazonian bananas start at larger diameters and are comparatively rare relative to the classical events, e.g., in boreal forests (Nieminen et al., 2018; Dada et al., 2018).

This striking contrast to other environments has inspired researchers to investigate the underlying mechanisms that could explain the absence of NPF as well as alternative particle sources that sustain the Amazonian aerosol population. Reasons for the absence of NPF within the PBL could be the following:

1. suppression by isoprene (e.g., Kiendler-Scharr et al., 2009; Kanawade et al., 2011; McFiggans et al., 2019; Yli-Juuti et al., 2020), which is the most abundant volatile organic compound (VOC) in the Amazonian atmosphere (e.g., Andreae et al., 2018; Yáñez-Serrano et al., 2020);

2. the very low concentrations of inorganic precursor gases such as sulfur dioxide (SO_2, being converted into sulfuric acid, H_2SO_4) as well as the bases ammonia (NH_3) and amines (NR_3) (Andreae et al., 1990; Trebs et al., 2004), which play key roles in the binary H_2SO_4–H_2O and ternary NH_3–H_2SO_4–H_2O nucleation mechanisms (Kirkby et al., 2011; Andreae et al., 2021);

3. the high levels of relative humidity (RH), which have been associated with a low occurrence of NPF (e.g., Bonn and Moortgat, 2003; Hamed et al., 2011; Hyvönen et al., 2005).

The occurrence of NPF is dependent on the local conditions at individual sites, including meteorology, biogenic emissions, and air pollution levels, but regional and synoptic scales are also very important for this process. Particle growth events lasting on the order of hours are particularly influenced by larger geographic scales. Nieminen et al. (2018) emphasized that the NPF occurrence and growth rates (GRs) show a geographically inhomogeneous distribution, indicating that the underlying mechanisms are as manifold as complex. Typical atmospheric GR ranges from 1 to 12 nm h^{-1} (Yli-Juuti et al., 2020). Further, different meteorological conditions have been associated with the occurrence of NPF and particle growth. Specifically, photochemical reactions under daytime conditions have been regarded as a driving force for both nucleation and condensational growth (e.g., Nieminen et al., 2018; Kerminen et al., 2018; Hamed et al., 2011; Ma and Birmili, 2015). This is in line with a

significantly higher occurrence of NPF under clear-sky conditions, as observed for instance in Hyytiälä, Finland, and British Columbia (Dada et al., 2017; Andreae et al., 2021). In addition, an association between the occurrence of NPF and convective clouds has been observed at different marine to continental sites (e.g., Perry and Hobbs, 1994; Clarke, 1992; Waddicor et al., 2012; De Reus et al., 2001; Wehner et al., 2015). Evidence of this phenomenon in the Amazon has also been reported by Andreae et al. (2018). While different potential explanations have emerged, the exact mechanisms, precursors, and spatial distribution in the context of clouds have remained unknown (Kerminen et al., 2018).

NPF has likely been altered as a result of industrialization, when anthropogenic emissions started to influence the atmospheric concentrations of trace species (Andreae et al., 2021). Relative to remote sites, rural and urban locations tend to show higher NPF frequencies (typically 10 %–30 % event days) and higher particle GR (4–12 nm h^{-1}) (Kerminen et al., 2018; Nieminen et al., 2018). This relates to the fundamental question of whether atmospheric concentrations of certain, mainly anthropogenically derived, species such as H_2SO_4 have to exceed certain thresholds for NPF to occur. Recent evidence of pure biogenic ion-induced nucleation under controlled laboratory (Kirkby et al., 2016) and under real atmospheric conditions (Rose et al., 2018; Zhao et al., 2020) highlights possible mechanisms for NPF pathways in a clean atmosphere.

Accordingly, environments with low anthropogenic influence are of particular interest to investigate processes under conditions that approximate a preindustrial state of the atmosphere. Amazonia is an ideal outdoor laboratory for such investigations under pristine conditions (Hamilton et al., 2014; Pöhlker et al., 2018). Of particular relevance is the wet season with its episodic occurrence of pristine periods, which allows for the study of atmospheric processes – such as the occurrence of sub-50 nm particles ($CN_{<50}$) – under conditions that approximate a preindustrial state of the rain forest atmosphere (Andreae et al., 2015). At the Amazon Tall Tower Observatory (ATTO) – which is located in a mostly untouched rain forest region and has become a landmark site for atmospheric research (Andreae et al., 2015; Pöhlker et al., 2019) – March to May represent the cleanest months of the year, with about 10 % of the time being considered pristine periods (Pöhlker et al., 2018).

Figure 1 illustrates the main sources of aerosol particles and CCN in Amazonia, which can be broadly grouped into the following three categories:

1. Biogenic particles are emitted by the rain forest ecosystem, which includes the release of primary biological aerosol particles (i.e., pollen, spores, bacteria, fragments). In addition, biogenic VOCs emitted by the ecosystem may undergo atmospheric oxidation, resulting in conversion into secondary organic aerosols (SOA). (e.g., Pöhlker et al., 2012; Huffman et al., 2012; Chen et al., 2015; Liu et al., 2016; Saturno et al., 2018a; Löbs et al., 2020; Prass et al., 2021).

2. Long-range transport of transatlantically advected African dust and pollution (e.g., Talbot et al., 1990; Pöhlker et al., 2018; Nascimento et al., 2021; Moran-Zuloaga et al., 2018; Holanda et al., 2020), as well as regional biomass burning smoke (Artaxo et al., 2013), which play an important role to increase the aerosol number concentration.

3. Driven by deep convective clouds, biogenic VOCs are transported into the upper troposphere (∼ 10 km), where VOC oxidation, nucleation of new aerosol particles, and initial particle growth occurs, fostered by low temperatures and a low preexisting aerosol surface area (Krejci et al., 2003; Andreae et al., 2018). Subsequently, the freshly formed particles are mixed downward into the PBL, where they continue to grow to CCN-relevant sizes (e.g., Krejci et al., 2003; Wang et al., 2016).

Several studies provide experimental and modeling support for the broad atmospheric relevance of UT particle production and the subsequent vertical mixing of the $CN_{<50}$ (e.g., Krejci, 2003; Krejci et al., 2005; Wang et al., 2016; Andreae et al., 2018; Williamson et al., 2019; Leino et al., 2019; Zhao et al., 2020; Varanda Rizzo et al., 2018; Machado et al., 2021). Figure 1 shows the presence of a $CN_{<50}$ pool in the Amazonian UT during the wet and dry seasons as well as an increase in D with decreasing altitude due to condensational particle growth. The downward motion of the $CN_{<50}$ can be driven by strong convective downdrafts or weaker downward motions in stratiform cloud regions (Wang et al., 2016). Zhao et al. (2020) recently suggested that pure organic NPF based on biogenic VOCs dominates above 13 km, whereas ternary NPF involving organics and H_2SO_4 dominates between 8 and 13 km. In addition, an increase of sub-50 nm particles was observed, in particular in the early morning hours, suggesting a connection between these increased concentrations with vertical transport and deep convective clouds, as well as with lightning density. Major mechanistic questions regarding the vertical transport of the $CN_{<50}$ remain open (e.g., Machado et al., 2021), however. This mechanism corroborates the fact that most of the observed sub-50 nm Aitken-mode particles in the PBL have relatively larger diameters (> 20 nm) due to the aging process while transported from the free troposphere into the PBL. It means that the ion-induced biogenic nucleation in the uppermost troposphere potentially plays an important role and, therefore, substantially contributes to the particle population in the free troposphere and in the PBL (Wang et al., 2016; Andreae et al., 2018; Glicker et al., 2019).

This study aims to identify and characterize the occurrence of particle growth events in the size range from 10 to 50 nm within the PBL of central Amazonia. While previous studies have documented the occurrence and properties of freshly

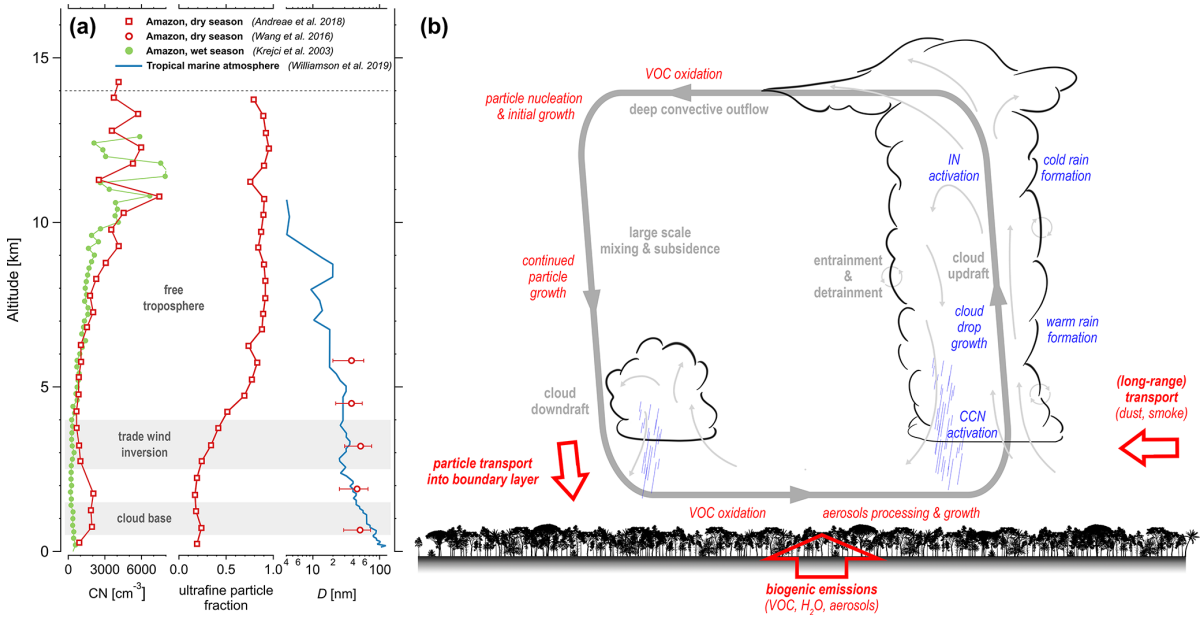

Figure 1. Conceptual scheme of sources, redistribution, processing, and removal of volatile organic compounds (VOCs), aerosol particles and cloud condensation nuclei (CCN) over the Amazon **(b)** in combination with previously measured vertical profiles of particle concentrations and sizes **(a)**. The scheme emphasizes the aerosol cycling in the course of deep convection, with an upward transport of VOCs and aerosol particles, new particle formation in the free troposphere with initial particle growth (Andreae et al., 2018), followed by the downward transport of sub-50 nm particles into the planetary boundary layer (Krejci et al., 2003; Wang et al., 2016). The three red arrows represent the main aerosol source categories in the Amazon, which are (i) primary and secondary particle formation from local and regional biogenic sources, (ii) long-range transport of dust, smoke, and other aerosols, and (iii) the vertical transport of sub-50 nm particles from aloft. The figure integrates concepts and data from various previous studies (i.e., Krejci et al., 2003; Baars et al., 2012; Wang et al., 2016; Andreae et al., 2018; Williamson et al., 2019).

nucleated particles at high altitudes (Krejci et al., 2003; Andreae et al., 2018; Williamson et al., 2019), their growth in the course of downward transport (Wang et al., 2016), and the appearance of sub-50 nm particles in the PBL (Varanda Rizzo et al., 2018; Wimmer et al., 2018), major questions remain open. With this study, we take a step beyond the existing knowledge, based on more than 6 years of aerosol measurements and complementary meteorological and satellite observations. In particular, we focus on a statistically broad characterization of Amazonian particle growth events (Amazonian bananas) by means of GR, CS, seasonality, and diurnal cycle, as well as their relationship to meteorological variables and deep convection. We also document growth events under clear-sky conditions and thus in the absence of deep convective mixing. Therefore, the knowledge obtained here about the sub-50 nm particle growth events addresses an important gap in our understanding of the Amazonian aerosol life cycle and will help to constrain the CCN sources and properties in this globally important ecosystem.

2 Measurements and data analysis

2.1 The Amazon Tall Tower Observatory (ATTO) site

The Amazon Tall Tower Observatory (ATTO) is located 150 km northeast of Manaus, Brazil, in a forest reserve. Detailed descriptions of the site, its location, instrumentation, and scientific missions can be found elsewhere (Andreae et al., 2015; Pöhlker et al., 2019). At the ATTO site, the first aerosol measurements were initiated in 2011 (e.g., Pöhlker et al., 2012; Saturno et al., 2018b). Since 2014, multiple continuous measurements of physical and chemical particle properties have been established and gradually extended (e.g., Pöhlker et al., 2016, 2018; Holanda et al., 2020; Saturno et al., 2018a; Schrod et al., 2020).

2.2 Terminology

According to Pöhlker et al. (2016), we define the Amazonian seasons as follows: the wet season spans from February to May, followed by the wet to dry transition period (WtoD) including June and July. The dry season extends from August to November, followed by the dry to wet transition period

(DtoW) including December and January. For the Amazonian submicron particle population, which is characterized by a multi-modal size distribution, we use the widely established terms Aitken mode (50–100 nm) and accumulation mode (100–1000 nm) (Pöhlker et al., 2016; Machado et al., 2021). In addition, we introduce the term sub-50 nm mode, defined as particles between 10 and 50 nm. We avoid using the term nucleation mode for this particle population as this term typically defines particles < 25 nm and refers to an aerosol population relatively soon after nucleation (Kulmala et al., 2012; Nieminen et al., 2018). The sub-50 nm particles analyzed here, however, have experienced initial aging and growth to diameters between 10 and 50 nm already. As an abbreviation, we use $CN_{<50}$ to refer to the particle fraction in the sub-50 nm mode. For the particle number concentrations in the individual modes, we use the symbols $N_{<50}$, N_{Ait}, and N_{acc}. N_{CN} is defined as the total particle number concentration.

2.3 Aerosol measurements

This study focuses on particle number size distributions (PNSDs) obtained from a scanning mobility particle sizer (SMPS) with an inlet located at 60 m above ground. The inlet used to sample the aerosols is installed on an 80 m high tower (02°08.602′ S, 59°00.033′ W; 130 m a.s.l.) at the ATTO site. The SMPS is manufactured by TSI Inc., and as classifiers we used model 3080 and, later, model 3082, coupled to a condensation particle counter (CPC) 3772. The inlet height was chosen to be approximately 30 m above the average canopy height, which enables measurements close to the canopy without direct contact with the largest trees. The SMPS is located in an air-conditioned laboratory container at the foot of the mast. Sample air is transported through a 25 mm diameter stainless steel tube (finetron tubes, Dockweiler AG, Neustadt-Glewe, Germany) and dried to a relative humidity (RH) below 40 %. An automatic regenerating silica gel adsorption aerosol dryer, as described in Tuch et al. (2009), was installed upstream of the instruments in 2014 and was replaced by a custom-built and automated condensation aerosol dryer in March 2020. For more detailed information on the aerosol measurements setup, see Andreae et al. (2015).

The SMPS measurements cover the particle size range from 10 to 400 nm and yield a temporal resolution of 5 min. The PNSD data cover more than 6 years, from February 2014 to September 2020, covering 1596 measurement days and comprising 426 272 sample runs in total. The data coverage of ~ 67 % over the entire time frame (i.e., February 2014 to September 2020) can be considered a robust data foundation and statistical basis for the observations and conclusion presented here.

The sizing accuracy of the SMPS was frequently checked with monodisperse polystyrene latex particles. Additionally, the data quality was continuously verified by complementary measurements with a condensation particle counter (CPC, model 5412, Grimm Aerosol Technik, Ainring, Germany) measuring the total particle number concentration (N_{CN}) >4 nm. All particle data were visually inspected for malfunction and contamination, further corrected for standard temperature and pressure (STP, 273.15 K, 1013.25 hPa) as well as inlet transmission efficiency according to Moran-Zuloaga et al. (2018). The PNSD data were used for this analysis if N_{CN} from SMPS and CPC agreed within 15 %.

$CN_{<50}$ are particularly prone to diffusion losses at surfaces (e.g., the tube surfaces of the inlet lines) (von der Weiden et al., 2009). Accordingly, the generally sparse occurrence of $CN_{<50}$ in the Amazon frequently raises questions about whether these results are (systematically) biased by unaccounted diffusion losses (e.g., in the 60 m long inlets). The observations outlined below suggest the absence of large and unaccounted for particle losses in the size range that is particularly relevant here (i.e., 10 to 100 nm) and further indicate that the observed PNSDs correctly reflect the actual atmospheric aerosol distribution:

- The inlet and particle transport is optimized for high particle transmission efficiency and short residence time of the sample air. According to the particle loss calculator provided by von der Weiden et al. (2009) and corresponding sensitivity tests, the 50 % transmission efficiency of the inlet at the lower end of the PNSD is reached at $D_{50\,\%} \approx 8$ nm. All PNSDs in this study have been corrected for diffusional, sedimentation, and inertial losses according to von der Weiden et al. (2009).

- Experiments with the SMPS running at the 60 m inlet line and a separate and mobile CPC running without inlet lines at the height of 60 m directly on the tower agreed well, which underlines that no significant fractions of $CN_{<50}$ were lost in the inlet lines.

- Finally, the PNSDs with the sparse particle occurrence < 20 nm reported here agree well with results in previous studies (e.g., Gunthe et al., 2009; Varanda Rizzo et al., 2018).

2.4 Multi-modal log-normal fitting of PNSDs

Each measured PNSD was fitted by a multi-modal log-normal distribution function, according to Heintzenberg (1994):

$$f\left(D_p, D_i, N_i, \sigma_i\right) = \sum_{i=1}^{n} \frac{N_i}{\sqrt{2\pi}\ln(\sigma_i)} \times \exp\left\{-\frac{\left[\ln(D_p) - \ln(D_i)\right]^2}{2\ln^2(\sigma_i)},\right\}, \quad (1)$$

where D_p is the particle diameter, and n is the number of aerosol size modes to be fitted (with $n \leq 3$; see Sect. 2.2). Each mode is characterized by three main parameters: the

mode number concentration N_i, the mode geometric median diameter D_i, and the mode geometric standard deviation σ_i. A script was developed – similarly to the procedure in Hussein et al. (2005) – to provide an automatic user-free decision algorithm to obtain the size modes according to the following steps:

1. In the first step, the maximum particle number concentration and the corresponding particle diameter, D_{dom}, are determined within the particle number size distribution. Within the size range of $-30\,\%$ to $+20\,\%$ of D_{dom}, a one-modal log-normal distribution is fitted.

2. The first one-modal fit is assigned as accumulation ($D_{\mathrm{Acc}} \in [100, 300]$), Aitken ($D_{\mathrm{Ait}} \in [50, 100]$), or sub-50 nm mode ($D_{<50} \in [9, 50]$), and two additional one-modal log-normal distributions are added for the remaining modes. The parameters of the three log-normal distributions are then varied within the mentioned diameter range and the standard deviation and for concentrations less than the maximum of the particle number size distribution.

3. The geometric standard (σ_i) deviation of all modes was constrained within the range of 1.1 to 1.55, which was optimized for the ATTO conditions.

4. Subsequently, a joint optimization of the previously obtained fit parameters (D_i, σ_i, and N_i) for the modes was conducted. The procedure is developed by fixing two of the modes and leaving the third free so that its parameters are again optimized by minimizing the least-squares. The optimization order in this process was to optimize the sub-50 nm mode, then the accumulation mode, and, finally, the Aitken mode. In this case, all the free diameters of the modes could vary between $0.5D_i$ and $1.5D_i$. As a measure of fitting quality, for each particle number size distribution, the algorithm compares the particle number concentrations of each bin of the measured and the fitted curve and obtains the R^2 value. We considered only fits in which the agreement returned $R^2 > 0.8$, which means that about 97 % of the data are covered by the developed mode fitting. Examples of fits can be seen in Fig. S1 in the Supplement.

5. Comparisons between the integrated particle number concentration from the SMPS measurements ($N_{\mathrm{conc,\,SMPS}}$) and log-normal fitted size distributions ($N_{\mathrm{conc},\sum n\mathrm{modes}}$) were made to further assure the quality of the fits. Within this data set, on average, fits with $R^2 = 0.97$ were obtained, which yielded a linear fit of $N_{\mathrm{conc,SMPS}}$ and $N_{\mathrm{conc},\sum n\mathrm{modes}}$ with $R^2 = 0.99$ (Fig. S2).

2.5 Identification of particle growth events

We analyzed the occurrence and properties of *particle growth events* (Amazonian banana plots) in the sub-50 nm and Aitken-mode size range. Characteristic examples of such growth events are shown and discussed in Sect. 3. The growth event identification is based on the following main steps:

1. All data were smoothed to eliminate single exceptionally high or low values to avoid possible bias due to short intense particle peaks or dips. The moving window has two dimensions: one in time and the other in size. The SMPS measurements last 5 min to get a full-size distribution. In order to reduce noise, we average the time window at 25 min. The second parameter is the particle size window, which accounts for five SMPS bins. This is also made to reduce noise in terms of particle size. These two choices were shown as ideal to get reliable data, following suggestions by Kulmala et al. (2012). We also performed several tests to verify if sudden events were missing and found that, in general, the method could cover them without significant losses.

2. All PNSD data were divided into 24 h subsets.

3. Particle growth event days were then automatically flagged based on the guidelines in Kulmala et al. (2012). These guidelines were slightly modified by increasing the size threshold for the initial growth event identification from 20 to 40 nm to account for the characteristics of the Amazonian banana plots and PNSDs.

4. Further following Kulmala et al. (2012), the total particle number concentration of particle diameters > 40 nm was then subtracted from the total particle number concentration of particle diameters $10 \leq D_p \leq 40$ nm. Positive values in the PNSDs are marked as regions of interest for the occurrence of $\mathrm{CN}_{<50}$ that could result in particle growth events. Days fulfilling these criteria are flagged as *particle growth event days*.

5. This method is sensitive to the integral particle number concentration in the Aitken and accumulation modes and their seasonal variation, which might result in false positive or false negative event flagging. To account for that, the results from the automated identification routine were visually inspected, and potentially misinterpreted events were excluded from the analysis. The inspection followed the procedure described in Dal Maso (2005), in which a particle growth event is characterized by (i) the appearance of a distinct new mode of particles in the PNSD, (ii) the particle size inside the sub-50 nm mode, (iii) the mode prevailing for more than 1 h, and (iv) it showing signs of growth in time.

2.6 Growth rate and condensation sink

The GR and the condensation sink (CS) – both important physical parameters in the characterization of growth events – were calculated following the procedures of Dal Maso (2005) and Kulmala et al. (2012). The GR is defined as the rate at which the mean geometric diameter D_p of the $CN_{<50}$ population changes linearly with time:

$$GR = \frac{dD_p}{dt} = \frac{\Delta D_p}{\Delta t} = \frac{D_{p_2} - D_{p_1}}{t_2 - t_1}\ (\mathrm{nm\,h^{-1}}), \quad (2)$$

where D_{p_1} is the geometric diameter of the sub-50 nm mode obtained by the multi-modal fit at the beginning of the growth event at time t_1, and D_{p_2} is the geometric diameter at the end of the growth event at time t_2. Thereby, the *beginning* of a growth event is defined as the moment at which D_p starts to increase. The *end* of a growth event is reached when either (i) D_p (10–50 nm) stops growing, (ii) the growth is interrupted due to sudden changes in air masses, or (iii) D_p reaches the Aitken mode – in this case, we selected D_2 as the last observed growth D_p inside the sub-50 nm mode. There were a few events in which the growth stopped for a while and, afterward, restarted again. In these cases, we considered the second growth to be a new growth event. The growth events considered in this study have a duration of at least 1 h.

A moving average smoothing filter was applied at the mean geometric diameter interval $D_{p_1} \le D_p \le D_{p_2}$, and the fit was obtained by applying a linear model fit at the referred diameter interval. The model returned the following parameters: R^2, p value, and GR. To assure the data quality during the analyses, fits were statistically tested, and only fits with $R^2 > 0.6$ and p value < 0.05 were accepted. Additionally, we performed visual inspections of the quality of each of the fits. It is worth mentioning that fits statistically tested with $R^2 > 0.6$ were able to represent the widest possible variability of growth events, without compromising the analyses.

The CS was calculated from the particle number concentration as (Dal Maso et al., 2002)

$$CS = 2\pi D \int_{D_{p,\min}}^{D_{p,\max}} D'_p \beta_m(D'_p) n(D'_p) dD'_p$$
$$= 2\pi D \sum_{D'_p} \beta_m(D'_{p,i}) D'_{p,i} N_i (\mathrm{s^{-1}}), \quad (3)$$

where N_i is the particle concentration at the diameter $D'_{p,i}$ of the ith size bin, D is the diffusion coefficient of the precursor condensable vapor, and β_m is the transition-regime correction (Fuchs and Sutugin, 1971), defined as

$$\beta_m = \frac{1 + Kn}{1 + 1.677Kn + 1.333Kn^2}, \quad (4)$$

which depends on the dimensionless Knudsen number, $Kn = 2\lambda/D_p$. The Kn parameter represents the ratio of two length scales, where λ is the effective mean free path of the vapor molecules in the gas (Dal Maso et al., 2002).

Physically, CS is a parameter that quantifies the ability of particles to remove condensable vapors from the atmosphere, incorporating them into the particle population and directly influencing the particle growth process. In this study, CS was calculated assuming $D = 0.117\ \mathrm{cm^{-2}\,s^{-1}}$, i.e., the value for sulfuric acid (H_2SO_4) (Gong et al., 2008), which is commonly used in the literature, allowing comparisons to other studies. We used the term CS_{growth} as the average CS during the particle growth event.

2.7 Meteorological parameter measurements

The meteorological parameters, air temperature (T), incoming shortwave radiation (SW), rainfall (P_{ATTO}), air pressure (p), and relative humidity (RH) were measured at an 80 m high tower (02°08.647′ S, 59°59.992′ W; 130 m a.s.l.) located approximately 100 m from the ATTO aerosol mast. The measurements performed at the 80 m tower ranged from 2013 to 2018. Specifically, SW and P_{ATTO} were measured at the top of the tower, whereas T, p, and RH were measured at 55, 55, and 81 m, respectively. From January 2019 to September 2020, the meteorological parameters air temperature (T), rainfall (P_{ATTO}), air pressure (p), and relative humidity (RH) were measured at the 325 m ATTO Tall Tower with a compact weather station (Lufft, WS600-LMB, G. Lufft Mess- und Regeltechnik GmbH, Fellbach, Germany). Overall, meteorological parameters span the time frame from May 2013 to September 2020. Furthermore, an optical fog sensor (OFS; Eigenbrodt GmbH, Königsmoor, Germany) measured the near-field visibility from September 2014 to December 2018 at the height of 50 m. Fog occurrence is defined as visibility below 5000 m, which represents a threshold for light fog. Detailed information on the meteorological instruments can be found in Andreae et al. (2015).

2.8 Equivalent potential temperature

Variations of the equivalent potential temperature, θ_e, have been used as a proxy to indicate downdraft occurrences (Machado et al., 2002; Betts et al., 2002; Varanda Rizzo et al., 2018; Wang et al., 2016; Gerken et al., 2016). θ_e quantifies the temperature of an air parcel, when lifted to a certain height where it condenses (characterized by its lift temperature, T_L), releasing the latent heat, and lowered adiabatically to 1000 hPa. In this study, θ_e was calculated from meteorological parameters measured in situ and was analyzed similarly to Wang et al. (2016) and Varanda Rizzo et al. (2018), using the definition described in Bolton (1980) as

$$\theta_e = T_k \left(\frac{1000}{p}\right)^{0.2854(1-2.8\times10^{-4}r)} \times \exp\left[\left(\frac{3.376}{T_L} - 0.00254\right) r(1+8.1\times10^{-4}r)\right] \quad \text{(K)}, \tag{5}$$

$$T_L = \frac{1}{\frac{1}{T_k - 55} - \frac{\ln\left(\frac{RH}{100}\right)}{2840}} \quad \text{(K)}, \tag{6}$$

where T_k is the ambient temperature in Kelvin, p and r are the ambient pressure (hPa) and the water mixing ratio (g kg^{-1}), respectively, and T_L is the lifting condensation level temperature in Kelvin. To obtain the variations in θ_e, it was necessary to subtract seasonality and diurnal variations.

The steps of this process are illustrated in Fig. S3 and are described as follows: θ'_e was obtained by subtracting the mean seasonal trend values, in which we considered both wet and dry seasons, for each year of the time series. Then, the calculated mean diurnal cycle of θ'_e was subtracted from θ'_e, at the same time of the day, resulting in a new time series: $\Delta\theta'_e$. The quantity $\Delta\theta'_e$ is the anomaly in θ_e and represents the deviation of θ_e from its expected value for that time of the day and season. Values of $\Delta\theta'_e < 0$ are a proxy for the occurrence of downdrafts and indicate a decrease in θ_e due to air masses from the free troposphere that enter the PBL, typically related to the occurrence of rain (Wang et al., 2016; Varanda Rizzo et al., 2018). Other processes may also be related to a decrease in θ_e, such as evaporation of rainfall, river breeze, and advection mechanisms.

It should be mentioned that two time series of meteorological data were used to calculate $\Delta\theta'_e$: the first one, with measurements conducted close to the canopy (2013–2018), and the second one, with measurements conducted at 325 m elevation (2019–September 2020). This was necessary because meteorological data are not available at the 80 m tower for the final period of analysis. The consistency of the $\Delta\theta'_e$ calculation was verified by comparing $\Delta\theta'_e$ for a 2-month period with overlapping measurements at the two height levels (January and February 2019), as shown in Fig. S4. Figure S5 shows the correlation between $\Delta\theta'_e$ obtained at the two levels, with the statistical results of the comparison. Although there are very small differences for single pairs of measurements, the overall agreement is reasonably good and, therefore, does not impact the conclusions of the analysis. These results encouraged us to use the meteorological data measured at 325 m height, which enabled us to extend the data analysis to the years 2019 and 2020. We can not rule out a very fine-scale stratification phenomenon close to the canopy, as observed by Zha et al. (2018), which could have some influence on $\Delta\theta'_e$ but to a minor extent, as observed by the comparison analysis. Further studies are required to examine this aspect in detail for the ATTO site.

2.9 GOES-16 cloud brightness temperature

This study uses infrared brightness temperature (Tir) data obtained by the Geostationary Operational Environmental Satellite (GOES), GOES-16, from November 2017 to April 2020. This data set comprises a total of 914 d with measurements every 10 min, as an indication of the troposphere's meteorological conditions. The Advance Baseline Imager (ABI) – a state-of-the-art 16-band radiometer on board GOES-16 – was employed in this study, specifically, Band 13, the infrared window at 10.3 µm. These measurements are less sensitive than other infrared bands to gas absorption, which allows the cloud-top brightness temperature to be estimated. An area of 3×3 pixels centered at ATTO was selected for obtaining the time series of Tir, representing around 6.0×6.0 km^2. Meteorological conditions representing shallow clouds/clear sky are described by a warm Tir and deep-convection conditions by a cold Tir. Here, we considered Tir > 280 K to be a nearly clear-sky condition, $245 \leq$ Tir < 280 K to correspond to shallow clouds and cumuliform clouds, and Tir < 245 K to correspond to all convective clouds associated with deep convection (Machado and Rossow, 1993; Machado et al., 2002). Tir under nearly clear-sky conditions corresponds roughly to the temperature in the PBL.

3 Results and discussion

3.1 Particle number size distributions for wet and dry season

In agreement with previous studies, our long-term PNSD measurements showed the distinct characteristics of the Amazonian wet- and dry-season aerosol populations (e.g., Roberts et al., 2001; Gunthe et al., 2009; Artaxo et al., 2013; Pöhlker et al., 2016; Varanda Rizzo et al., 2018). We chose a different representation of the typical PNSD shapes in Fig. 2 by showing them as frequency distributions (FDs). The PNSDs differ significantly between both seasons: during the wet season, clear Aitken and accumulation modes stand out, separated by a distinct Hoppel minimum (Hoppel et al., 1986). On average, the Aitken mode is centered at 71 nm, the Hoppel minimum is centered at 102 nm, and the accumulation mode is centered at 153 nm. In contrast, Fig. 2b shows the typical dry-season PNSDs characterized by a strong mono-modal shape with a dominating accumulation mode, reflecting the prevalence of biomass burning pollution (e.g., Rissler et al., 2006; Brito et al., 2014). On average, the accumulation mode is centered at 146 nm. In addition, the distribution in Fig. 2b reveals a contribution of the Aitken mode, centered at 68 nm (mean) and visible as a small shoulder on the dominant accumulation mode.

Regarding the abundance of $CN_{<50}$, the FDs in Fig. 2 reveal that aerosols in this size range are rather sparse – though not absent – during both seasons. The occurrence of $CN_{<50}$

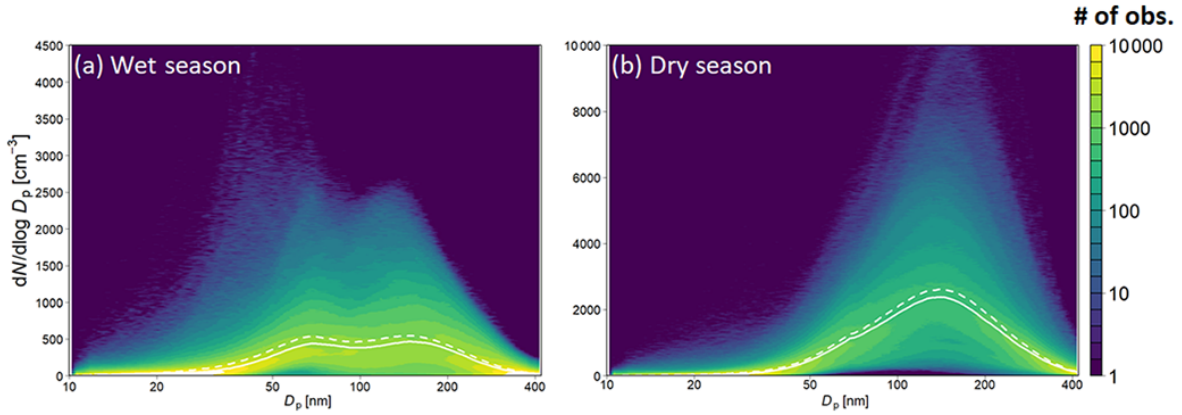

Figure 2. Frequency distributions (FDs) of particle number size distributions (PNSDs) for the Amazonian wet **(a)** and dry season **(b)**. The data basis comprises 6.5 years of SMPS data from February 2014 to September 2020. The color code denotes the number of observations. Solid lines represent the median and dashed lines the mean PNSDs. Please note the different *y* axes. The wet-season PNSD shows pronounced Aitken and accumulation modes. An overwhelming accumulation mode dominates the dry-season PNSD. The wet- and dry-season FDs of PNSDs emphasize a comparatively sparse occurrence of $CN_{<50}$, which form a weak but distinct mode below 50 nm.

in central Amazonia along with the absence of "classical" NPF, as is detected, e.g., in the Scandinavian boreal forests and shown in, e.g., Kulmala et al. (2004), Heintzenberg et al. (2017), Kerminen et al. (2018), and Dall'Osto et al. (2018), is well documented in the literature (e.g., Roberts et al., 2001; Pöhlker et al., 2016; Varanda Rizzo et al., 2018). Although occurring sparsely, the episodic presence of $CN_{<50}$ causes a distinct mode below about 50 nm, noticeable in the wet-season FDs in Fig. 2a. However, the $CN_{<50}$ do not show up clearly in the corresponding mean and median PNSDs. It is further worth noting that the PNSDs under the remote rain forest conditions at ATTO as shown here differ significantly from PNSDs that were obtained in the rain forest atmosphere with an influence of the urban emission plume from Manaus (e.g., Cirino et al., 2018; Fan et al., 2018; Wimmer et al., 2018; Glicker et al., 2019). These urban-influenced PNSDs are characterized by strongly enhanced particle concentrations below about 20 nm. As the mean and median PNSDs do not sufficiently reflect the abundance and properties of $CN_{<50}$ in Fig. 2, the following paragraphs summarize the in-depth analysis that allowed us to extract their event characteristics, seasonal and diurnal variability, and estimated significance.

3.2 Particle growth event characterization

The abundance of $CN_{<50}$, which show up as a weak, though noticeable, mode during the wet season (see the overall outline in Fig. 2a), results from the episodic occurrence of $CN_{<50}$ events and their subsequent growth. Figure 3 shows a typical example of an Amazonian banana plot representing two subsequent growth events, as frequently observed at ATTO. The first example in Fig. 3 starts in the morning hours around 08:30 local time (LT), with an average initial diameter slightly larger than 30 nm. The particles grow for about 4 h, reaching the Aitken mode size range up to ∼ 60 nm. On the same day, a second growth event starts around noon, with an average initial growth diameter slightly larger than 20 nm, growing during the afternoon hours. The initial diameters at the onset of the growth events in Fig. 3 are well above the lower size limit of the SMPS (i.e., 10 nm), which implies that the event characterization is not distorted or limited by the effectively measured size range.

The growth events shown here resemble the events reported by Wang et al. (2016). Note that in all previous studies in Amazonia, the growth events were observed during the wet season, suggesting that this event type is a typical wet-season phenomenon associated with precipitation (Zhou, 2002; Wimmer et al., 2018; Varanda Rizzo et al., 2018). The procedure described in Sect. 2.5 returned 254 characteristic particle growth events on 217 of the 1596 measurement days, corresponding to a frequency of occurrence of ∼ 14 % for event days. For the entire measurement period (February 2014–September 2020) this corresponds to about 30 event days per year. The events have a clear seasonality, with more cases in the wet season, corresponding to ∼ 88 % of events from January to June, while in the dry season from July to December, only ∼ 12 % were observed. Additional aspects of seasonality are discussed in Sect. 3.3.

The GR frequency distribution in Fig. 4a shows a clear peak centered around the median of 5.2 nm h^{-1}. The median GR of this study agrees well with the median GR of 5.5 nm h^{-1} obtained by Varanda Rizzo et al. (2018). Figure S6a contrasts the median GR obtained at different sites in Amazonia and worldwide and shows that the median GR from this study is within the GR ranges obtained at remote

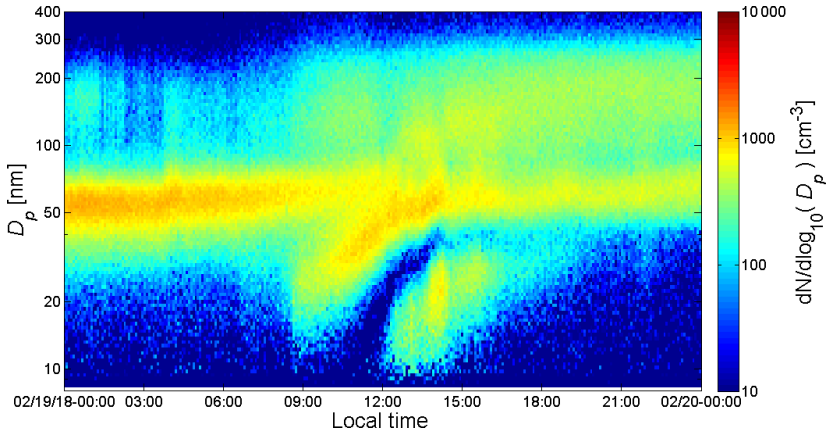

Figure 3. Characteristic examples of two $CN_{<50}$ growth events at ATTO on 19 and 20 February 2018. The temporal evolution of the particle number size distribution (PNSD) is shown as a heat map, emphasizing the pronounced Aitken mode as well as particle growth events from the sub-50 nm particle to the Aitken mode during daylight.

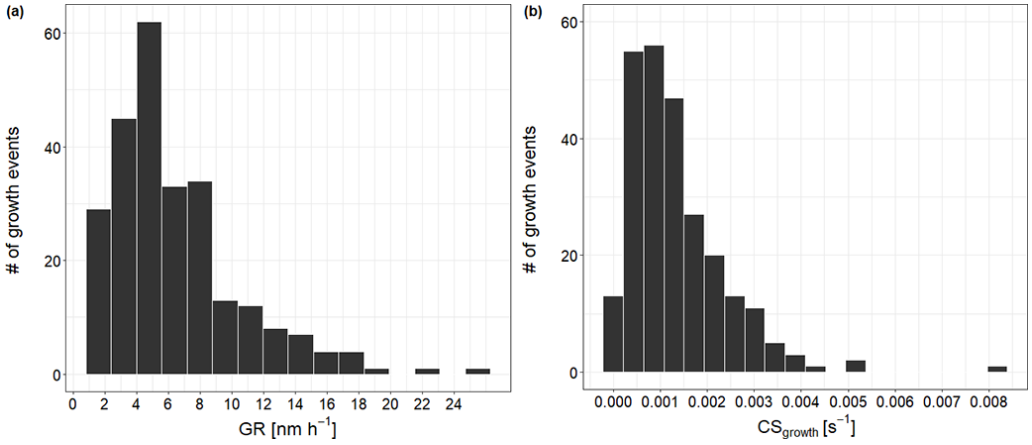

Figure 4. Histograms showing the frequency distribution of the growth rate, GR **(a)**, and condensation sink during the growth events, CS_{growth} **(b)**, for all observed 254 particle growth events.

boreal (0.5 to 5.3 nm h^{-1}) or polar sites (0.2 to 5.5 nm h^{-1}). The CS_{growth} frequency distribution in Fig. 4b shows a clear peak centered around the median of 1.1×10^{-3} s^{-1}. In contrast, the median CS calculated for all observation days is 3.2×10^{-3} s^{-1}, which corroborates that particle growth events at remote sites are expected when CS values are low (Fig. 6d). The Amazonian CS also agrees with what is observed in other remote regions (Fig. S6b). For example, boreal sites have an average CS ranging from 9.8×10^{-4} to 3.9×10^{-3} s^{-1} (Kerminen et al., 2018).

Figure 5a shows the FD of PNSDs exclusively for the periods of growth events, starting 3 h before the event's onset and lasting until the time when growth stopped being observed (according to Sect. 2.6). Figure 5b shows the separated $CN_{<50}$, Aitken, and accumulation modes for the median wet season. The characteristic multi-modal shape of the wet-season PNSDs stands out. The FD for the growth events further underlines the sparse particle abundance below 20 nm. Figure 5b shows that the Aitken and accumulation modes are the dominant modes of the median wet-season PNSD. The $CN_{<50}$ mode, although small and not readily perceptible from the median PNSD, has a significant contribution, however, and is centered at $D_{CN_{<50}} = 34$ nm, with $\sigma_{CN_{<50}} = 1.5$. For comparison, the diameters selected as the initial values for the growth events, $D_{p,i}$, have a median value of 26.1 nm, with 25th and 75th percentiles of 19 and 33 nm, respectively. The Aitken mode of the median distribution is centered at $D_{AIT} = 69$ nm, with $\sigma_{AIT} = 1.3$, and the accumulation mode is centered at $D_{ACC} = 149$ nm, with $\sigma_{ACC} = 1.5$. This clearly shows that the initial diameter of

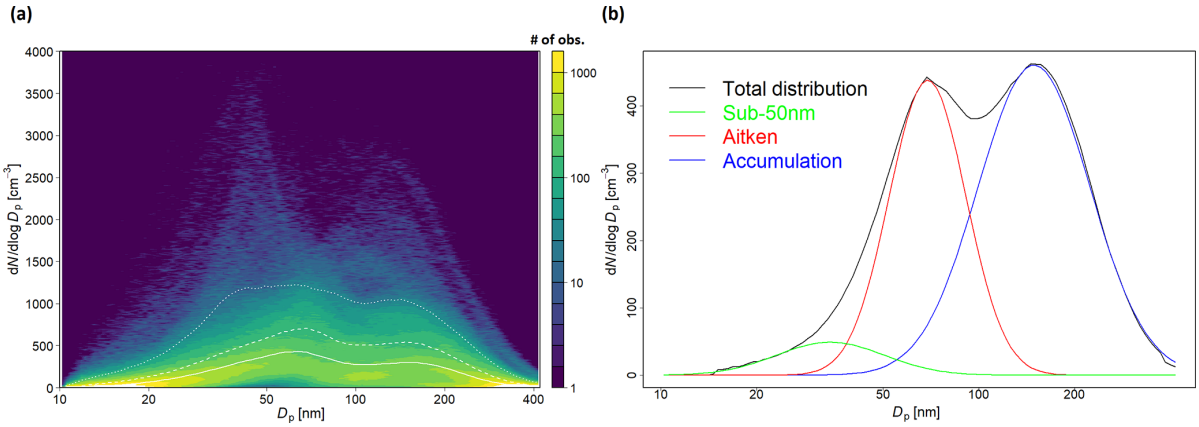

Figure 5. **(a)** Frequency distribution of particle number size distributions exclusively for growth event periods. The color code denotes the number of observations, solid lines indicate the median, and dashed lines indicate the 75th and 90th percentiles. The PNSDs for the growth events show a high frequency of $CN_{<50}$ and Aitken size modes. The FDs do not show any evidence of *open* PNSDs towards the lower detection limit. **(b)** Median wet-season PNSD (black line), showing its three log-normal modes: in green, the sub-50 nm size particle mode; in red, the Aitken mode; in blue, the accumulation mode; and in black, the total median distribution. The adjusted R^2 obtained for the calculated multi-modal log-normal fit is 0.99.

growth events in the Amazon is typically larger than reported in other regions (Nieminen et al., 2018).

3.3 Seasonality

The pronounced atmospheric seasonality in central Amazonia has been characterized by means of meteorological, aerosol, and cloud microphysical data in previous studies (e.g., Pöhlker et al., 2018, 2019; Moran-Zuloaga et al., 2018; Saturno et al., 2018a). Figure 6a shows the typical seasonality of precipitation at ATTO, P_{ATTO}. The highest rain rate occurs during the wet season, with P_{ATTO} peaking in March and April, while the minimum in P_{ATTO} occurs between July to September. A similarly pronounced seasonality can be found in various aerosol properties. The N_{CN} in the size range between 10 to 400 nm had its minimum in the wet-season months of March and April, with a median of $\sim 280\,cm^{-3}$, and its maximum in the dry-season months of August to November, with a median of $\sim 1400\,cm^{-3}$ (Fig. 6c).

The same pattern can be found in the monthly median CS in Fig. 6d. The strong seasonal differences in the physical aerosol properties – here manifested in a wide range of N_{CN} and different PNSD shapes – have a substantial influence on the concentration of available CCN and, thus, cloud microphysical processes in the Amazon Basin (Pöhlker et al., 2016, 2018). These results agree well with long-term measurements at another central Amazonian site (i.e., the ZF2 site) presented by Varanda Rizzo et al. (2018) and allow to put earlier campaign-wise measurements into a broader context (e.g., Roberts et al., 2001; Roberts, 2003; Zhou, 2002; Rissler et al., 2004, 2006; Martin et al., 2010).

Figure 6e shows the seasonal pattern in the $CN_{<50}$ growth event frequency. We found the highest frequencies during the wet season, peaking in April with about 26 %, and dropping down during the transition period (WtoD, June and July) to a minimum with almost zero events in August. The growth event occurrence stayed remarkably low during the dry-season months, with frequencies mostly below 3 % from July to November. Frequency levels increase again during the transition period (DtoW, December and January). The seasonality in growth event occurrence corresponds well with the seasonality in monthly rainfall and appears inversely related to the seasonality in N_{CN} and CS. This agrees with previous studies in the Amazon, suggesting a close link between generally low particle concentrations and the appearance of $CN_{<50}$- and Aitken-mode particles in the PBL (e.g., Krejci, 2003; Wang et al., 2016). The low CS might further favor the characteristic growth patterns of these events through the condensation of semi-volatile and low-volatility gaseous compounds on the $CN_{<50}$ particle fraction as available surfaces (see example in Fig. 3a) (Dal Maso, 2005; Dal Maso et al., 2007; Dada et al., 2017; Kerminen et al., 2018; Nieminen et al., 2018; Wiedensohler et al., 2019).

The N_{CN}, CS, and growth event occurrence in Fig. 6 are all based on the same multi-year SMPS data set. The underlying data availability is documented in Fig. 6b as the number of valid measurement days. To provide a seasonal overview, Table 1 shows statistical information on GR and CS_{growth} during the observed growth events, separated by the month of the year. In the wet season, when ~ 88 % of all growth events occurred, the GR values fluctuate around the median GR of $5.2\,nm\,h^{-1}$. The CS_{growth} shows a similar behavior, fluctuating around $1.1 \times 10^{-3}\,s^{-1}$. The low-

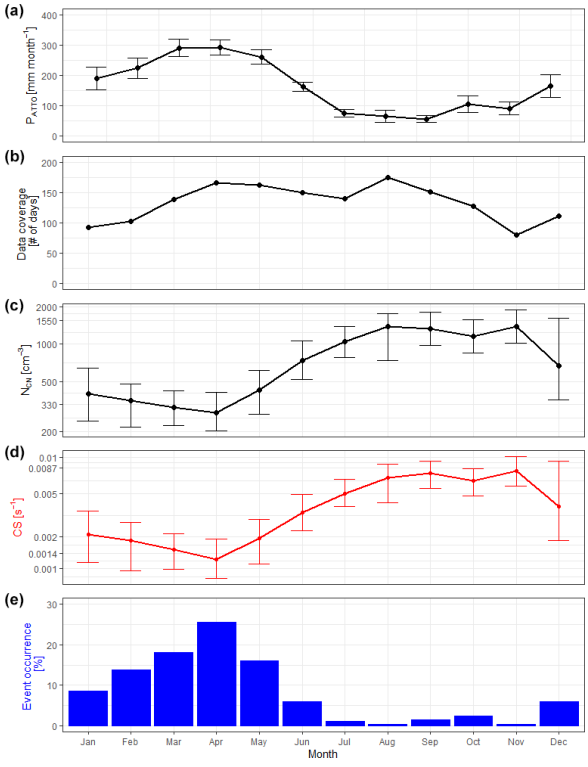

Figure 6. The seasonal cycles of selected meteorological and aerosol parameters presented as monthly averages for the entire observation period from February 2014 to June 2020. From top to bottom: **(a)** P_{ATTO} monthly rain measured at ATTO, where error bars denote the standard deviation. **(b)** SMPS data coverage as the number of measurement days. **(c)** Median total particle number concentration in the size range of 10 nm < D < 400 nm, calculated from SMPS data, where error bars denote the interquartile range (please note the logarithmic scale). **(d)** Median condensation sink per month calculated from SMPS data, where error bars refer to the interquartile range (please note the logarithmic scale). **(e)** Annual cycle of the occurrence of $CN_{<50}$ particle growth events.

est median GR of the wet season is found in March, with 3.7 nm h^{-1}, while the lowest CS_{growth} of the wet season is found in April, with 8.0×10^{-4} s^{-1}. The number of particle growth occurrences drops in the dry season, comprising only ∼ 12 % of the total growth events. During December, in the transition from the dry to wet season, the percentage of growth events starts to increase to ∼ 6 %. The average CS_{growth} (during growth events, Table 1) in the dry season is lower compared to the average monthly CS (see Fig. 6), indicating that growth events occur on days with a cleaner atmosphere compared to average dry-season conditions. The only exceptions are the events from October, whose median CS_{growth} was 4.4×10^{-3} s^{-1}.

Table 1. Monthly median with 25th and 75th percentiles (in parentheses) of GR and CS_{growth}. The percentage of growth events in each month is also presented. Note that the statistics shown refer to the growth events only.

Month	GR (nm h^{-1})	CS_{growth} ($\times 10^{-3}$ s^{-1})	Fraction of events (%)	No. of events
Jan	5.0 (2.5, 6.9)	1.2 (0.8, 1.6)	8.7	22
Feb	5.2 (3.9, 8.1)	1.3 (0.8, 2.1)	13.8	35
Mar	3.7 (2.6, 6.3)	1.0 (0.5, 1.5)	18.1	46
Apr	5.3 (4.5, 8.6)	0.8 (0.5, 1.2)	25.6	65
May	5.5 (4.0, 8.2)	1.1 (0.6, 1.9)	16.1	41
Jun	6.1 (4.6, 9.4)	2.5 (1.2, 3.0)	5.9	15
Jul	8.2 (6.2, 8.6)	3.4 (2.6, 3.8)	1.2	3
Aug	5.2 (5.2, 5.2)	1.1 (1.1, 1.1)	0.4	1
Sep	10.4 (3.7, 18.8)	1.7 (1.2, 1.9)	1.6	4
Oct	8.8 (4.9, 13.1)	4.4 (3.3, 5.2)	2.4	6
Nov	4.2 (4.2, 4.2)	3.7 (3.7, 3.7)	0.4	1
Dec	6.2 (4.7, 8.0)	1.2 (0.9, 1.5)	5.9	15

As outlined above, our results indicate that the occurrence of particle growth events is linked to the pronounced seasonality of the aerosol properties and the related underlying meteorological conditions and prevailing air mass history. In the dry season, regional and long-range-transported biomass burning aerosol from the Southern Hemisphere dominates the aerosol population in the lower troposphere (e.g., Moran-Zuloaga et al., 2018; Saturno et al., 2018b; Holanda et al., 2020). The resulting strong accumulation mode and, hence, the high CS likely suppress the growth of the smaller particles in the sub-50 nm mode. With the increase in precipitation (thus, in wet deposition) and the change in the average air mass history towards northern hemispheric origins, less polluted air masses arrive at the ATTO site (e.g., Moran-Zuloaga et al., 2018; Pöhlker et al., 2018). The number of particles of the accumulation mode and CS decreases significantly, coinciding with an increase in the occurrence of growth events.

3.4 Diurnal trends

The diurnal patterns of the growth event occurrence are shown in Fig. 7 in relation to meteorological parameters, such as air temperature (T), SW, P_{ATTO}, RH, and near-field visibility representing fog. Note that we contrasted the diurnal cycles for the entire observation period (i.e., February 2014 to September 2020, shown as solid lines) and the wet-season months (i.e., February to May, shown as dashed lines), since the majority of the growth events are observed during the wet season. The meteorological variables, T, SW, RH, and visibility were not discriminated with respect to days with and without events because no significant differences between event and non-event days were observed. Possible effects of deep convection, associated rainfall, and cloudiness are investigated in Sect. 3.5. In the diurnal cy-

Table 2. Median and 25th and 75th percentiles (in parenthesis) for Tir, $\Delta\theta'_e$, $D_{p,i}$, GR, and CS_{growth} for each hourly group. Tir, $\Delta\theta'_e$, and $D_{p,i}$ correspond to the onset of the particle growth event.

Group	Hour (local time)	Tir (K)	$\Delta\theta'_e$ (K)	GR ($nm\,h^{-1}$)	CS_{growth} ($\times 10^{-3}\,s^{-1}$)	$D_{p,i}$ (nm)	Fraction of events (%)
G1	01:00–05:59	269 (238, 283)	−0.8 (−4.6, 1.5)	3.8 (2.3, 5.5)	0.9 (0.4,1.5)	27.7 (21.7, 35.3)	16
G2	06:00–11:59	268 (236, 282)	−1.9 (−5.3, 2.1)	6.3 (4.2, 8.6)	1.2 (0.7, 2.0)	27.7 (20.6, 33.5)	53
G3	12:00–17:59	245 (219, 283)	−3.6 (−6.8, 0.5)	5.6 (4.0, 8.6)	1.2 (0.8, 1.5)	24.6 (19.4, 29.9)	21
G4	18:00–00:59	274 (227, 276)	0 (−4.3, 2.1)	4.2 (2.1, 6.3)	1.0 (0.6, 1.5)	27.8 (19.5, 32.7)	10

cles considering the whole period of observations, T and SW show the typical tropical rain forest conditions with about 12 h daylight and a remarkably low amplitude in T, spanning on average only 5 °C. Rainfall is most intense in the afternoon hours, with the highest precipitation intensity at 15:00 LT. The data also show a secondary maximum in the early morning, which has been associated with nocturnal long-lived mesoscale systems (Machado et al., 2021). The RH levels reach on average 100 % during the early morning and decrease during the day to around 75 %. Fog typically occurs in the second half of the night and often in the early morning before sunrise (i.e., between 03:00 and 07:00 LT), when T is lowest. Sporadically, fog also occurs shortly after rain showers, which is not reflected in the average conditions.

Figure 7e shows the diurnal cycle of the median $CN_{<50}$ number concentration, $N_{<50}$, during the particle growth event days (blue line) and for comparison, the median diurnal cycle of $N_{<50}$ comprising all measured PNSDs (black line). The particle concentration on growth event days is somewhat higher than that including all analyzed PNSDs, with median daily values and an interquartile range of 64 (38–108) cm^{-3}, compared to 49 (29–81) cm^{-3} for all days. The diurnal cycles of both the particle concentration during growth events and for the entire measurement period also show some similarities. Around 09:00 LT in the morning, there is a remarkable decrease until noon, which is followed by an increase towards midnight. The decrease starting in the late morning is likely due to increased mixing after the breakup of the nocturnal boundary layer and the development of a well-mixed boundary layer. Towards the late afternoon, the well-mixed layer is then shrinking due to decreasing solar radiation. The $N_{<50}$ diurnal cycle for growth event days shows further a strong increase from midnight to 09:00 LT, peaking at $N_{<50} = 88\,cm^{-3}$, compared to $N_{<50} = 56\,cm^{-3}$ at the same time for the total data. At this time, the difference between the growth event particle concentration and the average is largest and coincides with the highest occurrence of growth events.

The diurnal cycle of the growth event onsets has a rather broad maximum in the early morning hours from 06:00 to 10:00 LT. It peaks at about 07:00 LT and then gradually decreases towards noon (see Fig. 7f), which is in agreement with what is observed in Fig. 7e. In addition to the PBL

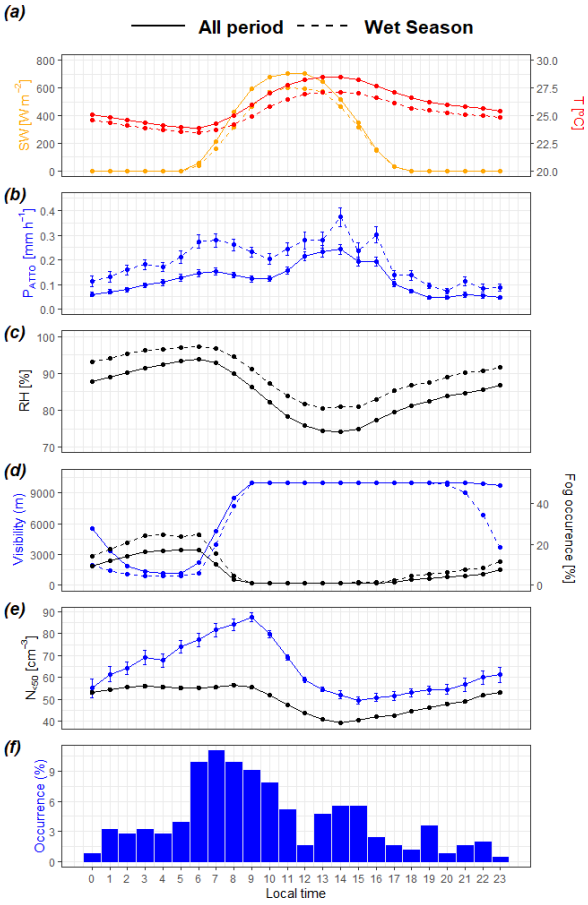

Figure 7. Diurnal cycle of selected meteorological parameters and the diurnal occurrence of particle growth events. From top to bottom: **(a)** incoming shortwave radiation (SW, orange) and air temperature (T, red) at 26 m (canopy level) height, **(b)** average local rain rate (P_{ATTO}, blue), **(c)** relative humidity (RH) at 26 m, **(d)** visibility (blue) measured by a fog monitor and fog occurrence (black) with lines representing the first quartile, **(e)** median diurnal cycle of $N_{<50}$ for all data (black) and only for the days on which particle growth events were observed (blue), and **(f)** the diurnal cycle of the particle growth event onsets. All error bars denote the standard error. The data shown represent all observations (full lines) and wet-season subsets (dashed lines).

development, particles are subject to atmospheric aging and likely condensation of semi-volatile and low-volatility compounds resulting in particle growth and a decrease in particle number concentration. It is interesting to note that the morning growth event maximum coincides with a maximum in RH and the occurrence of fog (see Fig. 7c, d). A second local and less pronounced maximum is visible from 13:00 to 15:00 LT. The growth events reported during daytime likely correspond to rainfall events, as reported by Machado et al. (2021) and probably the vertical transport of $CN_{<50}$ and Aitken size particles due to strong downdrafts in the course of convective rainfall and the injection of these particle populations into the PBL, as reported in Wang et al. (2016) and Andreae et al. (2018).

P_{ATTO} shows two maxima: a pronounced and rather defined maximum in the early morning at around 07:00 LT, which follows a gradual increase in precipitation during the second half of the night, and a broader maximum during the afternoon hours between 13:00 and 17:00 LT. Although about 74 % of the particle growth events occur during the day, there are still ∼ 26 % that take place during night conditions, between 19:00–05:00 LT. In particular, the occurrence of growth events from 01:00–05:00, which represents about 16 % of the total observed events, is evidence for complexity in the causes and mechanisms of particle injection and growth.

The evolution of the PBL also has a strong influence on the diurnal pattern. At night, the nocturnal PBL close to the forest canopy is decoupled from the residual layer above (Fisch et al., 2004). In the morning hours – as soon as convection becomes effective – air masses transported into and within the residual layer are mixed into lower levels and measured at the canopy level. Consequently, $CN_{<50}$ and Aitken-mode particles advected with the residual layer will be mixed downwards and appear at the 60 m inlet in the morning hours, typically around 08:00 LT. This behavior is in agreement with that observed in Fig. 7e, with the increase of $CN_{<50}$ throughout the night and in the early morning. Machado et al. (2021) discuss this daily mechanism of particle growth in more detail. Section 3.5 further discusses the meteorological conditions regarding convective downdrafts and the atmospheric conditions under which the growth events are observed.

A contrast in GR and CS is observed when day and night events are compared, as shown in Fig. 8. Daytime events, which correspond to ∼ 74 % of the events, have significantly higher GR and CS_{growth}, at 5.9 nm h^{-1} and 1.2×10^{-3} s^{-1}, respectively. The nighttime events, which account for ∼ 26 %, have GR and CS_{growth} of 4.0 nm h^{-1} and 9×10^{-4} s^{-1}, respectively. To verify the statistical significance of the difference between day and nighttime values, the Wilcoxon rank-sum test was applied. The p value obtained for GR is 3.6×10^{-6}, while the p value obtained for CS_{growth} is 2×10^{-2}, indicating that the data groups regarding day and night are statistically different considering a significance level of 5×10^{-2}. The observed differences are likely due

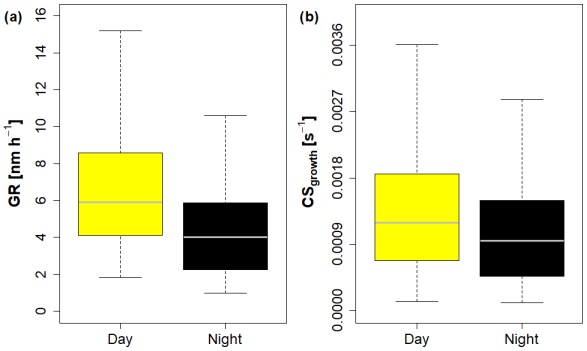

Figure 8. Box plot of **(a)** GR and **(b)** CS_{growth} related to growth events that occurred during the day or night. Nighttime events occurred between 19:00 and 05:00 LT, while daytime events occurred between 06:00 and 18:00 LT. The box represents the quartiles, whiskers represent 90th and 10th percentiles, and the horizontal lines represent the median.

to the different atmospheric mechanisms during daytime and nighttime. Figure 7a and f clearly indicate an increase of growth events with the increase in the intensity of solar radiation after sunrise. With increasing solar radiation, atmospheric aging and oxidation of possible precursor intensify. Sunlight also drives the dynamics of the PBL. Other phenomena also play an important role in daytime events, such as the peaks of precipitation that coincide with the peaks of growth events, which is discussed in more detail in Sect. 3.5. In contrast, the occurrence of nocturnal events may be related to different mechanisms such as local meteorological phenomena, horizontal advection, entrainment of air and particles from the free atmosphere into the PBL, and perhaps the contribution of biogenic sources from the surface.

3.5 Meteorological and cloud conditions during growth events

This section explores the weather and convective transport conditions linked to particle growth events. Figure 9a shows a histogram of the growth event frequency as a function of the associated anomaly of the equivalent potential temperature ($\Delta\theta_e'$) at the onset of the growth events (see Sect. 2.8). A negative $\Delta\theta_e'$ is an indicator for air mass downdrafts from higher altitudes, as has been shown for the events analyzed by Wang et al. (2016). We found that ∼ 63 % of events were likely associated with air mass downdrafts ($\Delta\theta_e' < 0$ K), whereas ∼ 37 % were associated with $\Delta\theta_e' > 0$ K. Figure 9b shows a histogram of all growth events as a function of the associated cloud brightness temperature, which is an indicator for deep convective clouds (Tir < 245 K) vs. clear-sky/shallow-cloud conditions (Tir > 280 K). For all events after 2017 (when Tir data are available), we found that ∼ 36 % were likely associated with deep convective clouds (Tir < 245 K, red), ∼ 26 % with clear sky/shallow clouds

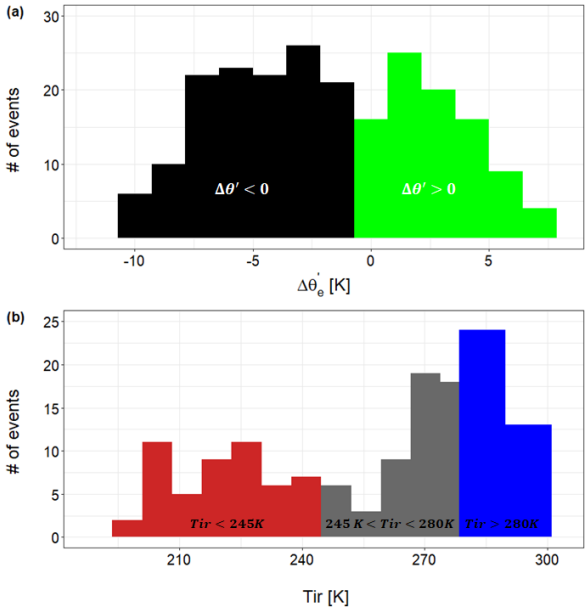

Figure 9. Histograms of **(a)** the values of $\Delta\theta_e'$ at the beginning of the particle growth events. Black bars represent events during downdraft conditions and the green bars during undefined conditions. **(b)** The values of Tir at the beginning of the particle growth events. Red bars represent events during deep-convection conditions, blue during clear-sky/shallow-cloud conditions, and gray during mixed-sky conditions.

(Tir > 280 K, blue), and ∼ 38 % with mixed-sky conditions (245 K < Tir < 280 K, gray).

The most contrasting Tir conditions were observed between the lower quartile (Tir < 228 K), representing deep convective cloud conditions, and the upper quartile (Tir > 281 K), representing clear-sky conditions, with 36 events contained in each group. As an example, four of these "extreme" events were selected (Fig. 10) for daytime and nighttime conditions. The growth events under clear-sky conditions are characterized by a trimodal aerosol population, with accumulation and Aitken modes as well as a third mode below 50 nm. As an example, the event on 14 March 2019 (daytime, clear sky) was characterized by the occurrence of a significant amount of $CN_{<50}$. The particle concentration for particles smaller than 50 nm increased already during nighttime (starting after 02:00 LT) and resulted in a pronounced peak around 08:00 LT. While during the late night and early morning, the mean modal diameter for these small particles is rather constant, particle growth started around 08:00 LT and lasted for about 10 h. These events could be associated with advection processes, e.g., by a downdraft in the gust front (clear sky nighttime) or by nighttime rainfall. Afterwards, subsequent growth begins in the early morning coinciding with the evolution of the PBL.

The events under deep convective conditions – both during daytime and nighttime – resemble the events reported by Wang et al. (2016). Here, downdrafts transport air masses into the lower atmosphere and, hence, inject $CN_{<50}$ upper tropospheric particles into the PBL, followed by particle growth into the Aitken mode. In both these cases, the atmosphere is very clean, with low concentrations in the accumulation mode. Before the growth event, most of the particle population is in the Aitken size mode, which is removed by the injection of upper or mid-tropospheric air during the downdraft event, so that only the $CN_{<50}$ aerosol population remained. Note that about 4 h after the start of the growth event, the accumulation-mode particles (re)appeared, probably by mixing with surrounding air masses.

Figure 11 shows box plots for GR in panel (a) and CS_{growth} in panel (b) for clear-sky and deep-convection conditions. The median GR for clear-sky conditions is 7.0 nm h^{-1}, whereas the median GR for deep-convection conditions is 3.8 nm h^{-1}. Regarding CS, under clear-sky conditions the median is 1.6×10^{-3} s^{-1}, while under deep convection, the median CS is 5×10^{-4} s^{-1}. The results show that different meteorological processes play an important role for the different particle growth events observed. The events that occurred under deep-convection conditions present much lower CS_{growth} and considerable lower GR. Two main factors may influence this result: the precipitation during deep-convection conditions cleans the atmosphere by wet scavenging, resulting in lower CS_{growth} values, and the presence of clouds reduces the availability of sunlight and thereby suppresses photochemical production of condensable species.

To further investigate typical conditions or processes related to the observed growth events, here we discriminate between different groups based on their daily frequency distribution. The growth events (see Fig. 7f) were divided into four groups (G1 to G4), where G1 and G4 represent nighttime, and G2 and G3 represent daytime events. The daytime events were divided considering the occurrence of two frequency peaks: the first peak, representing 53 % of the growth events, is included in G2, covering the time from 06:00 to 11:59 LT. The afternoon increase, representing 21 % of the growth events, is included in G3, covering the time from 12:00 to 17:59 LT. The nocturnal events were divided according to the evolution stage of the PBL. Events between 18:00 and 00:59 (G4), with 10 % of the events, are still influenced by some PBL turbulence but may also have had some influence from convective events in the late afternoon.

The growth events between 01:00 and 05:59 (G1), with 16 % of the total growth events, are the most enigmatic ones. They are not directly driven by photochemistry or variations in the PBL, since at this time the nocturnal PBL is already well established. Different mechanisms such as air mass entrainment into the PBL by, e.g., intermittent turbulence (Dias-Júnior et al., 2017), nighttime rainfall events, or even an unknown biogenic source could play a role in the aerosol particle dynamics of in this time period. Table 2

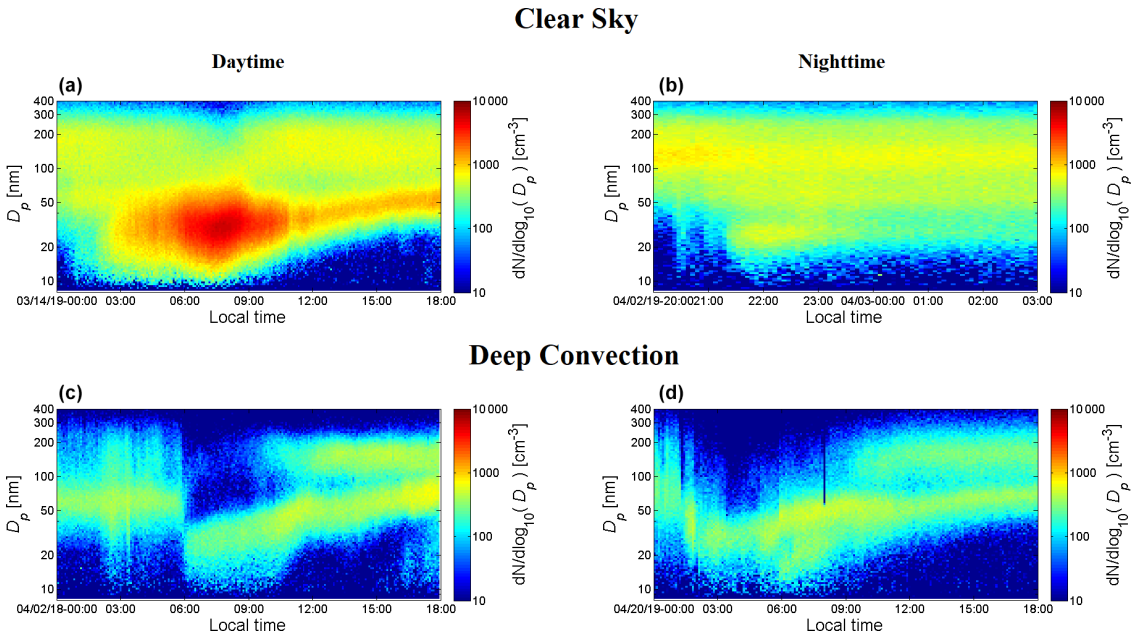

Figure 10. Selected particle growth events according to the Tir value at the onset of the event. Events under clear-sky/shallow-cloud conditions during daytime **(a, c)** and nighttime **(b, d)** were selected based on Tir > 281 K (third quartile), while deep-convection events were chosen based on Tir < 228 K (first quartile).

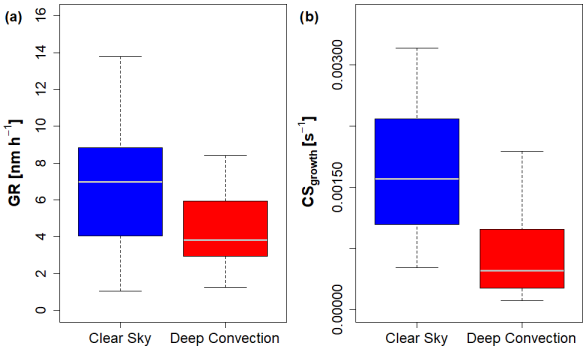

Figure 11. Box plot of **(a)** GR and **(b)** CS_{growth} for clear-sky conditions (Tir > 281 K) vs. deep-convection conditions (Tir < 228 K). Boxes represent the quartiles, whiskers represent 90th and 10th percentiles, and the horizontal line represents the median.

shows the median Tir, $\Delta\theta_e'$, the initial diameter at the onset of the growth event, $D_{p,i}$, and the GR and CS_{growth} for the four hourly groups.

The results indicate differences between the four groups (G1 to G4) regarding the Tir and $\Delta\theta_e'$ conditions during the event onset. The nocturnal groups G1 and G4 have median $\Delta\theta_e'$ of −0.8 and 0 K, respectively. Their median Tir indicates conditions closer to low clouds and clear skies, with median values equal to 269 and 274 K for G1 and G4, respectively. Figure 12 shows the average (mean and standard deviation) Tir for the entire event days separated for the different groups of events (blue). The Tir diurnal cycle shows clear differences between the groups. Within the G1 period, Tir shows a minimum at 04:00 LT, when the average brightness temperature reaches 256 K, indicating convective activity and early precipitation compared to all days.

The G4 group, with the smallest number of growth events, is not significantly different from the median diurnal cycle for all days, suggesting that this 10 % of growth cases appears not be related to specific meteorological events. There are signs of convection at 16:00 LT, which coincides with the precipitation peak in the afternoon. Afterward, Tir increases, going to clear-sky conditions during the night. The median GR for G1 and G4 varies from 3.8 to 4.2 nm h^{-1}, respectively, and CS_{growth} is approximately constant around 1.0×10^{-3} s^{-1}, while the median $D_{p,i}$ is similar for both nocturnal groups. The daytime groups G2 and G3 have the lowest median $\Delta\theta_e'$ at the onset of the events, with −1.9 and −3.6 K, respectively, indicating that convective downdraft activity plays an essential role during these growth events. For these two groups, the diurnal cycle of Tir presents lower values during the whole day compared to the overall average, and the G2 group also shows minima in the early morning coinciding with the precipitation peaks and also in the afternoon (Fig. 7b).

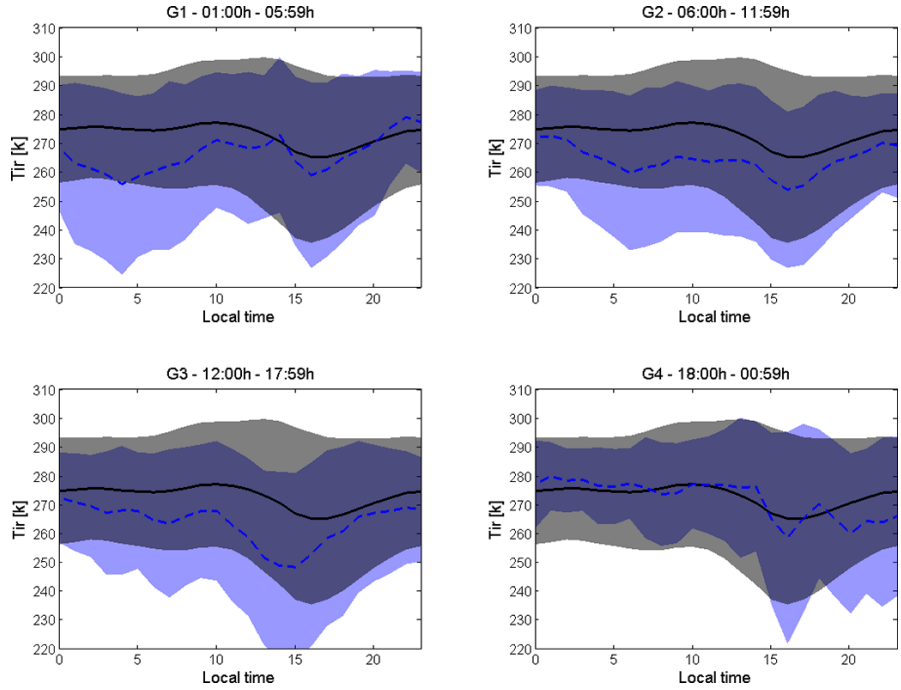

Figure 12. Average diurnal cycle of Tir for the event days in the groups G1 to G4. The dashed blue line represents the average diurnal cycle of Tir relating to the days when the particle growth events for a given group were observed. The black line represents the average diurnal cycle for all days on which PNSD measurements were made. The colored shading represents the standard deviations.

The G3 group is the one with the most convective characteristics. The Tir values indicate an occurrence of strong convective systems throughout the day, mainly in the afternoon. In particular, the pronounced decrease at 15:00 LT reaches deep-convection conditions, with Tir = 249 K, approximately 1 h earlier than expected considering the entire observation days. The median GR ranges from 6.3 to 5.6 nm h^{-1} in G2 and G3, respectively, and the median CS_{growth} remains similar for both groups, at 1.2×10^{-3} s^{-1}. The smaller value of GR in G3 compared to G2 (diurnal events) could be associated with deep-convection systems, which reduce the solar irradiance and thereby influence the photochemical processes. The presence of clouds has been associated with lowering GR and even lower occurrences of NPF and particle growth events (Dada et al., 2017; Kerminen et al., 2018). The median $D_{p,i}$ for G3 is the lowest of the four groups, at 24.6 nm, indicating that the strong convective downdrafts are more effective in transporting smaller particles from the free troposphere into the PBL, which agrees with what has been observed previously (Wang et al., 2016). Therefore, the growth events of groups G2 and G3 are probably influenced by the strong convective systems during daytime. In particular, the G3 group has the most significant characteristics of deep convection and intense occurrences of downdraft throughout the day.

When discriminating the growth events by positive or negative $\Delta\theta'_e$ at the event's onset (here defined as $\Delta t = 0$) and looking 10 h before and after this time, the different behavior of $\Delta\theta'_e$ and Tir near the growth event is evident. Figure 13 shows the behavior of the mean ensembles of $\Delta\theta'_e$ and Tir around $\Delta t = 0$ for $\Delta\theta'_e$ less than the 25th percentile (−5.3 K) and higher than the 75th percentile (+1.5 K) at the event's onset. Considering the case where $\Delta\theta'_e < -5.3$ K at the event's onset, both $\Delta\theta'_e$ and Tir strongly decrease from 10 h before the event and reach a minimum at $\Delta t = 0$, where $\Delta\theta'_e = -7.6$ K and Tir = 238 K, which represents deep-convection conditions with strong downdraft occurrence. Both parameters increase afterwards to cleaner sky conditions and out-of-downdraft conditions.

In contrast, for $\Delta\theta'_e > +1.5$ K at the event's onset, the ensembles show an opposite behavior of the parameters. The $\Delta\theta'_e$ presents an increasing tendency from 10 h before the event until $\Delta t = 0$, reaching a value of +4 K. Afterward, $\Delta\theta'_e$ decreases but always retains positive values, indicating that there is a class of growth events that may not be driven by convective downdrafts. The Tir values from 10 h before the events up to $\Delta t = 0$ are equivalent to conditions close to clear skies (Tir ∼ 280 K), which agrees with the results obtained for $\Delta\theta'_e$, as an indication of sky conditions not dominated by convection systems around the event's onset. After $\Delta t = 0$,

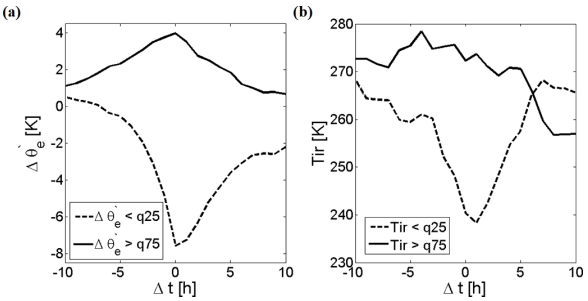

Figure 13. Ensemble analysis for **(a)** $\Delta\theta_e'$ and **(b)** Tir considering 10 h before and 10 h after the event's onset. The cases where $\Delta\theta_e'$ at the event's onset is less than the 25th percentile (dashed lines) and more than the 75th percentile (full lines) are shown. In total, 72 cases were considered in the analysis (36 cases for each condition).

Tir values decrease but without presenting deep-convection conditions. This shows that clear-sky events can be associated with either advection or subsidence bringing particulates from another area (e.g., a nearby rain event) or from the upper troposphere.

4 Summary and conclusions

This study reports the statistical characterization of aerosol particle growth events in the sub-50 nm size range (10–50 nm), based on continuous measurements (February 2014 to September 2020) of PNSDs at a remote site in central Amazonia. In total, 254 particle growth events were detected, comprising about 14 % of the analyzed days. Of all events, 88 % were found between January and June and 12 % between July and December. The diurnal cycle of the growth events shows that most of them occur during the daytime, accounting for 74 %, which still leaves a significant fraction of 26 % occurring during the night. During daytime, 53 % of the growth events start in the morning between 06:00 and 11:00 LT, with a pronounced peak at 07:00 LT, showing a relation to the photochemistry and links with the evolution of the PBL. These events also coincide with a precipitation peak in the morning. The nocturnal increase of $N_{<50}$ is likely related to convective systems that result in the precipitation peak in the morning. The subsequent decrease of $N_{<50}$ is likely due to condensation of semi- and less-volatile organic species on the sub-50 nm particles, resulting in growth. A second, less pronounced but significant peak occurs around 15:00 LT, coinciding with the strongest precipitation peak, also suggesting a relation to atmospheric convective systems.

The median GR, considering all the growth events, is 5.2 nm h^{-1}, which agrees with what was reported by Varanda Rizzo et al. (2018). The median CS_{growth} is 1.1×10^{-3} s^{-1}. Monthly variations in GR and CS show that during the wet season the growth events occur under low CS values, although the average CS_{growth} does not change much from month to month, oscillating around 1.1×10^{-3} s^{-1}. A remarkable contrast is observed when comparing daytime (median GR of 5.9 nm h^{-1} and median CS_{growth} of 1.2×10^{-3} s^{-1}) and nighttime growth events (median GR of 4.0 nm h^{-1} and median CS_{growth} of 9×10^{-4} s^{-1}).

Daytime events are directly influenced by sunlight, which controls photochemistry and hence the oxidation of SOA precursors. In contrast, nocturnal events may have different causes and mechanisms. One particular mechanism for nighttime growth events could be supported both by the continued deposition of condensables formed during the day and by the production of condensables at night by ozonolysis reactions. However, the direct influence of meteorology, entrainment of air masses, and perhaps the contribution of biogenic sources can not be ruled out. Upcoming flight and in situ campaigns are expected to provide new important insights into the main drivers of the sources for the different particle growth events. It is worth noting that, for primary biogenic emissions, there is still the need to identify the particle sources, although earlier studies have shown that the growth of secondary aerosol particles can be initiated by biogenically emitted potassium-salt-rich particles (Pöhlker et al., 2012). Also, a primary source close in the canopy would be fundamental for the aerosol particle maintenance in the PBL (Varanda Rizzo et al., 2018).

An analysis performed using $\Delta\theta_e'$ and Tir revealed that diverse atmospheric dynamics play different roles during particle growth event days. Many event onsets coincide with downdraft occurrences, when $N_{<50}$ appear and grow afterward. We also observed that accumulation-mode particles processed in clouds appear sporadically, causing a prominent Hoppel minimum. The growth events occurring under clear skies present GR and CS higher than those related to deep convection: the median GR and CS for clear-sky conditions are 7.0 nm h^{-1} and 1.6×10^{-3} s^{-1}, whereas under deep-convection conditions, the median GR and CS are 3.8 nm h^{-1} and 5×10^{-4} s^{-1}.

The events were further classified according to their frequency of occurrence throughout the day, showing that they are mostly driven by local convective activities (73 %). However, when analyzing the growth events by $\Delta\theta_e'$ at the event onset, the occurrence of downdrafts does not explain all the cases. The contrast is more evident in the ensembles of $\Delta\theta_e'$ and Tir when growth events and their respective occurrence days are selected by $\Delta\theta_e' >$ 75th percentile ($\Delta\theta_e' = +1.5$ K) at the event onset. For these events, representing about 27 % of the growth events, $\Delta\theta_e'$ is maximum and positive at time $\Delta t = 0$, and even 10 h before or after the growth event, it did not present negative values that could indicate the occurrence of convective downdrafts. Also, Tir fluctuates at around 270 K over the observed period, which represents shallow clouds, instead of convective systems conditions. In contrast, events with $\Delta\theta_e' <$ 25th percentile ($\Delta\theta_e' = -5.3$ K) at the event onset are associated with downdraft occurrences:

$\Delta\theta_e'$ strongly decreases 10 h after the growth event up to $\Delta t = 0$, which is also followed by a strong decrease in Tir.

Sources that could explain growth events in the absence of deep convection are perhaps related to primary biogenic aerosols emitted by the forest, smooth entrainment of air masses from the free troposphere into the PBL in the early morning or even different meteorological mechanisms such as gravity waves and particle production by lightning in the free troposphere, as reported by Machado et al. (2021). Another possible explanation is related to nighttime downdrafts far upwind, which get trapped above the nocturnal boundary layer and travel in the jet above the nocturnal inversion for potentially quite a large distance, being mixed down into the PBL after sunrise, as suggested by Krejci et al. (2005). Therefore future studies are required to unveil the aerosol sources that could explain the diversity of particle growth events observed in the lower troposphere over central Amazônia.

Data availability. The data of the key results presented here have been deposited in associated data files for use in follow-up studies. The SMPS data used in this study are available under https://doi.org/10.17617/3.90 (Franco et al., 2022a). Additional fog data used in this study are available under https://doi.org/10.17617/3.8z (Franco et al., 2022b). Additional equivalent potential temperature data, the anomaly of the potential temperature, and the characteristics of the 254 particle growth events analyzed in this study are available under https://doi.org/10.17617/3.8y (Franco et al., 2022c). Additional Tir data can be found on the portal https://edmond.mpdl.mpg.de/imeji/ (last access: 16 February 2022) collection /Q9NOaAlgWZTq7f9s (Machado et al., 2021). Additional ATTO data can be found in the ATTO data portal under https://www.attodata.org/ (last access: 16 February 2022, ATTO, 2022). For data requests beyond the available data, please refer to the corresponding authors.

Supplement. The supplement related to this article is available online at: https://doi.org/10.5194/acp-22-3469-2022-supplement.

Author contributions. MAF and FD contributed equally to this work. MAF, FD, and CP designed the study. MAF and FD analyzed the data. MAF, FD, LAK, BAH, FGM, JS, SC, JFdB, and SW collected and processed the ATTO aerosol data. LATM processed the satellite data. AA and MS collected the micrometeorological data at the INSTANT tower at ATTO. SW, FGM, PA, MOA, and UP provided essential scientific support for the ATTO measurements. DW supported the data management. MAF, CP, and FD wrote the paper. LATM, MOA, LVR, HMJB, JPN, FGM, MLP, SC, JFdB, and SC contributed with valuable ideas and comments to the analysis and the manuscript. All authors contributed to the discussion of the results as well as the finalization of the paper. PA and CP supervised the study.

Competing interests. At least one of the (co-)authors is a member of the editorial board of *Atmospheric Chemistry and Physics*. The peer-review process was guided by an independent editor, and the authors also have no other competing interests to declare.

Disclaimer. This paper contains results of research conducted under the Technical/Scientific Cooperation Agreement between the National Institute for Amazonian Research, the State University of Amazonas, and the Max-Planck-Gesellschaft e.V.; the opinions expressed are the entire responsibility of the authors and not of the participating institutions.

Publisher's note: Copernicus Publications remains neutral with regard to jurisdictional claims in published maps and institutional affiliations.

Acknowledgements. This work has been funded by the Max Planck Society (MPG) and FAPESP – Fundação de Amparo à Pesquisa do Estado de São Paulo. Marco A. Franco acknowledges the financial support of CNPq for the PhD scholarship, and CAPES, for a sandwich doctorate at the Max Planck Institute for Chemistry. For the operation of the ATTO site, we acknowledge the support by the Max Planck Society (MPG), the German Federal Ministry of Education and Research, and the Brazilian Ministério da Ciência, Tecnologia e Inovação (MCTI/FINEP) as well as the Amazon State University (UEA), FAPEAM, LBA/INPA, and SDS/CEUC/RDS-Uatumã. We acknowledge the support by the Instituto Nacional de Pesquisas da Amazônia (INPA). We would like to thank Reiner Ditz, Jürgen Kesselmeier, Susan Trumbore, Alberto Quesada, Thomas Disper, Thomas Klimach, Andrew Crozier, Björn Nillius, Uwe Schulz, Steffen Schmidt, Delano Campos, Sam Jones, Fábio Jorge, Hermes Braga Xavier, Nagib Alberto de Castro Souza, Adir Vasconcelos Brandão, Amauri Rodriguês Perreira, Antonio Huxley Melo Nascimento, Roberta Pereira de Souza, Bruno Takeshi, and Wallace Rabelo Costa for technical, logistical, and scientific support within the ATTO project.

Financial support. This research has been supported by the Fundação de Amparo à Pesquisa do Estado de São Paulo (FAPESP, grant no. 2017/17047-0), CNPq (grant no. 169842/2017-7), CAPES (grant no. 88887.368025/2019-00), the Max Planck Society (MPG), the German Federal Ministry of Education and Research (BMBF; contract nos. 01LB1001A, 01LK1602B, and 01LK2101B), and the Brazilian Ministério da Ciência, Tecnologia e Inovação (MCTI/FINEP; contract no. 01.11.01248.00).

The article processing charges for this open-access publication were covered by the Max Planck Society.

Review statement. This paper was edited by Veli-Matti Kerminen and reviewed by two anonymous referees.

References

Andreae, M., Berresheim, H., Bingemer, H., Jacob, D. J., Lewis, B., Li, S.-M., and Talbot, R. W.: The atmospheric sulfur cycle over the Amazon Basin: 2. Wet season, J. Geophys. Res.-Atmos., 95, 16813–16824, 1990.

Andreae, M. O.: The aerosol nucleation puzzle, Science, 339, 911–912, 2013.

Andreae, M. O., Acevedo, O. C., Araùjo, A., Artaxo, P., Barbosa, C. G. G., Barbosa, H. M. J., Brito, J., Carbone, S., Chi, X., Cintra, B. B. L., da Silva, N. F., Dias, N. L., Dias-Júnior, C. Q., Ditas, F., Ditz, R., Godoi, A. F. L., Godoi, R. H. M., Heimann, M., Hoffmann, T., Kesselmeier, J., Könemann, T., Krüger, M. L., Lavric, J. V., Manzi, A. O., Lopes, A. P., Martins, D. L., Mikhailov, E. F., Moran-Zuloaga, D., Nelson, B. W., Nölscher, A. C., Santos Nogueira, D., Piedade, M. T. F., Pöhlker, C., Pöschl, U., Quesada, C. A., Rizzo, L. V., Ro, C.-U., Ruckteschler, N., Sá, L. D. A., de Oliveira Sá, M., Sales, C. B., dos Santos, R. M. N., Saturno, J., Schöngart, J., Sörgel, M., de Souza, C. M., de Souza, R. A. F., Su, H., Targhetta, N., Tóta, J., Trebs, I., Trumbore, S., van Eijck, A., Walter, D., Wang, Z., Weber, B., Williams, J., Winderlich, J., Wittmann, F., Wolff, S., and Yáñez-Serrano, A. M.: The Amazon Tall Tower Observatory (ATTO): overview of pilot measurements on ecosystem ecology, meteorology, trace gases, and aerosols, Atmos. Chem. Phys., 15, 10723–10776, https://doi.org/10.5194/acp-15-10723-2015, 2015.

Andreae, M. O., Afchine, A., Albrecht, R., Holanda, B. A., Artaxo, P., Barbosa, H. M. J., Borrmann, S., Cecchini, M. A., Costa, A., Dollner, M., Fütterer, D., Järvinen, E., Jurkat, T., Klimach, T., Konemann, T., Knote, C., Krämer, M., Krisna, T., Machado, L. A. T., Mertes, S., Minikin, A., Pöhlker, C., Pöhlker, M. L., Pöschl, U., Rosenfeld, D., Sauer, D., Schlager, H., Schnaiter, M., Schneider, J., Schulz, C., Spanu, A., Sperling, V. B., Voigt, C., Walser, A., Wang, J., Weinzierl, B., Wendisch, M., and Ziereis, H.: Aerosol characteristics and particle production in the upper troposphere over the Amazon Basin, Atmos. Chem. Phys., 18, 921–961, https://doi.org/10.5194/acp-18-921-2018, 2018.

Andreae, M. O., Andreae, T. W., Ditas, F., and Pöhlker, C.: Frequent new particle formation at remote sites in the subboreal forest of North America, Atmos. Chem. Phys., 22, 2487–2505, https://doi.org/10.5194/acp-22-2487-2022, 2022.

Artaxo, P., Rizzo, L. V., Brito, J. F., Barbosa, H. M. J., Arana, A., Sena, E. T., Cirino, G. G., Bastos, W., Martin, S. T., and Andreae, M. O.: Atmospheric aerosols in Amazonia and land use change: from natural biogenic to biomass burning conditions, Faraday Discuss., 165, 203–235, https://doi.org/10.1039/c3fd00052d, 2013.

ATTO: ATTO data portal, https://www.attodata.org/, last access: 16 February 2022.

Baars, H., Ansmann, A., Althausen, D., Engelmann, R., Heese, B., Müller, D., Artaxo, P., Paixao, M., Pauliquevis, T., and Souza, R.: Aerosol profiling with lidar in the Amazon Basin during the wet and dry season, J. Geophys. Res.-Atmos., 117, D21, https://doi.org/10.1029/2012JD018338, 2012.

Betts, A. K., Gatti, L. V., Cordova, A. M., Dias, M. A. S., and Fuentes, J. D.: Transport of ozone to the surface by convective downdrafts at night, J. Geophys. Res.-Atmos., 107, LBA 13-1–LBA 13-6, https://doi.org/10.1029/2000JD000158, 2002.

Bolton, D.: The computation of equivalent potential temperature, Mon. Weather Rev., 108, 1046–1053, 1980.

Bonn, B. and Moortgat, G. K.: Sesquiterpene ozonolysis: Origin of atmospheric new particle formation from biogenic hydrocarbons, Geophys. Res. Lett., 30, 11, https://doi.org/10.1029/2003GL017000, 2003.

Brito, J., Rizzo, L. V., Morgan, W. T., Coe, H., Johnson, B., Haywood, J., Longo, K., Freitas, S., Andreae, M. O., and Artaxo, P.: Ground-based aerosol characterization during the South American Biomass Burning Analysis (SAMBBA) field experiment, Atmos. Chem. Phys., 14, 12069–12083, https://doi.org/10.5194/acp-14-12069-2014, 2014.

Chen, Q., Farmer, D. K., Rizzo, L. V., Pauliquevis, T., Kuwata, M., Karl, T. G., Guenther, A., Allan, J. D., Coe, H., Andreae, M. O., Pöschl, U., Jimenez, J. L., Artaxo, P., and Martin, S. T.: Submicron particle mass concentrations and sources in the Amazonian wet season (AMAZE-08), Atmos. Chem. Phys., 15, 3687–3701, https://doi.org/10.5194/acp-15-3687-2015, 2015.

Cirino, G., Brito, J., Barbosa, H. M., Rizzo, L. V., Tunved, P., de Sá, S. S., Jimenez, J. L., Palm, B. B., Carbone, S., Lavric, J. V., Souza, R. A., Wolff, S., Walter, D., Tota, J., Oliveira, M. B., Martin, S. T., and Artaxo, P.: Observations of Manaus urban plume evolution and interaction with biogenic emissions in GoAmazon 2014/5, Atmos. Environ., 191, 513–524, https://doi.org/10.1016/j.atmosenv.2018.08.031, 2018.

Clarke, A. D.: Atmospheric nuclei in the remote free-troposphere, J. Atmos. Chem., 14, 479–488, 1992.

Dada, L., Paasonen, P., Nieminen, T., Buenrostro Mazon, S., Kontkanen, J., Peräkylä, O., Lehtipalo, K., Hussein, T., Petäjä, T., Kerminen, V.-M., Bäck, J., and Kulmala, M.: Long-term analysis of clear-sky new particle formation events and nonevents in Hyytiälä, Atmos. Chem. Phys., 17, 6227–6241, https://doi.org/10.5194/acp-17-6227-2017, 2017.

Dada, L., Chellapermal, R., Buenrostro Mazon, S., Paasonen, P., Lampilahti, J., Manninen, H. E., Junninen, H., Petäjä, T., Kerminen, V.-M., and Kulmala, M.: Refined classification and characterization of atmospheric new-particle formation events using air ions, Atmos. Chem. Phys., 18, 17883–17893, https://doi.org/10.5194/acp-18-17883-2018, 2018.

Dall'Osto, M., Beddows, D. C. S., Asmi, A., Poulain, L., Hao, L., Freney, E., Allan, J. D., Canagaratna, M., Crippa, M., Bianchi, F., de Leeuw, G., Eriksson, A., Swietlicki, E., Hansson, H. C., Henzing, J. S., Granier, C., Zemankova, K., Laj, P., Onasch, T., Prevot, A., Putaud, J. P., Sellegri, K., Vidal, M., Virtanen, A., Simo, R., Worsnop, D., O'Dowd, C., Kulmala, M., and Harrison, R. M.: Novel insights on new particle formation derived from a pan-european observing system, Sci. Rep., 8, 1482, https://doi.org/10.1038/s41598-017-17343-9, 2018.

Dal Maso, M.: Formation and Growth of Fresh Atmospheric Aerosols Eight Years of Aerosol Size Distribution Data From SMEAR, Boreal Environ. Res., 10, 323–336, 2005.

Dal Maso, M., Kulmala, M., Lehtinen, K. E., Mäkelä, J., Aalto, P., and O'Dowd, C.: Condensation and coagulation sinks and formation of nucleation mode particles in coastal and boreal forest boundary layers, J. Geophys. Res.-Atmos., 107, PAR 2-1–PAR 2-10, https://doi.org/10.1029/2001JD001053, 2002.

Dal Maso, M., Sogacheva, L., Aalto, P. P., Riipinen, I., Komppula, M., Tunved, P., Korhonen, L., Suur-Uski, V., Hirsikko, A., KurtéN, T., Kerminen, V.-M., Lihavainen, H., Viisanen, Y., Hans-

son, H.-C., and Kulmala, M.: Aerosol size distribution measurements at four Nordic field stations: identification, analysis and trajectory analysis of new particle formation bursts, Tellus B, 59, 350–361, https://doi.org/10.1111/j.1600-0889.2007.00267.x, 2007.

De Reus, M., Krejci, R., Williams, J., Fischer, H., Scheele, R., and Ström, J.: Vertical and horizontal distributions of the aerosol number concentration and size distribution over the northern Indian Ocean, J. Geophys. Res.-Atmos., 106, 28629–28641, 2001.

Dias-Júnior, C. Q., Sá, L. D., Marques Filho, E. P., Santana, R. A., Mauder, M., and Manzi, A. O.: Turbulence regimes in the stable boundary layer above and within the Amazon forest, Agr. Forest Meteorol., 233, 122–132, https://doi.org/10.1016/j.agrformet.2016.11.001, 2017.

Fan, J., Rosenfeld, D., Zhang, Y., Giangrande, S. E., Li, Z., Machado, L. A. T., Martin, S. T., Yang, Y., Wang, J., Artaxo, P., Barbosa, H. M. J., Braga, R. C., Comstock, J. M., Feng, Z., Gao, W., Gomes, H. B., Mei, F., Pöhlker, C., Pöhlker, M. L., Pöschl, U., and de Souza, R. A. F.: Substantial convection and precipitation enhancements by ultrafine aerosol particles, Science, 359, 411–418, https://doi.org/10.1126/science.aan8461, 2018.

Fisch, G., Tota, J., Machado, L. A. T., Silva Dias, M. A. F., da F. Lyra, R. F., Nobre, C. A., Dolman, A. J., and Gash, J. H. C.: The convective boundary layer over pasture and forest in Amazonia, Theor. Appl. Climatol., 78, 47–59, https://doi.org/10.1007/s00704-004-0043-x, 2004.

Franco, M. A., Kremper, L. A., Ditas, F., Pöhlker, C., Artaxo, P., and Walter, D.: SMPS dataset at ATTO, Max Planck Society [data set], https://doi.org/10.17617/3.90, 2022a.

Franco, M. A., Ditas, F., Pöhlker, C., Artaxo, P., Walter, D., and Kremper, L. A.: Fog dataset at ATTO, Max Planck Society [data set], https://doi.org/10.17617/3.8z, 2022b.

Franco, M. A., Ditas, F., Pöhlker, C., Artaxo, P., and Walter, D.: Particle growth events and equivalent potential temperature at ATTO, Max Planck Society [data set], https://doi.org/10.17617/3.8y, 2022c.

Fuchs, N. and Sutugin, A.: High-dispersed aerosols, in: Topics in current aerosol research, Elsevier, p. 1, https://doi.org/10.1016/B978-0-08-016674-2.50006-6, 1971.

Gerken, T., Wei, D., Chase, R., Fuentes, J., Schumacher, C., Machado, L., Andreoli, R., Chamecki, M., Ferreira de Souza, R., Freire, L., Jardine, A., Manzi, A., Nascimento dos Santos, R., von Randow, C., dos Santos Costa, P., Stoy, P., Tóta, J., and Trowbridge, A.: Downward transport of ozone rich air and implications for atmospheric chemistry in the Amazon rainforest, Atmos. Environ., 124, 64–76, 2016.

Glicker, H. S., Lawler, M. J., Ortega, J., de Sá, S. S., Martin, S. T., Artaxo, P., Vega Bustillos, O., de Souza, R., Tota, J., Carlton, A., and Smith, J. N.: Chemical composition of ultrafine aerosol particles in central Amazonia during the wet season, Atmos. Chem. Phys., 19, 13053–13066, https://doi.org/10.5194/acp-19-13053-2019, 2019.

Gong, Y., Su, H., Cheng, Y., Liu, F., Wu, Z., Hu, M., Zeng, L., and Zhang, Y.: Analysis on concentration and source rate of precursor vapors participating in particle formation and growth at Xinken in the Pearl River Delta of China, Adv. Atmos. Sci., 25, 427–436, 2008.

Gunthe, S. S., King, S. M., Rose, D., Chen, Q., Roldin, P., Farmer, D. K., Jimenez, J. L., Artaxo, P., Andreae, M. O., Martin, S. T., and Pöschl, U.: Cloud condensation nuclei in pristine tropical rainforest air of Amazonia: size-resolved measurements and modeling of atmospheric aerosol composition and CCN activity, Atmos. Chem. Phys., 9, 7551–7575, https://doi.org/10.5194/acp-9-7551-2009, 2009.

Hamed, A., Korhonen, H., Sihto, S.-L., Joutsensaari, J., Järvinen, H., Petäjä, T., Arnold, F., Nieminen, T., Kulmala, M., Smith, J. N., Lehtinen, K. E. J., and Laaksonen, A.: The role of relative humidity in continental new particle formation, J. Geophys. Res.-Atmos., 116, D3, https://doi.org/10.1029/2010JD014186, 2011.

Hamilton, D. S., Lee, L. A., Pringle, K. J., Reddington, C. L., Spracklen, D. V., and Carslaw, K. S.: Occurrence of pristine aerosol environments on a polluted planet, P. Natl. Acad. Sci. USA, 111, 18466–18471, https://doi.org/10.1073/pnas.1415440111, 2014.

Heintzenberg, J.: Properties of the log-normal particle size distribution, Aerosol Sci. Technol., 21, 46–48, 1994.

Heintzenberg, J., Tunved, P., Galí, M., and Leck, C.: New particle formation in the Svalbard region 2006–2015, Atmos. Chem. Phys., 17, 6153–6175, https://doi.org/10.5194/acp-17-6153-2017, 2017.

Holanda, B. A., Pöhlker, M. L., Walter, D., Saturno, J., Sörgel, M., Ditas, J., Ditas, F., Schulz, C., Franco, M. A., Wang, Q., Donth, T., Artaxo, P., Barbosa, H. M. J., Borrmann, S., Braga, R., Brito, J., Cheng, Y., Dollner, M., Kaiser, J. W., Klimach, T., Knote, C., Krüger, O. O., Fütterer, D., Lavrič, J. V., Ma, N., Machado, L. A. T., Ming, J., Morais, F. G., Paulsen, H., Sauer, D., Schlager, H., Schneider, J., Su, H., Weinzierl, B., Walser, A., Wendisch, M., Ziereis, H., Zöger, M., Pöschl, U., Andreae, M. O., and Pöhlker, C.: Influx of African biomass burning aerosol during the Amazonian dry season through layered transatlantic transport of black carbon-rich smoke, Atmos. Chem. Phys., 20, 4757–4785, https://doi.org/10.5194/acp-20-4757-2020, 2020.

Hoppel, W., Frick, G., and Larson, R.: Effect of nonprecipitating clouds on the aerosol size distribution in the marine boundary layer, Geophys. Res. Lett., 13, 125–128, 1986.

Huffman, J. A., Sinha, B., Garland, R. M., Snee-Pollmann, A., Gunthe, S. S., Artaxo, P., Martin, S. T., Andreae, M. O., and Pöschl, U.: Size distributions and temporal variations of biological aerosol particles in the Amazon rainforest characterized by microscopy and real-time UV-APS fluorescence techniques during AMAZE-08, Atmos. Chem. Phys., 12, 11997–12019, https://doi.org/10.5194/acp-12-11997-2012, 2012.

Hussein, T., Dal Maso, M., Petaja, T., Koponen, I. K., Paatero, P., Aalto, P. P., Hameri, K., and Kulmala, M.: Evaluation of an automatic algorithm for fitting the particle number size distributions, Boreal Environ. Res., 10, 337–355, 2005.

Hyvönen, S., Junninen, H., Laakso, L., Dal Maso, M., Grönholm, T., Bonn, B., Keronen, P., Aalto, P., Hiltunen, V., Pohja, T., Launiainen, S., Hari, P., Mannila, H., and Kulmala, M.: A look at aerosol formation using data mining techniques, Atmos. Chem. Phys., 5, 3345–3356, https://doi.org/10.5194/acp-5-3345-2005, 2005.

Kanawade, V. P., Jobson, B. T., Guenther, A. B., Erupe, M. E., Pressley, S. N., Tripathi, S. N., and Lee, S.-H.: Isoprene suppression of new particle formation in a mixed deciduous forest, Atmos. Chem. Phys., 11, 6013–6027, https://doi.org/10.5194/acp-11-6013-2011, 2011.

Kerminen, V.-M., Chen, X., Vakkari, V., Petäjä, T., Kulmala, M., and Bianchi, F.: Atmospheric new particle formation and growth: review of field observations, Environ. Res. Lett., 13, 103003, https://doi.org/10.1088/1748-9326/aadf3c, 2018.

Kiendler-Scharr, A., Wildt, J., Dal Maso, M., Hohaus, T., Kleist, E., Mentel, T. F., Tillmann, R., Uerlings, R., Schurr, U., and Wahner, A.: New particle formation in forests inhibited by isoprene emissions, Nature, 461, 381–384, 2009.

Kirkby, J., Curtius, J., Almeida, J., Dunne, E., Duplissy, J., Ehrhart, S., Franchin, A., Gagne, S., Ickes, L., Kurten, A., Kupc, A., Metzger, A., Riccobono, F., Rondo, L., Schobesberger, S., Tsagkogeorgas, G., Wimmer, D., Amorim, A., Bianchi, F., Breitenlechner, M., David, A., Dommen, J., Downard, A., Ehn, M., Flagan, R., Haider, S., Hansel, A., Hauser, D., Jud,W., Junninen, H., Kreissl, F., Kvashin, A., Laaksonen, A., Lehtipalo, K., Lima, J., Lovejoy, E., Makhmutov, V., Mathot, S., Mikkila, J., Minginette, P., Mogo, S., Nieminen, T., Onnela, A., Pereira, P., Petaja, T., Schnitzhofer, R., Seinfeld, J., Sipila, M., Stozhkov, Y., Stratmann, F., Tome, A., Vanhanen, J., Viisanen, Y., Vrtala, A., Wagner, P., Walther, H., Weingartner, E., Wex, H., Winkler, P., Carslaw, K., Worsnop, D., Baltensperger, U., and Kulmala, M.: Role of sulphuric acid, ammonia and galactic cosmic rays in atmospheric aerosol nucleation, Nature, 476, 429–433, 2011.

Kirkby, J., Duplissy, J., Sengupta, K., Frege, C., Gordon, H., Williamson, C., Heinritzi, M., Simon, M., Yan, C., Almeida, J., Trostl, J., Nieminen, T., Ortega, I. K., Wagner, R., Adamov, A., Amorim, A., Bernhammer, A. K., Bianchi, F., Breitenlechner, M., Brilke, S., Chen, X. M., Craven, J., Dias, A., Ehrhart, S., Flagan, R. C., Franchin, A., Fuchs, C., Guida, R., Hakala, J., Hoyle, C. R., Jokinen, T., Junninen, H., Kangasluoma, J., Kim, J., Krapf, M., Kurten, A., Laaksonen, A., Lehtipalo, K., Makhmutov, V., Mathot, S., Molteni, U., Onnela, A., Perakyla, O., Piel, F., Petaja, T., Praplan, A. P., Pringle, K., Rap, A., Richards, N. A. D., Riipinen, I., Rissanen, M. P., Rondo, L., Sarnela, N., Schobesberger, S., Scott, C. E., Seinfeld, J. H., Sipila, M., Steiner, G., Stozhkov, Y., Stratmann, F., Tome, A., Virtanen, A., Vogel, A. L., Wagner, A. C., Wagner, P. E., Weingartner, E., Wimmer, D., Winkler, P. M., Ye, P. L., Zhang, X., Hansel, A., Dommen, J., Donahue, N. M., Worsnop, D. R., Baltensperger, U., Kulmala, M., Carslaw, K. S., and Curtius, J.: Ion-induced nucleation of pure biogenic particles, Nature, 533, 521–526, https://doi.org/10.1038/nature17953, 2016.

Krejci, R.: Evolution of aerosol properties over the rain forest in Surinam, South America, observed from aircraft during the LBA-CLAIRE 98 experiment, J. Geophys. Res., 108, 4561, https://doi.org/10.1029/2001JD001375, 2003.

Krejci, R., Strom, J., de Reus, M., Hoor, P., Williams, J., Fischer, H., and Hansson, H. C.: Evolution of aerosol properties over the rain forest in Surinam, South America, observed from aircraft during the LBA-CLAIRE 98 experiment, J. Geophys. Res.-Atmos., 108, https://doi.org/10.1029/2001jd001375, 2003.

Krejci, R., Ström, J., de Reus, M., Williams, J., Fischer, H., Andreae, M. O., and Hansson, H.-C.: Spatial and temporal distribution of atmospheric aerosols in the lowermost troposphere over the Amazonian tropical rainforest, Atmos. Chem. Phys., 5, 1527–1543, https://doi.org/10.5194/acp-5-1527-2005, 2005.

Kulmala, M., Vehkamäki, H., Petäjä, T., Dal Maso, M., Lauri, A., Kerminen, V.-M., Birmili, W., and McMurry, P.: Formation and growth rates of ultrafine atmospheric particles: a review of observations, J. Aerosol Sci., 35, 143–176, https://doi.org/10.1016/j.jaerosci.2003.10.003, 2004.

Kulmala, M., Petäjä, T., Nieminen, T., Sipilä, M., Manninen, H. E., Lehtipalo, K., Dal Maso, M., Aalto, P. P., Junninen, H., Paasonen, P., Riipinen, I., Lehtinen, K. E. J., Laaksonen, A., and Kerminen, V.-M.: Measurement of the nucleation of atmospheric aerosol particles, Nat. Protoc., 7, 1651–1667, https://doi.org/10.1038/nprot.2012.091, 2012.

Leino, K., Lampilahti, J., Poutanen, P., Väänänen, R., Manninen, A., Buenrostro Mazon, S., Dada, L., Franck, A., Wimmer, D., Aalto, P. P., Ahonen, L. R., Enroth, J., Kangasluoma, J., Keronen, P., Korhonen, F., Laakso, H., Matilainen, T., Sivola, E., Manninen, H. E., Lehtipalo, K., Kerminen, V.-M., Petäjä, T., and Kulmala, M.: Vertical profiles of sub-3 nm particles over the boreal forest, Atmos. Chem. Phys., 19, 4127–4138, https://doi.org/10.5194/acp-19-4127-2019, 2019.

Liu, Y., Brito, J., Dorris, M. R., Rivera-Rios, J. C., Seco, R., Bates, K. H., Artaxo, P., Duvoisin, S., Keutsch, F. N., Kim, S., Goldstein, A. H., Guenther, A. B., Manzi, A. O., Souza, R. A. F., Springston, S. R., Watson, T. B., McKinney, K. A., and Martin, S. T.: Isoprene photochemistry over the Amazon rainforest, P. Natl. Acad. Sci. USA, 113, 6125–6130, 2016.

Löbs, N., Barbosa, C. G. G., Brill, S., Walter, D., Ditas, F., de Oliveira Sá, M., de Araújo, A. C., de Oliveira, L. R., Godoi, R. H. M., Wolff, S., Piepenbring, M., Kesselmeier, J., Artaxo, P., Andreae, M. O., Pöschl, U., Pöhlker, C., and Weber, B.: Aerosol measurement methods to quantify spore emissions from fungi and cryptogamic covers in the Amazon, Atmos. Meas. Tech., 13, 153–164, https://doi.org/10.5194/amt-13-153-2020, 2020.

Ma, N. and Birmili, W.: Estimating the contribution of photochemical particle formation to ultrafine particle number averages in an urban atmosphere, Sci. Total Environ., 512, 154–166, 2015.

Machado, L. A., Laurent, H., and Lima, A. A.: Diurnal march of the convection observed during TRMM-WETAMC/LBA, J. Geophys. Res.-Atmos., 107, 8064, https://doi.org/10.1029/2001JD000338, 2002.

Machado, L. A. T. and Rossow, W. B.: Structural characteristics and radiative properties of tropical cloud clusters, Mon. Weather Rev., 121, 3234–3260, 1993.

Machado, L. A. T., Franco, M. A., Kremper, L. A., Ditas, F., Andreae, M. O., Artaxo, P., Cecchini, M. A., Holanda, B. A., Pöhlker, M. L., Saraiva, I., Wolff, S., Pöschl, U., and Pöhlker, C.: How weather events modify aerosol particle size distributions in the Amazon boundary layer, Atmos. Chem. Phys., 21, 18065–18086, https://doi.org/10.5194/acp-21-18065-2021, 2021.

Martin, S. T., Andreae, M. O., Althausen, D., Artaxo, P., Baars, H., Borrmann, S., Chen, Q., Farmer, D. K., Guenther, A., Gunthe, S. S., Jimenez, J. L., Karl, T., Longo, K., Manzi, A., Müller, T., Pauliquevis, T., Petters, M. D., Prenni, A. J., Pöschl, U., Rizzo, L. V., Schneider, J., Smith, J. N., Swietlicki, E., Tota, J., Wang, J., Wiedensohler, A., and Zorn, S. R.: An overview of the Amazonian Aerosol Characterization Experiment 2008 (AMAZE-08), Atmos. Chem. Phys., 10, 11415–11438, https://doi.org/10.5194/acp-10-11415-2010, 2010.

McFiggans, G., Mentel, T. F.,Wildt, J., Pullinen, I., Kang, S., Kleist, E., Schmitt, S., Springer, M., Tillmann, R., Wu, C., Zhao, D., Hallquist, M., Faxon, C., Le Breton, M., Hallquist, Å. M., Simpson, D., Bergström, R., Jenkin, M. E., Ehn, M., Thornton, J. A., Alfarra, M. R., Bannan, T. J., Percival, C. J., Priestley, M., Top-

ping, D., and Kiendler-Scharr, A.: Secondary organic aerosol reduced by mixture of atmospheric vapours, Nature, 565, 587–593, 2019.

Merikanto, J., Spracklen, D. V., Mann, G. W., Pickering, S. J., and Carslaw, K. S.: Impact of nucleation on global CCN, Atmos. Chem. Phys., 9, 8601–8616, https://doi.org/10.5194/acp-9-8601-2009, 2009.

Moran-Zuloaga, D., Ditas, F., Walter, D., Saturno, J., Brito, J., Carbone, S., Chi, X., Hrabě de Angelis, I., Baars, H., Godoi, R. H. M., Heese, B., Holanda, B. A., Lavrič, J. V., Martin, S. T., Ming, J., Pöhlker, M. L., Ruckteschler, N., Su, H., Wang, Y., Wang, Q., Wang, Z., Weber, B., Wolff, S., Artaxo, P., Pöschl, U., Andreae, M. O., and Pöhlker, C.: Long-term study on coarse mode aerosols in the Amazon rain forest with the frequent intrusion of Saharan dust plumes, Atmos. Chem. Phys., 18, 10055–10088, https://doi.org/10.5194/acp-18-10055-2018, 2018.

Nascimento, J. P., Bela, M. M., Meller, B. B., Banducci, A. L., Rizzo, L. V., Vara-Vela, A. L., Barbosa, H. M. J., Gomes, H., Rafee, S. A. A., Franco, M. A., Carbone, S., Cirino, G. G., Souza, R. A. F., McKeen, S. A., and Artaxo, P.: Aerosols from anthropogenic and biogenic sources and their interactions – modeling aerosol formation, optical properties, and impacts over the central Amazon basin, Atmos. Chem. Phys., 21, 6755–6779, https://doi.org/10.5194/acp-21-6755-2021, 2021.

Nieminen, T., Kerminen, V.-M., Petäjä, T., Aalto, P. P., Arshinov, M., Asmi, E., Baltensperger, U., Beddows, D. C. S., Beukes, J. P., Collins, D., Ding, A., Harrison, R. M., Henzing, B., Hooda, R., Hu, M., Hõrrak, U., Kivekäs, N., Komsaare, K., Krejci, R., Kristensson, A., Laakso, L., Laaksonen, A., Leaitch, W. R., Lihavainen, H., Mihalopoulos, N., Németh, Z., Nie, W., O'Dowd, C., Salma, I., Sellegri, K., Svenningsson, B., Swietlicki, E., Tunved, P., Ulevicius, V., Vakkari, V., Vana, M., Wiedensohler, A., Wu, Z., Virtanen, A., and Kulmala, M.: Global analysis of continental boundary layer new particle formation based on long-term measurements, Atmos. Chem. Phys., 18, 14737–14756, https://doi.org/10.5194/acp-18-14737-2018, 2018.

Perry, K. D. and Hobbs, P. V.: Further evidence for particle nucleation in clear air adjacent to marine cumulus clouds, J. Geophys. Res.-Atmos., 99, 22803–22818, 1994.

Pöhlker, C., Wiedemann, K. T., Sinha, B., Shiraiwa, M., Gunthe, S. S., Smith, M., Su, H., Artaxo, P., Chen, Q., Cheng, Y., Elbert, W., Gilles, M. K., Kilcoyne, A. L. D., Moffet, R. C., Weigand, M., Martin, S. T., Pöschl, U., and Andreae, M. O.: Biogenic potassium salt particles as seeds for secondary organic aerosol in the Amazon, Science, 337, 1075–1078, https://doi.org/10.1126/science.1223264, 2012.

Pöhlker, C., Walter, D., Paulsen, H., Könemann, T., Rodríguez-Caballero, E., Moran-Zuloaga, D., Brito, J., Carbone, S., Degrendele, C., Després, V. R., Ditas, F., Holanda, B. A., Kaiser, J. W., Lammel, G., Lavrič, J. V., Ming, J., Pickersgill, D., Pöhlker, M. L., Praß, M., Löbs, N., Saturno, J., Sörgel, M., Wang, Q., Weber, B., Wolff, S., Artaxo, P., Pöschl, U., and Andreae, M. O.: Land cover and its transformation in the backward trajectory footprint region of the Amazon Tall Tower Observatory, Atmos. Chem. Phys., 19, 8425–8470, https://doi.org/10.5194/acp-19-8425-2019, 2019.

Pöhlker, M. L., Pöhlker, C., Ditas, F., Klimach, T., Hrabe de Angelis, I., Araújo, A., Brito, J., Carbone, S., Cheng, Y., Chi, X., Ditz, R., Gunthe, S. S., Kesselmeier, J., Könemann, T., Lavrič, J. V., Martin, S. T., Mikhailov, E., Moran-Zuloaga, D., Rose, D., Saturno, J., Su, H., Thalman, R., Walter, D., Wang, J., Wolff, S., Barbosa, H. M. J., Artaxo, P., Andreae, M. O., and Pöschl, U.: Long-term observations of cloud condensation nuclei in the Amazon rain forest – Part 1: Aerosol size distribution, hygroscopicity, and new model parametrizations for CCN prediction, Atmos. Chem. Phys., 16, 15709–15740, https://doi.org/10.5194/acp-16-15709-2016, 2016.

Pöhlker, M. L., Ditas, F., Saturno, J., Klimach, T., Hrabě de Angelis, I., Araùjo, A. C., Brito, J., Carbone, S., Cheng, Y., Chi, X., Ditz, R., Gunthe, S. S., Holanda, B. A., Kandler, K., Kesselmeier, J., Könemann, T., Krüger, O. O., Lavrič, J. V., Martin, S. T., Mikhailov, E., Moran-Zuloaga, D., Rizzo, L. V., Rose, D., Su, H., Thalman, R., Walter, D., Wang, J., Wolff, S., Barbosa, H. M. J., Artaxo, P., Andreae, M. O., Pöschl, U., and Pöhlker, C.: Long-term observations of cloud condensation nuclei over the Amazon rain forest – Part 2: Variability and characteristics of biomass burning, long-range transport, and pristine rain forest aerosols, Atmos. Chem. Phys., 18, 10289–10331, https://doi.org/10.5194/acp-18-10289-2018, 2018.

Prass, M., Andreae, M. O., de Araùjo, A. C., Artaxo, P., Ditas, F., Elbert, W., Förster, J.-D., Franco, M. A., Hrabe de Angelis, I., Kesselmeier, J., Klimach, T., Kremper, L. A., Thines, E., Walter, D., Weber, J., Weber, B., Fuchs, B. M., Pöschl, U., and Pöhlker, C.: Bioaerosols in the Amazon rain forest: temporal variations and vertical profiles of Eukarya, Bacteria, and Archaea, Biogeosciences, 18, 4873–4887, https://doi.org/10.5194/bg-18-4873-2021, 2021.

Rissler, J., Swietlicki, E., Zhou, J., Roberts, G., Andreae, M. O., Gatti, L. V., and Artaxo, P.: Physical properties of the submicrometer aerosol over the Amazon rain forest during the wet-to-dry season transition - comparison of modeled and measured CCN concentrations, Atmos. Chem. Phys., 4, 2119–2143, https://doi.org/10.5194/acp-4-2119-2004, 2004.

Rissler, J., Vestin, A., Swietlicki, E., Fisch, G., Zhou, J., Artaxo, P., and Andreae, M. O.: Size distribution and hygroscopic properties of aerosol particles from dry-season biomass burning in Amazonia, Atmos. Chem. Phys., 6, 471–491, https://doi.org/10.5194/acp-6-471-2006, 2006.

Roberts, G. C.: Impact of biomass burning on cloud properties in the Amazon Basin, J. Geophys. Res., 108, 4062, https://doi.org/10.1029/2001JD000985, 2003.

Roberts, G. C., Andreae, M. O., Zhou, J., and Artaxo, P.: Cloud condensation nuclei in the Amazon Basin: "marine" conditions over a continent?, Geophys. Res. Lett., 28, 2807–2810, https://doi.org/10.1029/2000GL012585, 2001.

Rose, C., Zha, Q., Dada, L., Yan, C., Lehtipalo, K., Junninen, H., Mazon, S. B., Jokinen, T., Sarnela, N., Sipilä, M., Petäjä, T., Kerminen, V.-M., Bianchi, F., and Kulmala, M.: Observations of biogenic ion-induced cluster formation in the atmosphere, Sci. Adv., 4, eaar5218, https://doi.org/10.1038/s41586-018-0871-y, 2018.

Saturno, J., Ditas, F., Penning de Vries, M., Holanda, B. A., Pöhlker, M. L., Carbone, S., Walter, D., Bobrowski, N., Brito, J., Chi, X., Gutmann, A., Hrabe de Angelis, I., Machado, L. A. T., Moran-Zuloaga, D., Rüdiger, J., Schneider, J., Schulz, C., Wang, Q., Wendisch, M., Artaxo, P., Wagner, T., Pöschl, U., Andreae, M. O., and Pöhlker, C.: African volcanic emissions influencing atmospheric aerosols over the Amazon rain forest, Atmos. Chem.

Phys., 18, 10391–10405, https://doi.org/10.5194/acp-18-10391-2018, 2018a.

Saturno, J., Holanda, B. A., Pöhlker, C., Ditas, F., Wang, Q., Moran-Zuloaga, D., Brito, J., Carbone, S., Cheng, Y., Chi, X., Ditas, J., Hoffmann, T., Hrabe de Angelis, I., Könemann, T., Lavrič, J. V., Ma, N., Ming, J., Paulsen, H., Pöhlker, M. L., Rizzo, L. V., Schlag, P., Su, H., Walter, D., Wolff, S., Zhang, Y., Artaxo, P., Pöschl, U., and Andreae, M. O.: Black and brown carbon over central Amazonia: long-term aerosol measurements at the ATTO site, Atmos. Chem. Phys., 18, 12817–12843, https://doi.org/10.5194/acp-18-12817-2018, 2018b.

Schrod, J., Thomson, E. S., Weber, D., Kossmann, J., Pöhlker, C., Saturno, J., Ditas, F., Artaxo, P., Clouard, V., Saurel, J.-M., Ebert, M., Curtius, J., and Bingemer, H. G.: Long-term deposition and condensation ice-nucleating particle measurements from four stations across the globe, Atmos. Chem. Phys., 20, 15983–16006, https://doi.org/10.5194/acp-20-15983-2020, 2020.

Spracklen, D. V., Carslaw, K. S., Kulmala, M., Kerminen, V.-M., Sihto, S.-L., Riipinen, I., Merikanto, J., Mann, G. W., Chipperfield, M. P., Wiedensohler, A., Birmili, W., and Lihavainen, H.: Contribution of particle formation to global cloud condensation nuclei concentrations, Geophys. Res. Lett., 35, L06808, https://doi.org/10.1029/2007GL033038, 2008.

Talbot, R., Andreae, M., Berresheim, H., Artaxo, P., Garstang, M., Harriss, R., Beecher, K., and Li, S.: Aerosol chemistry during the wet season in central Amazonia: The influence of long-range transport, J. Geophys. Res.-Atmos., 95, 16955–16969, 1990.

Trebs, I., Meixner, F. X., Slanina, J., Otjes, R., Jongejan, P., and Andreae, M. O.: Real-time measurements of ammonia, acidic trace gases and water-soluble inorganic aerosol species at a rural site in the Amazon Basin, Atmos. Chem. Phys., 4, 967–987, https://doi.org/10.5194/acp-4-967-2004, 2004.

Tuch, T. M., Haudek, A., Müller, T., Nowak, A., Wex, H., and Wiedensohler, A.: Design and performance of an automatic regenerating adsorption aerosol dryer for continuous operation at monitoring sites, Atmos. Meas. Tech., 2, 417–422, https://doi.org/10.5194/amt-2-417-2009, 2009.

Varanda Rizzo, L., Roldin, P., Brito, J., Backman, J., Swietlicki, E., Krejci, R., Tunved, P., Petäjä, T., Kulmala, M., and Artaxo, P.: Multi-year statistical and modeling analysis of submicrometer aerosol number size distributions at a rain forest site in Amazonia, Atmos. Chem. Phys., 18, 10255–10274, https://doi.org/10.5194/acp-18-10255-2018, 2018.

von der Weiden, S.-L., Drewnick, F., and Borrmann, S.: Particle Loss Calculator – a new software tool for the assessment of the performance of aerosol inlet systems, Atmos. Meas. Tech., 2, 479–494, https://doi.org/10.5194/amt-2-479-2009, 2009.

Waddicor, D. A., Vaughan, G., Choularton, T. W., Bower, K. N., Coe, H., Gallagher, M., Williams, P. I., Flynn, M., Volz-Thomas, A., Pätz, H.-W., Isaac, P., Hacker, J., Arnold, F., Schlager, H., and Whiteway, J. A.: Aerosol observations and growth rates downwind of the anvil of a deep tropical thunderstorm, Atmos. Chem. Phys., 12, 6157–6172, https://doi.org/10.5194/acp-12-6157-2012, 2012.

Wang, J., Krejci, R., Giangrande, S., Kuang, C., Barbosa, H. M. J., Brito, J., Carbone, S., Chi, X., Comstock, J., Ditas, F., Lavric, J., Manninen, H. E., Mei, F., Moran-Zuloaga, D., Pöhlker, C., Pöhlker, M. L., Saturno, J., Schmid, B., Souza, R. A. F., Springston, S. R., Tomlinson, J. M., Toto, T., Walter, D., Wimmer, D., Smith, J. N., Kulmala, M., Machado, L. A. T., Artaxo, P., Andreae, M. O., Petäjä, T., and Martin, S. T.: Amazon boundary layer aerosol concentration sustained by vertical transport during rainfall, Nature, 539, 416–419, https://doi.org/10.1038/nature19819, 2016.

Wehner, B., Werner, F., Ditas, F., Shaw, R. A., Kulmala, M., and Siebert, H.: Observations of new particle formation in enhanced UV irradiance zones near cumulus clouds, Atmos. Chem. Phys., 15, 11701–11711, https://doi.org/10.5194/acp-15-11701-2015, 2015.

Wiedensohler, A., Ma, N., Birmili, W., Heintzenberg, J., Ditas, F., Andreae, M., and Panov, A.: Infrequent new particle formation over the remote boreal forest of Siberia, Atmos. Environ., 200, 167–169, https://doi.org/10.1016/j.atmosenv.2018.12.013, 2019.

Williamson, C. J., Kupc, A., Axisa, D., Bilsback, K. R., Bui, T., Campuzano-Jost, P., Dollner, M., Froyd, K., Hodshire, A. L., Jimenez, J. L., Kodros, J. K., Luo, G., Murphy, D. M., Nault, B. A., Ray, E. A., Weinzierl, B. B., Wilson, J. C., Yu, F., Yu, P., Pierce, J. F., and Brock C. A.: A large source of cloud condensation nuclei from new particle formation in the tropics, Nature, 574, 399–403, 2019.

Wimmer, D., Buenrostro Mazon, S., Manninen, H. E., Kangasluoma, J., Franchin, A., Nieminen, T., Backman, J., Wang, J., Kuang, C., Krejci, R., Brito, J., Goncalves Morais, F., Martin, S. T., Artaxo, P., Kulmala, M., Kerminen, V.-M., and Petäjä, T.: Ground-based observation of clusters and nucleation-mode particles in the Amazon, Atmos. Chem. Phys., 18, 13245–13264, https://doi.org/10.5194/acp-18-13245-2018, 2018.

Yáñez-Serrano, A. M., Bourtsoukidis, E., Alves, E. G., Bauwens, M., Stavrakou, T., Llusià, J., Filella, I., Guenther, A., Williams, J., Artaxo, P., Sindelarova, K., Doubalova, J., Kesselmeier, J., and Peñuelas, J.: Amazonian biogenic volatile organic compounds under global change, Glob. Change Biol., 26, 4722–4751, 2020.

Yli-Juuti, T., Mohr, C., and Riipinen, I.: Open questions on atmospheric nanoparticle growth, Commun. Chem., 3, 1–4, 2020.

Zha, Q., Yan, C., Junninen, H., Riva, M., Sarnela, N., Aalto, J., Quéléver, L., Schallhart, S., Dada, L., Heikkinen, L., Peräkylä, O., Zou, J., Rose, C., Wang, Y., Mammarella, I., Katul, G., Vesala, T., Worsnop, D. R., Kulmala, M., Petäjä, T., Bianchi, F., and Ehn, M.: Vertical characterization of highly oxygenated molecules (HOMs) below and above a boreal forest canopy, Atmos. Chem. Phys., 18, 17437–17450, https://doi.org/10.5194/acp-18-17437-2018, 2018.

Zhao, B., Shrivastava, M., Donahue, N. M., Gordon, H., Schervish, M., Shilling, J. E., Zaveri, R. A., Wang, J., Andreae, M. O., Zhao, C., Gaudet, B., Liu, Y., Fan, J. W., and Fast, J. D.: High concentration of ultrafine particles in the Amazon free troposphere produced by organic new particle formation, P. Natl. Acad. Sci., 117, 25344–25351, 2020.

Zhou, J.: Submicrometer aerosol particle size distribution and hygroscopic growth measured in the Amazon rain forest during the wet season, J. Geophys. Res., 107, 8055, https://doi.org/10.1029/2000JD000203, 2002.

Supplement of Atmos. Chem. Phys., 22, 3469–3492, 2022
https://doi.org/10.5194/acp-22-3469-2022-supplement

Atmospheric Chemistry and Physics Open Access

Supplement of

Occurrence and growth of sub-50 nm aerosol particles in the Amazonian boundary layer

Marco A. Franco et al.

Correspondence to: Marco A. Franco (marco.franco@usp.br) and Christopher Pöhlker (c.pohlker@mpic.de)

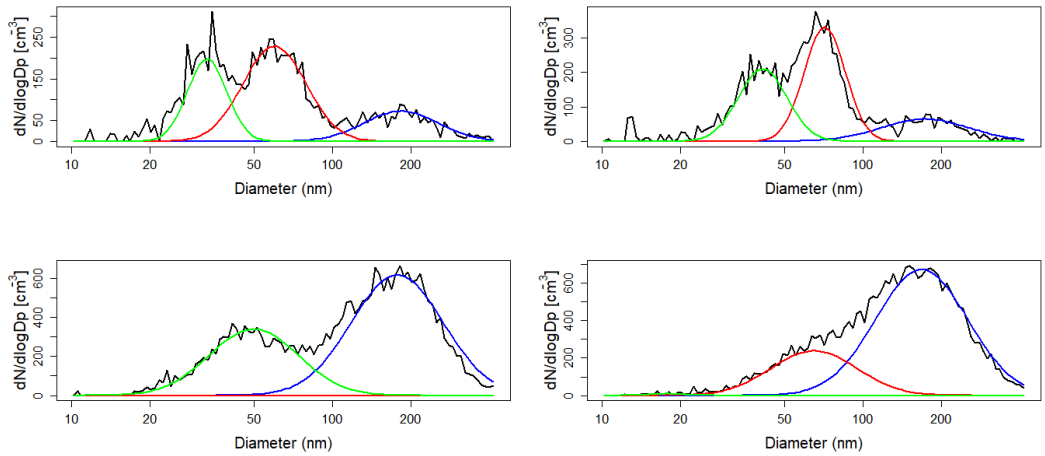

Figure S1. Examples of multi-modal log-normal fits obtained by the automatic algorithm. Sub-50 nm size particle mode (green) is defined as $10 \leq D_p < 50$, Aitken mode (red) is defined as $50 \leq D_p < 100$, and accumulation mode (blue) is defined as $100 \leq D_p \leq 400$.

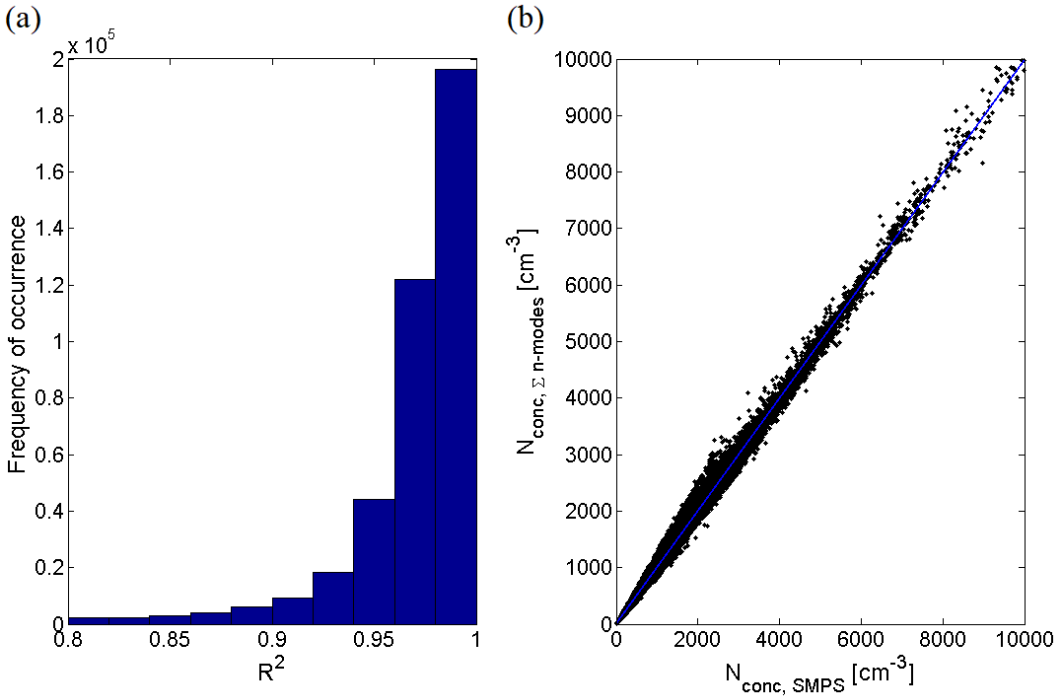

Figure S2. a) Histogram of the R^2 resulted from the multi-modal log-normal fits, considering only data with $R^2 > 0.8$. The average R^2 is 0.97. b) Linear fit of integrated $N_{conc,SMPS}$ and estimated $N_{conc,\sum nmodes}$, with $R^2 = 0.997$.

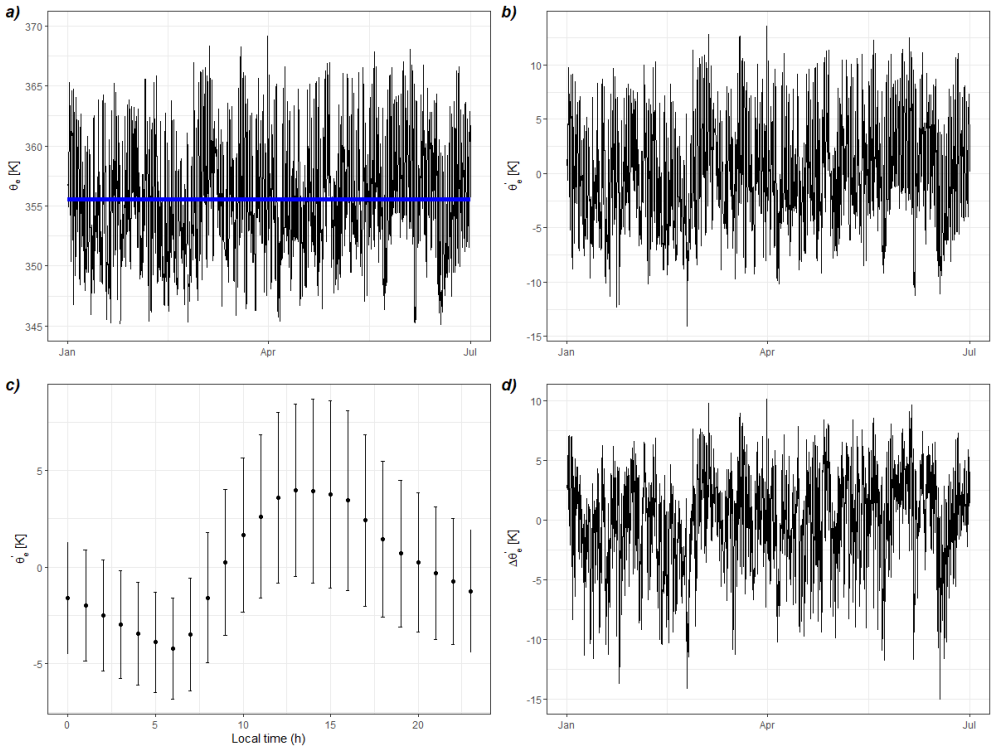

Figure S3. Illustration of the procedure to obtain the anomaly of the equivalent potential temperature ($\Delta\theta_e^{'}$ at a particular season. For didactic purposes, it was selected the wet season of 2018. a) The mean seasonal θ_e (blue line) is obtained from the time series of θ_e. b) Time series of θ_e detrended by its seasonal mean ($\theta_e^{'}$). c) The mean diurnal cycle of $\theta_e^{'}$. d) Time series of $\Delta\theta_e^{'}$, which represents the variations of θ_e at a specific time of the day at a particular season.

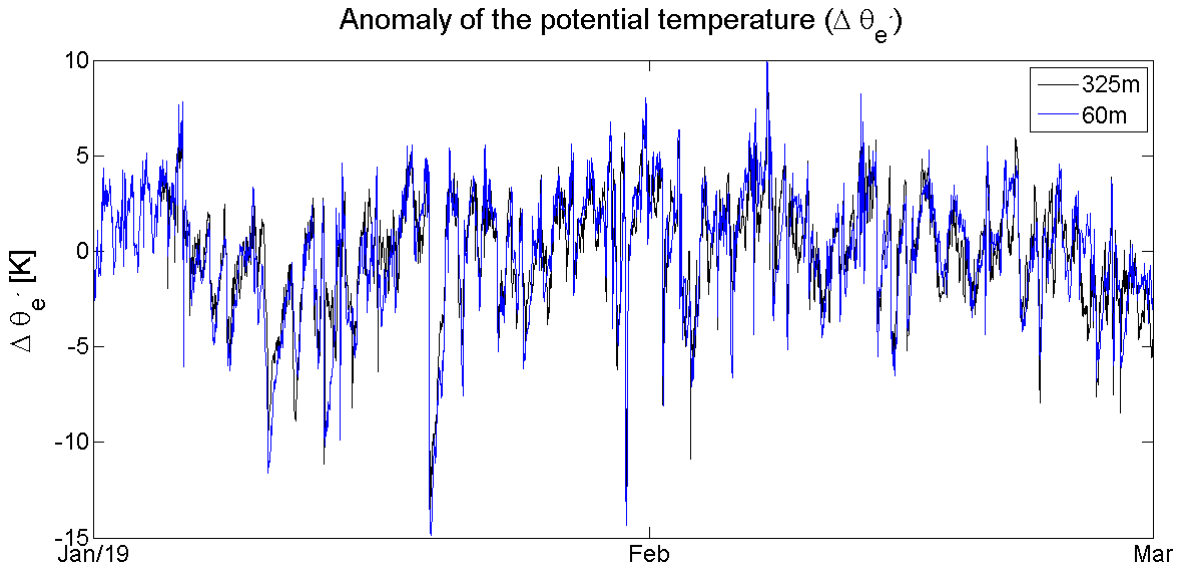

Figure S4. Time series of $\Delta\theta_e'$ calculated with meteorological measurements obtained simultaneously at ~60 (blue) and 325 m (black) high.

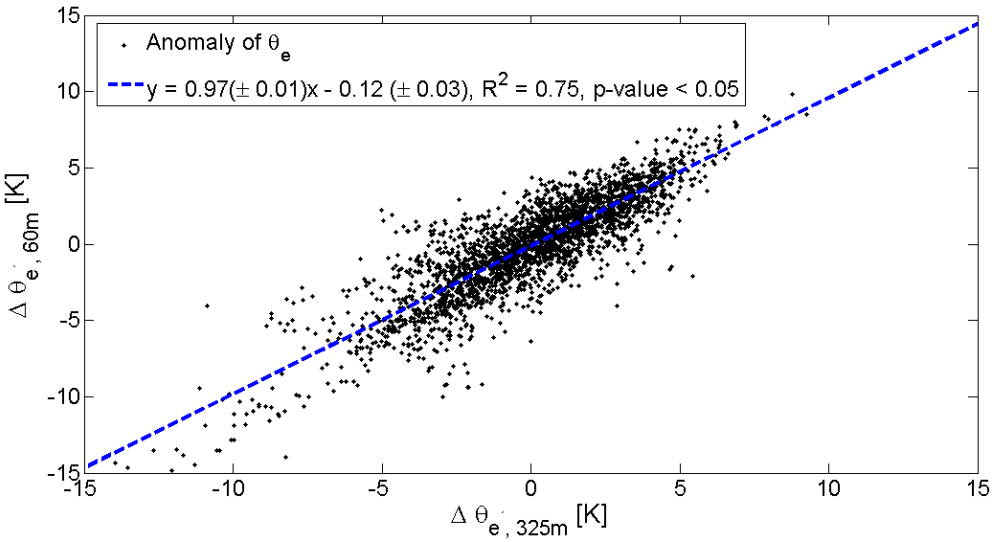

Figure S5. Correlation plot of $\Delta\theta_e'$ calculated with meteorological data obtained at ~60 and 325 m high. The blue line is the linear fit obtained from the data adjust.

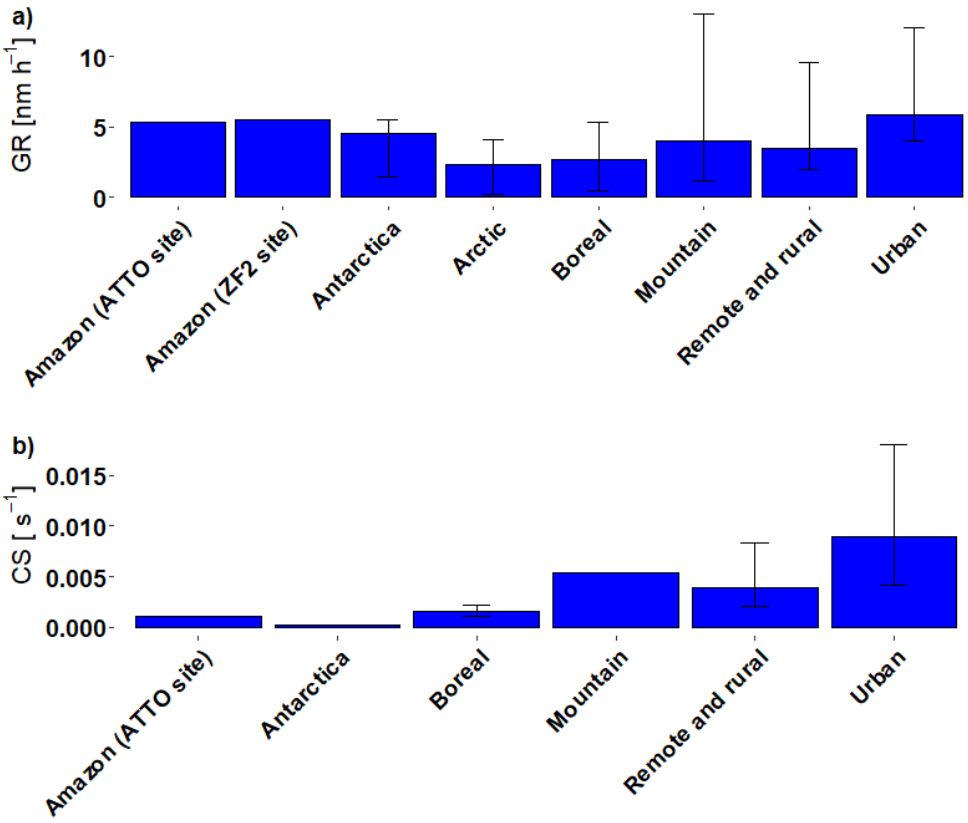

Figure S6. Comparative analysis of a) GR and b) CS at different site conditions. The error bars and the median data regarding the sites different from the Amazon sites denotes the 5th and 95th percentiles of the median GR and CS values obtained from different studies compiled by Kerminen et al. (2018) in its supplementary tables (available online at https://iopscience.iop.org/article/10.1088/1748-9326/aadf3c/data). For the Amazon sites, it was chosen to present only the medians of GR and CS, since the percentiles obtained in the studies refer to the different types of growth events analyzed, and not to different sites. In b), the missing sites did not present CS results in their respective articles.

2.4 High aerosol sensitivity of convective clouds over the Amazon

This chapter contains the manuscript that is currently under revision after submission to Science Advances.

Contribution to this publication by Leslie A. Kremper: I am the second author of this paper. In collaboration with F. Ditas and then taking over in 2019, I have been responsible as an instrument operator for the ATTO measurements of aerosol particle number size distributions obtained by a scanning mobility particle sizer (SMPS) as well as of total aerosol particle concentrations obtained by a condensation particle counter (CPC). I largely contributed to the data acquisition, field instrument maintenance, and data quality assurance. The SMPS and CPC represent the ground observations that are linked here to the satellite retrievals of cloud microphysical parameters and, therefore, are essential for the manuscript in this chapter. Beyond the data acquisition and processing, I contributed to the writing and data interpretation (e.g., size-segregated aerosol analysis and relevance for clouds) of this manuscript.

High aerosol sensitivity of convective clouds over the Amazon

Oliver Lauer[1], Leslie A. Kremper[1], Daniel Rosenfeld[2], Marco A. Franco[1,3], Meinrat O. Andreae[1,4,5], Paulo Artaxo[3], Ramon Campos Braga[1,6], Cléo Quaresma Dias-Júnior[7], Alessandro C. de Araújo[8], Florian Ditas[1,a], Avichay Efraim[2], Barbara Ervens[9], Bruna A. Holanda[1,a], Leonore Jungandreas[10], Ovid O. Krüger[1], Luiz A. T. Machado[1,3], Lianet Hernández Pardo[1,b], Ulrich Pöschl[1], Guy Pulik[2], Johannes Quaas[11], Youtong Zheng[12,13], Yannian Zhu[14,15], Christopher Pöhlker[1], and Mira L. Pöhlker[1,9,16]

[1] Multiphase Chemistry Department, Max Planck Institute for Chemistry, 55128 Mainz, Germany
[2] Institute of Earth Sciences, The Hebrew University of Jerusalem, Jerusalem, Israel
[3] Instituto de Física, Universidade de São Paulo, São Paulo, Brazil
[4] Scripps Institution of Oceanography, University of California San Diego, La Jolla, CA 92037, USA
[5] Department of Geology and Geophysics, King Saud University, Riyadh 145111, Saudi Arabia
[6] National Marine Science Centre, Southern Cross University, Coffs Harbour, NSW, Australia
[7] Department of Physics, Federal Institute of Pará (IFPA), Belém, PA, Brazil
[8] Empresa Brasileira de Pesquisa Agropecuária (Embrapa) Amazonia Oriental, CEP 66095-100, Belém, Brazil
[9] Université Clermont Auvergne, CNRS, SIGMA Clermont, Institut de Chimie de Clermont-Ferrand, 63000 Clermont-Ferrand, France
[10] German Center for Biodiversity Research, University Leipzig, Leipzig, Germany
[11] Faculty of Physics and Earth Sciences, Leipzig Institute for Meteorology, Leipzig University, Leipzig, Germany
[12] Atmospheric and Oceanic Sciences, Princeton University, Princeton, New Jersey, 08544, USA
[13] Department of Earth and Atmospheric Sciences, University of Houston, Houston, TX, USA
[14] School of Atmospheric Sciences, Nanjing University, 210023 Nanjing, China
[15] Joint International Research Laboratory of Atmospheric and Earth System Sciences & Institute for Climate and Global Change Research, Nanjing University, China
[16] Atmospheric Microphysics Department, Leibniz Institute for Tropospheric Research, Leipzig, Germany
[a] now at: Hessian Agency for Nature Conservation, Environment and Geology, Wiesbaden, Germany
[b] now at: Institute for Atmospheric and Environmental Sciences, Goethe University Frankfurt am Main, Germany

To whom correspondence should be addressed: C. Pöhlker (c.pohlker@mpic.de), M. L. Pöhlker (poehlker@tropos.de)

Abstract. Aerosols strongly influence clouds and climate but the effects of anthropogenic aerosols on cloud droplet concentrations and optical properties have remained largely uncertain in radiative forcing assessments. Here, we show that cloud droplet formation and growth of convective clouds in the central Amazon is largely aerosol-sensitive throughout the seasons, even under polluted conditions. Only highly polluted clouds close to deforestation fires become limited by updraft velocities rather than aerosol abundance. These results bridge pre-industrial-like atmospheric states and present-day pollution to quantify the cloud sensitivity across this particularly relevant aerosol concentration range in climate and Earth system models. Since our results are presentative for large parts of the basin, they generally improve our understanding of the hydrological cycle in the Amazonian ecosystem and beyond.

One sentence summary / Teaser: Ground-based and satellite observations show that convective clouds over the Amazon react sensitively to changes in the aerosol population throughout the seasons and over large parts of the basin.

Introduction

The effects of aerosols on clouds and climate have remained widely uncertain in assessing and modeling climate change[1]. Aerosol–cloud interactions contribute significant uncertainty to current radiative forcing estimates, especially due to a lack of knowledge of preindustrial aerosol and cloud conditions[2,3]. Accordingly, locations that today still approximate a preindustrial atmospheric state are of particular interest to understand and constrain the anthropogenic influence on cloud abundance and properties[4]. These locations, however, have become rare worldwide[5]. The Amazon is one of the few remaining continental places with episodes of pristine and pre-industrial-like atmospheric conditions[6,7]. It, therefore, represents a well-suited outdoor laboratory to investigate the responses and adjustments of cloud properties to aerosol perturbations across a wide range of atmospheric conditions, ranging from a largely unperturbed biosphere–atmosphere exchange in the wet season to heavy pollution in the dry season, also referred to as biomass burning season[8,9].

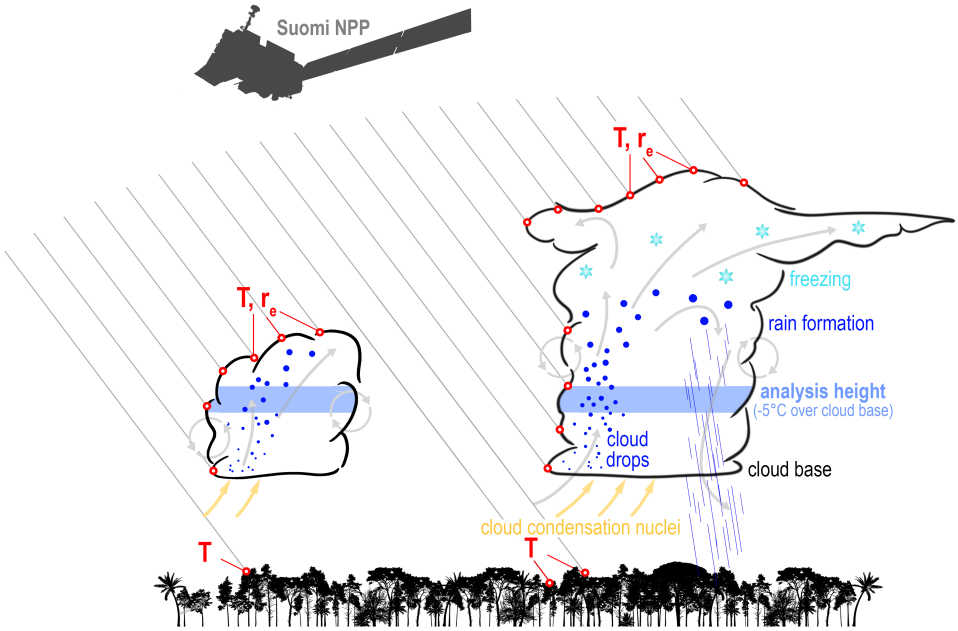

Figure 1. Microphysical processes, properties, and satellite observations of convective clouds: temperature (T) and effective radius of cloud droplets (r_e) as a function of height in evolving and fully developed cumulus clouds observed by Suomi-NPP satellite (see examples in Fig. 5). Under constant atmospheric conditions, the properties of clouds in different development states are interchangeable at the same temperature level, which means that a T-r_e profile of a cloud cluster and a profile tracking of a single convective cloud throughout its evolution provide the same information[10,11]. Following the temperature decrease with increasing height, the selected analysis height of this study is located $\Delta T = 5\,\mathrm{K}$ above cloud base, providing the cloud droplet effective radius ($r_{e,cb5}$) at that height.

The Amazonian aerosol population is characterized by a pronounced seasonality and a multimodal size distribution, spanning from few nanometers to tenths of micrometers (see Table S1 with reference values)[12,13]. A detailed understanding of the aerosol size distribution is a prerequisite for cloud microphysical studies. In combination with the chemical composition of the aerosols, it defines the number concentration ($N_{\mathrm{CCN}}(S)$) of cloud condensation nuclei (CCN) in an aerosol population, thus, the number of cloud droplets (N_{d}) at a given water vapor supersaturation (S), driven by a given updraft velocity (w) of the air masses at cloud base[14–16]. The ratio of aerosols that qualify as CCN ($N_{\mathrm{CCN}}(S)/N_{\mathrm{CN}}$) in an aerosol population is determined by the shape of its size distribution, the total particle number concentration, the particle hygroscopicity, and S. Typically, it increases with higher fractions of large particles as well as with an enhanced hygroscopicity[7,17]. Very high concentrations of large particles, however, can suppress S and yield low $N_{\mathrm{CCN}}(S)/N_{\mathrm{CN}}$.

Dense biomass burning smoke affects atmospheric thermodynamics and causes adjustments in the cloud micro- and macrophysical properties, such as the cloud dynamic evolution, the vertical profile of latent heat release, and precipitation formation[18–20]. Prominent examples of aerosol-induced changes of cloud physics are the 'cloud albedo effect'[21] and the 'cloud lifetime effect'[22]. The Twomey or cloud albedo effect refers to an aerosol-related increase in N_{d} and a corresponding decrease in the cloud droplet effective radius (r_{e}), which leads to more reflective clouds for a fixed cloud macro-structure and atmospheric thermodynamic conditions (i.e., the same liquid water content). The Albrecht or cloud lifetime effect refers to a decreased precipitation efficiency due to increased CCN and cloud droplet numbers[23]. This can delay the precipitation onset in the clouds to higher altitudes, cause a corresponding suppression of low-level rainout, and prolong cloud lifetime resulting in a larger cloud fraction[19,24–26]. Beyond their fundamental role in the climate system, these processes are also critically important for the rain forest ecosystem as they directly affect the hydrological cycle in the Amazon basin.

In order to represent these complex aerosol-cloud-precipitation processes more accurately in climate and Earth System models[27–29], we address here the effects of pristine aerosol conditions and a biomass-burning-driven increase in aerosol and CCN concentrations on the microphysics of convective clouds in the central Amazon. This observational three-year study on aerosol-cloud interactions combines in situ aerosol data from the Amazon Tall Tower Observatory (ATTO)[30] and high-resolution remote sensing observations of cloud microphysical properties from the Visible Infrared Imaging Radiometer Suite (VIIRS) on the Suomi National Polar-orbiting Partnership (NPP) satellite. Figure 1 illustrates the comparatively high spatial resolution ($\sim$ 375 m) of the VIIRS data to retrieve fundamental parameters, such as the cloud base height (H_{cb}), the droplet number concentration (N_{d}) and the effective cloud droplet radius (r_{e}) at and above the base of convective clouds on large geographic scales[31–33]. Details on the retrieval approach are outlined in the method section. These parameters were examined for their seasonality and their relation to the concentration and size distribution of the underlying aerosol field. Our findings help to understand and constrain the complex aerosol-cloud-precipitation interactions in the Amazonian hydrological cycle[34].

Results and Discussion

Seasonality of cloud microphysical properties

A variety of meteorological, trace gas, and aerosol parameters in central Amazonia show a pronounced seasonality[9,35–38]. These include the total aerosol particle number concentration (N_{CN}) and the black carbon mass concentration (M_{BC}), which are characterized by the typical oscillation between the clean wet (Feb to May) vs the polluted dry seasons (Aug to Nov), as shown in Fig. 2D and E. Pollution levels, here represented by M_{BC}, are peaking around September and are lowest – episodically even below detection limit – around April and May[7]. Here we show that the cloud parameters H_{cb}, N_d, and r_e are strongly seasonal as well (Fig. 2A, B, and C).

The base height of the convective clouds varies between $\sim 500\,\mathrm{m}$ in the wet and $\sim 1500\,\mathrm{m}$ in the dry season (Fig. 2A). These values agree well with previously reported planetary boundary layer (PBL) heights[39–41] as well as cloud base (CB) heights[24] in the Amazon. We obtained H_{cb} by applying four different methods and found that the satellite-based H_{cb} agrees well with other retrievals and direct measurements, which underlines the validity of the VIIRS approach. H_{cb} from the satellite observations and the ERA5 reanalysis data within a 50 times $50\,\mathrm{km}$ grid region around ATTO represent regional retrievals, whereas the ceilometer-derived H_{cb} as well as the lifting condensation level (LCL) calculated from ATTO meteorology data represent local retrievals. The calculated LCL-approach can be regarded as a lower limit for H_{cb}, since cloud formation is often delayed to higher altitudes due to the influence of dry air entrainment from the free atmosphere. In fact, the LCL-based H_{cb} accounts for the lowest values in Fig. 2A.

Similarly to N_{CN} and M_{BC}, the cloud parameters N_d and r_e show a clear seasonality (Fig. 2B and C). Due to condensational droplet growth, r_e initially increases adiabatically with height above cloud base[33]. In order to quantify the adiabatic growth rate of r_e, a common reference level is chosen. Throughout this study, $r_{e,cb5}$ represents the effective cloud droplet radius at $\Delta T = 5\,\mathrm{K}$ relative to the cloud base temperature, as illustrated in Fig. 1. At this cloud level – corresponding roughly to a height of $800\,\mathrm{m}$ above cloud base – clear differences in $r_{e,cb5}$ are expected for different CCN concentrations according to previous studies[24,43]. After reaching S_{max} close to the cloud base and throughout the initial phase of condensational droplet growth, N_d does not change significantly and, therefore, is not height-dependent in this range. This is valid as long as the cloud is adiabatic and no droplet evaporation or activation of additional CCN occurs[33]. This level is chosen, firstly because it is far enough from the cloud base to ensure stable adiabatic growth. Secondly, at this height, droplets are not yet big enough for efficient coalescence[33].

The wet season clouds are characterized by comparatively low droplet number concentrations with an average of $N_d = 300 \pm 180\,\mathrm{cm^{-3}}$ (arithmetic mean $\pm$ one standard deviation) and droplet growth to comparatively large sizes with $r_{e,cb5} = 12.7 \pm 2.2\,\mu\mathrm{m}$. The lowest N_d values of $150 \pm 40\,\mathrm{cm^{-3}}$ correspond to $r_{e,cb5} = 14.8 \pm 1.3\,\mu\mathrm{m}$. Dry season clouds, in contrast, are characterized by more (i.e., $N_d = 820 \pm 310\,\mathrm{cm^{-3}}$), though smaller, droplets (i.e., $r_{e,cb5} = 9.2 \pm 1.2\,\mu\mathrm{m}$). The highest N_d values of $1200 \pm 280\,\mathrm{cm^{-3}}$ correspond to $r_{e,cb5} = 8.0 \pm 0.9\,\mu\mathrm{m}$. Since observational data on N_d and r_e from the Amazon – especially seasonally resolved – is sparse, our results help to close this fundamental knowledge gap and agree well with the few existing

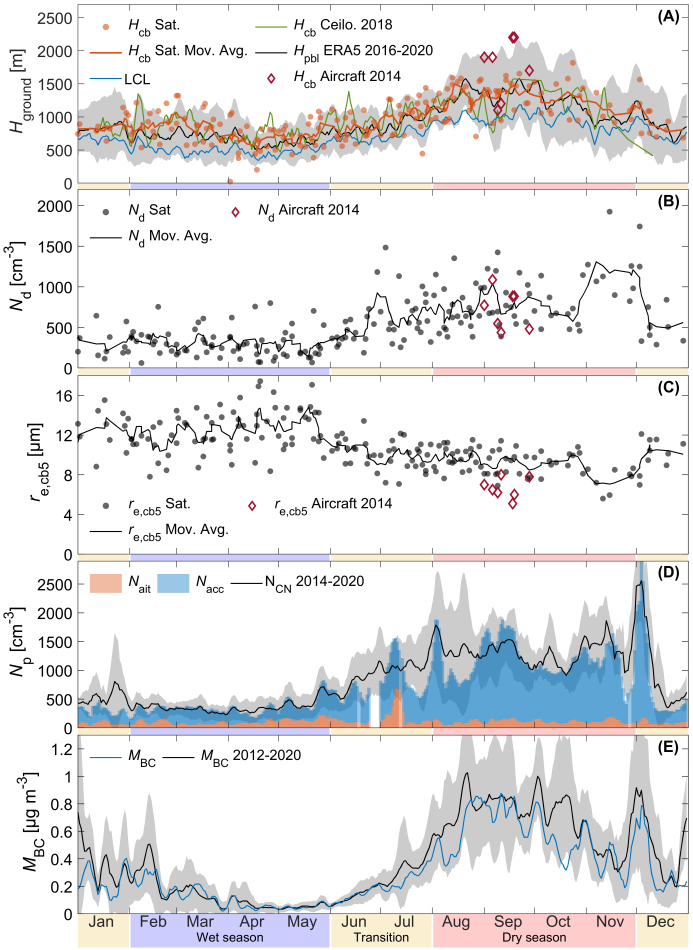

Figure 2. Seasonality of cloud microphysical and aerosol parameters in the ATTO region. Where not specified otherwise, the seasonal cycles represent the study's core period from 2017 to 2019. **(A)** Cloud base height (H_{cb}) obtained through four different approaches: VIIRS satellite retrieval ($H_{cb,sat}$), ATTO ceilometer measurements ($H_{cb,ceilo}$), ATTO lifting condensation level calculations (LCL), and ERA5 reanalysis data ($H_{pbl,ERA5}$). **(B,C)** The effective cloud droplet radius ($r_{e,cb5}$) and cloud droplet number concentration (N_d) were derived from VIIRS data. $r_{e,cb5}$ shown here was obtained at $\Delta T = 5$ K above cloud base as a defined reference to illustrate the droplet growth rate. The markers in **(A)**, **(B)** and **(C)** represent cloud scenes on individual days while the lines are five-point floating averages. Aircraft data from Braga *et al.*[42] are shown for comparison. **(D)** Aitken mode (N_{ait}), accumulation mode (N_{acc}), and total aerosol number concentrations (N_{CN}, black line as daily mean and gray shading as one standard deviation) from ATTO measurements. **(E)** Black carbon mass concentrations (M_{BC}) from ATTO measurements with three-year period of this study in blue and seven-year period in black (black line as daily mean and gray shading as one standard deviation).

studies[24,43–45]. Andreae *et al.*[24], for example, reported $r_{e,cb5}$ between $13-14\,\mu m$ for clean "green ocean conditions" as an upper limit and $r_{e,cb5}$ around $\sim 7\,\mu m$ for smoky conditions, with $\sim 5\,\mu m$ as an extreme minimum for pyrocumulus clouds.

The seasonality in N_d and $r_{e,cb5}$ generally follows the aerosol abundance, showing that the biomass burning-driven aerosol strongly modulates the cloud microphysical parameters, consistent with previous studies[7,46]. Especially, accumulation mode particles (i.e., 0.1 to 1 µm in diameter) are abundant and large enough to be the prime candidates for the majority of CCN. Under certain conditions, however, also Aitken mode particles can serve as CCN and, therefore, should not be neglected in accounting for total CCN concentrations. In the Amazon, such suitable conditions, under which a fraction of the Aitken mode particles can act as CCN, can be found in deep convective clouds during the wet season[47]. Figure 2D emphasizes that the seasonality in aerosol abundance is quite different between the aerosol size modes. While the accumulation mode is characterized by a pronounced seasonality, mainly driven by the occurrence of fires in the Amazon[48,49], the concentration of the Aitken mode particles is more constant, ranging between 200 and $300\,cm^{-3}$ throughout the seasons[12,13,50].

Aerosol- and updraft-sensitive cloud regimes

A simple yet instructive representation of the aerosol-cloud interactions under given atmospheric conditions is the relationship between N_{CN}, as a routinely measured aerosol parameter, and N_d. The shape and slope of such N_{CN} vs N_d curves in adiabatic parcels near the cloud base are determined by the interplay of w, S, as well as aerosol properties, such as composition and size distribution[51,52]. Figure 3 shows the N_{CN}-N_d relationship for the ATTO region, together with corresponding data sets from previous studies in the Amazon and worldwide. Within this N_{CN} vs N_d space, characteristic regimes of CCN activation and cloud droplet formation can be regarded as aerosol-limited (high w and low N_{CN}), updraft-limited (low w and high N_{CN}) or transitional, i.e., aerosol–and updraft-sensitive (Fig. 3B)[53,54].

The proximity of the N_{CN}-N_d curve to the one-to-one line indicates the extent to which the entire aerosol population has been activated as droplets. A close proximity indicates high activated aerosol fractions. The slope of the curve (dN_d/dN_{CN}) over a certain segment indicates the sensitivity of N_d to an increase in N_{CN}. An purely aerosol-limited CCN activation would correspond to a slope of 1 (i.e., $dN_d/dN_{CN} = 1$) and every additional aerosol particle would form a cloud droplet. In a purely updraft-limited regime, the slope would approach zero (i.e., $dN_d/dN_{CN} = 0$) and additional particles can be only activated if w is enhanced. The transitional regime where clouds are sensitive to changes in both aerosols and updraft is characterized by a slope between unity and zero, depending on N_{CN} and w as well as the slope of the cumulative aerosol size distribution around the critical diameters[47]. Under real atmospheric conditions, further processes like coagulation and mixing have to be taken into account in addition to the above considerations[54,62].

Figure 3 shows that the N_{CN}-N_d relationship at ATTO can be described as aerosol-sensitive over most of the relevant N_{CN} range. The multi-year N_{CN} frequency distribution ranges from clean continental air with a few hundreds of CN per cm^3 to polluted continental air with few thousands of CN per cm^3[63]. High N_{CN} levels above $\sim 3000\,cm^{-3}$ rarely occur at ATTO and have rather been observed in the proximity of major fires, such as in the deforestation hot spots in the southeastern

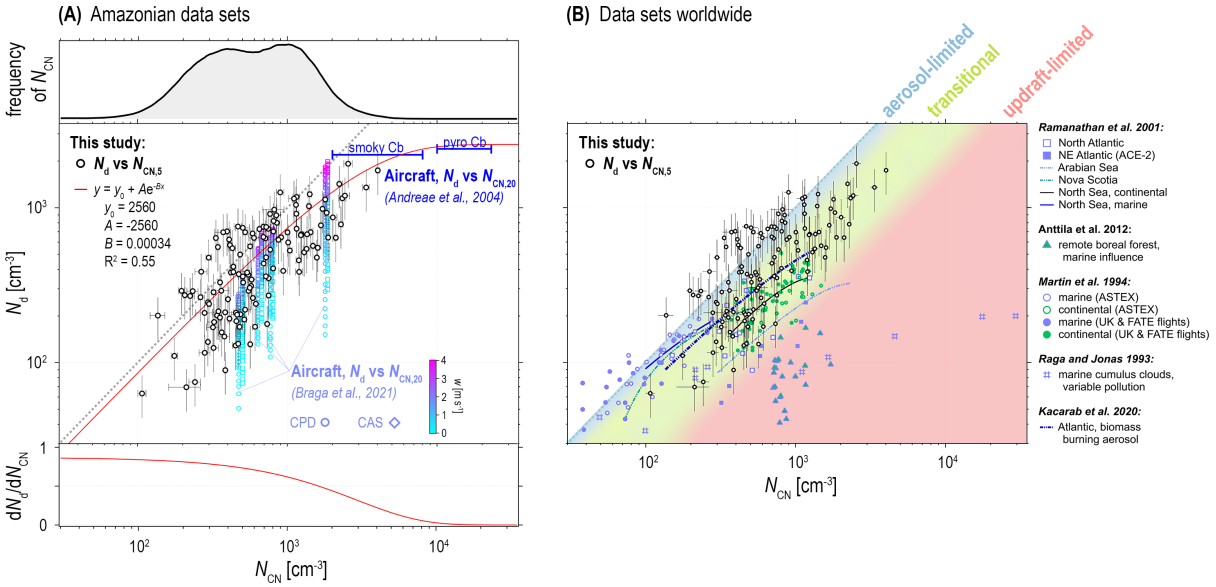

Figure 3. Relations between droplet number concentration, N_d, and total aerosol particle number concentration, N_{CN}, at cloud base in the ATTO region compared to data from earlier studies in the Amazon **(A)** and in other regions worldwide **(B)**. The ATTO data points (black circular markers) represent mean values with the error bars for one standard deviation in N_{CN} and 30 % error bars for the uncertainty in N_d according to Rosenfeld *et al.*[55]. Note that the N_{CN} data used here was obtained at 60 m assuming a well-mixed PBL with constant vertical aerosol size distributions[56]. Panel **(A)** combines the ATTO N_{CN}-N_d relationship with in situ aerosol and cloud observations from two aircraft campaigns: Braga *et al.*[57] reported N_d for flight average N_{CN} values as a function of the updraft velocity w. Andreae *et al.*[24] reported characteristic N_d values and N_{CN} ranges for highly polluted conditions over Amazonian fires. The empirical exponential fit in **(A)** includes the data from Andreae *et al.*[24]. Panel **(A)** also shows the N_{CN} frequency distribution at ATTO from 2014 to 2021 (top) as well as the slope dN_d/dN_{CN} of the empirical fit function (bottom). Panel **(B)** combines the ATTO N_{CN}-N_d relationship with data sets worldwide[18,58–61], which are subdivided into marine (blue) vs continental (green) environments here. The background shading in **(B)** illustrates the aerosol-limited (defined here through $N_d/N_{CN} \gtrapprox 0.9$), transitional (here $0.9 \gtrapprox N_d/N_{CN} \gtrapprox 0.2$), and updraft-limited (here $N_d/N_{CN} \lessapprox 0.2$) regimes, according to Reutter *et al.*[53]. The lower cut-off diameter of N_{CN} is ∼5 nm. In both panels, the 1:1 line is shown for orientation. Cloud probes specified in **(A)** are CCP = cloud combination probe and CAS = cloud and aerosol spectrometer[57].

Amazon[63–65]. The bottom panel in Fig. 3A shows that the highest sensitivity of $dN_d/dN_{CN} \approx 0.85$ occurs under wet season conditions with $N_{CN} \lessapprox 500\,cm^3$ (compare Table S1). The sensitivity drops below 0.5 at $N_{CN} \gtrapprox 1600\,cm^{-3}$, which corresponds to rather polluted dry season conditions. Expectedly, an increase in N_{CN} during the wet season has a larger effect on N_d and associated cloud microphysical processes than a corresponding increase in N_{CN} during the dry season, e.g. through an intensification of biomass burning[66]. Nevertheless, the sensitivity observed under dry season conditions in the central Amazon is still remarkably high. Note here that the N_{CN} frequency distribution at ATTO is characteristic for the atmospheric conditions

in central Amazonia, which implies that the high aerosol-sensitivity can also be regarded as representative for large parts of the basin, especially the largely untouched northern and western parts.

The N_{CN}-N_d relationship at ATTO also agrees well with data from the ACRIDICON-CHUVA aircraft campaign[57], which resolves N_d as a function of w for a given N_{CN} (Fig. 3A). This data illustrates the wide variability of N_d depending on updraft conditions at cloud base: for $w \gtrapprox 2\,\mathrm{m\,s^{-1}}$, the N_{CN}-N_d curve is much closer to the one-to-one line and appears much stronger aerosol-limited than for $w \lessapprox 2\,\mathrm{m\,s^{-1}}$. For the highest N_{CN} values observed at ATTO, the curve shows a tendency to level out as expected. This decrease in the slope $\mathrm{d}N_d/\mathrm{d}N_{CN}$ is consistent with the aircraft data in Andreae[63] on smoky and even pyro cumulonimbus (Cb) clouds in the southern Amazon. All these data sets can be described well with an empirical exponential fit function as shown in Fig. 3A.

Figure 3B embeds the ATTO N_{CN}-N_d curves into corresponding measurements from marine and continental environments worldwide. The comparatively close proximity of the Amazonian N_{CN}-N_d curve to the one-to-one line – representing high activated aerosol fractions – agrees well with the generally high CCN efficiencies observed in the central Amazon, where 50 to 90 % of all particles can be activated as CCN at a supersaturation of $S = 0.5\,\%$[7,50]. Such high CCN efficiencies are determined by the characteristic shape of the Amazonian aerosol size distribution, which typically has the majority of particles within the CCN-relevant size range and sufficiently low N_{CN} along with high S. Specifically, sub-50 nm particles are sparse, the accumulation mode typically dominates and accounts for ~70 % of the particles in the average distribution, and the Aitken mode is centered at comparatively large diameters between 67 and 71 nm[13] (and Table S1). Note for comparison that most marine data sets in Fig. 3B show lower activated fractions, which could result from generally lower updrafts in marine environments $<0.5\,\mathrm{m\,s^{-1}}$[60] as well as the typical shape of marine aerosol size distributions with a pronounced Aitken mode between 20 and 50 nm, which is much smaller than in the Amazon and therefore not particularly prone to act as CCN[67–70]. Note further that the marine N_{CN}-N_d curves tend to level off at lower $N_{CN} \lessapprox 1000\,\mathrm{cm^{-3}}$ than the continental curves, probably also associated with lower w above the ocean than above land. Moreover, wet season N_{CN} levels at ATTO overlap with the upper range of the marine N_{CN} data points, which re-emphasizes the concept of Green vs Blue Ocean conditions, in the sense that the pristine rain forest atmosphere resembles the pristine atmosphere over oceans[71,72].

Effective droplet radius and activation of Aitken mode particles as CCN

Figure 4A shows the relationship between N_{acc} and N_d. The accumulation mode represents the primary source of CCN and, therefore, accounts for the majority of the initial droplets at cloud base[7,50]. N_{acc} has been retrieved here from a multimodal fitting of the overall particle number size distribution according to Franco *et al.*[13], which allows to discriminate the roles of accumulation vs Aitken mode particles in the cloud droplet formation. The N_{acc} vs N_d scatter plot shows a comparatively tight relationship, which can be described by an empirical exponential fit. The BC mass concentration (M_{BC}) – widely used as a pollution marker and shown here by color-coding of the data points – increases with N_{acc} and exhibits two clusters of data points for the clean wet vs polluted dry seasons. Analogous to Fig. 3, the N_{acc}-N_d curve starts to level off at about $N_{acc} > 1000\,\mathrm{cm^{-3}}$, which implies that w increasingly becomes the limiting factor and an increasingly smaller fraction of the accumulation mode

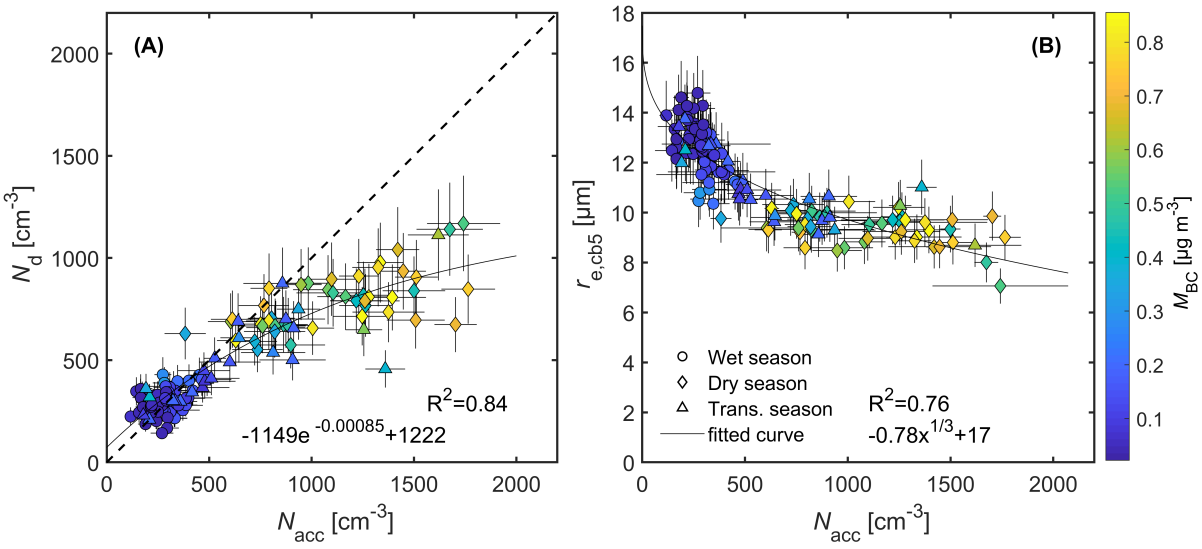

Figure 4. Dependence of cloud droplet evolution on aerosol particle number concentration in the accumulation mode (N_{acc}): droplet number concentration (N_d) and effective droplet radius (r_e) at a temperature $\Delta T = 5\,K$ above the cloud base. The N_d, as well as the r_e are the results from satellite analysis (both 5-point floating average). The shape of the markers denotes different seasons and the color of the markers indicates the black carbon (BC) mass concentration (M_{BC}) as a measure for biomass burning pollution. The solid black line represents an empirical exponential fit. The use of the floating average narrows the spread of the scatter diagrams and emphasises the seasonal variability at the same time. The same plot with raw data without applying a floating average can be found in Fig. S2. Figures S3, S4, and S5 resolve the relationship by season.

particles activates as CCN. At low N_{acc}, the slope dN_d/dN_{acc} approaches unity and even exceeds the one-to-one line. For N_{acc} around $100\,cm^{-3}$ as particularly clean wet season conditions, $N_{ait} \approx 70\,cm^{-3}$ are activated as CCN, corresponding to about 40 % of the wet season Aitken mode population (Table S1). This observational evidence for a contribution of the Aitken mode to cloud droplet formation is consistent with Pöhlker *et al.*[47], showing that this effect is particularly strong under conditions with low N_{CN} (Table S1) and a pronounced bimodal shape of the submicron aerosol population, as encountered during the Amazonian wet season[13,73]. The relevance of Aitken mode particles for N_d has also been emphasized in Braga *et al.*[57], where aircraft data and model simulations over the Amazon region and Atlantic Ocean were compared.

Figure 4B shows the inverse relationship between N_{acc} and $r_{e,cb5}$, emphasizing the relevance of the cloud albedo effect in the Amazon[21]. The relationship can be well described with an inverse cubic relationship, which is expected since the decrease in $r_{e,cb5}$ with increasing N_{acc} scales with the droplet volume. Note that under clean wet season conditions (i.e., $N_{acc} < 200\,cm^{-3}$), the average $r_{e,cb5}$ at the reference height $\sim 800\,m$ above cloud base already reaches the threshold of $\sim 14\,\mu m$, at which warm rain formation starts due to efficient droplet collision and coalescence[57,74]. This agrees with studies reporting a relatively low

height of warm rain formation under wet season conditions in the Amazon[44,75]. With increasing N_{acc} levels, mostly driven by biomass burning smoke, $r_{e,cb5}$ decreases substantially to about 7 µm. Note in this context that a r_e of $\sim$3.7 µm is the lower detection limit of the satellite retrieval (see method section).

In summary, we have related measured aerosol number concentrations of total particles (N_{CN}), Aitken mode particles (N_{ait}), and accumulation mode particles (N_{acc}) to satellite retrievals of droplet number concentration (N_d) and effective cloud droplet radius (r_e) at a reference height of $\sim$800 m above the base of convective clouds in the central Amazon over a period of three years. The results provide detailed insights into cloud microphysics, which are characterized by a pronounced seasonality with comparatively low number concentrations and fast cloud droplet growth rates in the wet season (i.e., $N_{CN} = 460 \pm 200\,\mathrm{cm}^{-3}$, $N_d = 300 \pm 180\,\mathrm{cm}^{-3}$, and $r_{e,cb5} = 13 \pm 2\,\mu\mathrm{m}$, all number given as mean values $\pm$ one standard deviation) and high droplet number concentrations with a slower droplet growth in the dry season ($N_{CN} = 1260 \pm 690\,\mathrm{cm}^{-3}$, $N_d = 820 \pm 310\,\mathrm{cm}^{-3}$, $r_{e,cb5} = 9 \pm 1\,\mu\mathrm{m}$). Both, N_d and r_e, are sensitive to changes in N_{CN}.

The N_{CN}-N_d relationship shows characteristics typical for aerosol sensitive clouds, emphasizing that the properties of convective clouds over the Amazon respond to changes in the aerosol population even during polluted conditions in the biomass burning season. With regard to the northwest-southeast gradient of air pollution in the Amazon basin, clouds in the largely untouched northwest are expected to be similarly or even more sensitive to changes in the aerosol population. Only highly polluted clouds close to heavy biomass burning in the southeast may become independent of N_{CN} corresponding to updraft-limited conditions. Based on long-term measurements, we obtained statistically robust relationships between aerosol and cloud parameters, which help to understand complex aerosol-cloud-precipitation interactions in the Amazonian hydrological cycle and constrain these processes in climate and Earth system models.

Materials and Methods

Satellite data analysis

The approach of this study is based on the retrieval of so-called T-r_e profiles, which estimate the vertical evolution of the effective cloud droplet radius (r_e) as a function of temperature (T) in a cluster of clouds. Satellite images were recorded by the VIIRS installed on the Suomi NPP satellite[76,77]. The VIIRS data are composed of 22 visible-to-infrared channels that measure the wavelength-dependent intensity of cloud-reflected sunlight and infrared emission in the spectral range from $0.6\,\mu m$ to $11.45\,\mu m$. Five out of the 22 channels provide a high spatial resolution of $375\,m$, while the other 17 channels provide a moderate resolution of $750\,m$[31,77]. The two high-resolution channels at $3.74\,\mu m$ and $11.45\,\mu m$ are primarily used in this study. The intensity of the emitted infrared radiation at a wavelength of $11.45\,\mu m$ is proportional to the temperature of the emitting object, approximating black body radiation (i.e., higher T implies higher intensity in the $11.45\,\mu m$ channel). The intensity of the radiation at a wavelength of $3.74\,\mu m$, which comprises reflected sun light and black body emission, is inversely correlated with the effective cloud droplet radius (i.e., smaller r_e entails higher radiance in the $3.74\,\mu m$ channel). The lower detection limit for r_e is around $3.5\,\mu m$ defined by the ratio between wavelength and r_e. The upper limit of r_e is $40\,\mu m$ due to an exponential drop in signal intensity.

Figure 1 provides an illustration of cloud processes and the VIIRS satellite observations. The T-r_e profiles were obtained from selected clouds or cloud ensembles within a certain area as shown by means of one example in Fig. 5. The overall region of interest (ROI), in which subregions (i.e., polygons) for the T-r_e profile retrieval were selected, is centered around ATTO and covers $40\,000\,km^2$ ($200 \times 200\,km^2$). Note that the ROI does not include the city of Manaus and its plume, which is directed most of the time towards the west[78,79]. Viewing angles are limited by shadows cast by the clouds if the angle between observer (satellite) and light source (sun) gets too wide. Suitable satellite zenith viewing angles (east-west direction) are limited to a range between -10°and 40°relative to the satellite path, which eliminates 60 % of all days for investigation, on which the satellite overpass was not close enough to ATTO. Solar zenith angles are limited between 0°and 65°, which makes ATTO a well-suited location as it is close to the equator and, thus, always fulfills this requirement. Further, the topography of the ATTO region is relatively flat. This largely avoids topography-forced updrafts and resulting instabilities in the PBL, as the approach of this study requires a homogeneous temperature profile in the boundary layer. Finally, the dark forest provides an ideal homogeneous background, in strong contrast to the highly reflective clouds. These factors as well as the broad spectrum of ground-based in situ aerosol observations make ATTO a suitable location for the long-term satellite investigation.

In total, 203 days from January 2017 to December 2019 had adequate conditions that allowed a retrieval of T-r_e profiles. Per overpass, multiple polygons were selected within the ROI (Fig. 5). All polygons were drawn by hand and meet the following requirements: (i) All clouds within the polygon are coupled with the PBL, so that the assumption of equal cloud properties at the same height for clouds in different development states is justified[11]. (ii) Each polygon includes visible ground areas as the ground temperature is needed to calculate H_{cb} (Fig. 1,[80]). (iii) The polygon includes clouds in different development states or

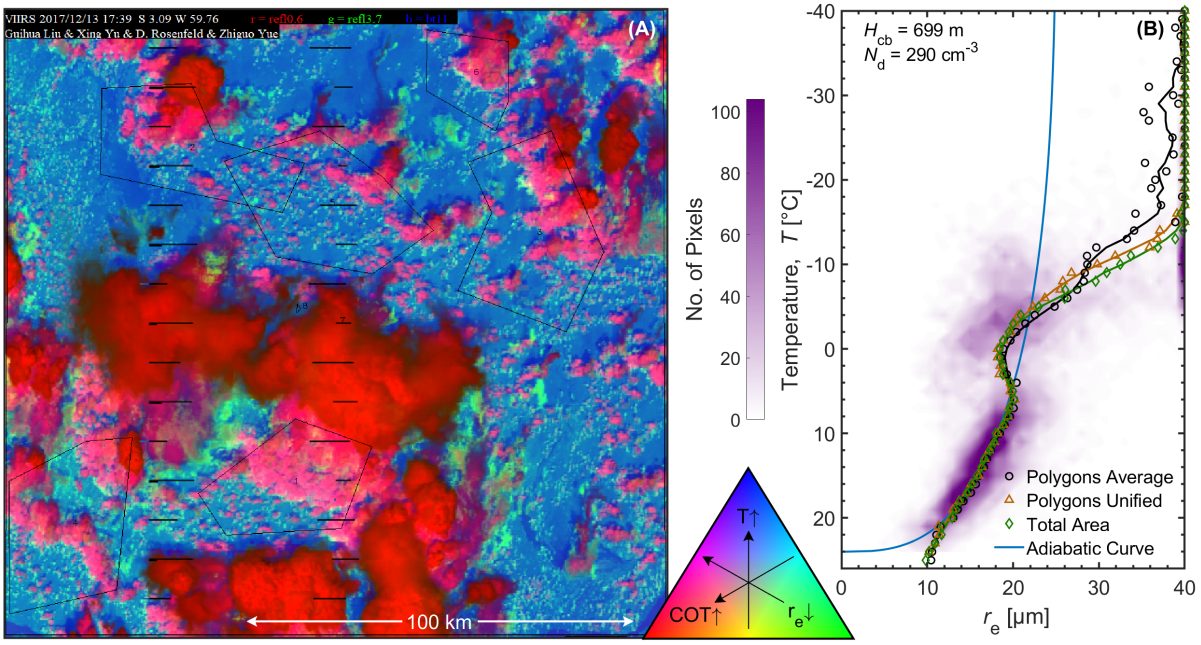

Figure 5. Exemplary VIIRS image of the ATTO region with the cloud scenery on 13 December 2017 **(A)** and the corresponding T-r_e profiles **(B)**. **(A)** The VIIRS image covers 200 km x 200 km with the ATTO site being marked as the white star. In the triangular color scale, blue indicates the highest temperatures (T) near the surface, representing cloud-free areas. Red indicates cloud optical thickness (COT) with intense, dark red showing high COT and thus regions of deep clouds, while pink shows regions with shallow convective clouds. Green color shows the inverse effective cloud droplet radius (r_e) with more intense green for smaller r_e. In this figure the teal pixels are low level clouds with low COT, small r_e and high T. The warmest pixels of these clouds have been interpreted as cloud base. The polygons in **(A)** show different regions that were averaged to retrieve the T-r_e profiles shown in **(B)**: Black polygons were analysed individually to retrieve individual T-r_e profiles that were subsequently averaged, yielding the black profile in **(B)** (averaged polygons). Brown polygons correspond to the combination of all black polygons treating it as one without overlap, yielding the brown T-r_e profile in **(B)** (unified polygons). The green T-r_e profile in **(B)** was obtained from the entire field of view in **(A)** (total area). The blue line in **(B)** shows the fitted adiabatic growth curve for this example case, calculated from the T-r_e profile and the adiabatic liquid water content (LWC) from National Centers for Environmental Prediction (NCEP) reanalysis data. The average H_{cb} is reported as 700 ± 130 m and N_d calculated from the fitted adiabatic growth curve is $290 \pm 110\,\mathrm{cm}^{-3}$.

fully developed clouds with a visible side profile to retrieve reliable T-r_e profiles (see e.g. example for cloud slope in Fig. 5). (iv) Cirrus, multi-layer, decoupled and semi-transparent clouds are avoided, as they distort the T-r_e profiles (see Fig. 6).

An exemplary VIIRS image is shown in Fig. 5A. It is an RGB-image (red, green, and blue), where each of the three base color channels represents one cloud property. Red is correlated with the cloud optical thickness (COT), green is inversely correlated with the effective cloud droplet radius (r_e), and blue is correlated with the temperature (T). The resulting color of each pixel

is proportional of each property related to the three base colors. For reliable T-r_e profiles, only coupled cumulus clouds with a clear field of view can be used. These show up as pink-colored clouds with teal edges. The pink color is a result of an average COT (medium red), high r_e at the cloud top (weak green), and a warm temperature compared to higher clouds (strong blue). The teal edge is a result of small COT (weak red), small r_e (strong green) and high temperature (strong blue). The ground is colored in strong blue, since it has the highest temperature. This representation of cloud properties also helps to avoid areas that can cause unwanted distortions: Clouds that are marked by bright green shading are decoupled mid-level clouds, as a result of small r_e and low temperatures, while semi-transparent cirrus clouds are displayed in dark red or black. They are cold and contain ice particles, which are detected as $r_e = 40 \mu m$ (Fig. 5A and Fig. 6A). Details on the coloring of the satellite plots can be found in Lensky and Rosenfeld[81]. For the retrieval of the T-r_e-profiles, the measured r_e values are binned into 1°C temperature intervals according to the corresponding pixel. For example, for every pixel with a temperature between 9.5°C and 10.5°C, the r_e values get binned together into a bin centered at 10°C. The 30th percentile (see explanation below) of r_e for each temperature is then the r_e used in the resulting T-r_e-profile for each polygon. For the T-r_e-profile retrieval within a given ROI, three different averaging methods were applied and compared:

1. *Polygons average*: Averaging of the individual T-r_e profiles from all individual polygons in Fig. 5A, which yielded the black profile in Fig. 5B.
2. *Polygons unified*: Retrieval of the T-r_e profile after merging all polygons in Fig. 5A and, thus, eliminating duplicated pixels, which yielded the brown profile in Fig. 5B.
3. *Total area*: Retrieval of the T-r_e profile from the entire VIIRS image, which yielded the green profile in Fig. 5B.

Figures 5B and 6B show the comparison of the T-r_e profiles from aforementioned methods: The T-r_e profiles from the *averaged polygons* and *unified polygons* approaches are comparable and vary only in some aspects. The T-r_e profile of the entire VIIRS image through the *total area* approach, however, can deviate strongly, especially when decoupled mid-level or cirrus clouds are present (Figure 6). The *unified polygons* approach yields the smoothest T-r_e profiles, but comparing all methods to model and ground data shows that the *averaged polygons* approach yields the best approximation of cloud properties, such as H_{cb} and cloud base T. This is expected, because the *unified polygons* use the warmest cloud pixel detected as cloud base, this leads to a systematic overestimation of the cloud base T and, in turn, results in an underestimation of H_{cb} for the *unified polygons* approach, while this bias is eliminated by the *averaged polygons* approach. Therefore the *averaged polygons* T-r_e profiles are used for all of the further analyses. Outliers within the same overpass are removed.

Here, we describe the T-r_e data analysis briefly, while more details can be found inZheng and Rosenfeld[80], Rosenfeld *et al.*[55], Yue *et al.*[32], and Efraim *et al.*[33]. Assuming a linear decrease in T with height in the boundary layer, the H_{cb} is calculated based on the temperature difference between the cloud bin that represents the highest temperature (in which 40 % of the pixels passed the cloud mask) and the average surface temperature T_{sfc} at 2 m above ground from reanalysis data[80], using the boundary layer dry lapse rate of 9.8 K/1000 m[82], with 130 m accuracy, due to the binning of T to 1 °C. The comparatively low resolution of the NCEP model requires a correction of H_{cb} with the satellite measured surface height. The cloud base temperature, T_{cb}, is

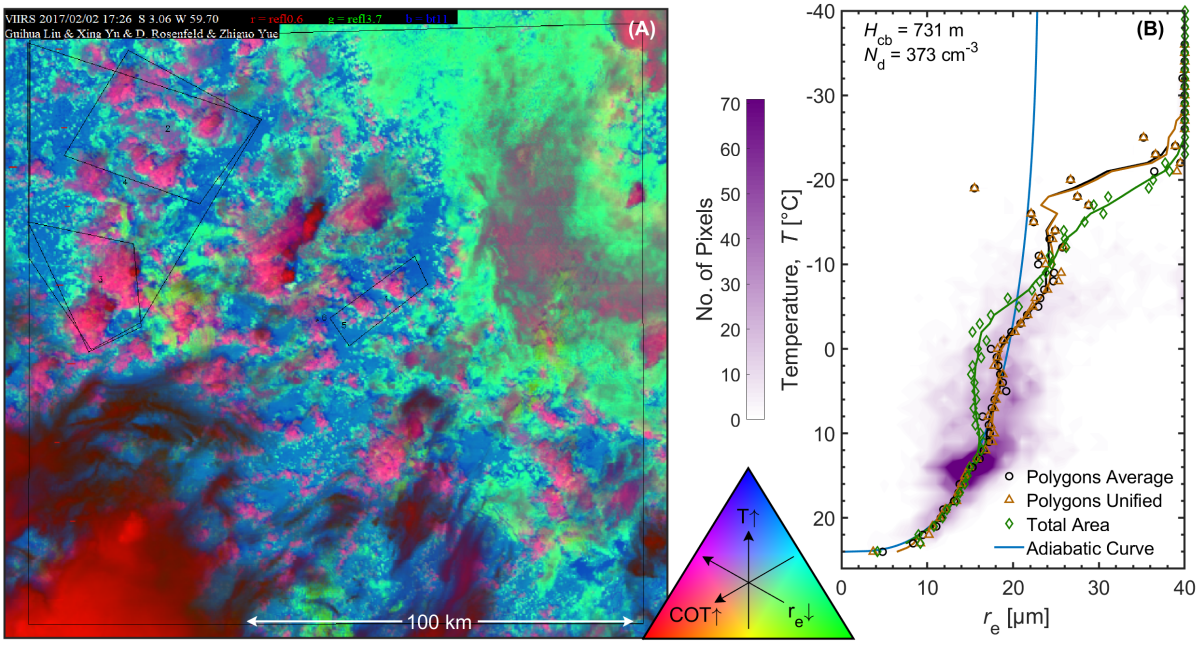

Figure 6. Exemplary VIIRS image of the ATTO region with the cloud scenery on 2 February 2017 **(A)** and the corresponding T-r_e profiles **(B)**. This example emphasizes the influences of distortions, like mid-level and cirrus clouds, on the T-r_e profiles, especially when different regions are considered (averaged polygons vs unified polygons vs total area). For details and layout aspects of this figure, refer to the caption of Fig. 5.

crucial for the calculation of N_d at cloud base. The inherent uncertainty for the VIIRS T measurement is $\pm 0.2\,°C$[83], which contributes significantly to the uncertainty in the calculated N_d. Likewise the accuracy of the cloud mask in predicting cloud pixels contributes to the uncertainty in N_d[84]. Assuming adiabatic growth, N_d is calculated by fitting the evolution of r_e with T and comparing it to the corresponding adiabatic liquid water content (LWC), based on T_{cb} and the NCEP reanalysis data, as described by Rosenfeld *et al.*[55]. The adiabatic LWC is corrected for entrainment effects by an empirical factor of 1/1.3 following Freud *et al.*[85]. According to Rosenfeld *et al.*[55], the uncertainty of the retrieved N_d is within 30 %, which includes environmental deficiencies such as additional aerosol entrainment from the free troposphere. The uncertainty of 30 % can be regarded as an upper limit. Recent improvements of the method have likely reduced the uncertainty. There has been no statistical analysis with aircraft data as a cross reference since the method was updated, therefore an uncertainty below 30 % can not be quantified yet. Multiple studies reported a systematic overestimation of the satellite-retrieved r_e by ~20 %[86–88]. To account for this widely recognized systematic overestimation, the 30th percentile value of all r_e within the same 1 K temperature bin are used. The average deviation of r_e found in this study lies between 5 and 15 %. The r_e at $\Delta T = 5$ K above cloud base represents the adiabatic growth rate after droplet activation. The level of $\Delta T = 5$ K is chosen, because the distance to the cloud base is

large enough to sufficiently represent the overall trend for the growth rate, while droplets are still predominantly smaller than 14 µm, even in the wet season, to prevent the influence of beginning coalescence[57,74].

The Amazon Tall Tower Observatory (ATTO)

The Amazon Tall Tower Observatory has been established in 2011/12 in central Amazonia to explore and monitor fundamental climatic, biogeochemical, and atmospheric parameters over decades[30]. The ATTO site (2.146°S, 59.006°W, 130 m above sea level) is located ∼150 km northeast of the city of Manaus, Brazil, in a region with largely untouched primary rain forest. An overview of the atmospheric, geographic, and ecological conditions as well as commonly encountered air masses can be found in Andreae *et al.*[30] and Pöhlker *et al.*[48]. Characteristic aerosol and CCN conditions at ATTO have been described in several studies[7,9,13,49,50,89].

Cloud base height and boundary layer height measurements at ATTO

During 2017 and 2018, the lifting condensation level (LCL) was calculated from temperature and humidity measurements at 60 m height on the 80 m tall walk-up tower[30]. In addition, cloud base height measurements have been conducted since 2015 with a CHM 15k-ceilometer, which is a single-wavelength elastic-backscatter lidar, originally sold by Jenoptik AG, Jena, Germany, since 2014 sold by Lufft GmbH, Fellbach, Germany[90,91]. Also the average boundary layer height (BLH) from ERA5 reanalysis data (https://www.ecmwf.int/en/forecasts/dataset/ecmwf-reanalysis-v5) for the region 50 km around ATTO is in good agreement with the cloud base height of coupled cumulus clouds[41].

Aerosol measurements at ATTO

Particle number size distributions were measured by a Scanning Mobility Particle Sizer (SMPS, TSI Inc., Shoreview, USA; model 3080 and later model 3082) with a condensation particle counter (CPC, model 3772). The instrument is sampling air from the 60 m inlet on the triangular mast and is located in an air-conditioned laboratory container at the foot of the tower. Sample air was transported through a stainless steel tube (finetron tubes, Dockweiler AG, Neustadt-Glewe, Germany) and dried by an automatic regenerating silica gel adsorption aerosol dryer, as described in Tuch *et al.*[92], to a relative humidity (RH) below 40 %. The SMPS measurements cover a particle diameter range from 10 to 400 nm. Frequent size accuracy tests were performed by using monodisperse polystyrene latex particles, and the data quality was continuously verified by complementary measurements by another condensation particle counter (CPC) running in parallel. Data were acquired and exported with the Aerosol Instrument Manager Software (AIM, Version 9 & 10, TSI Inc.) and corrected for standard temperature and pressure (STP, 273.15 K, 1013.25 hPa) as well as for inlet transmission losses following the approach as described in von der Weiden *et al.*[93] and Moran-Zuloaga *et al.*[89]. Further, the data were checked by visual inspection for instrument malfunction events. The acquired particle size distributions were fitted by a multi-modal log-normal distribution function developed by Franco *et al.*[13] to determine the Aitken and accumulation mode number concentrations. The Aitken mode (N_{ait}) is defined as particles with

diameters of 50 nm $< D <$ 100 nm and the accumulation mode (N_{acc}) as particles with diameters of 100 nm $< D <$ 400 nm. The total particle number concentration (N_{CN}) here is the integral of the entire SMPS size range (i.e., 10 to $400\,\mathrm{nm}$). The black carbon mass concentration (M_{BC}) was obtained through measurements of the aerosol light absorption coefficient at a wavelength of $637\,\mathrm{nm}$ by a multi-angle absorption photometer, (MAAP, model 5012, Thermo Electron Group, Waltham, USA), assuming a mass absorption cross section of $6.6\,\mathrm{m^2\,g^{-1}}$ [9].

Selection and processing of ground and satellite data

Only ATTO ground data between 16:00 and 17:30 UTC (12:00 and 13:30 local time), which is right before and during the satellite overpass (between 17:10 and 17:45 UTC), were considered and averaged for this analysis. This represents the closest approximation of the aerosol population that had served as CCN for the cloud(s) recorded in the VIIRS images. Both aerosol and cloud data can vary greatly on the scale of hours. They also do not necessarily follow the same trend, as environmental influences can affect both parameters independently. Therefore, all ATTO time series were pre-processed with a 5-point moving average to filter out most of the short-term variability to emphasize the characteristic seasonal conditions and trends. The floating 5-point average has been found in the course of an iterative evaluation process as the best compromise between noise reduction and preservation of details.

Acknowledgements.

This research has been funded by the Bundesministerium für Bildung und Forschung (BMBF contracts 01LB1001A, 01LK1602B, and 01LK2101B), the Brazilian Ministério da Ciência, Tecnologia e Inovação (MCTI/FINEP contract 01.11.01248.00), the Max Planck Society, the Conselho Nacional de Desenvolvimento Científico e Tecnológico (CNPq, Brazil) (process 200723/2015-4), the FAPESP (Fundação de Amparo à Pesquisa do Estado de São Paulo) (grant no. 2017/17047-0), the CNPq project (grant no. 169842/2017-7), the and CAPES project (grant no. 88887.368025/2019-00). For the operation of the ATTO site, we acknowledge the support by the Instituto Nacional de Pesquisas da Amazônia (INPA), the Amazon State University (UEA), the Large-Scale Biosphere-Atmosphere Experiment (LBA), FAPEAM, the Reserva de Desenvolvimento Sustentável do Uatumã (SDS/CEUC/RDS-Uatumã), the Max Planck Society, and the Max Planck Graduate Center with the Johannes Gutenberg University Mainz (MPGC). Particularly, we would like to thank the ATTO team members including Susan Trumbore, Alberto Quesada, Bruno Takeshi, Reiner Ditz, Stefan Wolff, Björn Nillius, Fernando Morais, Thomas Klimach, Roberta Pereira de Souza, Jürgen Kesselmeier, Andrew Crozier, Sam Jones, Delano Campos, Juarez Viegas, Sipko Bulthuis, Francisco Alcinei Gomes da Silva, Isabella Diogenes, Hermes Braga Xavier, Nagib Alberto de Castro Souza, Antonio Huxley Melo Nascimento, Valmir Ferreira de Lima, Feliciano de Souza Coelho, André Luiz Matos, Wallace Rabelo Costa, Amauri Rodriguês Perreira, Adir Vasconcelos Brandão, Davirley Gomes Silva, Thomas Disper, Torsten Helmer, Steffen Schmidt, Uwe Schulz, Uwe Schultz, Karl Kübler, Olaf Kolle, Martin Hertel, Kerstin Hippler, Steffen Schmidt and all further colleagues involved in the technical, logistical, and scientific support. We further thank Cristielen Perceval Machado for the support during finalization of the manuscript.

Author contribution. Author contributions according to Contributor Roles Taxonomy (CRediT, https://casrai.org/credit/): Conceptualization: MLP, DR, CP; Data curation: OL, LAK; Formal analysis: OL, LAK; Funding acquisition: MOA, PA, LATM, UP, CP, MLP; Investigation: OL, LAK, MAF, CQDJ, ACdA, FD, AE, BAH, OOK; Methodology: OL, CP, MLP; Project administration: CP, MLP; Resources: DR, PA, UP; Software: OL, AE, YoZ, YaZ; Supervision: DR, UP, CP, MLP; Validation: MOA, RCB, BE, LJ, LHP, JQ; Visualization: OL, CP; Writing – original draft: OL, CP, MLP; Writing – review & editing: All authors

Competing Interests. The authors declare that they have no conflict of interest.

Data Availability. The datasets presented here are available under https://doi.org/NNN. Additional ATTO data can be found in the ATTO data portal under https://www.attodata.org/.

References

[1] P. Forster, T. Storelvmo, K. Armour, W. Collins, J.-L. Dufresne, D. Frame, D. Lunt, T. Mauritsen, M. Palmer, M. Watanabe, M. Wild, H. Zhang, The Earth's Energy Budget, Climate Feedbacks, and Climate Sensitivity, *Climate Change 2021: The Physical Science Basis. Contribution of Working Group I to the Sixth Assessment Report of the Intergovernmental Panel on Climate Change*, V. Masson-Delmotte, P. Zhai, A. Pirani, S. Connors, C. Péan, S. Berger, N. Caud, Y. Chen, L. Goldfarb, M. Gomis, M. Huang, K. Leitzell, E. Lonnoy, J. Matthews, T. Maycock, T. Waterfield, O. Yelekçi, R. Yu, B. Zhou, eds. (Cambridge University Press, Cambridge, United Kingdom and New York, NY, USA, 2021), chap. 7.

[2] J. Mülmenstädt, G. Feingold, The radiative forcing of aerosol–cloud interactions in liquid clouds: Wrestling and embracing uncertainty, *Curr. Clim. Change Rep.* **4**, 23–40 (2018).

[3] K. S. Carslaw, L. A. Lee, C. L. Reddington, K. J. Pringle, A. Rap, P. M. Forster, G. W. Mann, D. V. Spracklen, M. T. Woodhouse, L. A. Regayre, J. R. Pierce, Large contribution of natural aerosols to uncertainty in indirect forcing, *Nature* **503**, 67 (2013).

[4] M. O. Andreae, Aerosols Before Pollution, *Science* **315**, 50–51 (2007).

[5] D. S. Hamilton, L. A. Lee, K. J. Pringle, C. L. Reddington, D. V. Spracklen, K. S. Carslaw, Occurrence of pristine aerosol environments on a polluted planet, *Proceedings of the National Academy of Sciences* **111**, 18466–18471 (2014).

[6] S. T. Martin, M. O. Andreae, P. Artaxo, D. Baumgardner, Q. Chen, A. H. Goldstein, A. Guenther, C. L. Heald, O. L. Mayol-Bracero, P. H. McMurry, T. Pauliquevis, U. Poschl, K. A. Prather, G. C. Roberts, S. R. Saleska, M. A. S. Dias, D. V. Spracklen, E. Swietlicki, I. Trebs, Sources and properties of Amazonian aerosol particles, *Reviews of Geophysics* **48**, RG2002 (2010).

[7] M. L. Pöhlker, F. Ditas, J. Saturno, T. Klimach, I. Hrabě de Angelis, A. C. Araùjo, J. Brito, S. Carbone, Y. Cheng, X. Chi, R. Ditz, S. S. Gunthe, B. A. Holanda, K. Kandler, J. Kesselmeier, T. Könemann, O. O. Krüger, J. V. Lavrič, S. T. Martin, E. Mikhailov, D. Moran-Zuloaga, L. V. Rizzo, D. Rose, H. Su, R. Thalman, D. Walter, J. Wang, S. Wolff, H. M. J. Barbosa, P. Artaxo, M. O. Andreae, U. Pöschl, C. Pöhlker, Long-term observations of cloud condensation nuclei over the Amazon rain forest – Part 2: Variability and characteristics of biomass burning, long-range transport, and pristine rain forest aerosols, *Atmos. Chem. Phys.* **18**, 10289–10331 (2018).

[8] U. Pöschl, S. T. Martin, B. Sinha, Q. Chen, S. S. Gunthe, J. A. Huffman, S. Borrmann, D. K. Farmer, R. M. Garland, G. Helas, J. L. Jimenez, S. M. King, A. Manzi, E. Mikhailov, T. Pauliquevis, M. D. Petters, A. J. Prenni, P. Roldin, D. Rose, J. Schneider, H. Su, S. R. Zorn, P. Artaxo, M. O. Andreae, Rainforest Aerosols as Biogenic Nuclei of Clouds and Precipitation in the Amazon, *Science* **329**, 1513–1516 (2010).

[9] J. Saturno, B. A. Holanda, C. Pöhlker, F. Ditas, Q. Wang, D. Moran-Zuloaga, J. Brito, S. Carbone, Y. Cheng, X. Chi, J. Ditas, T. Hoffmann, I. Hrabe de Angelis, T. Könemann, J. V. Lavrič, N. Ma, J. Ming, H. Paulsen, M. L. Pöhlker,

L. V. Rizzo, P. Schlag, H. Su, D. Walter, S. Wolff, Y. Zhang, P. Artaxo, U. Pöschl, M. O. Andreae, Black and brown carbon over central Amazonia: long-term aerosol measurements at the ATTO site, *Atmospheric Chemistry and Physics* **18**, 12817–12843 (2018).

[10] A. Arakawa, W. H. Schubert, Interaction of a Cumulus Cloud Ensemble with the Large-Scale Environment, Part I, *Journal of Atmospheric Sciences* **31**, 674 – 701 (1974).

[11] I. M. Lensky, D. Rosenfeld, The time-space exchangeability of satellite retrieved relations between cloud top temperature and particle effective radius, *Atmos. Chem. Phys.* **6**, 2887–2894 (2006).

[12] L. Varanda Rizzo, P. Roldin, J. Brito, J. Backman, E. Swietlicki, R. Krejci, P. Tunved, T. Petäjä, M. Kulmala, P. Artaxo, Multi-year statistical and modeling analysis of submicrometer aerosol number size distributions at a rain forest site in Amazonia, *Atmospheric Chemistry and Physics* **18**, 10255–10274 (2018).

[13] M. A. Franco, F. Ditas, L. A. Kremper, L. A. T. Machado, M. O. Andreae, A. Araújo, H. M. J. Barbosa, J. F. de Brito, S. Carbone, B. A. Holanda, F. G. Morais, J. P. Nascimento, M. L. Pöhlker, L. V. Rizzo, M. Sá, J. Saturno, D. Walter, S. Wolff, U. Pöschl, P. Artaxo, C. Pöhlker, Occurrence and growth of sub-50 nm aerosol particles in the Amazonian boundary layer, *Atmospheric Chemistry and Physics* **22**, 3469–3492 (2022).

[14] H. Köhler, The nucleus in and the growth of hygroscopic droplets, *Transactions of the Faraday Society* **32**, 1152–1161 (1936).

[15] W. E. Howell, THE GROWTH OF CLOUD DROPS IN UNIFORMLY COOLED AIR, *Journal of Atmospheric Sciences* **6**, 134 – 149 (1949).

[16] M. Andreae, D. Rosenfeld, Aerosol–cloud–precipitation interactions. Part 1. The nature and sources of cloud-active aerosols, *Earth-Science Reviews* **89**, 13–41 (2008).

[17] U. Dusek, G. P. Frank, L. Hildebrandt, J. Curtius, J. Schneider, S. Walter, D. Chand, F. Drewnick, S. Hings, D. Jung, S. Borrmann, M. O. Andreae, Size Matters More Than Chemistry for Cloud-Nucleating Ability of Aerosol Particles, *Science* **312**, 1375–1378 (2006).

[18] V. Ramanathan, P. J. Crutzen, J. T. Kiehl, D. Rosenfeld, Aerosols, Climate, and the Hydrological Cycle, *Science* **294**, 2119–2124 (2001).

[19] D. Rosenfeld, U. Lohmann, G. B. Raga, C. D. O'Dowd, M. Kulmala, S. Fuzzi, A. Reissell, M. O. Andreae, Flood or drought: How do aerosols affect precipitation?, *Science* **321**, 1309–1313 (2008).

[20] J. V. Martins, A. Marshak, L. A. Remer, D. Rosenfeld, Y. J. Kaufman, R. Fernandez-Borda, I. Koren, A. L. Correia, V. Zubko, P. Artaxo, Remote sensing the vertical profile of cloud droplet effective radius, thermodynamic phase, and temperature, *Atmospheric Chemistry and Physics* **11**, 9485–9501 (2011).

[21] S. Twomey, The Influence of Pollution on the Shortwave Albedo of Clouds, *Journal of Atmospheric Sciences* **34**, 1149–1152 (1977).

[22] B. A. Albrecht, Aerosols, Cloud Microphysics, and Fractional Cloudiness, *Science* **245**, 1227–1230 (1989).

[23] L. D. Rotstayn, Indirect forcing by anthropogenic aerosols: A global climate model calculation of the effective-radius and cloud-lifetime effects, *Journal of Geophysical Research: Atmospheres* **104**, 9369–9380 (1999).

[24] M. O. Andreae, D. Rosenfeld, P. Artaxo, A. A. Costa, G. P. Frank, K. M. Longo, M. A. F. Silva-Dias, A. MO, R. D, A. P, C. AA, F. GP, L. KM, S.-D. MA, M. O. Andreae, D. Rosenfeld, P. Artaxo, A. A. Costa, G. P. Frank, K. M. Longo, M. A. F. Silva-Dias, Smoking Rain Clouds over the Amazon, *Science* **303**, 1337–1342 (2004).

[25] G. Feingold, On smoke suppression of clouds in Amazonia, *Geophysical Research Letters* **32**, L02804 (2005).

[26] J. C. Lin, T. Matsui, R. A. Pielke, C. Kummerow, Effects of biomass-burning-derived aerosols on precipitation and clouds in the Amazon Basin: a satellite-based empirical study, *Journal of Geophysical Research* **111**, D19204 (2006).

[27] K. J. Pringle, K. S. Carslaw, D. V. Spracklen, G. M. Mann, M. P. Chipperfield, The relationship between aerosol and cloud drop number concentrations in a global aerosol microphysics model, *Atmospheric Chemistry and Physics* **9**, 4131–4144 (2009).

[28] J. Quaas, Approaches to observe anthropogenic aerosol-cloud interactions, *Current climate change reports* **1**, 297–304 (2015).

[29] J. Quaas, A. Arola, B. Cairns, M. Christensen, H. Deneke, A. M. L. Ekman, G. Feingold, A. Fridlind, E. Gryspeerdt, O. Hasekamp, Z. Li, A. Lipponen, P.-L. Ma, J. Mülmenstädt, A. Nenes, J. E. Penner, D. Rosenfeld, R. Schrödner, K. Sinclair, O. Sourdeval, P. Stier, M. Tesche, B. van Diedenhoven, M. Wendisch, Constraining the Twomey effect from satellite observations: issues and perspectives, *Atmospheric Chemistry and Physics* **20**, 15079–15099 (2020).

[30] M. O. Andreae, O. C. Acevedo, A. Araùjo, P. Artaxo, C. G. G. Barbosa, H. M. J. Barbosa, J. Brito, S. Carbone, X. Chi, B. B. L. Cintra, N. F. da Silva, N. L. Dias, C. Q. Dias-Júnior, F. Ditas, R. Ditz, A. F. L. Godoi, R. H. M. Godoi, M. Heimann, T. Hoffmann, J. Kesselmeier, T. Könemann, M. L. Krüger, J. V. Lavric, A. O. Manzi, A. P. Lopes, D. L. Martins, E. F. Mikhailov, D. Moran-Zuloaga, B. W. Nelson, A. C. Nölscher, D. Santos Nogueira, M. T. F. Piedade, C. Pöhlker, U. Pöschl, C. A. Quesada, L. V. Rizzo, C.-U. Ro, N. Ruckteschler, L. D. A. Sá, M. de Oliveira Sá, C. B. Sales, R. M. N. dos Santos, J. Saturno, J. Schöngart, M. Sörgel, C. M. de Souza, R. A. F. de Souza, H. Su, N. Targhetta, J. Tóta, I. Trebs, S. Trumbore, A. van Eijck, D. Walter, Z. Wang, B. Weber, J. Williams, J. Winderlich, F. Wittmann, S. Wolff, A. M. Yáñez Serrano, The Amazon Tall Tower Observatory (ATTO): overview of pilot measurements on ecosystem ecology, meteorology, trace gases, and aerosols, *Atmospheric Chemistry and Physics* **15**, 10723–10776 (2015).

[31] D. Rosenfeld, G. Liu, X. Yu, Y. Zhu, J. Dai, X. Xu, Z. Yue, High-resolution (375 m) cloud microstructure as seen from the NPP/VIIRS satellite imager, *Atmospheric Chemistry and Physics* **14**, 2479–2496 (2014).

[32] Z. Yue, D. Rosenfeld, G. Liu, J. Dai, X. Yu, Y. Zhu, E. Hashimshoni, X. Xu, Y. Hui, O. Lauer, Automated Mapping of Convective Clouds (AMCC) Thermodynamical, Microphysical, and CCN Properties from SNPP/VIIRS Satellite Data, *Journal of Applied Meteorology and Climatology* **58**, 887 – 902 (2019).

[33] A. Efraim, O. Lauer, D. Rosenfeld, R. Campos Braga, L. A. Kremper, F. M., U. Pöschl, Z. Y., C. Pöhlker, M. L. Pöhlker, Satellite detection of secondary drop activation aloft in deep convective clouds with warm rain, *in prep.* **2021** (2021).

[34] D. Rosenfeld, S. Sherwood, R. Wood, L. Donner, Climate Effects of Aerosol-Cloud Interactions, *Science* **343**, 379–380 (2014).

[35] P. Artaxo, J. V. Martins, M. A. Yamasoe, A. S. Procópio, T. M. Pauliquevis, M. O. Andreae, P. Guyon, L. V. Gatti, A. M. C. Leal, Physical and chemical properties of aerosols in the wet and dry seasons in Rondônia, Amazonia, *Journal of Geophysical Research: Atmospheres* **107**, LBA 49–1–LBA 49–14 (2002).

[36] G. C. Roberts, A. Nenes, J. H. Seinfeld, M. O. Andreae, Impact of biomass burning on cloud properties in the Amazon Basin, *Journal of Geophysical Research: Atmospheres* **108** (2003).

[37] L. V. Rizzo, P. Artaxo, T. Müller, A. Wiedensohler, M. Paixão, G. G. Cirino, A. Arana, E. Swietlicki, P. Roldin, E. O. Fors, K. T. Wiedemann, L. S. M. Leal, M. Kulmala, Long term measurements of aerosol optical properties at a primary forest site in Amazonia, *Atmospheric Chemistry and Physics* **13**, 2391–2413 (2013).

[38] D. Moran-Zuloaga, F. Ditas, D. Walter, J. Saturno, J. Brito, S. Carbone, X. Chi, I. Hrabě de Angelis, H. Baars, R. H. M. Godoi, B. Heese, B. A. Holanda, J. V. Lavrič, S. T. Martin, J. Ming, M. L. Pöhlker, N. Ruckteschler, H. Su, Y. Wang, Q. Wang, Z. Wang, B. Weber, S. Wolff, P. Artaxo, U. Pöschl, M. O. Andreae, C. Pöhlker, Long-term study on coarse mode aerosols in the Amazon rain forest with the frequent intrusion of Saharan dust plumes, *Atmospheric Chemistry and Physics* **18**, 10055–10088 (2018).

[39] G. Fisch, J. Tota, L. A. T. Machado, M. Dias, R. F. D. Lyra, C. A. Nobre, A. J. Dolman, J. H. C. Gash, The convective boundary layer over pasture and forest in Amazonia, *Theoretical and Applied Climatology* **78**, 47–59 (2004).

[40] A. Henkes, G. Fisch, L. A. T. Machado, J.-P. Chaboureau, Morning boundary layer conditions for shallow to deep convective cloud evolution during the dry season in the central Amazon, *Atmospheric Chemistry and Physics* **21**, 13207–13225 (2021).

[41] C. Q. Dias-Júnior, R. G. Carneiro, G. Fisch, F. A. F. D'Oliveira, M. Sörgel, S. Botía, L. A. T. Machado, S. Wolff, R. M. N. d. Santos, C. Pöhlker, Intercomparison of Planetary Boundary Layer Heights Using Remote Sensing Retrievals and ERA5 Reanalysis over Central Amazonia, *Remote Sensing* **14** (2022).

[42] R. C. Braga, D. Rosenfeld, R. Weigel, T. Jurkat, M. Andreae, M. Wendisch, M. Pöhlker, T. Klimach, U. Pöschl, C. Pöhlker, C. Voigt, C. Mahnke, S. Borrmann, R. Albrecht, S. Molleker, D. Vila, L. Machado, P. Artaxo, Comparing calculated

microphysical properties of tropical convective clouds at cloud base with measurements during the ACRIDICON-CHUVA campaign (2016).

[43] E. Freud, D. Rosenfeld, M. O. Andreae, A. A. Costa, P. Artaxo, Robust relations between CCN and the vertical evolution of cloud drop size distribution in deep convective clouds, *Atmospheric Chemistry and Physics* **8**, 1661–1675 (2008).

[44] R. C. Braga, D. Rosenfeld, R. Weigel, T. Jurkat, M. O. Andreae, M. Wendisch, U. Pöschl, C. Voigt, C. Mahnke, S. Borrmann, R. I. Albrecht, S. Molleker, D. A. Vila, L. A. T. Machado, L. Grulich, Further evidence for CCN aerosol concentrations determining the height of warm rain and ice initiation in convective clouds over the Amazon basin, *Atmospheric Chemistry and Physics* **17**, 14433–14456 (2017).

[45] M. A. Cecchini, L. A. T. Machado, M. O. Andreae, S. T. Martin, R. I. Albrecht, P. Artaxo, H. M. J. Barbosa, S. Borrmann, D. Fütterer, T. Jurkat, C. Mahnke, A. Minikin, S. Molleker, M. L. Pöhlker, U. Pöschl, D. Rosenfeld, C. Voigt, B. Weinzierl, M. Wendisch, Sensitivities of Amazonian clouds to aerosols and updraft speed, *Atmospheric Chemistry and Physics* **17**, 10037–10050 (2017).

[46] Y. J. Kaufman, T. Nakajima, Effect of Amazon Smoke on Cloud Microphysics and Albedo-Analysis from Satellite Imagery, *Journal of Applied Meteorology and Climatology* **32**, 729 – 744 (1993).

[47] M. L. Pöhlker, M. Zhang, R. Campos Braga, O. O. Krüger, U. Pöschl, B. Ervens, Aitken mode particles as CCN in aerosol- and updraft-sensitive regimes of cloud droplet formation, *Atmospheric Chemistry and Physics* **21**, 11723–11740 (2021).

[48] C. Pöhlker, D. Walter, H. Paulsen, T. Könemann, E. Rodríguez-Caballero, D. Moran-Zuloaga, J. Brito, S. Carbone, C. Degrendele, V. R. Després, F. Ditas, B. A. Holanda, J. W. Kaiser, G. Lammel, J. V. Lavrič, J. Ming, D. Pickersgill, M. L. Pöhlker, M. Praß, N. Löbs, J. Saturno, M. Sörgel, Q. Wang, B. Weber, S. Wolff, P. Artaxo, U. Pöschl, M. O. Andreae, Land cover and its transformation in the backward trajectory footprint region of the Amazon Tall Tower Observatory, *Atmospheric Chemistry and Physics* **19**, 8425–8470 (2019).

[49] B. A. Holanda, M. L. Pöhlker, D. Walter, J. Saturno, M. Sörgel, J. Ditas, F. Ditas, C. Schulz, M. A. Franco, Q. Wang, T. Donth, P. Artaxo, H. M. J. Barbosa, S. Borrmann, R. Braga, J. Brito, Y. Cheng, M. Dollner, J. W. Kaiser, T. Klimach, C. Knote, O. O. Krüger, D. Fütterer, J. V. Lavrič, N. Ma, L. A. T. Machado, J. Ming, F. G. Morais, H. Paulsen, D. Sauer, H. Schlager, J. Schneider, H. Su, B. Weinzierl, A. Walser, M. Wendisch, H. Ziereis, M. Zöger, U. Pöschl, M. O. Andreae, C. Pöhlker, Influx of African biomass burning aerosol during the Amazonian dry season through layered transatlantic transport of black carbon-rich smoke, *Atmospheric Chemistry and Physics* **20**, 4757–4785 (2020).

[50] M. L. Pöhlker, C. Pöhlker, F. Ditas, T. Klimach, I. Hrabe de Angelis, A. Araújo, J. Brito, S. Carbone, Y. Cheng, X. Chi, R. Ditz, S. S. Gunthe, J. Kesselmeier, T. Könemann, J. V. Lavrič, S. T. Martin, E. Mikhailov, D. Moran-Zuloaga, D. Rose, J. Saturno, H. Su, R. Thalman, D. Walter, J. Wang, S. Wolff, H. M. J. Barbosa, P. Artaxo, M. O. Andreae, U. Pöschl,

Long-term observations of cloud condensation nuclei in the Amazon rain forest – Part 1: Aerosol size distribution, hygroscopicity, and new model parametrizations for CCN prediction, *Atmos. Chem. Phys.* **16**, 15709–15740 (2016).

[51] J. Chen, Y. Liu, M. Zhang, Y. Peng, New understanding and quantification of the regime dependence of aerosol-cloud interaction for studying aerosol indirect effects, *Geophysical Research Letters* **43**, 1780–1787 (2016).

[52] J. Chen, Y. Liu, M. Zhang, Y. Peng, Height Dependency of Aerosol-Cloud Interaction Regimes, *Journal of Geophysical Research: Atmospheres* **123**, 491–506 (2018).

[53] P. Reutter, H. Su, J. Trentmann, M. Simmel, D. Rose, S. S. Gunthe, H. Wernli, M. O. Andreae, U. Pöschl, Aerosol- and updraft-limited regimes of cloud droplet formation: influence of particle number, size and hygroscopicity on the activation of cloud condensation nuclei (CCN), *Atmospheric Chemistry and Physics* **9**, 7067–7080 (2009).

[54] D. Chang, Y. Cheng, P. Reutter, J. Trentmann, S. M. Burrows, P. Spichtinger, S. Nordmann, M. O. Andreae, U. Pöschl, H. Su, Comprehensive mapping and characteristic regimes of aerosol effects on the formation and evolution of pyro-convective clouds, *Atmospheric Chemistry and Physics* **15**, 10325–10348 (2015).

[55] D. Rosenfeld, Y. Zheng, E. Hashimshoni, M. L. Pöhlker, A. Jefferson, C. Pöhlker, X. Yu, Y. Zhu, G. Liu, Z. Yue, B. Fischman, Z. Li, D. Giguzin, T. Goren, P. Artaxo, H. M. J. Barbosa, U. Pöschl, M. O. Andreae, Satellite retrieval of cloud condensation nuclei concentrations by using clouds as CCN chambers, *Proceedings of the National Academy of Sciences* **113**, 5828–5834 (2016).

[56] G. Adler, J. M. Flores, A. Abo Riziq, S. Borrmann, Y. Rudich, Chemical, physical, and optical evolution of biomass burning aerosols: A case study, *Atmospheric Chemistry and Physics* **11**, 1491–1503 (2011).

[57] R. C. Braga, B. Ervens, D. Rosenfeld, M. O. Andreae, J.-D. Förster, D. Fütterer, L. Hernández Pardo, B. A. Holanda, T. Jurkat-Witschas, O. O. Krüger, O. Lauer, L. A. T. Machado, C. Pöhlker, D. Sauer, C. Voigt, A. Walser, M. Wendisch, U. Pöschl, M. L. Pöhlker, Cloud droplet formation at the base of tropical convective clouds: closure between modeling and measurement results of ACRIDICON–CHUVA, *Atmospheric Chemistry and Physics* **21**, 17513–17528 (2021).

[58] G. B. Raga, P. R. Jonas, On the link between cloud-top radiative properties and sub-cloud aerosol concentrations, *Quarterly Journal of the Royal Meteorological Society* **119**, 1419–1425 (1993).

[59] G. M. Martin, D. W. Johnson, A. Spice, The Measurement and Parameterization of Effective Radius of Droplets in Warm Stratocumulus Clouds, *Journal of Atmospheric Sciences* **51**, 1823 – 1842 (1994).

[60] M. Kacarab, K. L. Thornhill, A. Dobracki, S. G. Howell, J. R. O'Brien, S. Freitag, M. R. Poellot, R. Wood, P. Zuidema, J. Redemann, A. Nenes, Biomass burning aerosol as a modulator of the droplet number in the southeast Atlantic region, *Atmospheric Chemistry and Physics* **20**, 3029–3040 (2020).

[61] T. Anttila, D. Brus, A. Jaatinen, A.-P. Hyvärinen, N. Kivekäs, S. Romakkaniemi, M. Komppula, H. Lihavainen, Relationships between particles, cloud condensation nuclei and cloud droplet activation during the third Pallas Cloud Experiment, *Atmospheric Chemistry and Physics* **12**, 11435–11450 (2012).

[62] H. Jia, J. Quaas, E. Gryspeerdt, C. Böhm, O. Sourdeval, Addressing the difficulties in quantifying droplet number response to aerosol from satellite observations, *Atmospheric Chemistry and Physics* **22**, 7353–7372 (2022).

[63] M. O. Andreae, Correlation between cloud condensation nuclei concentration and aerosol optical thickness in remote and polluted regions, *Atmospheric Chemistry and Physics* **9**, 543–556 (2009).

[64] P. Artaxo, L. V. Rizzo, J. F. Brito, H. M. J. Barbosa, A. Arana, E. T. Sena, G. G. Cirino, W. Bastos, S. T. Martin, M. O. Andreae, Atmospheric aerosols in Amazonia and land use change: from natural biogenic to biomass burning conditions, *Faraday Discussions* **165**, 203–235 (2013).

[65] J. Brito, L. V. Rizzo, W. T. Morgan, H. Coe, B. Johnson, J. Haywood, K. Longo, S. Freitas, M. O. Andreae, P. Artaxo, Ground-based aerosol characterization during the South American Biomass Burning Analysis (SAMBBA) field experiment, *Atmospheric Chemistry and Physics* **14**, 12069–12083 (2014).

[66] G. C. Roberts, A. Nenes, J. H. Seinfeld, M. O. Andreae, Impact of biomass burning on cloud properties in the Amazon Basin, *Journal of Geophysical Research: Atmospheres* **108** (2003).

[67] P. K. Quinn, D. B. Collins, V. H. Grassian, K. A. Prather, T. S. Bates, Chemistry and Related Properties of Freshly Emitted Sea Spray Aerosol, *Chemical Reviews* **115**, 4383–4399 (2015). PMID: 25844487.

[68] H. Wex, K. Dieckmann, G. C. Roberts, T. Conrath, M. A. Izaguirre, S. Hartmann, P. Herenz, M. Schäfer, F. Ditas, T. Schmeissner, S. Henning, B. Wehner, H. Siebert, F. Stratmann, Aerosol arriving on the Caribbean island of Barbados: physical properties and origin, *Atmospheric Chemistry and Physics* **16**, 14107–14130 (2016).

[69] X. Gong, H. Wex, J. Voigtländer, K. W. Fomba, K. Weinhold, M. van Pinxteren, S. Henning, T. Müller, H. Herrmann, F. Stratmann, Characterization of aerosol particles at Cabo Verde close to sea level and at the cloud level – Part 1: Particle number size distribution, cloud condensation nuclei and their origins, *Atmospheric Chemistry and Physics* **20**, 1431–1449 (2020).

[70] B. C. Schulze, S. M. Charan, C. M. Kenseth, W. Kong, K. H. Bates, W. Williams, A. R. Metcalf, H. H. Jonsson, R. Woods, A. Sorooshian, R. C. Flagan, J. H. Seinfeld, Characterization of Aerosol Hygroscopicity Over the Northeast Pacific Ocean: Impacts on Prediction of CCN and Stratocumulus Cloud Droplet Number Concentrations, *Earth and Space Science* **7**, e2020EA001098 (2020). E2020EA001098 2020EA001098.

[71] G. C. Roberts, M. O. Andreae, J. Zhou, P. Artaxo, Cloud condensation nuclei in the Amazon Basin: "marine" conditions over a continent?, *Geophysical Research Letters* **28**, 2807–2810 (2001).

[72] E. Williams, D. Rosenfeld, N. Madden, J. Gerlach, N. Gears, L. Atkinson, N. Dunnemann, G. Frostrom, M. Antonio, B. Biazon, R. Camargo, H. Franca, A. Gomes, M. Lima, R. Machado, S. Manhaes, L. Nachtigall, H. Piva, W. Quintiliano, L. Machado, P. Artaxo, G. Roberts, N. Renno, R. Blakeslee, J. Bailey, D. Boccippio, A. Betts, D. Wolff, B. Roy, J. Halverson, T. Rickenbach, J. Fuentes, E. Avelino, Contrasting convective regimes over the Amazon: Implications for cloud electrification, *Journal of Geophysical Research: Atmospheres* **107**, LBA 50–1–LBA 50–19 (2002).

[73] L. A. T. Machado, M. A. Franco, L. A. Kremper, F. Ditas, M. O. Andreae, P. Artaxo, M. A. Cecchini, B. A. Holanda, M. L. Pöhlker, I. Saraiva, S. Wolff, U. Pöschl, C. Pöhlker, How weather events modify aerosol particle size distributions in the Amazon boundary layer, *Atmospheric Chemistry and Physics* **21**, 18065–18086 (2021).

[74] D. Rosenfeld, G. Gutman, Retrieving microphysical properties near the tops of potential rain clouds by multispectral analysis of AVHRR data, *Atmospheric Research* **34**, 259–283 (1994). 11th conference on clouds and precipitation.

[75] I. M. Lensky, D. Rosenfeld, Satellite-based insights into precipitation formation processes in continental and maritime convective clouds at nighttime, *Journal of Applied Meteorology* **42**, 1227–1233 (2003).

[76] D. Hillger, T. Kopp, T. Lee, D. Lindsey, C. Seaman, S. Miller, J. Solbrig, S. Kidder, S. Bachmeier, T. Jasmin, T. Rink, First-Light Imagery from Suomi NPP VIIRS, *Bulletin of the American Meteorological Society* **94**, 1019 – 1029 (2013).

[77] D. Hillger, C. Seaman, C. Liang, S. Miller, D. Lindsey, T. Kopp, Suomi NPP VIIRS imagery evaluation, *Journal of Geophysical Research* **119**, 6440–6455 (2014).

[78] U. Kuhn, L. Ganzeveld, A. Thielmann, T. Dindorf, G. Schebeske, M. Welling, J. Sciare, G. Roberts, F. X. Meixner, J. Kesselmeier, J. Lelieveld, O. Kolle, P. Ciccioli, J. Lloyd, J. Trentmann, P. Artaxo, M. O. Andreae, Impact of Manaus City on the Amazon Green Ocean atmosphere: ozone production, precursor sensitivity and aerosol load, *Atmospheric Chemistry and Physics* **10**, 9251–9282 (2010).

[79] S. T. Martin, P. Artaxo, L. Machado, A. O. Manzi, R. A. F. Souza, C. Schumacher, J. Wang, T. Biscaro, J. Brito, A. Calheiros, K. Jardine, A. Medeiros, B. Portela, S. S. de Sá, K. Adachi, A. C. Aiken, R. Albrecht, L. Alexander, M. O. Andreae, H. M. J. Barbosa, P. Buseck, D. Chand, J. M. Comstock, D. A. Day, M. Dubey, J. Fan, J. Fast, G. Fisch, E. Fortner, S. Giangrande, M. Gilles, A. H. Goldstein, A. Guenther, J. Hubbe, M. Jensen, J. L. Jimenez, F. N. Keutsch, S. Kim, C. Kuang, A. Laskin, K. McKinney, F. Mei, M. Miller, R. Nascimento, T. Pauliquevis, M. Pekour, J. Peres, T. Petäjä, C. Pöhlker, U. Pöschl, L. Rizzo, B. Schmid, J. E. Shilling, M. A. S. Dias, J. N. Smith, J. M. Tomlinson, J. Tóta, M. Wendisch, The Green Ocean Amazon Experiment (GoAmazon2014/5) Observes Pollution Affecting Gases, Aerosols, Clouds, and Rainfall over the Rain Forest, *Bulletin of the American Meteorological Society* **98**, 981 – 997 (2016).

[80] Y. Zheng, D. Rosenfeld, Linear relation between convective cloud base height and updrafts and application to satellite retrievals, *Geophysical Research Letters* **42**, 6485–6491 (2015).

[81] I. M. Lensky, D. Rosenfeld, Clouds-Aerosols-Precipitation Satellite Analysis Tool (CAPSAT), *Atmospheric Chemistry and Physics* **8**, 6739–6753 (2008).

[82] Y. Zheng, D. Rosenfeld, Linear relation between convective cloud base height and updrafts and application to satellite retrievals, *Geophysical Research Letters* **42**, 6485–6491 (2015).

[83] D. Tobin, H. Revercomb, R. Knuteson, J. Taylor, F. Best, L. Borg, D. Deslover, G. Martin, H. Buijs, M. Esplin, R. Glumb, Y. Han, D. Mooney, J. Predina, L. Strow, L. Suwinski, L. Wang, Suomi-NPP CrIS radiometric calibration uncertainty, *Journal of Geophysical Research: Atmospheres* **118**, 10,589–10,600 (2013).

[84] Y. Zhu, D. Rosenfeld, X. Yu, G. Liu, J. Dai, X. Xu, Satellite retrieval of convective cloud base temperature based on the NPP/VIIRS Imager, *Geophysical Research Letters* **41**, 1308–1313 (2014).

[85] E. Freud, D. Rosenfeld, J. R. Kulkarni, Resolving both entrainment-mixing and number of activated CCN in deep convective clouds, *Atmospheric Chemistry and Physics* **11**, 12887–12890 (2011).

[86] D. Painemal, P. Zuidema, Assessment of MODIS cloud effective radius and optical thickness retrievals over the Southeast Pacific with VOCALS-REx in situ measurements, *Journal of Geophysical Research Atmospheres* **116** (2011).

[87] S. R. Noble, J. G. Hudson, MODIS comparisons with northeastern Pacific in situ stratocumulus microphysics, *Journal of Geophysical Research. Atmospheres* **120**, 8332 (2015).

[88] D. Painemal, D. Spangenberg, W. L. Smith, P. Minnis, B. Cairns, R. H. Moore, E. Crosbie, C. Robinson, K. L. Thornhill, E. L. Winstead, L. Ziemba, Evaluation of satellite retrievals of liquid clouds from the GOES-13 imager and MODIS over the midlatitude North Atlantic during the NAAMES campaign, *Atmos. Meas. Tech* **14**, 1–14 (2021).

[89] D. Moran-Zuloaga, F. Ditas, D. Walter, J. Saturno, J. Brito, S. Carbone, X. Chi, I. Hrabě de Angelis, H. Baars, R. H. M. Godoi, B. Heese, B. A. Holanda, J. V. Lavrič, S. T. Martin, J. Ming, M. L. Pöhlker, N. Ruckteschler, H. Su, Y. Wang, Q. Wang, Z. Wang, B. Weber, S. Wolff, P. Artaxo, U. Pöschl, M. O. Andreae, C. Pöhlker, Long-term study on coarse mode aerosols in the Amazon rain forest with the frequent intrusion of Saharan dust plumes, *Atmospheric Chemistry and Physics* **18**, 10055–10088 (2018).

[90] M. Wiegner, A. Geiß, Aerosol profiling with the Jenoptik ceilometer CHM15kx, *Atmospheric Measurement Techniques* **5**, 1953–1964 (2012).

[91] M. Hervo, Y. Poltera, A. Haefele, An empirical method to correct for temperature-dependent variations in the overlap function of CHM15k ceilometers, *Atmospheric Measurement Techniques* **9**, 2947–2959 (2016).

[92] T. M. Tuch, A. Haudek, T. Müller, A. Nowak, H. Wex, A. Wiedensohler, Design and performance of an automatic regenerating adsorption aerosol dryer for continuous operation at monitoring sites, *Atmospheric Measurement Techniques* **2**, 417–422 (2009).

[93] S.-L. von der Weiden, F. Drewnick, S. Borrmann, Particle Loss Calculator – a new software tool for the assessment of the performance of aerosol inlet systems, *Atmospheric Measurement Techniques* **2**, 479–494 (2009).

Supplement File of

High aerosol sensitivity of convective clouds over the Amazon

Lauer et al.

Correspondence:

Christopher Pöhlker <c.pohlker@mpic.de>

Mira L. Pöhlker <poehlker@tropos.de>

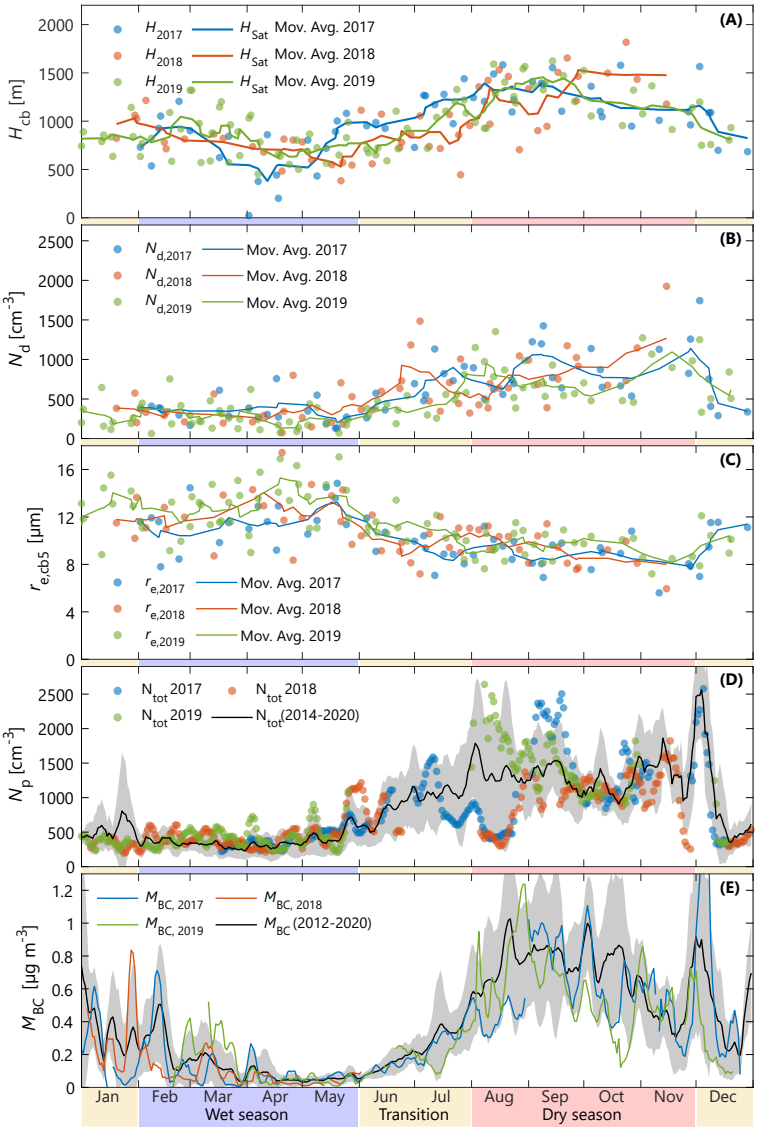

Fig. S1. Annual data separated by year. Data in all three years shows a similar annual trend. An outlier is the August aerosol data in panel D: the years 2017 and 2018 show a comparatively low average aerosol concentration, which contrasts with the much higher concentrations in 2019. The same period shows also the highest variance over the 6-year period, during which SMPS data is available. Even though aerosol data strongly increased in August 2019, the corresponding N_d is only slightly increased in comparison, indicating a low activation efficiency. During August 2019, ATTO received smoke from fires in the south with northwards wind directions.

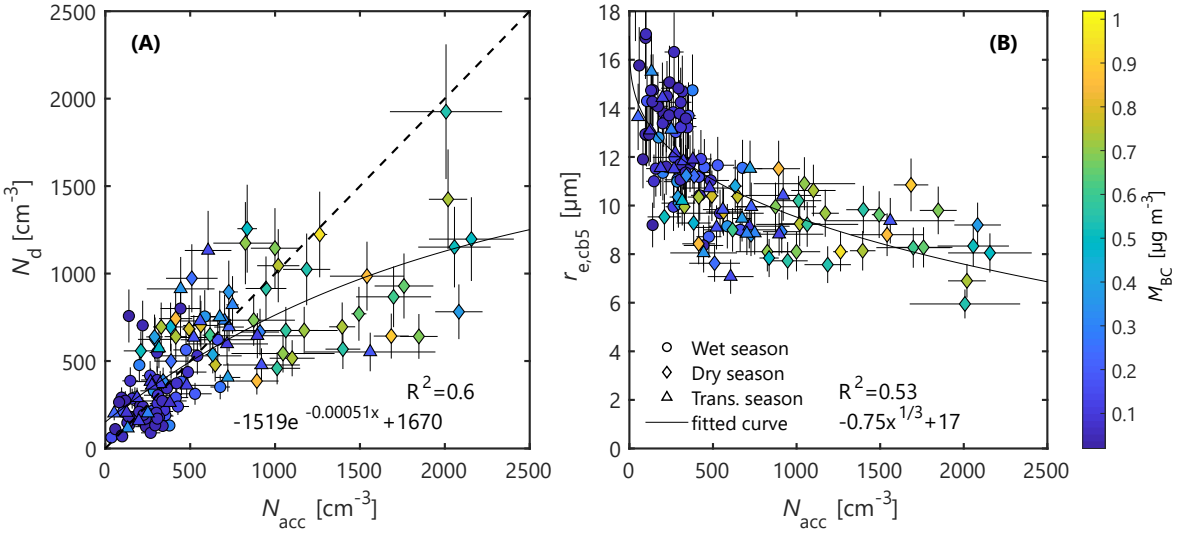

Fig. S2. Scatter plot with raw data. Shows overall the same trend as Fig. 4. The higher variability is related to the small time window of only 1.5 hours during each overflight and the changing conditions, especially in the dry season.

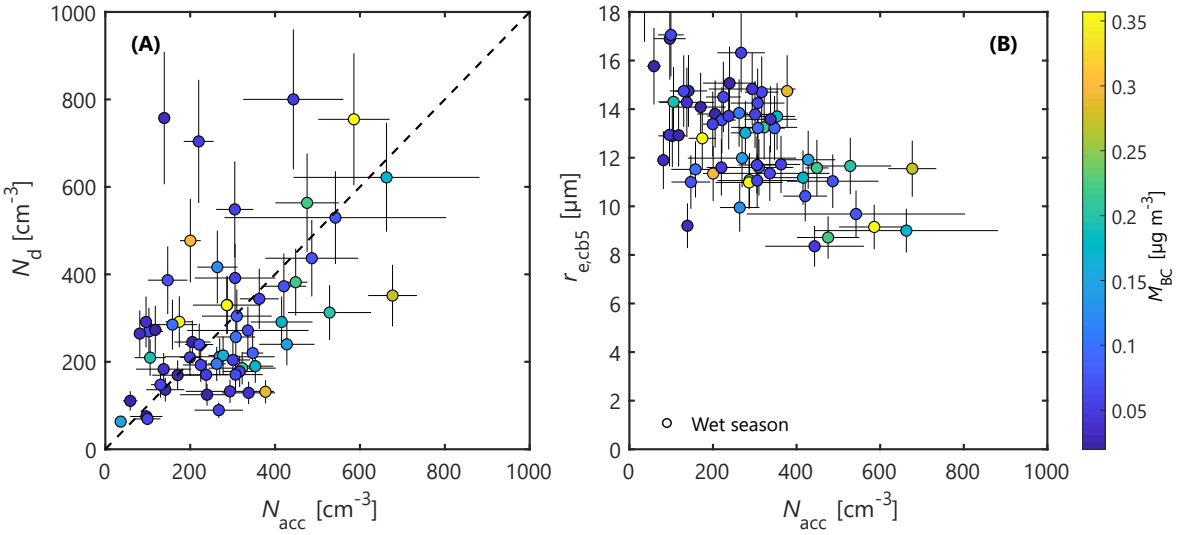

Fig. S3. Wet season scatter plot. More points above the 1:1-line compared to the other seasons, due to a stronger contribution of Aitken mode particles to N_d. Spread in results originate from less robust T-R_e fits. Because of the high growth rate, fewer amount of points can be considered for the adiabatic fit curve.

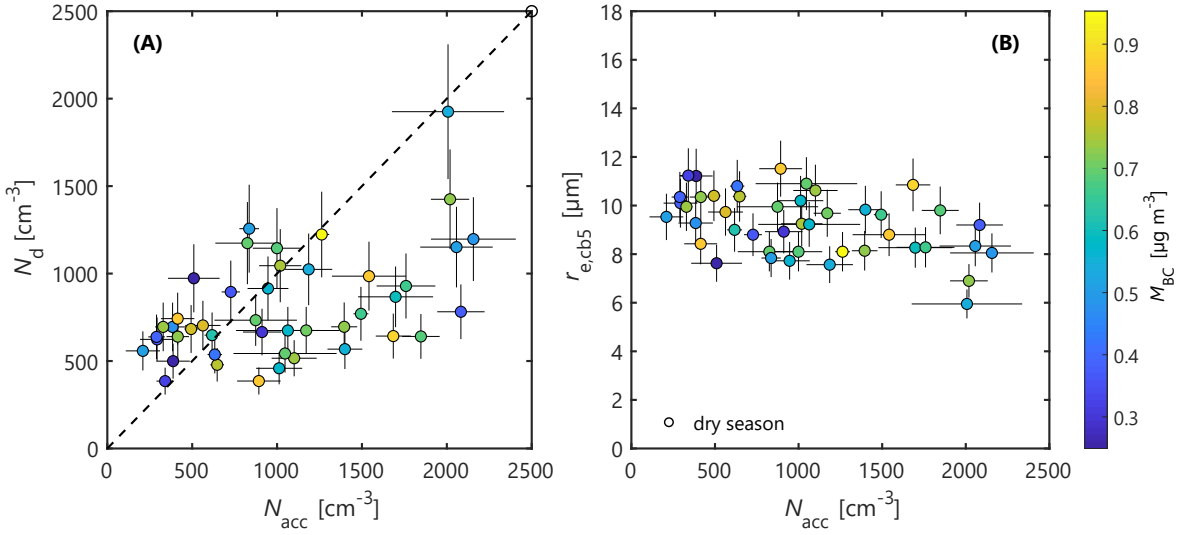

Fig. S4. Dry season Scatter plot. Very inconsistent conditions during this season result in large spread of results. Wind directions as well as aerosol loads and origin are constantly shifting during this time. Especially between the 3 different years, 2019 showed different overall conditions compared to 2017 and 2018, especially during August (see Fig. S1).

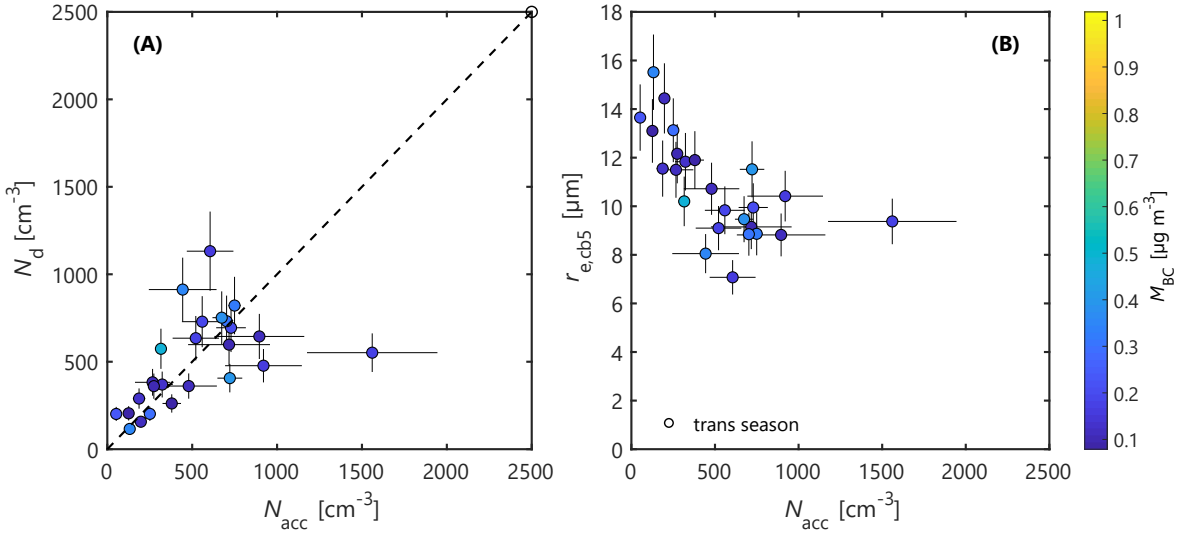

Fig. S5. Transition season scatter plot. Follows closest to the theoretical expected values. Overall low black carbon mass, but stable conditions with enough N_d activation for robust T-R_e profiles.

Table S1. Typical particle number concentrations under central Amazonian wet and dry season conditions. Specifically, the total number concentration of all condensation nuclei ($N_{\mathbf{CN}}$), the particle number concentrations of Aitken, accumulation, and coarse modes ($N_{\mathbf{Ait}}$, $N_{\mathbf{acc}}$, $N_{\mathbf{coarse}}$), as well as the corresponding mode peak diameters ($D_{\mathbf{Ait}}$, $D_{\mathbf{acc}}$, $D_{\mathbf{coarse}}$) are summarized here.

Parameter	Unit	Wet season	Dry season	References
N_{CN}	[cm^3]	$300 - 400$	$1250 - 1500$	Moran-Zuloaga et al. (2018); Varanda Rizzo et al. (2018)
N_{ait}	[cm^3]	$180 - 250$	$310 - 480$	Pöhlker et al. (2016); Varanda Rizzo et al. (2018)
N_{acc}	[cm^3]	$150 - 160$	$670 - 1350$	Pöhlker et al. (2016); Varanda Rizzo et al. (2018)
N_{coarse}	[cm^3]	0.4 ± 0.3	1.2 ± 0.8	Moran-Zuloaga et al. (2018); Prass et al. (2021)
D_{Ait}	[nm]	$67 - 71$	$68 - 71$	Pöhlker et al. (2016); Varanda Rizzo et al. (2018); Franco et al. (2022)
D_{acc}	[nm]	$153 - 172$	$146 - 161$	Pöhlker et al. (2016); Varanda Rizzo et al. (2018); Franco et al. (2022)
D_{coarse}	[nm]	$\sim$2000	$\sim$1500	Moran-Zuloaga et al. (2018), Andreae et al. (2015)

REFERENCES

Andreae, M. O., Acevedo, O. C., Araùjo, A., Artaxo, P., Barbosa, C. G. G., Barbosa, H. M. J., Brito, J., Carbone, S., Chi, X., Cintra, B. B. L., da Silva, N. F., Dias, N. L., Dias-Júnior, C. Q., Ditas, F., Ditz, R., Godoi, A. F. L., Godoi, R. H. M., Heimann, M., Hoffmann, T., Kesselmeier, J., Könemann, T., Krüger, M. L., Lavric, J. V., Manzi, A. O., Lopes, A. P., Martins, D. L., Mikhailov, E. F., Moran-Zuloaga, D., Nelson, B. W., Nölscher, A. C., Santos Nogueira, D., Piedade, M. T. F., Pöhlker, C., Pöschl, U., Quesada, C. A., Rizzo, L. V., Ro, C.-U., Ruckteschler, N., Sá, L. D. A., de Oliveira Sá, M., Sales, C. B., dos Santos, R. M. N., Saturno, J., Schöngart, J., Sörgel, M., de Souza, C. M., de Souza, R. A. F., Su, H., Targhetta, N., Tóta, J., Trebs, I., Trumbore, S., van Eijck, A., Walter, D., Wang, Z., Weber, B., Williams, J., Winderlich, J., Wittmann, F., Wolff, S., and Yáñez Serrano, A. M.: The Amazon Tall Tower Observatory (ATTO): overview of pilot measurements on ecosystem ecology, meteorology, trace gases, and aerosols, Atmospheric Chemistry and Physics, 15, 10 723–10 776, 2015.

Franco, M. A., Ditas, F., Kremper, L. A., Machado, L. A. T., Andreae, M. O., Araújo, A., Barbosa, H. M. J., de Brito, J. F., Carbone, S., Holanda, B. A., Morais, F. G., Nascimento, J. P., Pöhlker, M. L., Rizzo, L. V., Sá, M., Saturno, J., Walter, D., Wolff, S., Pöschl, U., Artaxo, P., and Pöhlker, C.: Occurrence and growth of sub-50 nm aerosol particles in the Amazonian boundary layer, Atmospheric Chemistry and Physics, 22, 3469–3492, 2022.

Moran-Zuloaga, D., Ditas, F., Walter, D., Saturno, J., Brito, J., Carbone, S., Chi, X., Hrabě de Angelis, I., Baars, H., Godoi, R. H. M., Heese, B., Holanda, B. A., Lavrič, J. V., Martin, S. T., Ming, J., Pöhlker, M. L., Ruckteschler, N., Su, H., Wang, Y., Wang, Q., Wang, Z., Weber, B., Wolff, S., Artaxo, P., Pöschl, U., Andreae, M. O., and Pöhlker, C.: Long-term study on coarse mode aerosols in the Amazon rain forest with the frequent intrusion of Saharan dust plumes, Atmospheric Chemistry and Physics, 18, 10 055–10 088, 2018.

Prass, M., Andreae, M. O., de Araùjo, A. C., Artaxo, P., Ditas, F., Elbert, W., Förster, J.-D., Franco, M. A., Hrabe de Angelis, I., Kesselmeier, J., Klimach, T., Kremper, L. A., Thines, E., Walter, D., Weber, J., Weber, B., Fuchs, B. M., Pöschl, U., and Pöhlker, C.: Bioaerosols in the Amazon rain forest: temporal variations and vertical profiles of Eukarya, Bacteria, and Archaea, Biogeosciences, 18, 4873–4887, 2021.

Pöhlker, M. L., Pöhlker, C., Ditas, F., Klimach, T., Hrabe de Angelis, I., Araújo, A., Brito, J., Carbone, S., Cheng, Y., Chi, X., Ditz, R., Gunthe, S. S., Kesselmeier, J., Könemann, T., Lavrič, J. V., Martin, S. T., Mikhailov, E., Moran-Zuloaga, D., Rose, D., Saturno, J., Su, H., Thalman, R., Walter, D., Wang, J., Wolff, S., Barbosa, H. M. J., Artaxo, P., Andreae, M. O., and Pöschl, U.: Long-term observations of cloud condensation nuclei in the Amazon rain forest – Part 1: Aerosol size distribution, hygroscopicity, and new model parametrizations for CCN prediction, Atmos. Chem. Phys., 2016.

Varanda Rizzo, L., Roldin, P., Brito, J., Backman, J., Swietlicki, E., Krejci, R., Tunved, P., Petäjä, T., Kulmala, M.,

and Artaxo, P.: Multi-year statistical and modeling analysis of submicrometer aerosol number size distributions at a rain forest site in Amazonia, Atmospheric Chemistry and Physics, 18, 10 255–10 274, 2018.

CHAPTER 3

Conclusions

Conclusions

Atmospheric aerosol have a significant impact on the atmospheric radiative transfer as well as the hydrological cycling in the Amazon rain forest by influencing cloud and precipitation formation. Despite many advances in our understanding of the Amazonian aerosol cycle, major questions on its sources, spatiotemmporal variability, atmospheric feedbacks, and overall roles in the Earth system have remained open. This emphasizes the importance to further investigate the biosphere-atmosphere interactions of the rain forest ecosystem and its perturbation by human activities. Through sample collection for laboratory analysis, combined with continuous online measurements at the Amazon Tall Tower Observatory (ATTO), this dissertation provides new insights into the role of natural and anthropogenic aerosol sources and their effects on aerosol composition and variability under clean and polluted atmospheric conditions.

Based on a large set of aerosol samples collected during several field campaigns, scanning electron microscopy combined with energy dispersive x-ray spectroscopy (SEM-EDX) has been used to analyze the size-resolved elemental composition of individual aerosol particles, with a particular focus on the inorganic fraction. The systematic sampling addressed the variability of the aerosol elemental composition in terms of the diurnal cycle and canopy conditions. With complementary data from online micrometeorological and aerosol measurements, relationships between the atmospheric conditions and the particle composition were established. It turned out that the wet season is not characterized by a homogeneously clean atmosphere, but is strongly influenced by the episodic occurrence of long-range transported (LRT) air masses bringing African dust, biomass burning smoke, and sea spray aerosol. All particles were dominated by organic matter, but also comprised a significant and diverse fraction of inorganic elements. Under the influence of LRT, the inorganic elemental signature was characterized by the dust and sea salt marker elements such as aluminum, iron, sodium and chlorine. Under the contrasting pristine conditions, it is characterized by biogenic tracer elements.

A targeted study addressed the clean rain forest conditions in the absence of LRT. It found a ubiquitous fraction of inorganic elements in the mostly carbon-dominated particles in all samples. The most prominent inorganic elements were potassium, chlorine, sulfur, sodium, and phosphorus, which were mostly attributed to biogenic sources in the rain forest ecosystem. Particles have been classified into categories with different physicochemical properties based on their inorganic composition and size. This indicates that different sources are involved in the intensive exchange between the biosphere and the atmosphere over large parts of the aerosol size distribution. These results are based on optimized sampling and automated SEM-EDX analysis, yielding a statistically robust data set that is representative for central Amazonian conditions. Building on and going beyond previous research (Pöschl et al., 2010; C. Pöhlker et al., 2012), these findings emphasize that biogenic salts of potentially different origins play a crucial role in the Amazonian aerosol cycle. These results clearly highlight the need for further studies on this fundamental and probably underestimated aspect of the Amazonian aerosol cycle.

In addition, aerosol particle number size distributions (PNSD) were measured with a scanning mobility particle sizer (SMPS) at the ATTO site over more than six years. This unique data set covers the aerosol variability in a size range from 10 to 400 nm

with high time resolution. The data resolves the seasonality and diel patterns of the aerosol and further resolves the effects of weather events on the abundance and size of the particles. Under clean conditions, the PNSDs are characterized by a multi-modal shape with distinct Aitken and accumulation modes. Under highly polluted conditions, the accumulation mode becomes dominant, covering the Aitken mode and leading to a mono-modal shape that demonstrates the prevalence of pollution aerosol. However, the sources and processes that contribute to the Aitken and accumulation modes, especially in the absence of heavy pollution, are poorly understood. In previous studies by Wang et al., 2016 and Andreae et al., 2018, the formation of new particles in the upper troposphere and their subsequent injection into the boundary layer has been identified as a significant source of particles. The results presented here complement these previous studies by providing ground-based observations on the occurrence of particles smaller than 50 nm and their subsequent growth into the Aitken mode. A significantly higher occurrence of these sub-50 nm events was detected during the clean wet season, especially during the day, emphasizing a contribution of photo-chemistry in particle growth. Combined with meteorological data, another relationship between growth events and convective activity was observed. These results support new particle formation in the upper troposphere as a relevant particle source. However, the analysis also showed that not all events are related to convective activity. In accordance with the SEM-EDX results, this finding emphasizes the potential relevance of primary biogenic emissions in the ultrafine size range for the aerosol cycling in the Amazon.

The PNSDs can be used to approximate the fraction of the aerosol population that can act as cloud condensation nuclei and, therefore, play a crucial role in aerosol-cloud interactions. The ground-based Aitken and accumulation mode particle concentrations were related to the satellite-derived droplet number concentration and effective cloud droplet radius in the ATTO region. Over a period of three years, this comparison showed a clear relationship between aerosol abundance and cloud microphysical properties. Analogous to the variability within the PNSDs, the cloud parameters show a pronounced seasonality. The results suggest that cloud droplet formation and growth in convective clouds is sensitive to changes in the aerosol population even under polluted conditions. These findings help to better constrain the complex aerosol-cloud-precipitation interactions in the Amazonian hydrological cycle.

Overall, this dissertation highlights the strength of combining systematic and targeted aerosol sampling for microspectroscopy with continuous online observations at the remote Amazon Tall Tower Observatory. By focusing primarily on very clean conditions during the Amazonian wet season, new insights into fundamental biogeochemical processes in the rain forest ecosystem could be obtained. The data and conclusions presented here can help to improve our understanding of Amazon forest in the Earth system and its representation in global models to address future transformation in the course of climate change.

Bibliography

Prospero, J. M.; Charlson, R. J.; Mohnen, V.; Jaenicke, R.; Delany, A. C.; Moyers, J.; Zoller, W., and Rahn, K.: "The atmospheric aerosol system: An overview". *Reviews of Geophysics*, 21, 7. (1983), pp. 1607–1629. DOI: 10.1029/RG021i007p01607.

Salati, E. and Vose, P. B.: "Amazon Basin: A System in Equilibrium". *Science*, 225, 4658. (1984), pp. 129–138. DOI: 10.1126/science.225.4658.129.

Talbot, R. W.; Andreae, M. O.; Andreae, T. W., and Harriss, R. C.: "Regional aerosol chemistry of the Amazon Basin during the dry season". *Journal of Geophysical Research: Atmospheres*, 93, D2. (1988), pp. 1499–1508. DOI: 10.1029/JD093iD02p01499.

Talbot, R. W.; Andreae, M. O.; Berresheim, H.; Artaxo, P.; Garstang, M.; Harriss, R. C.; Beecher, K. M., and Li, S. M.: "Aerosol chemistry during the wet season in central Amazonia: The influence of long-range transport". *Journal of Geophysical Research: Atmospheres*, 95, D10. (1990), pp. 16955–16969. DOI: 10.1029/JD095iD10p16955.

Artaxo, P.; Gerab, F., and Rabello, M. L. C.: "Elemental composition of aerosol particles from two atmospheric monitoring stations in the Amazon Basin". *Nuclear Instruments and Methods in Physics Research Section B: Beam Interactions with Materials and Atoms*, 75, 1. (1993), pp. 277–281. DOI: 10.1016/0168-583X(93)95658-R.

Pandis, S. N.; Wexler, A. S., and Seinfeld, J. H.: "Dynamics of Tropospheric Aerosols". *The Journal of Physical Chemistry*, 99, 24. (1995), pp. 9646–9659. DOI: 10.1021/j100024a003.

Song, C. H. and Carmichael, G. R.: "The aging process of naturally emitted aerosol (sea-salt and mineral aerosol) during long range transport". *Atmospheric Environment*, 33, 14. (1999), pp. 2203–2218. DOI: 10.1016/S1352-2310(98)00301-X.

Haywood, J. and Boucher, O.: "Estimates of the direct and indirect radiative forcing due to tropospheric aerosols: A review". *Reviews of Geophysics*, 38, 4. (2000), pp. 513–543. DOI: 10.1029/1999RG000078.

Raes, F.; Dingenen, R. V.; Vignati, E.; Wilson, J.; Putaud, J.-P.; Seinfeld, J. H., and Adams, P.: "Formation and cycling of aerosols in the global troposphere". *Atmospheric Environment*, 34, 25. (2000), pp. 4215–4240. DOI: 10.1016/S1352-2310(00)00239-9.

Yin, Y.; Levin, Z.; Reisin, T. G., and Tzivion, S.: "The effects of giant cloud condensation nuclei on the development of precipitation in convective clouds — a numerical study". *Atmospheric Research*, 53, 1. (2000), pp. 91–116. DOI: 10.1016/S0169-8095(99)00046-0.

Raga, G.; Castro, T., and Baumgardner, D.: "The impact of megacity pollution on local climate and implications for the regional environment: Mexico City". *Atmospheric Environment*, 35, 10. (2001), pp. 1805–1811. DOI: 10.1016/S1352-2310(00)00275-2.

Bauer, H.; Kasper-Giebl, A.; Löflund, M.; Giebl, H.; Hitzenberger, R.; Zibuschka, F., and Puxbaum, H.: "The contribution of bacteria and fungal spores to the organic carbon content of cloud water, precipitation and aerosols". *Atmospheric Research*. 2nd International Conference on Fog and Fog Collection, 64, 1. (2002), pp. 109–119. DOI: 10.1016/S0169-8095(02)00084-4.

Williams, J.; de Reus, M.; Krejci, R.; Fischer, H., and Ström, J.: "Application of the variability-size relationship to atmospheric aerosol studies: estimating aerosol lifetimes and ages". *Atmospheric Chemistry and Physics*, 2, 2. (2002), pp. 133–145. DOI: 10.5194/acp-2-133-2002.

Zhou, J.; Swietlicki, E.; Hansson, H. C., and Artaxo, P.: "Submicrometer aerosol particle size distribution and hygroscopic growth measured in the Amazon rain forest during the wet season". *Journal of Geophysical Research: Atmospheres*, 107, D20. (2002), LBA 22-1-LBA 22–10. DOI: 10.1029/2000JD000203.

Bauer, H.; Giebl, H.; Hitzenberger, R.; Kasper-Giebl, A.; Reischl, G.; Zibuschka, F., and Puxbaum, H.: "Airborne bacteria as cloud condensation nuclei". *Journal of Geophysical Research: Atmospheres*, 108, D21. (2003). DOI: 10.1029/2003JD003545.

Kulmala, M.: "How Particles Nucleate and Grow". *Science*, 302, 5647. (2003), pp. 1000–1001. DOI: 10.1126/science.1090848.

Roberts, G. C.; Nenes, A.; Seinfeld, J. H., and Andreae, M. O.: "Impact of biomass burning on cloud properties in the Amazon Basin". *Journal of Geophysical Research: Atmospheres*, 108, D2. (2003). DOI: 10.1029/2001JD000985.

Andreae, M. O.; Rosenfeld, D.; Artaxo, P.; Costa, A. A.; Frank, G. P.; Longo, K. M., and Silva-Dias, M. A. F.: "Smoking Rain Clouds over the Amazon". *Science*, 303, 5662. (2004), pp. 1337–1342. DOI: 10.1126/science.1092779.

Koren, I.; Kaufman, Y. J.; Remer, L. A., and Martins, J. V.: "Measurement of the Effect of Amazon Smoke on Inhibition of Cloud Formation". *Science*, 303, 5662. (2004), pp. 1342–1345. DOI: 10.1126/science.1089424.

Kaufman, Y. J.; Koren, I.; Remer, L. A.; Rosenfeld, D., and Rudich, Y.: "The effect of smoke, dust, and pollution aerosol on shallow cloud development over the Atlantic Ocean". *Proceedings of the National Academy of Sciences*, 102, 32. (2005), pp. 11207–11212. DOI: 10.1073/pnas.0505191102.

Lohmann, U. and Feichter, J.: "Global indirect aerosol effects: a review". *Atmospheric Chemistry and Physics*, 5, 3. (2005), pp. 715–737. DOI: 10.5194/acp-5-715-2005.

Oliveira, R. S.; Dawson, T. E.; Burgess, S. S. O., and Nepstad, D. C.: "Hydraulic redistribution in three Amazonian trees". *Oecologia*, 145, 3. (2005), pp. 354–363. DOI: 10.1007/s00442-005-0108-2.

Pöschl, U.: "Atmospheric Aerosols: Composition, Transformation, Climate and Health Effects". *Angewandte Chemie International Edition*, 44, 46. (2005), pp. 7520–7540. DOI: 10.1002/anie.200501122.

Dusek, U.; Frank, G. P.; Hildebrandt, L.; Curtius, J.; Schneider, J.; Walter, S.; Chand, D.; Drewnick, F.; Hings, S.; Jung, D.; Borrmann, S., and Andreae, M. O.: "Size Matters More Than Chemistry for Cloud-Nucleating Ability of Aerosol Particles". *Science*, 312, 5778. (2006), pp. 1375–1378. DOI: 10.1126/science.1125261.

Malhi, Y.; Wood, D.; Baker, T. R.; Wright, J.; Phillips, O. L.; Cochrane, T.; Meir, P.; Chave, J.; Almeida, S.; Arroyo, L.; Higuchi, N.; Killeen, T. J.; Laurance, S. G.; Laurance, W. F.; Lewis, S. L.; Monteagudo, A.; Neill, D. A.; Vargas, P. N.; Pitman, N. C. A.; Quesada, C. A.; Salomão, R.; Silva, J. N. M.; Lezama, A. T.; Terborgh, J.; Martínez, R. V., and Vinceti, B.: "The regional variation of aboveground live biomass in old-growth Amazonian forests". *Global Change Biology*, 12, 7. (2006), pp. 1107–1138. DOI: 10.1111/j.1365-2486.2006.01120.x.

Rissler, J.; Vestin, A.; Swietlicki, E.; Fisch, G.; Zhou, J.; Artaxo, P., and Andreae, M. O.: "Size distribution and hygroscopic properties of aerosol particles from dry-season biomass burning in Amazonia". *Atmospheric Chemistry and Physics*, 6, 2. (2006), pp. 471–491. DOI: 10.5194/acp-6-471-2006.

Sun, J. and Ariya, P. A.: "Atmospheric organic and bio-aerosols as cloud condensation nuclei (CCN): A review". *Atmospheric Environment*, 40, 5. (2006), pp. 795–820. DOI: 10.1016/j.atmosenv.2005.05.052.

Yu, H.; Kaufman, Y. J.; Chin, M.; Feingold, G.; Remer, L. A.; Anderson, T. L.; Balkanski, Y.; Bellouin, N.; Boucher, O.; Christopher, S.; DeCola, P.; Kahn, R.; Koch, D.; Loeb, N.; Reddy, M. S.; Schulz, M.; Takemura, T., and Zhou, M.: "A review of measurement-based assessments of the aerosol direct radiative effect and forcing". *Atmospheric Chemistry and Physics*, 6, 3. (2006), pp. 613–666. DOI: 10.5194/acp-6-613-2006.

Andreae, M. O.: "Aerosols Before Pollution". *Science*, 315, 5808. (2007), pp. 50–51. DOI: 10.1126/science.1136529.

Elbert, W.; Taylor, P. E.; Andreae, M. O., and Pöschl, U.: "Contribution of fungi to primary biogenic aerosols in the atmosphere: wet and dry discharged spores, carbohydrates, and inorganic ions". *Atmospheric Chemistry and Physics*, 7, 17. (2007), pp. 4569–4588. DOI: 10.5194/acp-7-4569-2007.

Möhler, O.; DeMott, P. J.; Vali, G., and Levin, Z.: "Microbiology and atmospheric processes: the role of biological particles in cloud physics". *Biogeosciences*, 4, 6. (2007), pp. 1059–1071. DOI: 10.5194/bg-4-1059-2007.

Andreae, M. O. and Rosenfeld, D.: "Aerosol–cloud–precipitation interactions. Part 1. The nature and sources of cloud-active aerosols". *Earth-Science Reviews*, 89, 1. (2008), pp. 13–41. DOI: 10.1016/j.earscirev.2008.03.001.

Bonan, G. B.: "Forests and Climate Change: Forcings, Feedbacks, and the Climate Benefits of Forests". *Science*, 320, 5882. (2008), pp. 1444–1449. DOI: 10.1126/science.1155121.

Kroll, J. H. and Seinfeld, J. H.: "Chemistry of secondary organic aerosol: Formation and evolution of low-volatility organics in the atmosphere". *Atmospheric Environment*, 42, 16. (2008), pp. 3593–3624. DOI: 10.1016/j.atmosenv.2008.01.003.

Lenton, T. M.; Held, H.; Kriegler, E.; Hall, J. W.; Lucht, W.; Rahmstorf, S., and Schellnhuber, H. J.: "Tipping elements in the Earth's climate system". *Proceedings of the National Academy of Sciences*, 105, 6. (2008), pp. 1786–1793. DOI: 10.1073/pnas.0705414105.

Zhang, R.; Khalizov, A. F.; Pagels, J.; Zhang, D.; Xue, H., and McMurry, P. H.: "Variability in morphology, hygroscopicity, and optical properties of soot aerosols during atmospheric processing". *Proceedings of the National Academy of Sciences*, 105, 30. (2008), pp. 10291–10296. DOI: 10.1073/pnas.0804860105.

Ansmann, A.; Baars, H.; Tesche, M.; Müller, D.; Althausen, D.; Engelmann, R.; Pauliquevis, T., and Artaxo, P.: "Dust and smoke transport from Africa to South America: Lidar profiling over Cape Verde and the Amazon rainforest". *Geophysical Research Letters*, 36, 11. (2009). DOI: 10.1029/2009GL037923.

Arraut, J. M. and Satyamurty, P.: "Precipitation and Water Vapor Transport in the Southern Hemisphere with Emphasis on the South American Region". *Journal of Applied Meteorology and Climatology*, 48, 9. (2009), pp. 1902–1912. DOI: 10.1175/2009JAMC2030.1.

Hallquist, M.; Wenger, J. C.; Baltensperger, U.; Rudich, Y.; Simpson, D.; Claeys, M.; Dommen, J.; Donahue, N. M.; George, C.; Goldstein, A. H.; Hamilton, J. F.; Herrmann, H.; Hoffmann, T.; Iinuma, Y.; Jang, M.; Jenkin, M. E.; Jimenez, J. L.; Kiendler-Scharr, A.; Maenhaut, W.; McFiggans, G.; Mentel, T. F.; Monod, A.; Prévôt, A. S. H.; Seinfeld, J. H.; Surratt, J. D.; Szmigielski, R., and Wildt, J.: "The formation, properties and impact of secondary organic aerosol: current and emerging issues". *Atmospheric Chemistry and Physics*, 9, 14. (2009), pp. 5155–5236. DOI: 10.5194/acp-9-5155-2009.

Kesselmeier, J.; Guenther, A.; Hoffmann, T.; Piedade, M. T., and Warnke, J.: "Natural Volatile Organic Compound Emissions From Plants and Their Roles in Oxidant Balance and Particle Formation". (2009). DOI: 10.1029/2008GM000717.

Martins, J. A.; Silva Dias, M. a. F., and Gonçalves, F. L. T.: "Impact of biomass burning aerosols on precipitation in the Amazon: A modeling case study". *Journal of Geophysical Research: Atmospheres*, 114, D2. (2009). DOI: 10.1029/2007JD009587.

Phillips, O. L.; Aragão, L. E. O. C.; Lewis, S. L.; Fisher, J. B.; Lloyd, J.; López-González, G.; Malhi, Y.; Monteagudo, A.; Peacock, J.; Quesada, C. A.; van der Heijden, G.; Almeida, S.; Amaral, I.; Arroyo, L.; Aymard, G.; Baker, T. R.; Bánki, O.; Blanc, L.; Bonal, D.; Brando, P.; Chave, J.; de Oliveira, Á. C. A.; Cardozo, N. D.; Czimczik, C. I.; Feldpausch, T. R.; Freitas, M. A.; Gloor, E.; Higuchi, N.; Jiménez, E.; Lloyd, G.; Meir, P.; Mendoza, C.; Morel, A.; Neill, D. A.; Nepstad, D.; Patiño, S.; Peñuela, M. C.; Prieto, A.; Ramírez, F.; Schwarz, M.; Silva, J.; Silveira, M.; Thomas, A. S.; Steege, H. ter; Stropp, J.; Vásquez, R.; Zelazowski, P.; Dávila, E. A.; Andelman, S.; Andrade, A.; Chao, K.-J.; Erwin, T.; Di Fiore, A.; C., E. H.; Keeling, H.; Killeen, T. J.; Laurance, W. F.; Cruz, A. P.; Pitman, N. C. A.; Vargas, P. N.; Ramírez-Angulo, H.; Rudas, A.; Salamão, R.; Silva, N.; Terborgh, J., and Torres-Lezama, A.: "Drought Sensitivity of the Amazon Rainforest". *Science*, 323, 5919. (2009), pp. 1344–1347. DOI: 10.1126/science.1164033.

Bristow, C. S.; Hudson-Edwards, K. A., and Chappell, A.: "Fertilizing the Amazon and equatorial Atlantic with West African dust". *Geophysical Research Letters*, 37, 14. (2010). DOI: 10.1029/2010GL043486.

George, I. J. and Abbatt, J. P. D.: "Heterogeneous oxidation of atmospheric aerosol particles by gas-phase radicals". *Nature Chemistry*, 2, 9. (2010), pp. 713–722. DOI: 10.1038/nchem.806.

Martin, S. T.; Andreae, M. O.; Artaxo, P.; Baumgardner, D.; Chen, Q.; Goldstein, A. H.; Guenther, A.; Heald, C. L.; Mayol-Bracero, O. L.; McMurry, P. H.; Pauliquevis, T.; Pöschl, U.; Prather, K. A.; Roberts, G. C.; Saleska, S. R.; Silva Dias, M. A.; Spracklen, D. V.; Swietlicki, E., and Trebs, I.: "Sources and properties of Amazonian aerosol particles". *Reviews of Geophysics*, 48, 2. (2010). DOI: 10.1029/2008RG000280.

Pope, F. D.: "Pollen grains are efficient cloud condensation nuclei". *Environmental Research Letters*, 5, 4. (2010), p. 044015. DOI: 10.1088/1748-9326/5/4/044015.

Pöschl, U.; Martin, S. T.; Sinha, B.; Chen, Q.; Gunthe, S. S.; Huffman, J. A.; Borrmann, S.; Farmer, D. K.; Garland, R. M.; Helas, G.; Jimenez, J. L.; King, S. M.; Manzi, A.; Mikhailov, E.; Pauliquevis, T.; Petters, M. D.; Prenni, A. J.; Roldin, P.; Rose, D.; Schneider, J.; Su, H.; Zorn, S. R.; Artaxo, P., and Andreae, M. O.: "Rainforest Aerosols as Biogenic Nuclei of Clouds and Precipitation in the Amazon". *Science*, 329, 5998. (2010), pp. 1513–1516. DOI: 10.1126/science.1191056.

de Leeuw, G.; Andreas, E. L.; Anguelova, M. D.; Fairall, C. W.; Lewis, E. R.; O'Dowd, C.; Schulz, M., and Schwartz, S. E.: "Production flux of sea spray aerosol". *Reviews of Geophysics*, 49, 2. (2011). DOI: 10.1029/2010RG000349.

Pan, Y.; Birdsey, R. A.; Fang, J.; Houghton, R.; Kauppi, P. E.; Kurz, W. A.; Phillips, O. L.; Shvidenko, A.; Lewis, S. L.; Canadell, J. G.; Ciais, P.; Jackson, R. B.; Pacala, S. W.; McGuire, A. D.; Piao, S.; Rautiainen, A.; Sitch, S., and Hayes, D.: "A Large and Persistent Carbon Sink in the World's Forests". *Science*, 333, 6045. (2011), pp. 988–993. DOI: 10.1126/science.1201609.

Shiraiwa, M.; Ammann, M.; Koop, T., and Pöschl, U.: "Gas uptake and chemical aging of semisolid organic aerosol particles". *Proceedings of the National Academy of Sciences*, 108, 27. (2011), pp. 11003–11008. DOI: 10.1073/pnas.1103045108.

Silvestrini, R. A.; Soares-Filho, B. S.; Nepstad, D.; Coe, M.; Rodrigues, H., and Assunção, R.: "Simulating fire regimes in the Amazon in response to climate change and deforestation". *Ecological Applications*, 21, 5. (2011), pp. 1573–1590. DOI: 10.1890/10-0827.1.

Arraut, J. M.; Nobre, C.; Barbosa, H. M. J.; Obregon, G., and Marengo, J.: "Aerial Rivers and Lakes: Looking at Large-Scale Moisture Transport and Its Relation to Amazonia and to Subtropical Rainfall in South America". *Journal of Climate*, 25, 2. (2012), pp. 543–556. DOI: 10.1175/2011JCLI4189.1.

Davidson, E. A.; de Araújo, A. C.; Artaxo, P.; Balch, J. K.; Brown, I. F.; C. Bustamante, M. M.; Coe, M. T.; DeFries, R. S.; Keller, M.; Longo, M.; Munger, J. W.; Schroeder, W.; Soares-Filho, B. S.; Souza, C. M., and Wofsy, S. C.: "The Amazon basin in transition". *Nature*, 481, 7381. (2012), pp. 321–328. DOI: 10.1038/nature10717.

Després, V. R.; Huffman, J. A.; Burrows, S. M.; Hoose, C.; Safatov, A. S.; Buryak, G.; Fröhlich-Nowoisky, J.; Elbert, W.; Andreae, M. O.; Pöschl, U., and Jaenicke, R.: "Primary biological aerosol particles in the atmosphere: a review". *Tellus B: Chemical and Physical Meteorology*, 64, 1. (2012), p. 15598. DOI: 10.3402/tellusb.v64i0.15598.

Griffiths, P. T.; Borlace, J.-S.; Gallimore, P. J.; Kalberer, M.; Herzog, M., and Pope, F. D.: "Hygroscopic growth and cloud activation of pollen: a laboratory and modelling study". *Atmospheric Science Letters*, 13, 4. (2012), pp. 289–295. DOI: 10.1002/asl.397.

Hoose, C. and Möhler, O.: "Heterogeneous ice nucleation on atmospheric aerosols: a review of results from laboratory experiments". *Atmospheric Chemistry and Physics*, 12, 20. (2012), pp. 9817–9854. DOI: 10.5194/acp-12-9817-2012.

Huffman, J. A.; Sinha, B.; Garland, R. M.; Snee-Pollmann, A.; Gunthe, S. S.; Artaxo, P.; Martin, S. T.; Andreae, M. O., and Pöschl, U.: "Size distributions and temporal variations of biological aerosol particles in the Amazon rainforest characterized by microscopy and real-time UV-APS fluorescence techniques during AMAZE-08". *Atmospheric Chemistry and Physics*, 12, 24. (2012), pp. 11997–12019. DOI: 10.5194/acp-12-11997-2012.

Kulmala, M.; Petäjä, T.; Nieminen, T.; Sipilä, M.; Manninen, H. E.; Lehtipalo, K.; Dal Maso, M.; Aalto, P. P.; Junninen, H.; Paasonen, P.; Riipinen, I.; Lehtinen, K. E. J.; Laaksonen, A., and Kerminen, V.-M.: "Measurement of the nucleation of atmospheric aerosol particles". *Nature Protocols*, 7, 9. (2012), pp. 1651–1667. DOI: 10.1038/nprot.2012.091.

Laskin, A.; Moffet, R. C.; Gilles, M. K.; Fast, J. D.; Zaveri, R. A.; Wang, B.; Nigge, P., and Shutthanandan, J.: "Tropospheric chemistry of internally mixed sea salt and organic particles: Surprising reactivity of NaCl with weak organic acids". *Journal of Geophysical Research: Atmospheres*, 117, D15. (2012), 2012JD017743. DOI: 10.1029/2012JD017743.

Pöhlker, C.; Wiedemann, K. T.; Sinha, B.; Shiraiwa, M.; Gunthe, S. S.; Smith, M.; Su, H.; Artaxo, P.; Chen, Q.; Cheng, Y.; Elbert, W.; Gilles, M. K.; Kilcoyne, A. L. D.; Moffet, R. C.; Weigand, M.; Martin, S. T.; Pöschl, U., and Andreae, M. O.: "Biogenic Potassium Salt Particles as Seeds for Secondary Organic Aerosol in the Amazon". *Science*, 337, 6098. (2012), pp. 1075–1078. DOI: 10.1126/science.1223264.

Artaxo, P.; V. Rizzo, L.; F. Brito, J.; J. Barbosa, H. M.; Arana, A.; T. Sena, E.; G. Cirino, G.; Bastos, W.; T. Martin, S., and O. Andreae, M.: "Atmospheric aerosols in Amazonia and land use change: from natural biogenic to biomass burning conditions". *Faraday Discussions*, 165, 0. (2013), pp. 203–235. DOI: 10.1039/C3FD00052D.

Bond, T. C.; Doherty, S. J.; Fahey, D. W.; Forster, P. M.; Berntsen, T.; DeAngelo, B. J.; Flanner, M. G.; Ghan, S.; Kärcher, B.; Koch, D.; Kinne, S.; Kondo, Y.; Quinn, P. K.; Sarofim, M. C.; Schultz, M. G.; Schulz, M.; Venkataraman, C.; Zhang, H.; Zhang, S.; Bellouin, N.; Guttikunda, S. K.; Hopke, P. K.; Jacobson, M. Z.; Kaiser, J. W.; Klimont, Z.; Lohmann, U.; Schwarz, J. P.; Shindell, D.; Storelvmo, T.; Warren, S. G., and Zender, C. S.: "Bounding the role of black carbon in the climate system: A scientific assessment". *Journal of Geophysical Research: Atmospheres*, 118, 11. (2013), pp. 5380–5552. DOI: 10.1002/jgrd.50171.

Carslaw, K. S.; Lee, L. A.; Reddington, C. L.; Pringle, K. J.; Rap, A.; Forster, P. M.; Mann, G. W.; Spracklen, D. V.; Woodhouse, M. T.; Regayre, L. A., and Pierce, J. R.: "Large contribution of natural aerosols to uncertainty in indirect forcing". *Nature*, 503, 7474. (2013), pp. 67–71. DOI: 10.1038/nature12674.

Huffman, J. A.; Prenni, A. J.; DeMott, P. J.; Pöhlker, C.; Mason, R. H.; Robinson, N. H.; Fröhlich-Nowoisky, J.; Tobo, Y.; Després, V. R.; Garcia, E.; Gochis, D. J.; Harris, E.; Müller-Germann, I.; Ruzene, C.; Schmer, B.; Sinha, B.; Day, D. A.; Andreae, M. O.; Jimenez, J. L.; Gallagher, M.; Kreidenweis, S. M.; Bertram, A. K., and Pöschl, U.: "High concentrations of biological aerosol particles and ice nuclei during and after rain". *Atmospheric Chemistry and Physics*, 13, 13. (2013), pp. 6151–6164. DOI: 10.5194/acp-13-6151-2013.

Rizzo, L. V.; Artaxo, P.; Müller, T.; Wiedensohler, A.; Paixão, M.; Cirino, G. G.; Arana, A.; Swietlicki, E.; Roldin, P.; Fors, E. O.; Wiedemann, K. T.; Leal, L. S. M., and Kulmala, M.: "Long term measurements of aerosol optical properties at a primary forest site in Amazonia". *Atmospheric Chemistry and Physics*, 13, 5. (2013), pp. 2391–2413. DOI: 10.5194/acp-13-2391-2013.

Choobari, O. A.; Zawar-Reza, P., and Sturman, A.: "The global distribution of mineral dust and its impacts on the climate system: A review". *Atmospheric Research*, 138. (2014), pp. 152–165. DOI: 10.1016/j.atmosres.2013.11.007.

Hamilton, D. S.; Lee, L. A.; Pringle, K. J.; Reddington, C. L.; Spracklen, D. V., and Carslaw, K. S.: "Occurrence of pristine aerosol environments on a polluted planet". *Proceedings of the National Academy of Sciences*, 111, 52. (2014), pp. 18466–18471. DOI: 10.1073/pnas.1415440111.

Hilker, T.; Lyapustin, A. I.; Tucker, C. J.; Hall, F. G.; Myneni, R. B.; Wang, Y.; Bi, J.; Mendes de Moura, Y., and Sellers, P. J.: "Vegetation dynamics and rainfall sensitivity of the Amazon". *Proceedings of the National Academy of Sciences*, 111, 45. (2014), pp. 16041–16046. DOI: 10.1073/pnas.1404870111.

Andreae, M. O.; Acevedo, O. C.; Araùjo, A.; Artaxo, P.; Barbosa, C. G. G.; Barbosa, H. M. J.; Brito, J.; Carbone, S.; Chi, X.; Cintra, B. B. L.; da Silva, N. F.; Dias, N. L.; Dias-Júnior, C. Q.; Ditas, F.; Ditz, R.; Godoi, A. F. L.; Godoi, R. H. M.; Heimann, M.; Hoffmann, T.; Kesselmeier, J.; Könemann, T.; Krüger, M. L.; Lavric, J. V.; Manzi, A. O.; Lopes, A. P.; Martins, D. L.; Mikhailov, E. F.; Moran-Zuloaga, D.; Nelson, B. W.; Nölscher, A. C.; Santos Nogueira, D.; Piedade, M. T. F.; Pöhlker, C.; Pöschl, U.; Quesada, C. A.; Rizzo, L. V.; Ro, C.-U.; Ruckteschler, N.; Sá, L. D. A.; de Oliveira Sá, M.; Sales, C. B.; dos Santos, R. M. N.; Saturno, J.; Schöngart, J.; Sörgel, M.; de Souza, C. M.; de Souza, R. a. F.; Su, H.; Targhetta, N.; Tóta, J.; Trebs, I.; Trumbore, S.; van Eijck, A.; Walter, D.; Wang, Z.; Weber, B.; Williams, J.; Winderlich, J.; Wittmann, F.; Wolff, S., and Yáñez-Serrano, A. M.: "The Amazon Tall Tower Observatory (ATTO): overview of pilot measurements on ecosystem ecology, meteorology, trace gases, and aerosols". *Atmospheric Chemistry and Physics*, 15, 18. (2015), pp. 10723–10776. DOI: 10.5194/acp-15-10723-2015.

Doughty, C. E.; Metcalfe, D. B.; Girardin, C. a. J.; Amézquita, F. F.; Cabrera, D. G.; Huasco, W. H.; Silva-Espejo, J. E.; Araujo-Murakami, A.; da Costa, M. C.; Rocha, W.; Feldpausch, T. R.; Mendoza, A. L. M.; da Costa, A. C. L.; Meir, P.; Phillips, O. L., and Malhi, Y.: "Drought impact on forest carbon dynamics and fluxes in Amazonia". *Nature*, 519, 7541. (2015), pp. 78–82. DOI: 10.1038/nature14213.

Hassett, M. O.; Fischer, M. W. F., and Money, N. P.: "Mushrooms as Rainmakers: How Spores Act as Nuclei for Raindrops". *PLOS ONE*, 10, 10. (2015), e0140407. DOI: 10.1371/journal.pone.0140407.

Pöschl, U. and Shiraiwa, M.: "Multiphase Chemistry at the Atmosphere–Biosphere Interface Influencing Climate and Public Health in the Anthropocene". *Chemical Reviews*, 115, 10. (2015), pp. 4440–4475. DOI: 10.1021/cr500487s.

Quinn, P. K.; Collins, D. B.; Grassian, V. H.; Prather, K. A., and Bates, T. S.: "Chemistry and Related Properties of Freshly Emitted Sea Spray Aerosol". *Chemical Reviews*, 115, 10. (2015), pp. 4383–4399. DOI: 10.1021/cr500713g.

Yáñez-Serrano, A. M.; Nölscher, A. C.; Williams, J.; Wolff, S.; Alves, E.; Martins, G. A.; Bourtsoukidis, E.; Brito, J.; Jardine, K.; Artaxo, P., and Kesselmeier, J.: "Diel and seasonal changes of biogenic volatile organic compounds within and above an Amazonian rainforest". *Atmospheric Chemistry and Physics*, 15, 6. (2015), pp. 3359–3378. DOI: 10.5194/acp-15-3359-2015.

China, S.; Wang, B.; Weis, J.; Rizzo, L.; Brito, J.; Cirino, G. G.; Kovarik, L.; Artaxo, P.; Gilles, M. K., and Laskin, A.: "Rupturing of Biological Spores As a Source of Secondary Particles in Amazonia". *Environmental Science & Technology*, 50, 22. (2016), pp. 12179–12186. DOI: 10.1021/acs.est.6b02896.

Fröhlich-Nowoisky, J.; Kampf, C. J.; Weber, B.; Huffman, J. A.; Pöhlker, C.; Andreae, M. O.; Lang-Yona, N.; Burrows, S. M.; Gunthe, S. S.; Elbert, W.; Su, H.; Hoor, P.; Thines, E.; Hoffmann, T.; Després, V. R., and Pöschl, U.: "Bioaerosols in the Earth system: Climate, health, and ecosystem interactions". *Atmospheric Research*, 182. (2016), pp. 346–376. DOI: 10.1016/j.atmosres.2016.07.018.

Jickells, T. D.; Baker, A. R., and Chance, R.: "Atmospheric transport of trace elements and nutrients to the oceans". *Philosophical Transactions of the Royal Society A: Mathematical, Physical and Engineering Sciences*, 374, 2081. (2016), p. 20150286. DOI: 10.1098/rsta.2015.0286.

Paasonen, P.; Kupiainen, K.; Klimont, Z.; Visschedijk, A.; Denier van der Gon, H. A. C., and Amann, M.: "Continental anthropogenic primary particle number emissions". *Atmospheric Chemistry and Physics*, 16, 11. (2016), pp. 6823–6840. DOI: 10.5194/acp-16-6823-2016.

Wang, J.; Krejci, R.; Giangrande, S.; Kuang, C.; Barbosa, H. M. J.; Brito, J.; Carbone, S.; Chi, X.; Comstock, J.; Ditas, F.; Lavric, J.; Manninen, H. E.; Mei, F.; Moran-Zuloaga, D.; Pöhlker, C.; Pöhlker, M. L.; Saturno, J.; Schmid, B.; Souza, R. A. F.; Springston, S. R.; Tomlinson, J. M.; Toto, T.; Walter, D.; Wimmer, D.; Smith, J. N.; Kulmala, M.; Machado, L. A. T.; Artaxo, P.; Andreae, M. O.; Petäjä, T., and Martin, S. T.: "Amazon boundary layer aerosol concentration sustained by vertical transport during rainfall". *Nature*, 539, 7629. (2016), pp. 416–419. DOI: 10.1038/nature19819.

Whitehead, J. D.; Darbyshire, E.; Brito, J.; Barbosa, H. M. J.; Crawford, I.; Stern, R.; Gallagher, M. W.; Kaye, P. H.; Allan, J. D.; Coe, H.; Artaxo, P., and McFiggans, G.: "Biogenic cloud nuclei in the central Amazon during the transition from wet to dry season". *Atmospheric Chemistry and Physics*, 16, 15. (2016), pp. 9727–9743. DOI: 10.5194/acp-16-9727-2016.

Cardoso, D.; Särkinen, T.; Alexander, S.; Amorim, A. M.; Bittrich, V.; Celis, M.; Daly, D. C.; Fiaschi, P.; Funk, V. A.; Giacomin, L. L.; Goldenberg, R.; Heiden, G.; Iganci, J.; Kelloff, C. L.; Knapp, S.; Cavalcante de Lima, H.; Machado, A. F. P.; dos Santos, R. M.; Mello-Silva, R.; Michelangeli, F. A.; Mitchell, J.; Moonlight, P.; de Moraes,

P. L. R.; Mori, S. A.; Nunes, T. S.; Pennington, T. D.; Pirani, J. R.; Prance, G. T.; de Queiroz, L. P.; Rapini, A.; Riina, R.; Rincon, C. A. V.; Roque, N.; Shimizu, G.; Sobral, M.; Stehmann, J. R.; Stevens, W. D.; Taylor, C. M.; Trovó, M.; van den Berg, C.; van der Werff, H.; Viana, P. L.; Zartman, C. E., and Forzza, R. C.: "Amazon plant diversity revealed by a taxonomically verified species list". *Proceedings of the National Academy of Sciences*, 114, 40. (2017), pp. 10695–10700. DOI: 10.1073/pnas.1706756114.

Cecchini, M. A.; Machado, L. A. T.; Andreae, M. O.; Martin, S. T.; Albrecht, R. I.; Artaxo, P.; Barbosa, H. M. J.; Borrmann, S.; Fütterer, D.; Jurkat, T.; Mahnke, C.; Minikin, A.; Molleker, S.; Pöhlker, M. L.; Pöschl, U.; Rosenfeld, D.; Voigt, C.; Weinzierl, B., and Wendisch, M.: "Sensitivities of Amazonian clouds to aerosols and updraft speed". *Atmospheric Chemistry and Physics*, 17, 16. (2017), pp. 10037–10050. DOI: 10.5194/acp-17-10037-2017.

Chor, T. L.; Dias, N. L.; Araújo, A.; Wolff, S.; Zahn, E.; Manzi, A.; Trebs, I.; Sá, M. O.; Teixeira, P. R., and Sörgel, M.: "Flux-variance and flux-gradient relationships in the roughness sublayer over the Amazon forest". *Agricultural and Forest Meteorology*, 239. (2017), pp. 213–222. DOI: 10.1016/j.agrformet.2017.03.009.

Hantson, S.; Knorr, W.; Schurgers, G.; Pugh, T. A. M., and Arneth, A.: "Global isoprene and monoterpene emissions under changing climate, vegetation, CO2 and land use". *Atmospheric Environment*, 155. (2017), pp. 35–45. DOI: 10.1016/j.atmosenv.2017.02.010.

Rizzolo, J. A.; Barbosa, C. G. G.; Borillo, G. C.; Godoi, A. F. L.; Souza, R. A. F.; Andreoli, R. V.; Manzi, A. O.; Sá, M. O.; Alves, E. G.; Pöhlker, C.; Angelis, I. H.; Ditas, F.; Saturno, J.; Moran-Zuloaga, D.; Rizzo, L. V.; Rosário, N. E.; Pauliquevis, T.; Santos, R. M. N.; Yamamoto, C. I.; Andreae, M. O.; Artaxo, P.; Taylor, P. E., and Godoi, R. H. M.: "Soluble iron nutrients in Saharan dust over the central Amazon rainforest". *Atmospheric Chemistry and Physics*, 17, 4. (2017), pp. 2673–2687. DOI: 10.5194/acp-17-2673-2017.

Saturno, J.; Pöhlker, C.; Massabò, D.; Brito, J.; Carbone, S.; Cheng, Y.; Chi, X.; Ditas, F.; Hrabě de Angelis, I.; Morán-Zuloaga, D.; Pöhlker, M. L.; Rizzo, L. V.; Walter, D.; Wang, Q.; Artaxo, P.; Prati, P., and Andreae, M. O.: "Comparison of different Aethalometer correction schemes and a reference multi-wavelength absorption technique for ambient aerosol data". *Atmospheric Measurement Techniques*, 10, 8. (2017), pp. 2837–2850. DOI: 10.5194/amt-10-2837-2017.

Andreae, M. O.; Afchine, A.; Albrecht, R.; Holanda, B. A.; Artaxo, P.; Barbosa, H. M. J.; Borrmann, S.; Cecchini, M. A.; Costa, A.; Dollner, M.; Fütterer, D.; Järvinen, E.; Jurkat, T.; Klimach, T.; Konemann, T.; Knote, C.; Krämer, M.; Krisna, T.; Machado, L. A. T.; Mertes, S.; Minikin, A.; Pöhlker, C.; Pöhlker, M. L.; Pöschl, U.; Rosenfeld, D.; Sauer, D.; Schlager, H.; Schnaiter, M.; Schneider, J.; Schulz, C.; Spanu, A.; Sperling, V. B.; Voigt, C.; Walser, A.; Wang, J.; Weinzierl, B.; Wendisch, M., and Ziereis, H.: "Aerosol characteristics and particle production in the upper troposphere over the Amazon Basin". *Atmospheric Chemistry and Physics*, 18, 2. (2018), pp. 921–961. DOI: 10.5194/acp-18-921-2018.

Kerminen, V.-M.; Chen, X.; Vakkari, V.; Petäjä, T.; Kulmala, M., and Bianchi, F.: "Atmospheric new particle formation and growth: review of field observations". *Environmental Research Letters*, 13, 10. (2018), p. 103003. DOI: 10.1088/1748-9326/aadf3c.

Moran-Zuloaga, D.; Ditas, F.; Walter, D.; Saturno, J.; Brito, J.; Carbone, S.; Chi, X.; Hrabě de Angelis, I.; Baars, H.; Godoi, R. H. M.; Heese, B.; Holanda, B. A.; Lavrič, J. V.; Martin, S. T.; Ming, J.; Pöhlker, M. L.; Ruckteschler, N.; Su, H.; Wang, Y.; Wang, Q.; Wang, Z.; Weber, B.; Wolff, S.; Artaxo, P.; Pöschl, U.; Andreae, M. O., and Pöhlker, C.: "Long-term study on coarse mode aerosols in the Amazon rain forest with the frequent intrusion of Saharan dust plumes". *Atmospheric Chemistry and Physics*, 18, 13. (2018), pp. 10055–10088. DOI: 10.5194/acp-18-10055-2018.

Mülmenstädt, J. and Feingold, G.: "The Radiative Forcing of Aerosol–Cloud Interactions in Liquid Clouds: Wrestling and Embracing Uncertainty". *Current Climate Change Reports*, 4, 1. (2018), pp. 23–40. DOI: 10.1007/s40641-018-0089-y.

Pfannerstill, E. Y.; Nölscher, A. C.; Yáñez-Serrano, A. M.; Bourtsoukidis, E.; Keßel, S.; Janssen, R. H. H.; Tsokankunku, A.; Wolff, S.; Sörgel, M.; Sá, M. O.; Araújo, A.; Walter, D.; Lavrič, J.; Dias-Júnior, C. Q.; Kesselmeier, J., and Williams, J.: "Total OH Reactivity Changes Over the Amazon Rainforest During an El Niño Event". *Frontiers in Forests and Global Change*, 1. (2018).

Pöhlker, M. L.; Ditas, F.; Saturno, J.; Klimach, T.; Hrabě de Angelis, I.; Araùjo, A. C.; Brito, J.; Carbone, S.; Cheng, Y.; Chi, X.; Ditz, R.; Gunthe, S. S.; Holanda, B. A.; Kandler, K.; Kesselmeier, J.; Könemann, T.; Krüger, O. O.; Lavrič, J. V.; Martin, S. T.; Mikhailov, E.; Moran-Zuloaga, D.; Rizzo, L. V.; Rose, D.; Su, H.; Thalman, R.; Walter, D.; Wang, J.; Wolff, S.; Barbosa, H. M. J.; Artaxo, P.; Andreae, M. O.; Pöschl, U., and Pöhlker, C.: "Long-term observations of cloud condensation nuclei over the Amazon rain forest – Part 2: Variability and characteristics of biomass burning, long-range transport, and pristine rain forest aerosols". *Atmospheric Chemistry and Physics*, 18, 14. (2018), pp. 10289–10331. DOI: 10.5194/acp-18-10289-2018.

Saturno, J.; Holanda, B. A.; Pöhlker, C.; Ditas, F.; Wang, Q.; Moran-Zuloaga, D.; Brito, J.; Carbone, S.; Cheng, Y.; Chi, X.; Ditas, J.; Hoffmann, T.; Hrabe de Angelis, I.; Könemann, T.; Lavrič, J. V.; Ma, N.; Ming, J.; Paulsen, H.; Pöhlker, M. L.; Rizzo, L. V.; Schlag, P.; Su, H.; Walter, D.; Wolff, S.; Zhang, Y.; Artaxo, P.; Pöschl, U., and Andreae, M. O.: "Black and brown carbon over central Amazonia: long-term aerosol measurements at the ATTO site". *Atmospheric Chemistry and Physics*, 18, 17. (2018), pp. 12817–12843. DOI: 10.5194/acp-18-12817-2018.

Staal, A.; Tuinenburg, O. A.; Bosmans, J. H. C.; Holmgren, M.; van Nes, E. H.; Scheffer, M.; Zemp, D. C., and Dekker, S. C.: "Forest-rainfall cascades buffer against drought across the Amazon". *Nature Climate Change*, 8, 6. (2018), pp. 539–543. DOI: 10.1038/s41558-018-0177-y.

Varanda Rizzo, L.; Roldin, P.; Brito, J.; Backman, J.; Swietlicki, E.; Krejci, R.; Tunved, P.; Petäjä, T.; Kulmala, M., and Artaxo, P.: "Multi-year statistical and modeling analysis of submicrometer aerosol number size distributions at a rain forest site in Amazonia". *Atmospheric Chemistry and Physics*, 18, 14. (2018), pp. 10255–10274. DOI: 10.5194/acp-18-10255-2018.

Wimmer, D.; Buenrostro Mazon, S.; Manninen, H. E.; Kangasluoma, J.; Franchin, A.; Nieminen, T.; Backman, J.; Wang, J.; Kuang, C.; Krejci, R.; Brito, J.; Goncalves Morais, F.; Martin, S. T.; Artaxo, P.; Kulmala, M.; Kerminen, V.-M., and Petäjä, T.: "Ground-based observation of clusters and nucleation-mode particles in the

Amazon". *Atmospheric Chemistry and Physics*, 18, 17. (2018), pp. 13245–13264. DOI: 10.5194/acp-18-13245-2018.

Barkhordarian, A.; Saatchi, S. S.; Behrangi, A.; Loikith, P. C., and Mechoso, C. R.: "A Recent Systematic Increase in Vapor Pressure Deficit over Tropical South America". *Scientific Reports*, 9, 1. (2019), p. 15331. DOI: 10.1038/s41598-019-51857-8.

Brock, C. A.; Williamson, C.; Kupc, A.; Froyd, K. D.; Erdesz, F.; Wagner, N.; Richardson, M.; Schwarz, J. P.; Gao, R.-S.; Katich, J. M.; Campuzano-Jost, P.; Nault, B. A.; Schroder, J. C.; Jimenez, J. L.; Weinzierl, B.; Dollner, M.; Bui, T., and Murphy, D. M.: "Aerosol size distributions during the Atmospheric Tomography Mission (ATom): methods, uncertainties, and data products". *Atmospheric Measurement Techniques*, 12, 6. (2019), pp. 3081–3099. DOI: 10.5194/amt-12-3081-2019.

Lee, S.-H.; Gordon, H.; Yu, H.; Lehtipalo, K.; Haley, R.; Li, Y., and Zhang, R.: "New Particle Formation in the Atmosphere: From Molecular Clusters to Global Climate". *Journal of Geophysical Research: Atmospheres*, 124, 13. (2019), pp. 7098–7146. DOI: 10.1029/2018JD029356.

Pöhlker, C.; Walter, D.; Paulsen, H.; Könemann, T.; Rodríguez-Caballero, E.; Moran-Zuloaga, D.; Brito, J.; Carbone, S.; Degrendele, C.; Després, V.; Ditas, F.; Holanda, B. A.; Kaiser, J. W.; Lammel, G.; Lavrič, J. V.; Ming, J.; Pickersgill, D.; Pöhlker, M. L.; Praß, M.; Löbs, N.; Saturno, J.; Sörgel, M.; Wang, Q.; Weber, B.; Wolff, S.; Artaxo, P.; Pöschl, U., and Andreae, M. O.: "Land cover and its transformation in the backward trajectory footprint region of the Amazon Tall Tower Observatory". *Atmospheric Chemistry and Physics*, 19, 13. (2019), pp. 8425–8470. DOI: 10.5194/acp-19-8425-2019.

Adachi, K.; Oshima, N.; Gong, Z.; de Sá, S.; Bateman, A. P.; Martin, S. T.; de Brito, J. F.; Artaxo, P.; Cirino, G. G.; Sedlacek III, A. J., and Buseck, P. R.: "Mixing states of Amazon basin aerosol particles transported over long distances using transmission electron microscopy". *Atmospheric Chemistry and Physics*, 20, 20. (2020), pp. 11923–11939. DOI: 10.5194/acp-20-11923-2020.

Holanda, B. A.; Pöhlker, M. L.; Walter, D.; Saturno, J.; Sörgel, M.; Ditas, J.; Ditas, F.; Schulz, C.; Franco, M. A.; Wang, Q.; Donth, T.; Artaxo, P.; Barbosa, H. M. J.; Borrmann, S.; Braga, R.; Brito, J.; Cheng, Y.; Dollner, M.; Kaiser, J. W.; Klimach, T.; Knote, C.; Krüger, O. O.; Fütterer, D.; Lavrič, J. V.; Ma, N.; Machado, L. A. T.; Ming, J.; Morais, F. G.; Paulsen, H.; Sauer, D.; Schlager, H.; Schneider, J.; Su, H.; Weinzierl, B.; Walser, A.; Wendisch, M.; Ziereis, H.; Zöger, M.; Pöschl, U.; Andreae, M. O., and Pöhlker, C.: "Influx of African biomass burning aerosol during the Amazonian dry season through layered transatlantic transport of black carbon-rich smoke". *Atmospheric Chemistry and Physics*, 20, 8. (2020), pp. 4757–4785. DOI: 10.5194/acp-20-4757-2020.

Hubau, W. et al.: "Asynchronous carbon sink saturation in African and Amazonian tropical forests". *Nature*, 579, 7797. (2020), pp. 80–87. DOI: 10.1038/s41586-020-2035-0.

Liu, L.; Cheng, Y.; Wang, S.; Wei, C.; Pöhlker, M. L.; Pöhlker, C.; Artaxo, P.; Shrivastava, M.; Andreae, M. O.; Pöschl, U., and Su, H.: "Impact of biomass burning aerosols on radiation, clouds, and precipitation over the Amazon: relative importance of aerosol–cloud and aerosol–radiation interactions". *Atmospheric Chemistry*

and Physics, 20, 21. (2020), pp. 13283–13301. DOI: 10.5194/acp-20-13283-2020.

Löbs, N.; Barbosa, C. G. G.; Brill, S.; Walter, D.; Ditas, F.; de Oliveira Sá, M.; de Araújo, A. C.; de Oliveira, L. R.; Godoi, R. H. M.; Wolff, S.; Piepenbring, M.; Kesselmeier, J.; Artaxo, P.; Andreae, M. O.; Pöschl, U.; Pöhlker, C., and Weber, B.: "Aerosol measurement methods to quantify spore emissions from fungi and cryptogamic covers in the Amazon". *Atmospheric Measurement Techniques*, 13, 1. (2020), pp. 153–164. DOI: 10.5194/amt-13-153-2020.

Ramsay, R.; Di Marco, C. F.; Sörgel, M.; Heal, M. R.; Carbone, S.; Artaxo, P.; de Araùjo, A. C.; Sá, M.; Pöhlker, C.; Lavric, J.; Andreae, M. O., and Nemitz, E.: "Concentrations and biosphere–atmosphere fluxes of inorganic trace gases and associated ionic aerosol counterparts over the Amazon rainforest". *Atmospheric Chemistry and Physics*, 20, 24. (2020), pp. 15551–15584. DOI: 10.5194/acp-20-15551-2020.

Schrod, J.; Thomson, E. S.; Weber, D.; Kossmann, J.; Pöhlker, C.; Saturno, J.; Ditas, F.; Artaxo, P.; Clouard, V.; Saurel, J.-M.; Ebert, M.; Curtius, J., and Bingemer, H. G.: "Long-term deposition and condensation ice-nucleating particle measurements from four stations across the globe". *Atmospheric Chemistry and Physics*, 20, 24. (2020), pp. 15983–16006. DOI: 10.5194/acp-20-15983-2020.

Fearnside, P. M.: "The intrinsic value of Amazon biodiversity". *Biodiversity and Conservation*, 30, 4. (2021), pp. 1199–1202. DOI: 10.1007/s10531-021-02133-7.

Gatti, L. V.; Basso, L. S.; Miller, J. B.; Gloor, M.; Gatti Domingues, L.; Cassol, H. L. G.; Tejada, G.; Aragão, L. E. O. C.; Nobre, C.; Peters, W.; Marani, L.; Arai, E.; Sanches, A. H.; Corrêa, S. M.; Anderson, L.; Von Randow, C.; Correia, C. S. C.; Crispim, S. P., and Neves, R. A. L.: "Amazonia as a carbon source linked to deforestation and climate change". *Nature*, 595, 7867. (2021), pp. 388–393. DOI: 10.1038/s41586-021-03629-6.

Machado, L. A. T.; Franco, M. A.; Kremper, L. A.; Ditas, F.; Andreae, M. O.; Artaxo, P.; Cecchini, M. A.; Holanda, B. A.; Pöhlker, M. L.; Saraiva, I.; Wolff, S.; Pöschl, U., and Pöhlker, C.: "How weather events modify aerosol particle size distributions in the Amazon boundary layer". *Atmospheric Chemistry and Physics*, 21, 23. (2021), pp. 18065–18086. DOI: 10.5194/acp-21-18065-2021.

Prass, M.; Andreae, M. O.; de Araùjo, A. C.; Artaxo, P.; Ditas, F.; Elbert, W.; Förster, J.-D.; Franco, M. A.; Hrabe de Angelis, I.; Kesselmeier, J.; Klimach, T.; Kremper, L. A.; Thines, E.; Walter, D.; Weber, J.; Weber, B.; Fuchs, B. M.; Pöschl, U., and Pöhlker, C.: "Bioaerosols in the Amazon rain forest: temporal variations and vertical profiles of Eukarya, Bacteria, and Archaea". *Biogeosciences*, 18, 17. (2021), pp. 4873–4887. DOI: 10.5194/bg-18-4873-2021.

Artaxo, P.; Hansson, H. C.; Machado, L. A. T., and Rizzo, L. V.: "Tropical forests are crucial in regulating the climate on Earth". *PLOS Climate*, 1, 8. (2022), e0000054. DOI: 10.1371/journal.pclm.0000054.

Artaxo, P.; Hansson, H.-C.; Andreae, M. O.; Bäck, J.; Alves, E. G.; Barbosa, H. M. J.; Bender, F.; Bourtsoukidis, E.; Carbone, S.; Chi, J.; Decesari, S.; Després, V. R.; Ditas, F.; Ezhova, E.; Fuzzi, S.; Hasselquist, N. J.; Heintzenberg, J.; Holanda, B. A.; Guenther, A.; Hakola, H.; Heikkinen, L.; Kerminen, V.-M.; Kontkanen, J.; Krejci,

R.; Kulmala, M.; Lavric, J. V.; Leeuw, G. de; Lehtipalo, K.; Machado, L. A. T.; McFiggans, G.; Franco, M. A. M.; Meller, B. B.; Morais, F. G.; Mohr, C.; Morgan, W.; Nilsson, M. B.; Peichl, M.; Petäjä, T.; Praß, M.; Pöhlker, C.; Pöhlker, M. L.; Pöschl, U.; Randow, C. V.; Riipinen, I.; Rinne, J.; Rizzo, L. V.; Rosenfeld, D.; Dias, M. A. F. S.; Sogacheva, L.; Stier, P.; Swietlicki, E.; Sörgel, M.; Tunved, P.; Virkkula, A.; Wang, J.; Weber, B.; Yáñez-Serrano, A. M.; Zieger, P.; Mikhailov, E.; Smith, J. N., and Kesselmeier, J.: "Tropical and Boreal Forest – Atmosphere Interactions: A Review". 74, 1. (2022), pp. 24–163. DOI: 10.16993/tellusb.34.

Barbosa, C. G. G.; Taylor, P. E.; Sá, M. O.; Teixeira, P. R.; Souza, R. A. F.; Albrecht, R. I.; Barbosa, H. M. J.; Sebben, B.; Manzi, A. O.; Araújo, A. C.; Prass, M.; Pöhlker, C.; Weber, B.; Andreae, M. O., and Godoi, R. H. M.: "Identification and quantification of giant bioaerosol particles over the Amazon rainforest". *npj Climate and Atmospheric Science*, 5, 1. (2022), pp. 1–10. DOI: 10.1038/s41612-022-00294-y.

Borma, L. S.; Costa, M. H.; da Rocha, H. R.; Arieira, J.; Nascimento, N. C. C.; Jaramillo-Giraldo, C.; Ambrosio, G.; Carneiro, R. G.; Venzon, M.; Neto, A. F.; van der Hoff, R.; Oliveira, B. F. A.; Rajão, R., and Nobre, C. A.: "Beyond Carbon: The Contributions of South American Tropical Humid and Subhumid Forests to Ecosystem Services". *Reviews of Geophysics*, 60, 4. (2022), e2021RG000766. DOI: 10.1029/2021RG000766.

Boulton, C. A.; Lenton, T. M., and Boers, N.: "Pronounced loss of Amazon rainforest resilience since the early 2000s". *Nature Climate Change*, 12, 3. (2022), pp. 271–278. DOI: 10.1038/s41558-022-01287-8.

Dias-Júnior, C. Q.; Carneiro, R. G.; Fisch, G.; D'Oliveira, F. A. F.; Sörgel, M.; Botía, S.; Machado, L. A. T.; Wolff, S.; Santos, R. M. N. dos, and Pöhlker, C.: "Intercomparison of Planetary Boundary Layer Heights Using Remote Sensing Retrievals and ERA5 Reanalysis over Central Amazonia". *Remote Sensing*, 14, 18. (2022), p. 4561. DOI: 10.3390/rs14184561.

Franco, M. A.; Ditas, F.; Kremper, L. A.; Machado, L. A. T.; Andreae, M. O.; Araújo, A.; Barbosa, H. M. J.; de Brito, J. F.; Carbone, S.; Holanda, B. A.; Morais, F. G.; Nascimento, J. P.; Pöhlker, M. L.; Rizzo, L. V.; Sá, M.; Saturno, J.; Walter, D.; Wolff, S.; Pöschl, U.; Artaxo, P., and Pöhlker, C.: "Occurrence and growth of sub-50 nm aerosol particles in the Amazonian boundary layer". *Atmospheric Chemistry and Physics*, 22, 5. (2022), pp. 3469–3492. DOI: 10.5194/acp-22-3469-2022.

Tang, K.; Sánchez-Parra, B.; Yordanova, P.; Wehking, J.; Backes, A.; Pickersgill, D. A.; Maier, S.; Sciare, J.; Pöschl, U.; Weber, B., and Fröhlich-Nowoisky, J.: "Bioaerosols and atmospheric ice nuclei in a Mediterranean dryland: community changes related to rainfall". *Biogeosciences*, 19, 1. (2022), pp. 71–91. DOI: 10.5194/bg-19-71-2022.

Adebiyi, A.; Kok, J.; Murray, B. J.; Ryder, C. L.; Stuut, J.-B. W.; Kahn, R. A.; Knippertz, P.; Formenti, P.; Mahowald, N. M.; Pérez García-Pando, C.; Klose, M.; Ansmann, A.; Samset, B. H.; Ito, A.; Balkanski, Y.; Di Biagio, C.; Romanias, M. N.; Huang, Y., and Meng, J.: "A review of coarse mineral dust in the Earth system". *Aeolian Research*, 60. (2023), p. 100849. DOI: 10.1016/j.aeolia.2022.100849.

Durgante, F. M.; Higuchi, N.; Ohashi, S.; Householder, J. E.; Lima, A. J. N.; Ishizuka, M.; Wittmann, F.; dos Santos, J.; Carneiro, V. M. C.; Xu, X.; do Nascimento, C. C.; Schöngart, J.; Piedade, M. T. F.; Schmitt, A. R. K.; Alves, Y. L. A.; Lehman, J.; Gimenez, B. O.; Baggio, P. M.; de Ourique, L. K., and Trumbore, S.: "Soil fertility and drought interact to determine large variations in wood production for a hyperdominant Amazonian tree species". *Frontiers in Forests and Global Change*, 5. (2023).

Gomes Alves, E.; Aquino Santana, R.; Quaresma Dias-Júnior, C.; Botía, S.; Taylor, T.; Yáñez-Serrano, A. M.; Kesselmeier, J.; Bourtsoukidis, E.; Williams, J.; Lembo Silveira de Assis, P. I.; Martins, G.; de Souza, R.; Duvoisin Júnior, S.; Guenther, A.; Gu, D.; Tsokankunku, A.; Sörgel, M.; Nelson, B.; Pinto, D.; Komiya, S.; Martins Rosa, D.; Weber, B.; Barbosa, C.; Robin, M.; Feeley, K. J.; Duque, A.; Londoño Lemos, V.; Contreras, M. P.; Idarraga, A.; López, N.; Husby, C.; Jestrow, B., and Cely Toro, I. M.: "Intra- and interannual changes in isoprene emission from central Amazonia". *Atmospheric Chemistry and Physics*, 23, 14. (2023), pp. 8149–8168. DOI: 10.5194/acp-23-8149-2023.

Holanda, B. A.; Franco, M. A.; Walter, D.; Artaxo, P.; Carbone, S.; Cheng, Y.; Chowdhury, S.; Ditas, F.; Gysel-Beer, M.; Klimach, T.; Kremper, L. A.; Krüger, O. O.; Lavric, J. V.; Lelieveld, J.; Ma, C.; Machado, L. A. T.; Modini, R. L.; Morais, F. G.; Pozzer, A.; Saturno, J.; Su, H.; Wendisch, M.; Wolff, S.; Pöhlker, M. L.; Andreae, M. O.; Pöschl, U., and Pöhlker, C.: "African biomass burning affects aerosol cycling over the Amazon". *Communications Earth & Environment*, 4, 1. (2023), pp. 1–15. DOI: 10.1038/s43247-023-00795-5.

Khadir, T.; Riipinen, I.; Talvinen, S.; Heslin-Rees, D.; Pöhlker, C.; Rizzo, L.; Machado, L. A. T.; Franco, M. A.; Kremper, L. A.; Artaxo, P.; Petäjä, T.; Kulmala, M.; Tunved, P.; Ekman, A. M. L.; Krejci, R., and Virtanen, A.: "Sink, Source or Something In-Between? Net Effects of Precipitation on Aerosol Particle Populations". *Geophysical Research Letters*, 50, 19. (2023), e2023GL104325. DOI: 10.1029/2023GL104325.

Leppla, D.; Zannoni, N.; Kremper, L.; Williams, J.; Pöhlker, C.; Sá, M.; Solci, M. C., and Hoffmann, T.: "Varying chiral ratio of pinic acid enantiomers above the Amazon rainforest". *Atmospheric Chemistry and Physics*, 23, 2. (2023), pp. 809–820. DOI: 10.5194/acp-23-809-2023.

Liu, T.; Zhang, J.; Cao, J.; Zheng, H.; Zhan, C.; Liu, H.; Zhang, L.; Xiao, K.; Liu, S.; Xiang, D., and Zhang, D.: "Identification of coexistence of biological and non-biological aerosol particles with DAPI (4′,6-diamidino-2-phenylindole) stain". *Particuology*, 72. (2023), pp. 49–57. DOI: 10.1016/j.partic.2022.02.009.

Pöhlker, M. L.; Pöhlker, C.; Quaas, J.; Mülmenstädt, J.; Pozzer, A.; Andreae, M. O.; Artaxo, P.; Block, K.; Coe, H.; Ervens, B.; Gallimore, P.; Gaston, C. J.; Gunthe, S. S.; Henning, S.; Herrmann, H.; Krüger, O. O.; McFiggans, G.; Poulain, L.; Raj, S. S.; Reyes-Villegas, E.; Royer, H. M.; Walter, D.; Wang, Y., and Pöschl, U.: "Global organic and inorganic aerosol hygroscopicity and its effect on radiative forcing". *Nature Communications*, 14, 1. (2023), p. 6139. DOI: 10.1038/s41467-023-41695-8.

Pugliese, G.; Ingrisch, J.; Meredith, L. K.; Pfannerstill, E. Y.; Klüpfel, T.; Meeran, K.; Byron, J.; Purser, G.; Gil-Loaiza, J.; van Haren, J.; Dontsova, K.; Kreuzwieser, J.; Ladd, S. N.; Werner, C., and Williams, J.: "Effects of drought and recovery

on soil volatile organic compound fluxes in an experimental rainforest". *Nature Communications*, 14, 1. (2023), p. 5064. DOI: 10.1038/s41467-023-40661-8.

Personal List of Publications

Kremper, Leslie A.; Moran-Zuloaga, D.; Kandler, K.; Förster, J.-D.; Quaresma Dias-Júnior, C.; Ditas, F.; Hrabe de Angelis, I.; Saturno, J.; Walter, D.; Artaxo, P.; Andreae, M. O.; Pöschl, U., and Pöhlker, C.: "Contrasting the elemental composition of amazonian aerosol under african dust influx vs pristine conditions". (in preparation)

Kremper, Leslie A.; Brill, S.; Förster, J.-D.; Artaxo, P.; Pöschl, U.; Kandler, K., and Pöhlker, C.: "Ubiquitous biogenic salts in the amazonian aerosol observed by electron microspectroscopy". (in preparation)

Lauer, O.; Kremper, Leslie A.; Rosenfeld, D.; Franco Marco A.and Andreae, M. O.; Artaxo, P.; Campos Braga, R.; Dias-Júnior, C. Q.; Araújo, A. C. de; Ditas, F.; Efraim, A.; Ervens, B.; Holanda, B. A.; Jungandreas, L.; Krüger, O. O.; Machado, L. A. T.; Hernández Pardo, L.; Pöschl, U.; Pulik, G.; Quaas, J.; Zheng, Y.; Zhu, Y.; Pöhlker, C., and Pöhlker, M. L.: "High aerosol sensitivity of amazonian clouds throughout the seasons". *Science Advances - under revision*. (2023)

Franco, M. A.; Ditas, F.; Kremper, Leslie A.; Machado, L. A. T.; Andreae, M. O.; Araújo, A.; Barbosa, H. M. J.; de Brito, J. F.; Carbone, S.; Holanda, B. A.; Morais, F. G.; Nascimento, J. P.; Pöhlker, M. L.; Rizzo, L. V.; Sá, M.; Saturno, J.; Walter, D.; Wolff, S.; Pöschl, U.; Artaxo, P., and Pöhlker, C.: "Occurrence and growth of sub-50 nm aerosol particles in the Amazonian boundary layer". *Atmospheric Chemistry and Physics*, 22, 5. (2022), pp. 3469–3492. DOI: 10.5194/acp-22-3469-2022

Khadir, T.; Riipinen, I.; Talvinen, S.; Heslin-Rees, D.; Pöhlker, C.; Rizzo, L.; Machado, L. A. T.; Franco, M. A.; Kremper, Leslie A.; Artaxo, P.; Petäjä, T.; Kulmala, M.; Tunved, P.; Ekman, A. M. L.; Krejci, R., and Virtanen, A.: "Sink, Source or Something In-Between? Net Effects of Precipitation on Aerosol Particle Populations". *Geophysical Research Letters*, 50, 19. (2023), e2023GL104325. DOI: 10.1029/2023GL104325

Holanda, B. A.; Franco, M. A.; Walter, D.; Artaxo, P.; Carbone, S.; Cheng, Y.; Chowdhury, S.; Ditas, F.; Gysel-Beer, M.; Klimach, T.; Kremper, Leslie A.; Krüger, O. O.; Lavric, J. V.; Lelieveld, J.; Ma, C.; Machado, L. A. T.; Modini, R. L.; Morais, F. G.; Pozzer, A.; Saturno, J.; Su, H.; Wendisch, M.; Wolff, S.; Pöhlker, M. L.; Andreae, M. O.; Pöschl, U., and Pöhlker, C.: "African biomass burning affects aerosol cycling over the Amazon". *Communications Earth & Environment*, 4, 1. (), pp. 1–15. DOI: 10.1038/s43247-023-00795-5

Leppla, D.; Zannoni, N.; Kremper, Leslie; Williams, J.; Pöhlker, C.; Sá, M.; Solci, M. C., and Hoffmann, T.: "Varying chiral ratio of pinic acid enantiomers above the Amazon rainforest". *Atmospheric Chemistry and Physics*, 23, 2. (2023), pp. 809–820. DOI: 10.5194/acp-23-809-2023

Efraim, A.; Lauer, O.; Rosenfeld, D.; Braga, R. C.; Franco, M. A.; Kremper, Leslie A.; Zhu, Y.; Pöschl, U.; Pöhlker, C.; Andreae, M. O.; Artaxo, P.; de Araújo, A. C., and Pöhlker, M. L.: "Satellite-Based Detection of Secondary Droplet Activation in Convective Clouds". *Journal of Geophysical Research: Atmospheres*, 127, 12. (2022), e2022JD036519. DOI: 10.1029/2022JD036519

Machado, L. A. T.; Franco, M. A.; Kremper, Leslie A.; Ditas, F.; Andreae, M. O.; Artaxo, P.; Cecchini, M. A.; Holanda, B. A.; Pöhlker, M. L.; Saraiva, I.; Wolff, S.; Pöschl, U., and Pöhlker, C.: "How weather events modify aerosol particle size distributions in the Amazon boundary layer". *Atmospheric Chemistry and Physics*, 21, 23. (2021), pp. 18065–18086. DOI: 10.5194/acp-21-18065-2021

Prass, M.; Andreae, M. O.; de Araùjo, A. C.; Artaxo, P.; Ditas, F.; Elbert, W.; Förster, J.-D.; Franco, M.; Hrabe de Angelis, I.; Kesselmeier, J.; Klimach, T.; Kremper, Leslie A.; Thines, E.; Walter, D.; Weber, J.; Weber, B.; Fuchs, B. M.; Pöschl, U., and Pöhlker, C.: "Bioaerosols in the Amazon rain forest: temporal variations and vertical profiles of Eukarya, Bacteria, and Archaea". *Biogeosciences*, 18, 17. (2021), pp. 4873–4887. DOI: 10.5194/bg-18-4873-2021

Mikhailov, E. F.; Pöhlker, M. L.; Reinmuth-Selzle, K.; Vlasenko, S. S.; Krüger, O. O.; Fröhlich-Nowoisky, J.; Pöhlker, C.; Ivanova, O. A.; Kiselev, A. A.; Kremper, Leslie A., and Pöschl, U.: "Water uptake of subpollen aerosol particles: hygroscopic growth, ccn activation, and liquid-liquid phase separation". *Atmos. Chem. Phys. Discuss.*, 2020. (2020), pp. 1–44. DOI: 10.5194/acp-2020-1224

Efraim, A.; Braga, R. C.; Rosenfeld, D.; Lauer, O.; Franco, M. A.; Kremper, Leslie A.; Pöhlker, C.; Andreae, M. O.; Quaresma Dias-Junior, C., and Pöhlker, M. L.: "Satellite-based detection of secondary droplet activation during condensational growth in convective clouds". *Atmospheric Research - under revision*. (2023)

Unfer, G. R.; Machado, L. A.; Albrecht, R. I.; Cecchini, M. A.; Hartwig, H.; Kremper, L. A.; Magina, F. C.; Pöhlker, M. L.; Vilà-Guerau de Arellano, J.; Williams, E.; Wolff, S., and Pöhlker, C.: "Surface Ozone Concentration associated with the Atmospheric Electric Field in the Amazon". (in preparation)

Franco, M. A.; Valiati, R.; Holanda, B. A.; Meller, B. B.; Kremper, Leslie A.; Rizzo, L. V.; Carbone, S.; Morais, F. G.; Nascimento, J. P.; Andreae, M. O.; Cecchini, M. A.; Machado, L. A. T.; Ponczek, M.; Pöschl, U.; Walter, D.; Pöhlker, C., and Artaxo, P.: "Vertically resolved aerosol variability in the Amazonian boundary layer under clean wet season conditions". *Atmospheric Chemistry and Physics - under revision*. (2023)

Machado, L. A. T.; Unfer, G. R.; Brill, S.; Hildmann, S.; Pöhlker, C.; Williams, J.; Hartwig, H.; Andreae, M. O.; Artaxo, P.; Cheng, Y.; Curtius, J.; Franco, M. A.; Cecchini, M. A.; Edtbauer, A.; Hoffmann, T.; Holanda, B.; Kremper, Leslie A.; Meller, B. B.; Pöhlker, M. L.; Quesada, C. A.; Ringsdorf, A.; Riipinen, I.; Wolff, S.; Lelieveld,

J., and Pöschl, U.: “Frequent nanoparticle bursts in the Amazon rainforest”. *Nature - under revision*. (2023)

Prass, M.; Brüwer, J.; Klimach, T.; Kremper, Leslie A.; Hrabe de Angelis, I.; Andreae, M. O.; de Araújo, A. C.; Artaxo, P.; Brill, S.; Ditas, F.; Förster, J.-D.; Pickersgill, D.; Walter, D.; Fuchs, B. M.; Pöschl, U., and Pöhlker, C.: “Bimodal bioaerosol population in the Amazon observed by automated fluorescence microscopy”. (in preparation)